

1 **Title:** Global continental and ocean basin reconstructions since 200 Ma

2  
3 **Authors:** Seton, M.<sup>1\*</sup>, Müller R.D.<sup>1</sup>, Zahirovic, S.<sup>1</sup>, Gaina, C.<sup>2#</sup>, Torsvik, T.<sup>2,3,4,5</sup>,  
4 Shephard, G.<sup>1</sup>, Talsma, A.<sup>1</sup>, Gurnis, M.<sup>6</sup>, Turner, M.<sup>6</sup>, Maus, S.,<sup>7</sup> and Chandler, M.<sup>8</sup>

5  
6 <sup>1</sup> EarthByte Group, School of Geosciences, Madsen Building F09, University of Sydney, NSW, 2006,  
7 Australia

8 <sup>2</sup> Centre for Geodynamics, Geological Survey of Norway, Leiv Eirikssons vei 39, N-7491  
9 Trondheim, Norway

10 <sup>3</sup> Physics of Geological Processes/School of Geosciences, University of Oslo, 0316 Oslo, Norway

11 <sup>4</sup> Center for Advanced Study, Norwegian Academy of Science and Letters, Drammensveien 78,  
12 0271 Oslo, Norway

13 <sup>5</sup> School of Geosciences, University of the Witwatersrand, Wits 2050, South Africa

14 <sup>6</sup> Seismological Laboratory, California Institute of Technology, Pasadena, California, USA

15 <sup>7</sup> National Geophysical Data Center, NOAA, Boulder, Colorado, USA

16 <sup>8</sup> School of Ocean and Earth Science and Technology (SOEST), University of Hawai'i at Manoa,  
17 1680 East-West Rd., POST # 806, Honolulu, HI 96822, USA

18  
19 \* Corresponding author: email - [maria.seton@sydney.edu.au](mailto:maria.seton@sydney.edu.au), phone - +61 2 9351 4255

20 # Now at Physics of Geological Processes/School of Geosciences, University of Oslo, 0316 Oslo,  
21 Norway

22  
23 **Journal:** Earth Science Reviews

24  
25 **Abstract**

26 Global plate motion models provide a spatial and temporal framework for  
27 geological data and have been effective tools for exploring processes occurring at  
28 the earth's surface. However, published models either have insufficient temporal  
29 coverage or fail to treat tectonic plates in a self-consistent manner. They usually  
30 consider the motions of selected features attached to tectonic plates, such as  
31 continents, but generally do not explicitly account for the continuous evolution  
32 of plate boundaries through time. In order to explore the coupling between the  
33 surface and mantle, plate models are required that extend over at least a few  
34 hundred million years and treat plates as dynamic features with dynamically  
35 evolving plate boundaries. We have constructed a new type of global plate  
36 motion model consisting of a set of continuously-closing topological plate

37 polygons with associated plate boundaries and plate velocities since the break-  
38 up of the supercontinent Pangea. Our model is underpinned by plate motions  
39 derived from reconstructing the seafloor-spreading history of the ocean basins  
40 and motions of the continents and utilizes a hybrid absolute reference frame,  
41 based on a moving hotspot model for the last 100 million years, and a true-polar  
42 wander corrected paleomagnetic model for 200 to 100 Ma. Detailed regional  
43 geological and geophysical observations constrain plate boundary inception or  
44 cessation, and time-dependent geometry. Although our plate model is primarily  
45 designed as a reference model for a new generation of geodynamic studies by  
46 providing the surface boundary conditions for the deep earth, it is also useful for  
47 studies in disparate fields when a framework is needed for analyzing and  
48 interpreting spatio-temporal data.

49

50 Keywords: plate reconstructions, plate motion model, Panthalassa, Laurasia,  
51 Tethys, Gondwana.

52

### 53 **1. Introduction**

54 Plate tectonic reconstructions are essential for providing a spatio-temporal  
55 context to geological and geophysical data and help uncover the driving forces of  
56 supercontinent break-up, separation and accretion, linkages between surface  
57 processes and the deep earth, modes of intra-plate deformation and mechanisms  
58 behind geological processes. Currently, plate reconstructions fall into three main  
59 categories: 1. “Geologically current” models based on present day plate motions  
60 from GPS measurements (Argus and Heflin, 1995), space geodesy e.g. GEODVEL  
61 (Argus et al., 2010) or a combination of spreading rates, fault azimuths and GPS  
62 measurements e.g. NUVEL-1 (DeMets et al., 2010; DeMets et al., 1990) and  
63 MORVEL (DeMets et al., 2010); 2. Traditional plate tectonic models based on the  
64 interpretation of the seafloor spreading record and/or paleomagnetic data to  
65 reconstruct the ocean basins, continents and terranes within an absolute  
66 reference framework (Golonka, 2007; Golonka and Ford, 2000; Müller et al.,  
67 2008b; Schettino and Scotese, 2005; Scotese, 1991; Scotese et al., 1988); 3.  
68 Coupled geodynamic–plate models, which model plate boundary locations and  
69 mantle density heterogeneity to predict past and/or present plate motions

70 (Conrad and Lithgow-Bertelloni, 2002; Hager and O'Connell, 1981; Lithgow-  
71 Bertelloni and Richards, 1998; Stadler et al., 2010).

72

73 “Geologically current” plate models provide the most accurate representation of  
74 global plate motions, are available in several global reference frameworks and  
75 can be independently verified with present day observations. However, they are  
76 limited from the Pliocene to present. Traditional plate tectonic reconstructions  
77 have good temporal coverage, which may extend as far back as the Paleozoic, but  
78 are often instantaneous snapshots rather than dynamically evolving models. For  
79 example, rather than representing plates in terms of their evolving shape, these  
80 models are generally built on rotating selected objects that form part of plates,  
81 such as continents, back through time, without addressing the implied evolution  
82 of the surrounding mid-ocean ridges, transform faults and subduction zones in a  
83 self-consistent manner. This limits the adaptability of traditional plate motion  
84 models, as they cannot easily be used as boundary conditions for geodynamic  
85 models. This is particularly acute for tracking the evolution of subduction since  
86 static plate reconstructions cannot simultaneously trace the continuous rollback  
87 of subduction zones while having slabs coupled to the subducting plate. Coupled  
88 geodynamic-plate models, which use numerical calculations to predict past and  
89 present plate motions, are sensitive to initial boundary conditions, as well as  
90 physical mantle properties, all subject to uncertainties and often work only for  
91 selected or interpolated timesteps. In addition, these published plate models are  
92 usually available in a form that does not easily lend itself to an exploration of the  
93 plate kinematic parameter space, in terms of testing alternative models in a  
94 geodynamic sense.

95

96 The rapid improvement in computational capability and efficiency (in terms of  
97 algorithms and hardware) with the simultaneous advancement in geodynamic  
98 modeling tools capable of addressing a range of applications, has created a need  
99 within the earth sciences community for a “deep-time” (i.e. time scales of a few  
100 hundred million years) reference plate motion model provided in digital form in  
101 such a way that it can be easily used, modified, and updated to address a variety  
102 of geological problems on a global scale. To ensure self-consistency, tectonic

103 plates and plate boundaries should be explicitly modeled as dynamically  
104 evolving features rather than the previous paradigm, which modeled the motion  
105 of discrete tectonic blocks, without much thought to the shape, size and  
106 boundaries between tectonic plates.

107

108 We have developed a “deep-time” reference plate motion model consisting of a  
109 set of dynamic topological plate polygons using the approach described in Gurnis  
110 et al. (2012) with associated plate boundaries and plate velocities since the  
111 break-up of Pangea (~200 Ma). Our model is underpinned by plate motions  
112 derived from reconstructing the seafloor-spreading history of the ocean basins  
113 and motions of the continents and built around a hybrid absolute reference  
114 frame. In reconstructing the ocean floor, we use satellite-derived gravity  
115 anomalies (Sandwell and Smith, 2009) (Figure 1) and an updated set of magnetic  
116 anomaly identifications to construct seafloor spreading isochrons for all the  
117 major oceanic plates. We use a combination of public and in-house magnetic  
118 anomaly data, which were line leveled and then gridded, to produce global  
119 magnetic anomaly grids and compare with our seafloor spreading isochrones  
120 (Figures 2,3, 5-7, 9, 11, 13, 14). We derive a global set of finite rotations for  
121 relative motions between all the major plates. In addition, we restore now-  
122 subducted oceanic crust for the major plates following the methodology in  
123 Müller et al. (2008b), by using evidence of subduction, slab windows and  
124 anomalous volcanism from onshore geology and the rules of plate tectonics. We  
125 create a set of dynamically closed plate polygons in one million year time  
126 intervals, which evolve from a series of dynamically evolving plate boundaries  
127 (Figures 18-28).

128

129 In building a topological closed plate polygon network, we have deliberately  
130 excluded many of the smaller tectonic plates and micro-plates in order to be able  
131 to produce a self-consistent global dataset for the community. The method of  
132 Gurnis et al. (2012) allows for construction of more detailed topological plate  
133 polygon networks. The data involved in reproducing our models are being made  
134 publicly available enabling researchers to either use our model as a framework  
135 in which to build upon for their particular area of expertise, input into

136 geodynamic simulations as surface boundary conditions or to understand the  
137 context of regional tectonics. We hope that this paper and the accompanying  
138 data will help those researchers from disparate fields critically evaluate plate  
139 reconstructions, determine areas in need of further analysis, use as a basis to  
140 further refine models and explore the limitations and sources of error inherent  
141 in plate motion models.

142

## 143 **2. Methodology**

144 There are four main components that comprise our plate motion model: an  
145 absolute reference frame, the relative motions between tectonic plates linked via  
146 a plate circuit, the geomagnetic polarity timescale and a collection of plate  
147 boundaries that combine to form a network of continuously closed plate  
148 polygons. The continuously closed plate polygons were created using *GPlates*  
149 software ([www.gplates.org](http://www.gplates.org)).

150

### 151 **2.1 Absolute Reference Frames**

152 The anchor for any global plate motion model is an absolute reference frame (i.e.  
153 how the plates move relative to a fixed reference system, such as the spin axis).  
154 A comprehensive discussion of absolute reference frames and the merits of each  
155 can be found in Torsvik et al. (2008). Our model uses a hybrid reference frame,  
156 which merges a moving Indian/Atlantic hotspot reference frame (O'Neill et al.,  
157 2005) back to 100 Ma with a paleomagnetically-derived true polar wander  
158 corrected reference frame (Steinberger and Torsvik, 2008) back to 200 Ma. This  
159 reference frame links to the global plate circuit through Africa, as Africa has been  
160 surrounded by mid-ocean ridges for at least the last 170 million years and,  
161 according to Torsvik et al. (2008), Africa has moved less than 500 km over the  
162 past 100 million years.

163

164 All the major tectonic plates are linked to Africa via the seafloor spreading or  
165 rifting back to 200 Ma, except the Pacific and associated plates, such as the  
166 Farallon, Izanagi, Phoenix and Kula. The Pacific plate can only be linked to the  
167 plate circuit for times younger than 83.5 Ma, after the establishment of seafloor  
168 spreading between the Pacific and west Antarctic plates. Prior to this time we

169 switch to a fixed Pacific hotspot reference frame for the Pacific plate, using a  
170 combination of Wessel and Kroenke (2008) and Wessel et al. (2006). We assume  
171 that the Pacific reference frame is fixed relative to other hotspots as we have no  
172 reliable model for whether the Pacific mantle plumes moved relative to each  
173 other or relative to the Earth's spin axis before 83.5 Ma, although some authors  
174 have invoked motion between some hotspots in the Pacific to account for paleo-  
175 latitude estimates from paleomagnetic data for the Ontong-Java Plateau (Riisager  
176 et al., 2003).

177

## 178 ***2.2 Relative Plate Motions***

179 In building our relative plate motion model, we combine published and new  
180 magnetic anomaly identifications (magnetic anomaly picks) and their associated  
181 rotations to construct a global set of seafloor spreading isochrons (see Section 3  
182 Regional continental and ocean floor reconstructions for details). This is largely  
183 based on the global plate model presented in Müller et al. (2008a), which builds  
184 upon the present day seafloor agegrid work of Müller et al. (1997) and includes a  
185 database consisting of over 70,000 magnetic anomaly identifications, extinct and  
186 active spreading ridge locations and boundary locations defining the transition  
187 from continental to oceanic crust. Seafloor spreading isochrons were  
188 constructed at Chrons 5o (10.9 Ma), 6o (20.1 Ma), 13y (33.1 Ma), 18o (40.1 Ma),  
189 21o (47.9 Ma), 25y (55.9 Ma), 31y (67.7 Ma), 34y (83.5 Ma), M0 (120.4 Ma), M4  
190 (126.7 Ma), M10 (131.9 Ma), M16 (139.6 Ma), M21 (147.7 Ma), and M25 (154.3  
191 Ma) with more detailed timesteps during major tectonic events. A finer set of  
192 seafloor spreading isochrons was drawn in back-arc and marginal basins.

193 Quoted ages use Cande and Kent (1995) for times after 83.5 Ma and Gradstein et  
194 al. (1994) for times prior to 83.5 Ma. The letter "y" stands for young end of  
195 chron and "o" for old end of chron. We verify our isochron interpretation by  
196 correlating with the magnetic lineations in the World Digital Magnetic Anomaly  
197 Map (WDMAM) (Maus et al., 2007), the Earth Magnetic Anomaly Grid (EMAG2)  
198 (Maus et al., 2009) and our own preferred magnetic anomaly compilation (Figure  
199 2). EMAG2 includes a compilation of both ship-track and long-wavelength  
200 satellite magnetic anomaly data with trend-gridding based on the Müller et al.  
201 (2008a) isochrons in most areas, hence WDMAM and our own compilation are

202 preferred for correlation. We constrain fracture zone locations using global  
203 gravity from satellite altimetry (Sandwell and Smith, 1997, 2005) (Figure 1). The  
204 boundary between oceanic and continental lithosphere was taken from Müller et  
205 al. (2008a), except where otherwise stated in the text.

206

207 The computation of finite rotations and construction of seafloor spreading  
208 isochrons is relatively straightforward for areas where both flanks of a spreading  
209 system are preserved (e.g. Atlantic, SE Indian Ridge, Pacific-Antarctic Ridge), but  
210 becomes more problematic in other settings. When only one flank of a spreading  
211 system is preserved (e.g. Pacific-Farallon, Pacific-Kula, Pacific-Izanagi, Pacific-  
212 Phoenix), we compute half-stage rotations (stage rotation between adjacent  
213 isochrons on one flank) and double the half-stage angle (i.e. assume that  
214 spreading was symmetrical) to create a full stage rotation, following the  
215 methodology of Stock and Molnar (1988). This assumption of spreading  
216 symmetry is reasonable as the maximum cumulative spreading asymmetry  
217 globally is only 10%, on average (Müller et al., 1998b). In instances where crust  
218 from both flanks has been subducted, we rely on the onshore geological record  
219 (e.g. mapping of major sutures, terrane boundaries and active and ancient  
220 magmatic arcs) to help define the locations of paleo-plate boundaries and use  
221 inferences from younger, preserved crust to estimate earlier spreading  
222 directions and rates. Where continental terranes have crossed ocean basins we  
223 use the implied history of mid-ocean ridge evolution and subduction to create  
224 synthetic ocean floor by constructing isochrons based on assuming spreading  
225 symmetry and ensuring triple junction closure. The location of mid-ocean ridges  
226 as they intersect continents can be further constrained by tracking slab window  
227 formation along continental margins (Thorkelson, 1996) and their correlation to  
228 anomalous geochemistry and volcanism (Bradley et al., 1993; Breitsprecher et  
229 al., 2003; Madsen et al., 2006; Sisson and Pavlis, 1993), elevated geothermal  
230 gradients (Bradley et al., 1993; Lewis et al., 2000; Thorkelson, 1996) and the  
231 eruption of massive sulphides (Haeussler et al., 1995; Rosenbaum et al., 2005).  
232 We do not use arguments for the location subduction based on mantle  
233 tomography as our model is solely underpinned by surface constraints.

234

235 Triple junction closure follows the rules set out in McKenzie and Morgan (1969)  
236 where we assume that the ridge axes are perpendicular to the spreading  
237 direction, transform faults are purely strike-slip features, plates are rigid and  
238 spreading is symmetrical. We use the finite difference method to compute  
239 spreading along the third arm of a triple junction. In addition, we assume that  
240 ridge-ridge-ridge triple junctions are stable features, but note that there is  
241 evidence that fast seafloor spreading rates cause triple junction instability and  
242 complexities in spreading (Bird and Naar, 1994).

243

### 244 ***2.3 Geomagnetic Polarity Timescales***

245 Geomagnetic polarity timescales (GPTS) correlate the reversals of the Earth's  
246 geomagnetic field, most often the sequence of magnetic anomalies recorded on  
247 the ocean floor, to those based on biostratigraphy, cyclostratigraphy (which  
248 includes Earth's orbital variations), absolute ages from radiometric studies and  
249 average spreading rates for interpolation.

250

251 The early GPTS for the Cenozoic (Heirtzler, 1968) and Mesozoic (Larson and  
252 Pitman, 1972) have been superseded by a range of updated timescales. Cande  
253 and Kent (1995) (CK95) developed a timescale for the Cenozoic (0-83.5 Ma)  
254 based on a model of smoothly varying spreading rates in the South Atlantic  
255 (Cande and Kent, 1992) with the inclusion of astronomical information for the  
256 past 5.23 million years. Gradstein et al. (1994) (G94) presented an integrated  
257 geomagnetic and stratigraphic Mesozoic timescale, which is commonly merged  
258 with the CK95 timescale to create a hybrid timescale through to the Mesozoic  
259 (e.g. (Müller et al., 2008b)). The GTS2004 timescale (Gradstein et al., 2004)  
260 recalibrated CK95 using alternative tie-points from updated radiometric ages  
261 and astronomical tuning for the Cenozoic and updated the Mesozoic timescale  
262 using the methodology of Cande and Kent (1992) and additional radiometric age  
263 constraints. The most recent GPTS (Gee and Kent, 2007) is a hybrid model,  
264 which uses CK95 for the Cenozoic and CENT94 (Channell, 1995) for the Mesozoic  
265 and includes sub-chrons from Lowrie and Kent (2004). The choice of GPTS (i.e.  
266 the ages assigned to each magnetic anomaly chron) has major implications for  
267 the timing of geological events and the significance of geological processes. For

268 example, the inferred mid-Cretaceous seafloor spreading pulse (Larson, 1995) is  
269 apparent if using the CK94G95 timescale but diminished if using GTS2004 due to  
270 a ~4 million year difference in the age assigned to M0 (~120 Ma) (Seton et al.,  
271 2009).

272

273 The occurrence of magnetic reversals in the so-called Jurassic Quiet Zone is not a  
274 widely accepted explanation for magnetic anomalies of ages 157 million years  
275 and older, which are rather modeled as geomagnetic intensity variations (Gee  
276 and Kent, 2007). Despite this, geomagnetic timescales based on detailed  
277 magnetic anomalies collected closer to the seafloor (using a deep towed  
278 magnetometer) in regions of high seafloor spreading rates (in the Pacific ocean)  
279 suggest the existence of a range of short reversals spanning from M29 to M40  
280 (Sager et al., 1998) or M29 to M44 (Tivey et al., 2006) (T06). Dating of Jurassic  
281 Quiet Zone based on the timescale of Sager et al. (1998) has been also attempted  
282 in the Central Atlantic ocean by Roeser et al. (2002) and Bird et al. (2007).

283

284 We ensure our data, including magnetic anomaly identifications, finite rotations  
285 and seafloor spreading isochrons are calibrated to one timescale. We choose the  
286 CK95 geomagnetic reversal timescale for the Cenozoic (to Chron 34y; 0-83.5 Ma),  
287 G94 for the Mesozoic (Chron M0-M33; 120.4-158.1 Ma) and T06 for the Jurassic  
288 (Chron M34-M44; 160.3-169.7 Ma), as our standard. Our continuously closed  
289 plate polygons can be combined using either timescale.

290

#### 291 ***2.4 Continuously Closed Plate Polygons***

292 A network of tectonic plates, bounded by a series of plate boundaries, combine to  
293 cover the surface of the Earth. Most plate tectonic models reconstruct features  
294 on the surface of the Earth without regard to the plate margins and are created in  
295 time intervals that are too sparse for current needs. These models are  
296 insufficient for studies that couple motions of the plates to other dynamic earth  
297 processes, for example mantle convection and oceanic and atmospheric  
298 circulation. This prompted Gurnis et al. (2012) to develop a novel methodology  
299 to create a set of dynamically closed plate polygons back in time. The  
300 continuously closing plate (CCP) methodology works by assigning a different

301 Euler pole for each plate boundary that constitutes a plate polygon, ensuring that  
302 the polygon remains topologically closed as a function of time (Gurnis et al.,  
303 2012). The feature is built into the plate reconstruction software *GPlates*  
304 (Boyden et al., 2011).

305

306 We use the CCP method and the base set of plate polygons in Gurnis et al. (2012)  
307 to create a new set of dynamically closed plate polygons based on the plate  
308 motion model presented in this study for the last 200 million years. The plate  
309 polygons are built using a series of plate boundaries, the location and timing of  
310 which have been determined by using present day plate boundaries (Bird, 2003),  
311 geological evidence for locations of island arcs, magmatic arcs, sutures and major  
312 faults through time as well as an analysis of plate motion vectors based on our  
313 kinematic model. The Euler poles describing the motion of each plate margin is  
314 derived from the plate tectonic model presented in this study. Each plate  
315 boundary feature within the dataset has a set of feature-specific attributes  
316 assigned. For example, mid-ocean ridge features include information on the  
317 plate to the left and right of the spreading ridge and whether it is an active or  
318 extinct feature; subduction zones contain information regarding the polarity of  
319 subduction, dip angle (when known) and the duration of activity; transform  
320 faults track the sense and direction of motion.

321

322 Our set of continuously closed plate polygons covers the entire surface of the  
323 Earth with no gaps in one million year time intervals. These can be used as input  
324 into geodynamic modeling software, to extract plate velocity data for each  
325 tectonic plate through time, to reconstruct raster data and to “cookie-cut”  
326 geological data based on tectonic plate. Using the CCP algorithm code in *GPlates*,  
327 the time interval between closed polygons can be made arbitrarily small and is  
328 only limited to how the underlying start and end ages of both margins and  
329 polygons has been encoded. For ease of use, the polygons are presented as static  
330 polygons at 1 million year time intervals. All data are available in digital format  
331 and can be downloaded from the following location:

332 [ftp://ftp.earthbyte.org/earthbyte/GlobalPlateModel/Seton\\_etal\\_Data.zip](ftp://ftp.earthbyte.org/earthbyte/GlobalPlateModel/Seton_etal_Data.zip).

333

### 334 **3. Regional continental and ocean floor reconstructions**

335 In the following section, we will describe the plate kinematic models we used for  
336 each region of the world. We separate the globe into four main regions: the  
337 Atlantic and Arctic; the Pacific and Panthalassa; the Tethys and Indian/Southern  
338 Ocean; and marginal and back-arc basins. We suggest that the accompanying  
339 data with this paper be loaded in order to most easily follow the plate  
340 boundaries and configurations mentioned in the text.

341

#### 342 ***3.1 Atlantic and Arctic***

##### 343 *3.1.1 South Atlantic*

344 Over the recent decades there has been considerable debate on the exact timing  
345 and kinematics of the opening of the South Atlantic ocean. It is commonly  
346 accepted that rifting in the South Atlantic occurred progressively from south to  
347 north along reactivated older tectonic lineaments dating from the late Triassic-  
348 early Jurassic (Daly et al., 1989) and was associated with substantial intra-  
349 continental deformation within Africa and South America (Eagles, 2007; Moulin  
350 et al., 2010; Nürnberg and Müller, 1991; Torsvik et al., 2009; Unternehr et al.,  
351 1988). To account for these motions, South America and Africa are subdivided  
352 using Jurassic-Cretaceous sedimentary basins, which document the various rift  
353 phases related to the dispersal of west Gondwana. South America is commonly  
354 subdivided into the Patagonia, Colorado and Parana subplates and Africa into  
355 South, Northwest and Northeast Africa (Nürnberg and Müller, 1991; Torsvik et  
356 al., 2009) (Figure 2). Internal deformation within both continents is required to  
357 minimize gaps/overlaps in full-fit reconstructions (see discussions in Eagles,  
358 (2007), Moulin et al. (2010) and Torsvik et al. (2009)).

359

360 Rifting prior to seafloor spreading in the southernmost Atlantic (“Falkland  
361 segment”) is believed to have occurred in the early Jurassic (190 Ma) and  
362 involved dextral movement between Patagonia and the Colorado sub-plate until  
363 the early Cretaceous (126.7 Ma) (Torsvik et al., 2009) (Figure 2). Opening  
364 propagated northward into the “Southern/Austral segment” adjacent to the  
365 Colorado sub-plate in the late Jurassic (around 150 Ma) based on late Jurassic-  
366 early Cretaceous sediment fill and activation (Nürnberg and Müller, 1991) and

367 the onset of deformation for a “fit” reconstruction using spreading rate  
368 interpolation (Eagles, 2007) or early Cretaceous (140 Ma) according to Schettino  
369 and Scotese (2005). The model of Torsvik et al. (2009) suggest that rifting was  
370 accommodated between the Colorado and Parana subplates, Colorado and Africa,  
371 and Parana and Africa from 150 Ma and was associated with dextral strike-slip  
372 motion between Patagonia/Colorado subplate and Parana (Nürnberg and Müller,  
373 1991; Torsvik et al., 2009). Further north, rifting adjacent to the Parana subplate  
374 and south of the Walvis Ridge/Rio Grande Rise is believed to have occurred by  
375 about 130 Ma (Nürnberg and Müller, 1991), 132 Ma corresponding to the  
376 Parana-Etendeka magmatic event peak (Torsvik et al., 2009), 134 Ma based on  
377 the presence of Anomaly M10 and the GTS2004 timescale (Moulin et al., 2010) or  
378 135 Ma based on dating of the continent-ocean transition (Bradley, 2008). The  
379 oldest magnetic anomaly that has been identified is M4 (~127 Ma) (Nürnberg  
380 and Müller, 1991; Torsvik et al., 2009) adjacent to Falkland and Parana/Chacos  
381 basin. Coincident with opening along the South Atlantic rift was the activation of  
382 the West and Central African Rift systems and the Central African Shear Zone  
383 (Binks and Fairhead, 1992; Genik, 1992; Guiraud and Maurin, 1992; Torsvik et  
384 al., 2009).

385

386 The “Central” segment of the South Atlantic margin (Figure 2) is characterized by  
387 widespread Aptian salt basin formation. Rifting continued propagating  
388 northward and extended into the African interior, active in the Benue Trough by  
389 at least 118 Ma (Nürnberg and Müller, 1991), although earlier extension in the  
390 Benue Trough is possible (Torsvik et al., 2009). The onset of seafloor spreading  
391 in the “Central” segment is difficult to ascertain because the oceanic crust  
392 adjacent to the margin formed during the Cretaceous Normal Superchron (CNS),  
393 however Anomaly M0 has been identified extending to latitude 22°S (Müller et  
394 al., 1999; Nürnberg and Müller, 1991)(Cande et al., 1988). Torsvik et al. (2009)  
395 used the shape and age of the Aptian salt basins to further refine the opening  
396 history in this section of the margin and suggested that seafloor spreading only  
397 reached north of the Walvis Ridge-Rio Grande Rise at ~112 Ma, much later than  
398 120.4 Ma suggested by previous models.

399

400 The “Equatorial” segment of the South Atlantic margin (Figure 2) was the  
401 youngest region of plate break-up. Magnetic anomalies cannot be interpreted  
402 due to equatorial formation of the oceanic crust relative to spreading direction.  
403 However, Anomaly 33 and fracture zone segments are well defined. Seafloor  
404 spreading is believed to have propagated into this area after Anomaly M0 (120.4  
405 Ma) (Nürnberg and Müller, 1991), ~100 Ma (Torsvik et al., 2009), 105 Ma  
406 (Moulin et al., 2010) or 102-96 Ma (Eagles, 2007), corresponding to a subtle  
407 bend in the fracture zones in the South Atlantic. Either coincident or subsequent  
408 to the opening of the equatorial segment, the areas undergoing continental  
409 extension in the African interior ceased but only after a short-lived  
410 compressional phase in the late Cretaceous (around 85-80 Ma) observed in  
411 folding and faulting across seismic sections (Binks and Fairhead, 1992; Nürnberg  
412 and Müller, 1991; Schettino and Scotese, 2005).

413

414 The spreading history along the entire length of the South Atlantic from Anomaly  
415 34 (83.5 Ma) onwards is relatively uncomplicated with most studies in  
416 agreement that largely symmetrical spreading occurred after Anomaly 34 to the  
417 present day (LaBrecque and Rabinowitz, 1977; Moulin et al., 2010; Nürnberg and  
418 Müller, 1991; Shaw and Cande, 1990; Torsvik et al., 2009). The stability and  
419 symmetry of this spreading system during the Cenozoic led to this region being  
420 used as a type example for calibrating the geomagnetic reversal timescale (Cande  
421 and Kent, 1992).

422

423 Recent models have been developed to refine rifting and minimize misfits in the  
424 South Atlantic. Although no model accurately restores all continental margins  
425 without gaps or overlaps, we find that the model of Torsvik et al. (2009) agrees  
426 well with continental stretching rates and conjugate margin rifting episodes. We  
427 therefore implement the model of Torsvik et al. (2009) for the early rifting phase  
428 of the South Atlantic, including intra-continental deformation in South America  
429 and Africa but adjust their rotations to be consistent with the Gradstein et al.  
430 (1994) timescale for the Mesozoic. In the early Jurassic (190 Ma), we follow a  
431 plate boundary between Patagonia and South Africa connected to the Permian-  
432 Triassic to Jurassic rifting in the Karoo Basin (Banks et al., 1995; Catuneanu et al.,

433 2005) and along the Agulhas-Falkland Fracture Zone to the Panthalassic  
434 subduction zone to the west. The South Atlantic central rift propagated  
435 northward, with extension between Colorado, Parana and Africa from 150 Ma.  
436 Rifting reached the African continental interior through the West and Central  
437 African Rift Zones, along the Central African Shear Zone at 131.7 Ma, connecting  
438 with the West and Central African Rift Zones. These continental rift zones  
439 encompass the major hydrocarbon-producing Cretaceous basins of the Central  
440 and West African rift system from East Niger to Sudan. We cease rifting in the  
441 interior of Africa at about 85 Ma.

442

443 We use the model of Nürnberg and Müller (1991) for the seafloor spreading  
444 record but refine the timing of the onset of seafloor spreading to 132 Ma to  
445 correspond to the peak of magmatism (Torsvik et al., 2009). In addition, we  
446 switch to the updated Cenozoic rotations of Müller et al. (1999) from Anomaly  
447 34 to the present day. The poles presented in Müller et al. (1999) are similar to  
448 those of Shaw and Cande (1990) but reflect finer scale changes in spreading  
449 direction due to the inversion method used for fracture zone interpretation  
450 (Müller et al., 1999). Our seafloor spreading isochrons match well with the  
451 magnetic lineations observed in our magnetic anomaly grid (Figure 2), although  
452 poor data coverage hinders broad scale correlation.

453

454 We also incorporate spreading in the Agulhas Basin (southernmost South  
455 Atlantic) between South America and the Malvinas Plate (LaBrecque and Hayes,  
456 1979; Marks and Stock, 2001) from Anomaly 34 (83.5 Ma) to Anomaly 30 (~66  
457 Ma) according to the rotations of Nürnberg and Müller (1991). The extinct  
458 spreading ridge associated with this spreading system as well as distinct fracture  
459 zone trends are clearly observed in satellite gravity data (Marks and Stock, 2001)  
460 (Figure 1).

461

### 462 *3.1.2 Central Atlantic*

463 The Central Atlantic contains of the region between North America conjugate to  
464 Northwest Africa bounded by Pico and Gloria Fracture Zones to the north and  
465 the 15° 20'N and Guinean Fracture Zones to the south (Figure 3). Break-up

466 marked the beginning of Pangea separation and involved at least a three-plate  
467 system between North America, Northwest Africa and the Moroccan Meseta  
468 (Figure 3). Rifting was controlled by pre-existing structures leading to the  
469 formation of a series of rift basins during late Triassic-early Jurassic between  
470 North America and Northwest Africa (Klitgord and Schouten, 1986; Lemoine,  
471 1983), which subsequently filled with salt and became inactive during plate  
472 separation. In addition, transtensional rifting between Northwest Africa and the  
473 Moroccan Meseta formed rift basins along the Atlas rift (Labails et al. 2010). The  
474 first stage of Atlas Mountain uplift occurred during the opening of the Central  
475 Atlantic (Beauchamp, 1998). Incorporating motion along the Atlas rift has  
476 implications for full-fit reconstructions of the Central Atlantic.

477

478 The establishment of seafloor spreading in the Central Atlantic is debated, with  
479 ages ranging from 175 Ma marked by the West African Coast Magnetic Anomaly  
480 and East Coast Magnetic Anomaly and an extrapolation of spreading rates  
481 (Klitgord and Schouten, 1986; Müller et al., 1999; Müller and Roest, 1992), 170-  
482 171 Ma based on a review of global passive margins (Bradley, 2008),  
483 diachronous opening with 200 Ma in the south progressing to 185 Ma in the  
484 north based on dating of post-rift sediment deposition (Withjack et al., 1998) and  
485 200 Ma according to model of Schettino and Turco (2009). A recent re-  
486 evaluation of the Central Atlantic opening (Labails et al., 2010) suggests that the  
487 earliest seafloor spreading occurred at 190 Ma (maximum at 203 Ma) based on  
488 an updated magnetic anomaly grid and interpretation of salt basins offshore  
489 Morocco and North America (Sahabi et al., 2004). In this model, spreading was  
490 initially very slow at half-spreading rates of ~8 mm/yr with an increase in  
491 spreading rate and direction at 170 Ma to ~17 mm/yr and spreading asymmetry  
492 until Anomaly M0 (120.4 Ma). This is in contrast to previous models (Bird et al.,  
493 2007; Klitgord and Schouten, 1986) that invoke an early ridge jump at 170 Ma  
494 rather than significant spreading asymmetry to account for increased crustal  
495 accretion onto the North American plate.

496

497 Anomalies M25-M0 (~154-120 Ma) and 34-30 (~84-65 Ma) are well established  
498 primarily due to the density of data on the western flank (Klitgord and Schouten,

499 1986; Müller et al., 1999; Müller and Roest, 1992). The spreading rates in the  
500 Central Atlantic in the Cenozoic are quite slow making identification of magnetic  
501 anomalies more difficult than for the Mesozoic (Klitgord and Schouten, 1986).  
502 Anomalies from 25 (~56 Ma) onwards have been identified quite consistently  
503 between studies (Klitgord and Schouten, 1986; Müller et al., 1999; Müller and  
504 Roest, 1992) with the main difference occurring between Anomalies 8-5 (~26-10  
505 Ma) due to finer constraints on fracture zone trends using the models by Müller  
506 and Roest (1992) and Müller et al. (1999).

507

508 We have implemented the early break-up history of Labails et al. (2010) to  
509 define the Jurassic-early Cretaceous history of the Central Atlantic as a highly  
510 asymmetric, slow spreading system. We initiate the Central Atlantic rift prior to  
511 200 Ma together with a transtensional plate boundary between Northwest Africa  
512 and Morocco along the Atlas rift using rotations derived from Labails. et al.  
513 (2010). The Central Atlantic rift connects to a major transform fault along the  
514 Jacksonville Fracture Zone to the south linking with Mesozoic rift basins in the  
515 Caribbean (see Section 3.4.1 Caribbean). To the north, the Central Atlantic rift  
516 extends into the northern Atlantic, where Triassic/Jurassic rifts are observed  
517 (see Section 3.1.3 North Atlantic). Immediately following the initiation of  
518 seafloor spreading in the Central Atlantic was the cessation of transtensional  
519 motion along the Atlas rift and the first stage of uplift of the Atlas Mountains  
520 (Beauchamp, 1998).

521

522 We initiate seafloor spreading at 190 Ma (Labails et al. 2010) and subsequently  
523 use the magnetic anomaly picks from Klitgord and Schouten (1986) and  
524 rotations from Müller et al. (1997) for M25-M0 (~154-120 Ma). Spreading  
525 propagated northward between the Iberia-Newfoundland margin during  
526 Anomaly M20 (~146 Ma) (Müller et al., 1997) (Figure 4). To the south,  
527 spreading in the Central Atlantic connected with the Equatorial Atlantic in the  
528 late Cretaceous. We incorporate the Cenozoic rotations from Müller et al. (1999),  
529 which have been updated from those of Müller and Roest (1992) and use the  
530 isochrons from Müller et al. (2008a) . The isochrons match well with the gridded

531 magnetic anomalies (Figure 3) and fracture zone identifications from global  
532 satellite gravity (Sandwell and Smith, 2009) (Figure 1).

533

### 534 *3.1.3 Northern Atlantic*

535 The Northern Atlantic encompasses the area between Newfoundland-Iberia and  
536 the Eurasian Basin in the Arctic Ocean (Figure 3 and 5). It includes active and  
537 extinct spreading systems, ridge-hotspot interactions related to the Iceland  
538 plume, volcanic and magma-poor margins and microcontinent formation (e.g. Jan  
539 Mayen). The Northern Atlantic underwent episodic continental extension in the  
540 Permo-Triassic, late Jurassic, early and mid Cretaceous, with reactivation and  
541 basin formation largely following pre-existing structures from the closure of the  
542 Iapetus Ocean and subsequent Baltica-Laurentia collision (400-450 Ma) (Dore et  
543 al., 1999; Kimbell et al., 2005; Silva et al., 2000; Skogseid et al., 2000). Seafloor  
544 spreading propagated from the Central Atlantic starting in the late Cretaceous in  
545 six distinct phases: Iberia-Newfoundland, Porcupine-North America, Eurasia-  
546 Greenland (conjugate to Rockall), North America-Greenland (Labrador Sea),  
547 Eurasia-Greenland (Greenland and Norwegian Sea and Jan Mayen), North  
548 America-Eurasia (Eurasian Basin, Arctic Ocean) (Figure 3-5).

549

#### 550 3.1.3.1 Iberia-Newfoundland

551 The Iberia-Newfoundland margin is a type example of a highly extended, magma-  
552 poor, rifted continental margin (Boillot et al., 1988; Hopper et al., 2004; Peron-  
553 Pinvidic et al., 2007; Srivastava et al., 2000) with two main phases of extension.  
554 Extension between the late Triassic to early Jurassic formed large rift basins  
555 within the continental lithosphere of both margins (Tucholke and Whitmarsh,  
556 2006) and was followed by a period of quiescence in the early-mid Jurassic  
557 marked by subsidence and the accumulation of shallow-water carbonates  
558 (Tankard and Welsink, 1987). The second phase of deformation, from late  
559 Jurassic to early Cretaceous, formed a wide zone of layered basalts, gabbros and  
560 serpentinitised mantle ("transitional" crust) indicative of seafloor spreading and  
561 mantle exhumation (Peron-Pinvidic et al., 2007; Sibuet et al., 2007; Srivastava et  
562 al., 1990b; Tucholke and Whitmarsh, 2006).

563

564 The onset and location of normal seafloor spreading is widely debated. The  
565 interpretation of low amplitude magnetic anomalies as old as Anomaly M21  
566 (~147 Ma) related to ultraslow seafloor spreading within the southern part of  
567 the transition zone (Sibuet et al., 2007; Srivastava et al., 2000) is the oldest  
568 seafloor spreading age assigned to the margin. Other studies have instead  
569 suggested younger ages for the onset of seafloor spreading: Anomalies M3-M5  
570 (~124-128 Ma) based on deep sea drilling and seismic refraction (Russell and  
571 Whitmarsh, 2003; Whitmarsh and Miles, 1995) and late Aptian (~112-118 Ma)  
572 based on stratigraphic studies (Tucholke et al., 2007). Although the earliest  
573 timing of seafloor spreading remains controversial, reconstructions between the  
574 Iberia and Newfoundland margin from Anomaly M0 (~120 Ma) onwards are well  
575 established with changes in spreading rates occurring at Anomaly 25 (~56 Ma)  
576 coincident with the initiation of spreading further north in the Norwegian-  
577 Greenland Sea (Srivastava et al., 2000; Srivastava and Tapscott, 1986).

578

579 Related to the development of the Iberia-Newfoundland margin is the opening of  
580 the Bay of Biscay north of Iberia and the motion of the Iberia block itself. The  
581 Bay of Biscay formed at a ridge-ridge-ridge triple junction (Klitgord and  
582 Schouten, 1986) commonly believed to have opened in the late Cretaceous (110-  
583 83.5 Ma) according to Müller et al. (1997). However, Anomalies M0 to 33 (~120-  
584 79 Ma) have been identified (Sibuet et al., 2004) suggesting that seafloor  
585 spreading initiated in the Bay of Biscay at the same time as an increase in  
586 spreading rate and cessation of mantle exhumation along the Iberia-  
587 Newfoundland margin (Sibuet et al., 2007). The end of seafloor spreading  
588 occurred at Anomaly 33 (~79 Ma) (Roest and Srivastava, 1991; Sibuet et al.,  
589 2004).

590

591 Most models agree that the Iberian continental block was fixed relative to Africa  
592 since the start of rifting along the Iberia-Newfoundland margin until Anomaly 10  
593 (~28 Ma) (Srivastava and Tapscott, 1986) based on geological evidence from the  
594 Pyrenees and geophysical data from the Northern Atlantic (Roest and Srivastava,  
595 1991; Sibuet et al., 2004). The location of the plate boundary is proposed to have  
596 been located north of the Kings Trough from M0 (~120 Ma) to the Eocene

597 (Srivastava et al., 1990), extended along the Kings Trough into the Bay of Biscay  
598 and along the Pyrenees from the Eocene to Anomaly 10 (~28 Ma) (Klitgord and  
599 Schouten, 1986; Roest and Srivastava, 1991; Whitmarsh and Miles, 1995) and  
600 after a southward ridge jump along the Azores transform fault and Straits of  
601 Gibraltar (Klitgord and Schouten, 1986; Roest and Srivastava, 1991).

602

603 In our plate kinematic model, we use the boundary between continental and  
604 oceanic crust interpretation of Todd et al. (1988) for the Newfoundland margin  
605 and Boillot and Winterer (1988) and Srivastava et al. (2000) for the Iberia  
606 margin. We take the age given by Srivastava et al. (2000) for the initiation of  
607 ultra-slow seafloor spreading based on their interpretation of magnetic  
608 anomalies back to M20 (~146 Ma) as we believe this corresponds to the  
609 boundary between true continental crust and oceanic/transitional crust. Our  
610 seafloor spreading isochrons are based on Müller et al. (1997) and correlate well  
611 with magnetic anomaly grids (Figure 3).

612

613 In our plate model, we fix Iberia to Africa from the initiation of seafloor  
614 spreading in the Eocene and use the rotations of Srivastava and Tapscott (1986)  
615 for seafloor spreading between the Iberia-Newfoundland margin (~146 Ma) to  
616 Anomaly 10 (~28 Ma) (Figure 4). We define the plate boundary between Iberia  
617 and Eurasia along the Kings Trough through the Pyrenees, connecting with the  
618 northern Tethyan subduction zone (Figure 4). In addition, we incorporate  
619 spreading in the Bay of Biscay between Iberia and Eurasia based on timing of  
620 Sibuet et al. (2004) (~120 Ma) and the finite difference method for the rate and  
621 direction of spreading. After Anomaly 10 (~28 Ma), we incorporate a southern  
622 jump of the plate boundary to the Azores transform fault and along the Straits of  
623 Gibraltar leading to the capture of Iberia by the Eurasian plate (Figure 4).

624

### 625 3.1.3.2 Porcupine -North America

626 The Porcupine Abyssal Plain is bounded by the Kings Trough, Labrador Sea and  
627 Charlie Gibbs Fracture Zone (Figure 3 and 4). The existence of the Porcupine  
628 Plate as an independent plate during the Eocene-Oligocene was first  
629 hypothesized by Srivastava and Tapscott (1986) in order to account for

630 overlapping reconstructed anomalies in the Porcupine Abyssal Plain when using  
631 a single pole of rotation for North Atlantic opening and to explain Eocene  
632 deformation recorded along the north Biscay and Porcupine margins. The need  
633 for a separate Porcupine Plate was challenged by Gerstell and Stock (1994) when  
634 they computed new rotations for Eurasia-North America without overlaps  
635 between the magnetic anomalies. However, these reconstructions were  
636 themselves challenged as they could not account for the observed intra-plate  
637 deformation recorded both onshore and offshore in the Porcupine Abyssal Plain  
638 (Srivastava and Roest, 1996).

639

640 A major phase of rifting occurred from the late Jurassic to early Cretaceous,  
641 marked by the formation of extensional basins along both margins (Rowley and  
642 Lottes, 1988) and the deposition of syn-rift sediments in the Barremian/late  
643 Hauterivian 130-125 Ma (De Graciansky et al., 1985). Seafloor spreading began  
644 by at least the mid-late Albian (110-105 Ma) based on the dating of the  
645 sediments above tholeiitic basalt from DSDP sites 550 and 551 and an Aptian  
646 regional unconformity (De Graciansky et al., 1985) and supported by the  
647 interpretation of Anomaly 34 (~84 Ma) seaward of this location (Müller and  
648 Roest, 1992; Srivastava and Tapscott, 1986). Further refinement based on  
649 magnetic anomalies is not possible as the early part of this crust was formed  
650 during the CNS.

651

652 Magnetic anomalies from 34 (~84 Ma) are well identified in the Porcupine  
653 Abyssal Plain and initially formed as a continuous spreading ridge to the north  
654 and south (i.e. between North America and Eurasia) (Figure 4). Magnetic  
655 anomalies between 25-13 (~56-33 Ma) record the motion of the independent  
656 Porcupine plate relative to Eurasia (Müller and Roest, 1992; Srivastava and  
657 Roest, 1989; Srivastava and Tapscott, 1986). Spreading in the Porcupine Abyssal  
658 Plain was coincident with spreading in the Labrador Sea between Anomalies 34-  
659 13 (~84-33 Ma). After Anomaly 13 (~33 Ma), the Porcupine plate ceased its  
660 independent motion and spreading continued via North America-Eurasia motion.

661

662 We use the rotations of Srivastava and Roest (1989) for the initial rift phase  
663 between the Porcupine and North American Plate and incorporate the onset of  
664 break-up and seafloor spreading at 110 Ma (Müller et al., 1997), marked by a  
665 regional unconformity and dating of sediments at DSDP 550 (De Graciansky et  
666 al., 1985). We use our preferred rotations from Srivastava and Roest (1989) for  
667 the early spreading phase and the initiation of independent motion of the  
668 Porcupine Plate between Anomalies 25 and 13 (~56-33 Ma) (Figure 4). This  
669 results in a small clockwise rotation of Eurasia and counter-clockwise rotation of  
670 Iberia relative to the Porcupine Plate. The cessation of independent Porcupine  
671 motion coincides with the cessation of seafloor spreading in the neighboring  
672 Labrador Sea and the establishment of a simple two-plate system (North  
673 America and Eurasia) to describe the plate motions in the North Atlantic (Figure  
674 4). From Anomaly 13 (~33 Ma) onwards, we use the rotations of Lawver et al.  
675 (1990). A comparison with fracture zone traces and satellite gravity data reveals  
676 a slight mismatch due to the compression inferred from our model and  
677 supported by the seafloor spreading fabric (Srivastava and Roest, 1996).

678

#### 679 3.1.3.3 Rockall-North America/Greenland

680 The Rockall region in the North Atlantic encompasses spreading between the  
681 Rockall Plateau conjugate to North America along its southern arm and  
682 conjugate to Greenland along its northern arm (Figure 3). A failed rift basin in  
683 the Rockall Trough exists adjacent to the Eurasian margin. Previous authors  
684 have determined that Rockall behaved as an independent plate throughout part  
685 of its history (Müller and Roest, 1992; Srivastava and Roest, 1989) but recent re-  
686 analysis of the magnetic anomalies and satellite gravity data can be explained by  
687 Eurasia-North America and Eurasia-Greenland motion (Gaina et al., 2002).

688

689 The Rockall Plateau underwent periods of extension in the early Triassic, early  
690 and mid-Jurassic and early, mid and late Cretaceous (Knott et al., 1993). The  
691 majority of rifting in the Rockall Trough occurred in the mid-late Cretaceous,  
692 continuing into the Eocene after an earlier Triassic-Jurassic rift phase (Cole and  
693 Peachey, 1999). Simultaneous rifting in the Porcupine Abyssal Plain occurred in  
694 the Cretaceous (Srivastava and Tapscott, 1986). Spreading between the Rockall

695 Plateau and North America was established at ~83 Ma independent of the  
696 Eurasian plate according to the models of Müller and Roest (1992) and  
697 Srivastava and Roest (1989) or as part of the Eurasian plate from Anomaly 33  
698 (~79 Ma) based on a reinterpretation of magnetic anomalies and fracture zone  
699 locations from satellite gravity data (Gaina et al., 2002) or 83 Ma according to  
700 Cole and Peachey (1999). Spreading propagated to the northwest into the  
701 Labrador Sea (Gaina et al., 2002; Müller and Roest, 1992; Rowley and Lottes,  
702 1988; Srivastava and Tapscott, 1986).

703

704 The establishment of a three-plate system between North America,  
705 Eurasia/Rockall and Greenland occurred after Anomaly 25 (~56 Ma) (Gaina et  
706 al., 2002; Rowley and Lottes, 1988; Srivastava and Tapscott, 1986). After the  
707 cessation of spreading in the Labrador Sea, the system reorganized into a two-  
708 plate system with spreading between Rockall/Eurasia and Greenland along the  
709 Reykjanes Ridge (Srivastava and Tapscott, 1986) after Anomaly 13 (~33 Ma) to  
710 the present day (Figure 3).

711

712 In constructing our model for spreading in the Rockall region, we separate the  
713 margin into two segments: Rockall Plateau/Eurasia relative to North America  
714 and Rockall Plateau/Eurasia relative to Greenland. Preceding the opening of the  
715 ocean basin between Rockall and North America, rifting occurred in the Rockall  
716 Trough (landward of the Rockall Plateau) in the mid-late Cretaceous, coincident  
717 with rifting in the Porcupine Basin to the south (Figure 4). The main rift phase  
718 then jumped westward between the Rockall Plateau (fixed to Greenland) and  
719 North America at ~85 Ma (Gaina et al., 2002), similar to previous studies  
720 (Rowley and Lottes, 1988). We follow the plate boundaries in this area from  
721 Srivastava and Tapscott (1986) for the earliest part of its history. Rifting  
722 progressed to seafloor spreading by Chron 33o (~79 Ma) (Gaina et al., 2002) and  
723 propagated into the Labrador Sea (Gaina et al., 2002) (Figure 4). We follow the  
724 plate reconstructions of Gaina et al. (2002) whereby spreading initiated between  
725 the Rockall Plateau and Greenland after Chron 25 forming a triple junction  
726 between the North American, Greenland and Eurasian plates (Figure 4). As the  
727 pole of rotation describing Eurasia-North America motion accounts for the

728 magnetic anomalies in the area, we do not incorporate motion between the  
729 Rockall Plateau and Eurasia, as proposed by other authors (Müller and Roest,  
730 1992; Srivastava and Roest, 1989).

731

732 Seafloor spreading isochrons were constructed based on the magnetic anomaly  
733 identification and finite rotations of Gaina et al. (2002) and compared to the  
734 several magnetic anomaly datasets (Figure 3). We find that there is generally  
735 good agreement between the gridded magnetic anomaly data and our seafloor  
736 spreading isochrons but find interpretation difficult proximal to the spreading  
737 axis. This may be due to the thermal influence of the Iceland hotspot on the mid-  
738 ocean ridge together with slow seafloor spreading rates. We find very good  
739 agreement between our fracture zone trends and those expressed in the satellite  
740 gravity data (Figure 1).

741

#### 742 3.1.3.4 Labrador Sea and Baffin Bay

743 The Labrador Sea is located between North America and Greenland south of  
744 Baffin Bay in the Canadian Arctic (Figure 3). Continental stretching in the  
745 Labrador Sea produced a narrow and symmetrical margin with less than 100 km  
746 of extension (Dunbar and Sawyer, 1989) at around 130 Ma (Umpleby, 1979)  
747 based on the dating of pre to early syn-rift sediments. Rifting in the Labrador Sea  
748 is believed to have begun only after the initiation of seafloor spreading in the  
749 Rockall Trough (Srivastava and Tapscott, 1986).

750

751 The onset of seafloor spreading in the Labrador Sea is quite controversial. The  
752 oldest magnetic anomaly identified in the area is Anomaly 33 (~79 Ma) but  
753 spreading is believed to have initiated earlier during the CNS around 90-92 Ma  
754 (Gaina et al., 2002; Roest and Srivastava, 1989; Rowley and Lottes, 1988). An  
755 analysis of reprocessed seismic data (Chalmers, 1991; Chalmers and Laursen,  
756 1995) suggests seafloor spreading began much later at Anomaly 27 (~61 Ma)  
757 with thin continental crust extending into the region where older magnetic  
758 anomalies have been interpreted. However, this young age is inconsistent with  
759 the sedimentary-tectonic history of the basins around the Labrador Sea which  
760 record post-rift deposition and a phase of thermal subsidence around 100-62 Ma

761 and fault block rotation between 80-63 Ma. Other estimates for the onset of  
762 seafloor spreading come from an analysis of global passive margins (Bradley,  
763 2008), invoking an age of between 109 Ma and 68 Ma for the initiation of  
764 spreading.

765

766 An interpretation of seafloor spreading anomalies by Roest and Srivastava  
767 (1989) produced similar results to Srivastava and Tapscott (1986) except for a  
768 re-identification of Anomaly 25 (~56 Ma), which yielded a more symmetrical  
769 spreading system implying a significant change in spreading direction in the  
770 Labrador Sea. The change in spreading direction was linked to the initiation of  
771 the Greenland-Eurasia plate boundary and a change in spreading direction  
772 experienced in the Central and South Atlantic (Rowley and Lottes, 1988).  
773 Spreading is believed to have continued to Chron 7 (~25 Ma) (Rowley and  
774 Lottes, 1988) or just after Chron 13 (~33 Ma) (Gaina et al., 2002; Roest and  
775 Srivastava, 1989).

776

777 Northward propagation of the Labrador Sea rift into Baffin Bay through the  
778 Davis Strait (Figure 3) has been dated to the late Aptian-early Cenomanian (110-  
779 100 Ma) by the deposition of fluvial sediments during active rifting and occurred  
780 at least 20 million years after the initiation of rifting in the Labrador Sea.

781 Although there are no identifiable magnetic anomalies in Baffin Bay, seismic  
782 refraction profiles indicate that the area is floored by oceanic crust (Chalmers  
783 and Pulvertaft, 2001) and is predicted by the Labrador Sea opening model of  
784 Roest and Srivastava (1989). The cessation of seafloor spreading in Baffin Bay  
785 may have been coincident with the termination of spreading in the Labrador Sea.

786

787 For the Labrador Sea and Baffin Bay, we use a set of rotations that are based on  
788 the model presented in Gaina et al. (2002) and Roest and Srivastava (1989). We  
789 model continental extension starting at 135 Ma by extrapolation to match the  
790 Mesozoic basins on the North American and conjugate Greenland margin. We  
791 invoke seafloor spreading at chron 33 (~79 Ma) and incorporate a major change  
792 in spreading direction between Chrons 31-25 (68-56 Ma), which was  
793 subsequently followed by oblique spreading and eventually cessation of

794 spreading after Anomaly 13 (33 Ma) (Gaina et al., 2002; Roest and Srivastava,  
795 1989) (Figure 4). The extinct ridge matches well with a gravity low observed in  
796 the satellite gravity anomalies (Sandwell and Smith, 2009). We infer that the  
797 spreading axis in the Labrador Sea and Baffin Bay were joined across the Davis  
798 Strait via left-lateral transform faults (Roest and Srivastava, 1989; Rowley and  
799 Lottes, 1988) from 63 Ma. We model the cessation of spreading in Baffin Bay to  
800 be coincident with the Labrador Sea at 33 Ma (Figure 4).

801

802 We use the magnetic anomaly identifications of Gaina et al. (2002) to construct  
803 seafloor spreading isochrons in the Labrador Sea. The magnetic lineations in this  
804 area are not well resolved (Figure 3) and may be due to a combination of high  
805 sedimentation rates, spreading obliquity and data resolution. However, a  
806 continuation of magnetic lineations from the Rockall segment into the southern  
807 Labrador Sea (i.e. the expression of the triple junction) is clearly observed.  
808 Although we agree that oceanic crust floors Baffin Bay, no magnetic lineations  
809 can be resolved from the global gridded magnetic anomaly data (Figure 3 and 5).

810

#### 811 3.1.3.5 Greenland-Eurasia and Jan Mayen Microcontinent

812 The separation of Greenland and Eurasia is occurring along the Reykjanes Ridge  
813 adjacent to the Rockall Plateau, through Iceland and along the Kolbeinsey and  
814 Mohns Ridge in the Norwegian and Greenland Seas (Figure 3 and 5). The margin  
815 has undergone several rift phases since the Triassic primarily during the mid  
816 Jurassic-early Cretaceous and late Cretaceous-early Cenozoic (Brekke, 2000).  
817 The late Jurassic-early Cretaceous rift phase created most of the basin structures  
818 in the hydrocarbon-bearing MØre and VØring Basins, offshore Norway (Skogseid  
819 et al., 2000). The final rift phase at the Campanian-Maastrichtian boundary (~70  
820 Ma) (Skogseid et al., 2000) was followed by volcanism (mid Paleocene to early  
821 Eocene) and finally to break-up and volcanism prior to Chron 25 (~56 Ma).

822

823 Traditionally, spreading between Greenland and Eurasia is modeled as a two-  
824 plate system with seafloor spreading initiating around 55-56 Ma, near the  
825 Paleocene-Eocene boundary (Rowley and Lottes, 1988; Skogseid, 1994;  
826 Srivastava and Tapscott, 1986; Talwani and Eldholm, 1977). An updated

827 interpretation including new geophysical data suggests that the system  
828 underwent several plate boundary changes since the inception of seafloor  
829 spreading around Anomaly 25 (~56 Ma) (Gaina et al., 2009). Fracture zone  
830 trends mark changes in spreading direction at Chron 21 (~47 Ma) and Chron 18  
831 (~40 Ma) (Gaina et al., 2009). A major reorganization of the system occurred at  
832 Anomaly 13 (~33 Ma) with relative motion between Greenland and Eurasia  
833 migrating from NW-SE to NE-SW, leading to the cessation of spreading in the  
834 Labrador Sea, the amalgamation of Greenland with North America and the  
835 cessation of spreading in the Norway Basin.

836

837 Spreading in the Norway Basin (part of the Norwegian Sea) was initiated at 56  
838 Ma isolating the Jan Mayen microcontinent (which was still fixed to Greenland)  
839 from the Møre and Vøring basin margin. Spreading along the extinct Aegir Ridge  
840 formed magnetic lineations (fan-shaped from Chron 21) in the Norway Basin  
841 until about Anomaly 13 (33-30 Ma) when the spreading ridge jumped westward,  
842 likely as a result of ridge-hotspot interactions and initiated spreading along the  
843 Kolbeinsey Ridge (Gaina et al., 2009). This is in contrast to a model of  
844 simultaneous spreading east and west of Jan Mayen at Anomaly 13 (~33 Ma),  
845 initiation of spreading along the Kolbeinsey Ridge at Anomaly 7 (~25 Ma) and  
846 cessation of spreading in the Norway basin at Anomaly 7 (~25 Ma) (Nunns,  
847 1983; Talwani and Eldholm, 1977). Using new marine geophysical data, Gaina et  
848 al. (2009) suggest further complications in the rifting and spreading history of  
849 the Jan Mayen microcontinent and Faeroe Islands with numerous triple junctions  
850 and ridge propagators leading to significant continental stretching and the  
851 formation of rift-related basins. The Mohns Ridge was connected to the Aegir  
852 Ridge from the initiation of spreading at ~55-56 Ma until 30 Ma and the  
853 cessation of spreading in the Norway Basin. After the seaward ridge jump, the  
854 Mohns Ridge linked to the Kolbeinsey Ridge defining the boundary between  
855 Greenland and Eurasia.

856

857 We use a combination of magnetic anomaly picks and rotations from Gaina et al.  
858 (2002) and Gaina et al. (2009) to reconstruct the entire Greenland-Eurasia  
859 margin. We do not incorporate the complex spreading (triple junctions and

860 ridge propagators) around the Jan Mayen microcontinent implied by the model  
861 of Gaina et al. (2009), but envisage that these will be incorporated in a further  
862 release. In our model, spreading initiates along the entire Greenland-Eurasia  
863 margin at 56 Ma, initially connecting up to the spreading in the Eurasian Basin to  
864 the north and the Greenland-Eurasia-North America triple junction in the south  
865 (Figure 5). At 33 Ma, spreading between North America and Greenland in the  
866 Labrador Sea ceased fusing the two plates together, shutting down the  
867 Greenland-Eurasia-North America triple junction and leading to a change in  
868 spreading rate and direction along the Greenland-Eurasia spreading system. The  
869 Jan Mayen microcontinent rifted off the Norwegian margin at 56 Ma forming the  
870 fan-shaped Norway Basin along the Aegir Ridge between 56 and 33-30 Ma  
871 (Figure 5). The Aegir Ridge connected to the Mohns Ridge in the north and  
872 Reykjanes Ridge in the south via a series of transform faults. Spreading then  
873 jumped to the Kolbeinsey Ridge at 30 Ma, connecting with the Mohns Ridge  
874 further north and forming the present day plate configuration (Figure 5). A  
875 comparison between our resultant seafloor spreading isochrons and the  
876 magnetic anomaly grids reveals that our trends match quite well with the  
877 magnetic lineations from the gridded dataset.

878

#### 879 3.1.3.6 Lomonosov Ridge-Eurasia (Eurasian Basin)

880 The Eurasian Basin is the youngest ocean basin within the Arctic Ocean and was  
881 formed by spreading between the Lomonosov Ridge and the Barents Shelf along  
882 the Gakkel and Nansen Ridges (Figure 5). The continental nature of the  
883 Lomonosov Ridge has been confirmed through seismic reflection imaging (Jokat  
884 et al., 1992) and ACEX drilling (Moran et al., 2006). The broad scale early rift  
885 phase mimic those of the North Atlantic margin but are less well constrained due  
886 to the remoteness of the region, data quality and persistent ice-coverage.  
887 Although the Barents Shelf is agreed to have formed part of the Eurasian margin,  
888 there is debate in the literature as to whether the Lomonosov Ridge has been  
889 fixed to the North American plate since at least 80 Ma (Rowley and Lottes, 1988;  
890 Srivastava and Tapscott, 1986) or whether it operated as an independent plate  
891 until at least Anomaly 13 (~33 Ma) (Brozena et al., 2003; Jackson and  
892 Gunnarsson, 1990). The lack of evidence for contemporaneous seafloor

893 spreading in other parts of the Arctic Ocean and the good fit of the magnetic  
894 anomalies in the Eurasian Basin are cited as reasons for the Lomonosov Ridge  
895 being part of the North American Plate. However, a recent compilation of marine  
896 geophysical data identified a feature that resembles an extinct spreading ridge  
897 near the Lomonosov Ridge, which possibly connected spreading in the Eurasian  
898 Basin with spreading in the Labrador Sea (Brozena et al., 2003), thus requiring  
899 independent motion of the Lomonosov Ridge.

900

901 The last rifting phase (late Cretaceous) led to break-up and seafloor spreading at  
902 68 Ma (Rowley and Lottes, 1988) or around Anomaly 25 (~56 Ma) (Gaina et al.,  
903 2002; Srivastava, 1985) in the south around Svalbard and at 50 Ma in the Laptev  
904 Sea (Rowley and Lottes, 1988). There appears to be a consensus in early studies  
905 that the oldest magnetic anomaly that can be confidently identified is Anomaly  
906 25-24 (~56-53 Ma) (Gaina et al., 2002; Rowley and Lottes, 1988; Srivastava,  
907 1985; Srivastava and Tapscott, 1986), yet there is space landward of Anomalies  
908 25-24 (~56-53 Ma) to suggest that seafloor spreading initiated earlier. The early  
909 spreading phase was the result of transtensional opening (Rowley and Lottes,  
910 1988) producing slow seafloor spreading rates, strike-slip motion between  
911 Svalbard and Greenland (Srivastava and Tapscott, 1986) and displacement along  
912 the Nares Strait (Srivastava, 1985). After Chron 13 (33 Ma), true seafloor  
913 spreading was established coincident with the major reorganization of the  
914 Greenland-Eurasia system and cessation of Labrador Sea spreading. Currently,  
915 the Eurasian Basin is undergoing the slowest observed seafloor spreading rates,  
916 with a full rate of ~10-13 mm/yr.

917

918 We have used the magnetic anomaly picks and finite rotations of Gaina et al.  
919 (2002) to describe the opening of the Eurasian Basin from Anomaly 24 (~53 Ma)  
920 to the present day. The rotations used are the same as for North America-  
921 Eurasia. We incorporate the plate boundary model of Rowley and Lottes (1988)  
922 whereby the Gakkel and Nansen Ridges connect to the Baffin Bay ridge axis  
923 through the Nares Strait and Mohns Ridge via a major strike-slip fault with minor  
924 compression between Greenland and Svalbard (Figure 5). In our interpretation,  
925 we couple the Lomonosov Ridge with North America as the rotations of Gaina et

926 al. (2002) to describe North America-Eurasia motion do not result in overlap of  
927 the magnetic anomalies. The seafloor spreading isochrons we implement are  
928 digitised from Gaina et al. (2002) and match well with the magnetic anomaly grid  
929 (Figure 5).

930

#### 931 *3.1.4 Arctic Basins*

932 The Arctic Ocean encompasses the Eurasian and Amerasia Basins (divided into  
933 the Canada, Makarov and Podvodnikov Basins) as well as numerous continental  
934 blocks such as the Lomonosov, Mendeleev, Alpha, Northwind and Chukchi Ridges  
935 (Figure 5). The Cenozoic Eurasian Basin (see Section 3.1.3.6 Eurasian Basin) has  
936 a distinct spreading history from the late Jurassic-Cretaceous Amerasia Basin.  
937 The early Mesozoic evolution of the Arctic region involves the closure of the  
938 South Anyui Basin along the North Siberian subduction zone, marked by the  
939 South Anyui suture (Kuzmichev, 2009; Nokleberg et al., 2001; Sokolov et al.,  
940 2002). This resulted in pre-breakup rifting in the earliest Jurassic, forming the  
941 Dinkum and Banks graben systems in Alaska and North America, respectively  
942 and the subsequent isolation of the Northwind and Chukchi Ridge by the earliest  
943 late Cretaceous (Grantz et al., 1998).

944

945 The rifting and opening of the Canada Basin is believed to have resulted from  
946 anticlockwise rotation of the North Slope Alaska-Chukotka Block away from the  
947 Canadian Arctic Islands, with a possible early strike-slip component, sometime  
948 from the late Jurassic to mid Cretaceous (Alvey et al., 2008; Carey, 1955; Grantz  
949 et al., 1998; Rowley and Lottes, 1988). Although the rotation model is supported  
950 by paleomagnetic data (Halgedahl and Jarrard, 1987), the fan-shaped nature of  
951 the magnetic lineations (Taylor et al., 1981) and crustal thickness mapping  
952 (Alvey et al., 2008), the exact timing of the rotation of Alaska and formation of  
953 the Canada Basin is debated. The dating of the magnetic anomalies in the Canada  
954 Basin is difficult due to extensive volcanic overprinting, low amplitude signature  
955 of the magnetic anomalies and high sedimentation rates. Anomalies M25-M11  
956 (~154-132 Ma) have been tentatively identified (Srivastava and Tapscott, 1986;  
957 Taylor et al., 1981), but other magnetic anomaly interpretations are possible. An  
958 analysis of rift-related structures and stratigraphy (Grantz et al., 1998) reveals

959 that the opening of the Canada Basin could have occurred as early as the late  
960 Jurassic-earliest Cretaceous. Less well-accepted models exist to explain the  
961 opening of the Canada Basin such as a non-rotational, step-wise late Jurassic-late  
962 Cretaceous opening model (Lane, 1997) and a model involving trapped crust  
963 from Kula-Pacific spreading (Churkin and Trexler, 1980).

964

965 Following the opening of the Canada Basin, Alvey et al. (2008) postulated that  
966 the Mendeleev and Alpha Ridges in the central Arctic formed either: 1. During  
967 continental rifting from the Canadian margin in the late Jurassic trapping Jurassic  
968 ocean floor in the Marakov/Podvodnikov Basin (Grantz et al., 1998); 2. During  
969 continental rifting from the Lomonosov Ridge forming the  
970 Marakov/Podvodnikov Basins during the late Cretaceous-mid Eocene (Alvey et  
971 al., 2008); 3. A hybrid model which includes an element of Jurassic ocean floor in  
972 the Podvodnikov Basin and a Cenozoic Marakov Basin (Alvey et al., 2008) or 4.  
973 The ridges formed purely via LIP emplacement related to the Iceland plume in  
974 the late Cretaceous (Dove et al., 2010; Forsyth, 1986; Jokat et al., 2003; Lawver et  
975 al., 2002; Lawver and Mueller, 1994) overprinting old oceanic crust.

976 Interpretations suggesting a Cenozoic age for the Marakov Basin match well with  
977 the identification of Anomalies 34-21 (~84-46 Ma; late Cretaceous-mid Eocene)  
978 (Taylor et al., 1981) as well crustal thickness estimates (Alvey et al., 2008) in the  
979 Marakov Basin, but crustal thickness estimates postulate that the Podvodnikov  
980 Basin must be floored by older oceanic floor (Alvey et al., 2008). The volcanic  
981 nature of the Mendeleev and Alpha Ridges has been confirmed from recovered  
982 basalt samples of late Cretaceous age (Jokat et al., 2003), an age slightly younger  
983 than the predicted location of the Iceland plume around 130 Ma  
984 (Hauterivian/Berremian) (Lawver and Muller, 1994). However, this does not  
985 preclude a continental nature for the Mendeleev and Alpha Ridges. Subsequent  
986 to the opening of the Marakov/Podvodnikov Basins, the locus of spreading  
987 jumped to the Eurasian Basin at ~56 Ma, forming the youngest piece of ocean  
988 floor in the Arctic domain.

989

990 We have incorporated a model whereby initial rifting occurred between the  
991 North American and Alaskan margin in the early Jurassic (~210-200 Ma)

992 followed by the isolation of the Northwind and Chukchi Ridges by the earliest  
993 late Cretaceous, triggered by the subduction of the Anyui Ocean. We invoke a  
994 simple counterclockwise rotational model for the opening of the Canada Basin  
995 whereby the North Slope of Alaska starts to rotate at 145 Ma (latest Jurassic)  
996 with seafloor spreading initiating at 142 Ma (Berriasian), with a much lower  
997 spreading rate in the south due to its proximity to the pole of rotation, creating  
998 fan-shaped anomalies. The timing is consistent with paleomagnetic data from  
999 Alaska but is inconsistent with previous magnetic anomaly interpretations  
1000 (Srivastava and Tapscott, 1986; Taylor et al., 1981). Cessation of spreading in  
1001 the Canada Basin and rotation of North Slope occurred at 118 Ma, coincident  
1002 with a change in the southern North Slope margin from largely strike-slip to  
1003 convergence due to a change in spreading direction in Panthalassa. We use the  
1004 finite rotations and seafloor spreading isochrons from Model 1 presented in  
1005 Alvey et al. (2008), however modify the isochrons to extend the interpretation of  
1006 the Canada Basin over the Alpha Ridge and into the Marakov Basin. The  
1007 isochrons are not constrained by magnetic anomaly identifications but rather are  
1008 a synthetic interpretation of the timing and orientation of spreading based on the  
1009 rotation of the North Slope of Alaska. Hence, we do not expect an exact  
1010 correlation with the magnetic anomaly grid.

1011

1012 The preferred model presented in Alvey et al. (2008) based on crustal thickness  
1013 estimates, invokes Cenozoic spreading in the Marakov Basin. We do not  
1014 incorporate a younger Marakov Basin as this would require either a short-lived  
1015 subduction zone along either the Lomonosov or Mendeleev Ridge during the  
1016 opening of this basin for which there is no geological evidence. Instead, we  
1017 suggest that the Alpha and Mendeleev Ridges are predominately LIP-related  
1018 features associated with the Iceland plume that overprinted the Canada Basin in  
1019 the early Cretaceous (Lawver and Muller, 1994) and not part of a rifted Cenozoic  
1020 continental margin. In our model the Makarov and parts of the Podvodnikov  
1021 Basin form the northern extent of the Canada Basin. We do agree with Alvey et  
1022 al. (2008) that there may be a trapped piece of Jurassic ocean floor from the  
1023 Anyui Basin in the Podvodnikov Basin, which would explain the anomalous  
1024 crustal thickness and would provide a mechanism for the Mendeleev Ridge

1025 having some continental affinities as continental material may have been  
1026 isolated during Jurassic rifting.

1027

### 1028 ***3.2 Pacific Ocean and Panthalassa***

1029 Present day seafloor spreading in the Pacific basin involves nine oceanic plates:  
1030 the Pacific, Antarctic, Nazca, Cocos and Juan De Fuca plates and the smaller  
1031 Rivera, Galapagos, Easter and Juan Fernandez micro-plates along the East Pacific  
1032 Rise (Bird, 2003) (Figure 1). Additionally, the Pacific basin seafloor spreading  
1033 record preserves clear evidence that several now extinct plates (e.g. Farallon,  
1034 Phoenix, Izanagi, Kula, Aluk and Bauer plates) existed within the Pacific and  
1035 proto-Pacific basin (Panthalassa) since at least the Jurassic/Cretaceous. In  
1036 addition, the onshore geological record from the Pacific margins provides  
1037 evidence for the opening and closure of several marginal basins, particularly  
1038 along the western North American margin.

1039

1040 Previous plate tectonic models of the Pacific have largely focused on identifying  
1041 magnetic lineations and deriving relative plate motions between presently active  
1042 plates where both sides of the spreading ridge are preserved (e.g. Juan De Fuca-  
1043 Pacific spreading (Atwater, 1970, 1990; Atwater and Severinghaus, 1990; Caress  
1044 et al., 1988; Engebretson et al., 1984; Stock and Molnar, 1988; Wilson, 1988),  
1045 Pacific-Antarctic spreading (Cande et al., 1998; Larter et al., 2002; Stock and  
1046 Molnar, 1987), the east Pacific Rise (Cande et al., 1982; Tebbens and Cande,  
1047 1997) and Cocos and Nazca spreading (Wilson, 1996)). Other plate tectonic  
1048 models have focused on identifying magnetic lineations in the older parts of the  
1049 Pacific, particularly the north and western Pacific, where conjugate magnetic  
1050 lineations no longer exist as they have been subducted (e.g. Kula-Pacific  
1051 (Atwater, 1990; Engebretson et al., 1984; Lonsdale, 1988b; Mammerickx and  
1052 Sharman, 1988; Rea and Dixon, 1983), Izanagi-Pacific (Handschumacher et al.,  
1053 1988b; Larson et al., 1972; Nakanishi et al., 1992; Nakanishi and Winterer, 1998;  
1054 Sager and Pringle, 1987; Sager et al., 1988b; Woods and Davies, 1982), Farallon-  
1055 Pacific (Atwater, 1970; 1990; Atwater and Severinghaus, 1989; Caress, et al.,  
1056 1988; Engebretson, et al., 1984; Stock and Molnar, 1988 (Wilson, 1988), Phoenix-  
1057 Pacific spreading (Cande et al., 1998; Larson et al., 2002; Larter et al., 2002; Stock

1058 and Molnar, 1987; Sutherland and Hollis, 2001; Viso et al., 2005) and the plates  
1059 related to the break-up of the Ontong Java-Hikurangi-Manihiki Plateaus (Taylor,  
1060 2006)). Beyond this, few studies have attempted to derive relative plate rotation  
1061 models of these now vanished plates (e.g. (Engebretson et al., 1985; Stock and  
1062 Molnar, 1988)) to establish a longer tectonic history of the Pacific plate where  
1063 minimal or no information about the seafloor spreading record exists.

1064

1065 Another common approach to constrain plate tectonic models of the Pacific has  
1066 been through the interpretation of the onshore geology, in particular examining  
1067 anomalous volcanism and geochemistry associated with ridge subduction,  
1068 crustal shortening rates and events, accretion of exotic terranes, ophiolite  
1069 emplacement, large-scale crustal deformation and massive sulphide and other  
1070 subduction related ore-deposit formation (e.g. (Bradley et al., 1993; Haeussler et  
1071 al., 1995; Madsen et al., 2006; Sun et al., 2007)). This information is sometimes  
1072 translated into a schematic representation of past plate configurations based  
1073 purely on the onshore record but these plate reconstruction schematics are often  
1074 only snapshots in time rather than evolving and are not quantitatively derived  
1075 through the seafloor spreading record. Nevertheless, they are helpful in  
1076 developing conceptual models for the evolution of now vanished ocean crust.

1077

1078 Engebretson, et al. (1985) presented a quantitative plate kinematic model of the  
1079 seafloor spreading record focused on the northern Pacific basin for the past 180  
1080 million years and is currently the most comprehensive and often cited study on  
1081 Pacific plate reconstructions. This study enabled subsequent authors to place  
1082 their regional tectonic reconstructions and geological observations into a Pacific-  
1083 wide tectonic framework. The model of Engebretson, et al. (1985) is based on an  
1084 absolute reference frame using fixed Atlantic and fixed Pacific hotspots (Morgan,  
1085 1972) with relative plate motions for the Pacific, Farallon, Izanagi, Kula and  
1086 Phoenix plates determined by computing the displacements of each plate relative  
1087 to the absolute reference frame rather than via plate circuit closure as is  
1088 commonly used. Since the publication of Engebretson, et al. (1985), additional  
1089 data acquisition, updated interpretations and more accurate magnetic anomaly

1090 timescales have been published, providing improved constraints on the Izanagi-  
1091 Pacific, Phoenix-Pacific, Farallon-Phoenix and Pacific-Antarctic ridges.

1092

1093 The Pacific triangle is an area of the western Pacific where three Mesozoic  
1094 magnetic lineation sets (Japanese, Hawaiian and Phoenix lineations) intersect  
1095 (Figure 6), recording the birth of the Pacific plate from three “parents”: the  
1096 Farallon, Izanagi and Phoenix plates. The evolution of the three parent plates has  
1097 influenced the development of subsequent seafloor spreading systems in the  
1098 Pacific. The northwestern (Japanese) lineations represent spreading between  
1099 the Pacific and Izanagi plates and young towards the west-northwest, the  
1100 easternmost (Hawaiian) lineations represent spreading between the Pacific and  
1101 Farallon plates and young towards the east and the southernmost (Phoenix)  
1102 lineations represent spreading between the Pacific and Phoenix plates and young  
1103 towards the south (Atwater, 1990; Nakanishi et al., 1992) (Figure 6). These  
1104 three plates radiated out from the emerging Pacific plate during the Mesozoic  
1105 and existed prior to the establishment of the Pacific plate in a simple ridge-ridge-  
1106 ridge configuration. We will present an assessment of the Pacific and  
1107 Panthalassa by describing each parent plate with their associated children.

1108

### 1109 *3.2.1 Izanagi Plate*

1110 The M-sequence Japanese magnetic lineation set found in the westernmost  
1111 Pacific represents the last preserved fragments of a westward-younging Jurassic-  
1112 Cretaceous spreading system (Figure 6). Early reconstructions of the area linked  
1113 the Japanese lineation set to the younger, Cenozoic seafloor spreading history of  
1114 the Pacific-Kula ridge (Larson et al., 1972). To reconcile the geometry of the  
1115 preserved NE-SW trending Japanese lineations with the E-W trending Cenozoic  
1116 lineations formed by Pacific-Kula spreading, Woods and Davies (1982)  
1117 introduced the idea of an independent Izanagi plate, although some models still  
1118 prefer a single Kula plate (Norton, 2007). Due to progressive subduction since  
1119 the Mesozoic, the entire crust that floored the Izanagi plate as well as the portion  
1120 of the Pacific plate recording the death of the Izanagi has been lost, leaving  
1121 behind only the Mesozoic fragment of the Pacific plate. This complicates  
1122 reconstructions as few present day constraints exist to tie down tectonic

1123 parameters for the evolution of the area. Additionally, there are no constraints  
1124 on the history of the Izanagi plate prior to the birth of the Pacific plate.  
1125  
1126 Magnetic anomalies M33-M0 (~158-120 Ma) of the Japanese lineation set have  
1127 been confidently identified in the northwest Pacific (Atwater, 1989;  
1128 Handschumacher et al., 1988a; Nakanishi et al., 1992; Nakanishi and Winterer,  
1129 1998; Sager et al., 1988a; Sager and Pringle, 1987; Sager and Pringle, 1988). A  
1130 recent deep-tow magnetometer survey over the Pigafetta Basin in the vicinity of  
1131 ODP drill site 801C revealed a low amplitude magnetic anomaly sequence  
1132 extending to M44 (~170 Ma), within the Jurassic Quiet Zone (Tivey et al., 2006)  
1133 with Anomaly M42 (~168 Ma) corresponding to the location of ODP drill site  
1134 801C (Tominaga et al., 2008). Previous interpretations infer the oldest crust in  
1135 the Pacific to be 175 Ma (Engebretson et al., 1985; Müller et al., 1997) based on  
1136 interpolation to the centre of the Pacific triangle, but this age appears to be  
1137 inconsistent with the recent dating of magnetic anomalies and the dating from  
1138 ODP site 801C, which is located ~750 km from the inferred centre of the Pacific  
1139 triangle. After the initiation of spreading between the Pacific and Izanagi plates,  
1140 the ridge underwent some instability with one or more proposed ridge jumps  
1141 postulated to explain the anomalously large distance between the adjacent  
1142 isochrons along a spreading corridor between M33-29 (~158-156 Ma) (Sager et  
1143 al., 1998). Analysis of the magnetic anomalies and seafloor fabric flanking this  
1144 proposed ridge jump has not found an abandoned spreading centre. Spreading  
1145 continued with relatively high seafloor spreading rates between M29-25 (~156-  
1146 154 Ma) (Nakanishi et al., 1992) before decreasing to average rates until M21  
1147 (~147 Ma).  
1148  
1149 The fracture zone pattern observed in the satellite gravity data and mapped via  
1150 ship track data (Nakanishi and Winterer, 1998; Sager et al., 1988a; Sager et al.,  
1151 1998) indicates a large 24° clockwise rotation of the Izanagi plate relative to the  
1152 Pacific at M21 (~147 Ma) (Sager et al., 1999), particularly evident along the  
1153 Kashima Fracture Zone near the Izu-Bonin-Mariana trench (Figure 6). The  
1154 change in spreading direction from NW-SE to NNW-SSE coincides with the  
1155 eruption of the Shatsky Rise at the Izanagi-Farallon-Pacific triple junction

1156 (Nakanishi et al., 1999; Sager et al., 1999) followed by the progressive  
1157 reorganization and migration of the triple junction centre for a period of about 2  
1158 million years. The period between Anomalies M21-20 (~147-145 Ma) also  
1159 corresponds to changes in spreading rate and direction in the Pacific, Atlantic  
1160 and Indian Oceans (Nakanishi et al., 1999; Sager et al., 1988). The youngest  
1161 identified Japanese lineation corresponds to M0 (~120 Ma) (Nakanishi et al.,  
1162 1999; Sager et al., 1999; Tominaga and Sager, 2010) trending similar to the post-  
1163 M20 (~145 Ma) lineations (Figure 6). This would suggest no measured change  
1164 in spreading direction between at least 145-120 Ma. The oceanic crust to the  
1165 north of M0 (~120 Ma) is inferred to have formed during the CNS and represents  
1166 the youngest preserved oceanic lithosphere associated with Izanagi-Pacific  
1167 spreading.

1168

1169 Previous interpretations have tied the cessation of spreading between the Pacific  
1170 and Izanagi plates to the onset of spreading between the Kula and Pacific plates  
1171 (Engebretson et al., 1985), sometime between 83.5-70 Ma (Atwater, 1989;  
1172 Lonsdale, 1988) (see Section 3.2.2.1 Kula plate). In these models, the orientation  
1173 of the Izanagi-Pacific ridge is depicted as a side-stepping E-W oriented ridge  
1174 perpendicular to the East Asian margin. As the oldest discernable Japanese  
1175 magnetic lineation is oriented NE-SW, an E-W oriented mid-ocean ridge requires  
1176 a major change in spreading direction post-M0 (~120 Ma). However, there are  
1177 no fracture zones present in the post-Mesozoic crust of the NW Pacific to suggest  
1178 a major change in spreading direction during the CNS (Figure 1).

1179

1180 An alternative approach to constrain the orientation and cessation of the Izanagi-  
1181 Pacific ridge is through an analysis of the onshore geological record in east Asia  
1182 together with the preserved seafloor spreading record in the NW Pacific (Seton  
1183 et al., In Prep; Whittaker et al., 2007). The younging northwestward sequence of  
1184 magnetic lineations and the presence of Indian-type mantle geochemical  
1185 signatures in various volcanic arcs of the northwest Pacific (Straub et al., 2009)  
1186 indicate a ridge subducted under east Asia at some time in the past. Whittaker et  
1187 al. (2007) assumed no change in spreading direction of the Pacific-Izanagi from  
1188 M0 (~120 Ma) onwards as there is no evidence for a major change in spreading

1189 direction post-M0 (~120 Ma) resulting in the mid ocean ridge intersecting the  
1190 east Asian margin in a sub-parallel fashion. The timing for the intersection of the  
1191 ridge with the margin forming a slab window can be constrained through a  
1192 number of geological observations from Japan and Korea. The geology in  
1193 southern and central Japan records a pulse of volcanism and anomalous heatflow  
1194 measurements (Agar et al., 1989; DiTullio, 1993; Lewis and Byrne, 2001;  
1195 Sakaguchi, 1996) indicative of the presence of a slab window in the late  
1196 Cretaceous-early Cenozoic. The cessation of granitic plutonism in Korea suggests  
1197 that subduction was terminated along east Asia around 60-50 Ma (Sagong et al.,  
1198 2005). In addition, seismic tomography profiles across east Asia reveal a break  
1199 in the continuity of slab material in the mid-mantle (Seton et al., In Prep)  
1200 possibility indicating the subduction of a mid-ocean ridge and slab break-off  
1201 event. Based on this model, the cessation of spreading between the Izanagi and  
1202 Pacific plates (i.e. the death of the Izanagi plate) occurred around 55-50 Ma  
1203 followed by the complete subduction of the Izanagi plate along the East Asian  
1204 margin by 40 Ma. In this model, the cessation of spreading between the Izanagi  
1205 and Pacific plate is not correlated with the initiation of spreading in the Kula  
1206 plate, as suggested by previous studies.

1207

1208 We model the Mesozoic-early Cenozoic evolution of the Izanagi plate using  
1209 constraints still preserved on the Pacific plate. We define the onset of spreading  
1210 between the Pacific and Izanagi plates to 190 Ma, 15-20 million years earlier  
1211 than previous interpretations. We base our age estimation, which is a maximum  
1212 age, on the following:

- 1213 1. The location of the oldest identified magnetic anomaly, M44 (~170 Ma)  
1214 (Tivey et al., 2006) is over 750 km from the inferred centre of the Pacific  
1215 triangle
- 1216 2. ODP site 801C, which lies within M42 (~168 Ma) is consistent with the  
1217 dating of microfossils overlying pillow basalts (Lancelot et al., 1990; Tivey  
1218 et al., 2006)
- 1219 3. An extrapolation of intermediate seafloor spreading rates (~30-40  
1220 mm/yr) from the location of M44 to the centre of the Pacific triangle  
1221 suggests an approximate age to be closer to around 190 Ma.

1222 4. A younger age for the initiation of seafloor spreading between the  
1223 Izanagi-Pacific, Farallon-Pacific and Phoenix-Pacific would require  
1224 anomalously high spreading rates or substantial spreading asymmetry.  
1225 This cannot be discounted as Tominaga et al. (2008) suggest a rapid  
1226 spreading rate of ~75 mm/yr. Therefore, we believe an age of 190 Ma for  
1227 the birth of the Pacific plate is a maximum age.

1228

1229 We have incorporated the Japanese magnetic lineations and fracture zones of  
1230 Nakanishi et al. (1999) and Sager et al. (1988) together with fracture zone traces  
1231 based on satellite gravity anomaly data (Sandwell and Smith, 2009) to define the  
1232 seafloor spreading history between the Izanagi and Pacific plates. Our resultant  
1233 seafloor spreading isochrons match well with the magnetic lineations seen in our  
1234 magnetic anomaly grid from M25 (~154 Ma) onwards when the magnetic  
1235 anomaly signature is strongest (Figure 6). Magnetic lineations prior to M25  
1236 (~154 Ma) have larger variability (Tominaga and Sager, 2010) and are not  
1237 observed in our magnetic anomaly grid (Figure 6) (see Tominaga and Sager  
1238 (2010) for details). The ridge jump prior to M26 (~155 Ma) postulated by Sager  
1239 et al. (1998) has not incorporated as we were unable to identify magnetic  
1240 lineations or an abandoned ridge. In addition, the conjugate ridge flank is  
1241 absent.

1242

1243 We incorporate the major 24° clockwise change in spreading direction at M21  
1244 (~147 Ma) (Sager et al., 1988) primarily constrained via the Kashima Fracture  
1245 Zone which shows continuity from at least M28-M10 (~156-130 Ma) (Figure 6).  
1246 This major change in spreading direction is coincident with the eruption of the  
1247 southern-end of the Shatsky Rise at the Farallon-Izanagi-Pacific triple junction  
1248 followed by triple junction instability. According to the model of Sager et al.  
1249 (1988) two simultaneous triple junctions and at least nine small, short-lived  
1250 ridge jumps occurred at the Pacific-Farallon-Izanagi junction. This led to an 800  
1251 km northeast jump in the triple junction centre clearly observed in the gridded  
1252 magnetic anomaly dataset between M21 (~147 Ma) and M16 (~138 Ma) (Figure  
1253 6). Due to the complexity of the triple junction solutions and the lack of  
1254 preserved data between the Izanagi and Farallon plates, we incorporate a simple

1255 model whereby the Pacific-Izanagi-Farallon triple junction remains in a ridge-  
1256 ridge-ridge configuration during its entire history. As the instability of this triple  
1257 junction is believed to have existed for only 2 million years (Sager et al., 1999),  
1258 we believe that our assumption is reasonable and follows the broad scale  
1259 development of the area.

1260

1261 The fracture zones in the westernmost Pacific do not show a major change in  
1262 trend after M20 (~146 Ma) (Figure 6). No discernable fracture zone trends after  
1263 M0 indicate the direction of motion during the CNS hence we assume that no  
1264 change in the direction of motion occurred from M20 to the CNS and use a fixed  
1265 stage rotation pole for this entire period. As much of the evidence for the late  
1266 Cretaceous-early Cenozoic history of the Izanagi plate has been lost due to  
1267 subduction along the east Asian margin, we assume no major change in  
1268 spreading rate, direction and accretion from M0 (last dated anomaly, ~120 Ma)  
1269 to the cessation of spreading along the Izanagi-Pacific ridge.

1270

1271 Finite rotations were computed for Izanagi-Pacific spreading using the half-stage  
1272 pole method and assuming spreading symmetry and rely heavily on fracture  
1273 zones traces for direction of motion. For younger times when no preserved crust  
1274 exists, we assume an intermediate full spreading rate of ~80 mm/yr (similar to  
1275 the spreading rate in the late Cretaceous), spreading symmetry and a consistent  
1276 spreading direction to model the position of the mid-ocean ridge. We find that  
1277 this results in the Pacific-Izanagi ridge intersecting the east Asian margin around  
1278 55-50 Ma in a sub-parallel orientation and is consistent with geological and  
1279 seismic tomography observations, as explained in Seton et al. (In Prep). Our  
1280 model suggests that spreading continued along the Pacific-Izanagi ridge after the  
1281 establishment of the Kula-Pacific ridge to the east, contrary to most previous  
1282 models. The preserved seafloor spreading record in the regions adjacent to the  
1283 Pacific-Izanagi ridge preserve no evidence to suggest a readjustment of the plate  
1284 driving forces due to the merging of two major plates (i.e. the death of the  
1285 Izanagi plate) prior to 55 Ma. Instead, we find that spreading between the Kula  
1286 and Pacific plates underwent a major change in spreading rate and direction at  
1287 Anomaly 24 (~55-53 Ma), which resulted in a dramatic doubling of the

1288 spreading rate of the Kula plate and a counter-clockwise change in spreading  
1289 direction from largely N-S to NW-SE. Our model is in stark contrast to the  
1290 prevailing models for the Izanagi-Pacific and Kula-Pacific ridge, but our  
1291 interpretation is kinematically self-consistent, matches geological observations  
1292 and can be linked to the subduction history as seen in seismic tomography  
1293 (Seton et al., In Prep).

1294

1295 The birth of the Izanagi plate is far more uncertain. The Izanagi plate must have  
1296 existed prior to the birth of the Pacific plate as part of a three-plate ridge-ridge-  
1297 ridge triple junction with the Farallon and Phoenix plates, based on the rules of  
1298 triple junction closure. However, there is no crust preserved in the seafloor  
1299 spreading record reflecting this early history as it has been progressively  
1300 subducted under the east Asian margin. We model a simple geometry whereby  
1301 the spreading direction between the Izanagi-Farallon plates is constrained by the  
1302 oldest Pacific-Izanagi and Pacific-Farallon isochrons via triple junction closure,  
1303 intermediate spreading rates and spreading symmetry. We constructed the  
1304 positions of the spreading ridges by computing small circle arcs between  
1305 Izanagi-Pacific, Farallon-Pacific and Phoenix-Pacific spreading. The spreading  
1306 direction between the Izanagi and Phoenix plates is similarly constrained using  
1307 triple junction closure between the Pacific-Izanagi and Pacific-Phoenix plates  
1308 and the length of the spreading ridges determined by intersection with the  
1309 Pacific margins.

1310

### 1311 *3.2.2 Farallon Plate*

1312 Early mapping of magnetic lineations in the western Pacific identified a set of  
1313 NW-SE trending Mesozoic magnetic lineations loosely bounded by the Shatsky  
1314 and Hess Rises and the Mid Pacific Mountains (Figure 6 and 7). These lineations,  
1315 termed the Hawaiian lineations, formed during NE-SW directed spreading  
1316 between the Pacific and now extinct Farallon plate between at least M29-M0  
1317 (~156-120 Ma) (Atwater and Severinghaus, 1990; Larson et al., 1972). The  
1318 Mesozoic oceanic crust on the Farallon plate subducted under North America  
1319 beginning in the late Mesozoic (Bunge and Grand, 2000) and clearly imaged as  
1320 seismically fast material under central and eastern North America (Bunge and

1321 Grand, 2000; Liu et al., 2010). The Hawaiian lineations show a clockwise change  
1322 in spreading direction at M11 (~133 Ma) (Atwater and Severinghaus, 1990;  
1323 Sager et al., 1988a) with no major change in spreading direction during the early  
1324 history of Pacific-Farallon spreading due to the uniformity of the magnetic  
1325 lineations (Figure 6) even though fracture zone traces prior to M25 (~154 Ma)  
1326 are absent (Figure 1). The pole of rotation to describe Mesozoic spreading was  
1327 likely located in the south or equatorial Pacific due to the slightly fan-shaped  
1328 nature of the lineations (Figure 6 and 7).

1329

1330 The Hawaiian lineations form a magnetic bight with the Japanese lineation set in  
1331 the north and trace the Pacific-Farallon-Izanagi triple junction (Figure 6). The  
1332 Shatsky Rise erupted along the triple junction centre between M21-19 (~147-  
1333 143 Ma), as confirmed by ODP leg 198 (Mahoney et al., 2005) either as a result of  
1334 a mantle plume head reaching the surface or decompression melting at a mid-  
1335 ocean ridge (Mahoney et al., 2005; Sager, 2005). The eruption of the Shatsky  
1336 Rise was coincident with an 800 km, nine-stage jump in the location of the triple  
1337 junction during which time the triple junction switched between ridge-ridge-  
1338 ridge and ridge-ridge-transform configurations (Nakanishi et al., 1999). The  
1339 triple junction regained its stability after the initial eruptive phase followed by  
1340 waning volcanism forming the Papanin Ridge along the triple junction centre  
1341 until M1 (~121-124 Ma) (Nakanishi et al., 1999).

1342

1343 In the south, the Hawaiian lineations disappear beneath the Mid-Pacific  
1344 Mountains obscuring the trace of the Pacific-Farallon-Phoenix triple junction.  
1345 Further east, the Hawaiian lineations form a complex junction with several  
1346 discrete fan-shaped lineation sets (e.g. Magellan and Mid-Pacific Mountain  
1347 lineation sets) (Tamaki and Larson, 1988) characteristic of crust that formed  
1348 during microplate formation at fast-spreading triple junction centers. These fan-  
1349 shaped lineations were active between M15-M1 (~138-121 Ma). In addition, a  
1350 set of short ENE-WSW trending lineations south of the Mid-Pacific Mountains  
1351 have been identified as M21 (~147 Ma) to M14 (~136 Ma) (Nakanishi and  
1352 Winterer, 1998) and are suggested to have formed between the Phoenix plate  
1353 and the postulated Trinidad plate.

1354

1355 East of the M-anomalies is a wide zone of crust which formed during the CNS.  
1356 Indicators of spreading direction are observed in the prominent Mendocino,  
1357 Pioneer, Murray, Molokai and Clarion fracture zones (Figure 1 and 7). The  
1358 Mendocino, Molokai and Clarion fracture zones record two clear changes in  
1359 spreading direction: one between M0 and the middle of the CNS (Granot et al.,  
1360 2009) and another clockwise change to almost E-W trending sometime towards  
1361 the end of the CNS (Atwater, 1989; Searle et al., 1993b). No clearer indication of  
1362 timing has been established. The isochrons that bound the beginning and end of  
1363 the CNS in this region cannot be restored without significant misfit along length.  
1364 Atwater et al. (1993), therefore proposed that spreading asymmetry and/or a  
1365 series of ridge jumps must have occurred during the CNS between smaller  
1366 segment of the ocean floor bounding the two isochrons. The Hess, Liliuokalani  
1367 and Sculpin ridges were suggested as possible remnants of this early spreading  
1368 history, whereas others suggest that they were instead related to the formation  
1369 of the Hess Rise (Hillier, 2007). Oceanic crust that formed by Pacific-Farallon  
1370 spreading during the CNS has also been identified in the central-south Pacific,  
1371 east of the Manihiki Rise suggesting that the Pacific-Farallon ridge propagated to  
1372 southward after the Mesozoic (Figure 8).

1373

1374 The Cenozoic lineations record five major episodes of break-up of the Farallon  
1375 plate including the formation of the Kula, Vancouver, Cocos, Nazca and Juan De  
1376 Fuca plates (Figure 8) and extend almost the entire length of the eastern Pacific  
1377 Ocean. In the northeast Pacific, the lineations are some of the best-mapped in  
1378 the world, as observed in the magnetic grid compilation (Figure 7). Spreading  
1379 appears simple for the early Cenozoic with progressive complexity approaching  
1380 the trench. The most prominent bend observed in all fracture zones in the  
1381 northeast Pacific occurred just prior to Chron 33 (~79 Ma) where spreading  
1382 changed from roughly E-W to ENE-WSW (Atwater et al., 1993). Atwater et al.  
1383 (1993) suggested that the inferred continuity of the spreading system provides  
1384 evidence of a simple two-plate system during this time, negating the need for  
1385 microplate formation (e.g. Chinook plate). Anomaly 33 (~79 Ma) corresponds to  
1386 the oldest clearly identified magnetic anomaly related to Pacific-Kula spreading

1387 (Atwater, 1989; Lonsdale, 1988) (see Section 3.2.2.1 Kula plate), marking the  
1388 minimum timing for the initial break-up of the Farallon plate. Spreading was  
1389 reasonably steady between Chrons 32-24 (~71-53 Ma), connecting with  
1390 spreading along the Kula-Pacific ridge to the north at the Great Magnetic Bight  
1391 (Figure 7). Anomaly 24 (~55-53 Ma; late Paleocene-early Eocene) corresponds  
1392 to a major hemisphere-wide plate reorganization event and is manifested in a  
1393 20° clockwise change in spreading direction between the Pacific and Farallon  
1394 plates from WSW-ENE to E-W (Atwater, 1989), a change in spreading direction  
1395 between Pacific-Kula plates (Lonsdale, 1988) and the break-up of the Farallon  
1396 plate into the Vancouver plate at either Chron 24 (~55-53 Ma) (Atwater, 1989)  
1397 or 23 (~51-52 Ma) (Menard, 1978; Rosa and Molnar, 1988) (Figure 8). The  
1398 break-up of the Farallon plate occurred in between the Pioneer and Murray  
1399 fracture zones (Atwater, 1989) (Figure 7) with oblique compression and slow  
1400 relative motion (Rosa and Molnar, 1988). At this time, the mid-ocean ridge was  
1401 located proximal to the subduction zone and was followed by a period of  
1402 complex spreading and/or spreading instability forming a “disturbed zone”  
1403 between Anomalies 19-12 (~41-31 Ma) (Atwater, 1989). Another major change  
1404 in spreading direction is recorded in the seafloor spreading record between the  
1405 Murray and Pioneer fracture zones at Anomaly 10 (~28 Ma), forming the  
1406 Monterey and Arguello plates (Atwater, 1989). South of the Murray fracture  
1407 zone, the Guadalupe plate formed between Anomalies 7-5 (~25-10 Ma)  
1408 (Atwater, 1989; Mammerickx and Klitgord, 1982). These plates formed  
1409 progressively as transform faults intersected with the Farallon subduction zone.  
1410 After Chron 10 (~28 Ma), the Vancouver plate is often referred to as the Juan De  
1411 Fuca plate, coinciding with the establishment of the San Andreas fault no earlier  
1412 than 30 Ma (Atwater, 1970) (Figure 8).

1413

1414 Spreading between the Pacific and Farallon plates during the Mesozoic occurred  
1415 in the region conjugate to the North American margin. However, starting in the  
1416 CNS, the Pacific-Farallon spreading extended southward as far south as the  
1417 Eltanin fracture zone in the South Pacific (Figure 7 and 9). Magnetic anomalies  
1418 34 (~84 Ma) to 6 (~20 Ma) on the Pacific plate associated with Pacific-Farallon  
1419 spreading conjugate to the South American margin have been identified (Cande

1420 et al., 1982; Herron, 1972; Mayes et al., 1990). This is restricted to Anomalies  
1421 23-6 (~52-20 Ma) on the Nazca plate (Cande and Haxby, 1991). Seafloor  
1422 spreading between Anomalies 34-21 (~84-47 Ma) was reasonably stable until a  
1423 major reorganization of the spreading system at Chron 21 (~47 Ma), observed in  
1424 fracture zone trends in the South Pacific (Mayes et al., 1990). The cessation of  
1425 spreading between the Pacific and Farallon plates occurred during break up into  
1426 the Cocos and Nazca plates at 23 Ma (see Section 3.2.2.3 Nazca and Cocos plates).

1427

1428 Our model for spreading between the Pacific and Farallon plates incorporates  
1429 spreading initiation at 190 Ma, based on the evidence presented earlier in the  
1430 manuscript (see Section 3.2.1 Izanagi plate), even though the oldest Hawaiian  
1431 lineation identified is M29 (~156 Ma). The model we have implemented closely  
1432 follows that of Atwater and Severinghaus (1990). We use their seafloor  
1433 spreading isochrons, with adjustments based on Nakanishi et al. (1992), for the  
1434 Mesozoic lineations. Our resultant seafloor spreading isochrons match well with  
1435 our magnetic anomaly grid (Figure 6 and 7) in the north and central sections of  
1436 the Mesozoic lineations but fail to account for the fan-shaped lineations in the  
1437 south. This is a direct consequence of our decision to exclude the reconstruction  
1438 of numerous microplates at the Pacific-Farallon-Phoenix triple junction (e.g.  
1439 Magellan, Mid-Pacific Mountains and Trinidad lineation sets) and instead focus  
1440 our model the board-scale development of the area. To the north, the Hawaiian  
1441 Mesozoic lineations show a clear magnetic bight with the Japanese lineations  
1442 (Figure 6 and 7), highlighting the geometric stability of the of the Pacific-Izanagi-  
1443 Farallon triple junction from M29-M22 (~156-148 Ma). A major clockwise  
1444 change in spreading direction is recorded in the Japanese lineations and fracture  
1445 zones at M21 (~147 Ma) leading to a period of instability of the Pacific-Izanagi-  
1446 Farallon triple junction (see Section 3.2.1 Izanagi plate). Interestingly, this does  
1447 not correspond to an adjustment of the Pacific-Farallon relative plate motion  
1448 suggesting that the adjustment was related to the Shatsky Rise rather than a  
1449 regional or global plate reorganization.

1450

1451 Finite rotations for the Pacific-Farallon ridge were derived using the half-stage  
1452 pole method with an assumption of spreading symmetry and average spreading

1453 rates. Reconstruction of the Pacific-Izanagi-Farallon, Pacific-Phoenix-Farallon  
1454 and Pacific-Kula-Farallon triple junctions additionally followed the principles of  
1455 triple junction closure. Although ridge jumps have been proposed for early CNS  
1456 spreading (Atwater et al., 1993), we have followed a simple model of seafloor  
1457 spreading throughout the CNS as we cannot identify remnant features describing  
1458 the proposed ridge jumps without access to high-resolution multibeam  
1459 bathymetry data. Towards the end of the CNS, constraining the precise timing of  
1460 the change in spreading direction observed in the Mendocino, Molokai and  
1461 Clarion fracture zones is difficult. We extrapolate using the Müller et al. (2008a)  
1462 model and suggest that a change in spreading direction between the Pacific and  
1463 Farallon plates occurred at 103 Ma, closely corresponding with the observed  
1464 bend in Pacific hotspots at ~99 Ma, implied by Veevers (2000) and Wessel and  
1465 Kroenke (2008), based on an updated seamount dataset.

1466

1467 The Shatsky Rise formed at the Izanagi-Farallon-Pacific triple junction and as a  
1468 consequence, part of the Shatsky Rise must have erupted onto the Farallon and  
1469 Izanagi plates. We have modeled the conjugate Shatsky Rise (Farallon) and find  
1470 that it intersects the North American margin at 90 Ma, correlating well with the  
1471 onset of the Laramide Orogeny in western North America and a shallow  
1472 seismically fast region underlying western North America (Liu et al., 2010). As  
1473 the geological evidence and seismic tomography images are independent of the  
1474 plate reconstructions used, our assumption of largely symmetrical seafloor  
1475 spreading and average spreading rates between Pacific-Farallon appears to be  
1476 reasonable.

1477

1478 After the CNS, we model seafloor spreading based on Atwater and Severinghaus  
1479 (1990) for the northeast Pacific but without small-scale ridge adjustments  
1480 associated with plate break-up events (Figure 8). We concur with the  
1481 interpretation of Atwater et al. (1993) that the most notable change in spreading  
1482 direction observed in all northeast Pacific fracture zones occurred at Chron 33  
1483 (~79 Ma). This timing corresponds to our initiation of seafloor spreading  
1484 between the Kula and Pacific plates and establishment of the Pacific-Kula-  
1485 Farallon triple junction (see Section 3.2.2.1 Kula plate) (Figure 8). Further

1486 southward, the Pacific-Farallon ridge extended to the Eltanin fracture zone and  
1487 Pacific-Farallon-Antarctic triple junction. Spreading along the Pacific-Antarctic  
1488 and Farallon-Antarctic ridges initiated at Chron 34 (~83.5 Ma) (see Section  
1489 3.2.3.1 Pacific-Antarctic spreading). Our model for the southeast Pacific is  
1490 similar to that of Mayes et al. (1990) with no major change in spreading rate  
1491 between Anomalies 33-21 (~79-47 Ma) followed by a change in spreading  
1492 direction after Chron 21 (~47 Ma), recorded in the fracture zones in the South  
1493 Pacific particularly along the Eltanin fracture zone. At this time, the Pacific-  
1494 Farallon spreading ridge extended further southward, connecting up with  
1495 spreading associated with the Aluk Plate.

1496

1497 The break-up of the Farallon plate into the Vancouver plate at Chron 24 (~53  
1498 Ma) (Atwater, 1989) resulted in minor relative motion along the Pioneer fracture  
1499 zone (Figure 7 and 8). Our finite rotations to describe Pacific-Vancouver  
1500 spreading are taken from Müller et al. (1997). As the Pacific-Farallon ridge  
1501 approached the North American subduction zone, spreading became more  
1502 complex with the formation of numerous microplates, ridge jump and  
1503 propagation events. Our model incorporates the Vancouver and Juan De Fuca  
1504 plates (Figure 8) but excludes the other proposed microplates, such as the  
1505 Monterey, Arguello and Guadalupe plates, as no published poles of rotation to  
1506 describe their history are available. Spreading between the Pacific and Farallon  
1507 plates ceased in the area to the west of South and Central America at 23 Ma  
1508 (Chron 6B) as the plate separated into the Cocos and Nazca plates.

1509

#### 1510 3.2.2.1 Kula Plate

1511 The existence of the Kula plate during the late Cretaceous to the  
1512 Paleocene/Eocene has been known since the early identification of northward  
1513 younging, E-W trending magnetic anomalies in the northern Pacific (Atwater,  
1514 1990; Hayes and Heirtzler, 1968; Lonsdale, 1988a; Mammerickx and Sharman,  
1515 1988; Rea and Dixon, 1983) (Figure 7). These magnetic anomalies, located north  
1516 of the Chinook Trough, represent only the southern (Pacific) flank of Kula-Pacific  
1517 spreading, the remainder having been subducted beneath the Aleutian trench.  
1518 The initiation of the Pacific-Kula ridge occurred within the Farallon plate and

1519 marks the first stage of Farallon plate break-up. Additionally, prevailing models  
1520 of the Pacific (e.g. (Engebretson et al., 1985)) imply cessation of spreading along  
1521 the Izanagi-Pacific ridge preceded the establishment of the Pacific-Kula Ridge,  
1522 therefore suggesting that Pacific-Izanagi and Pacific-Kula spreading was not  
1523 simultaneous. This assumption has implications for the formation of the  
1524 northern Pacific and plate driving forces in the area.

1525

1526 The oldest well recognized magnetic anomaly associated with Kula-Pacific  
1527 spreading is either Anomaly 31 (~68 Ma) or possibly 32 (~71 Ma) (Lonsdale,  
1528 1988a; Rea and Dixon, 1983) although some authors interpret Anomaly 33 (~79  
1529 Ma) (Mammerickx and Sharman, 1988) and tentatively Anomaly 34 (~83.5 Ma)  
1530 (Atwater, 1990; Norton, 2007). The conventional view is that after the death of  
1531 the Izanagi plate, the locus of rifting and spreading jumped eastward to the  
1532 Chinook Trough where E-W trending magnetic lineations formed via simple  
1533 Kula-Pacific spreading. However, Rea and Dixon (1983) postulated that two  
1534 spreading ridges formed along existing Pacific-Farallon fracture zones after a  
1535 change in spreading direction at ~83.5 Ma forming a second plate, the Chinook  
1536 plate, south of the Chinook Trough.

1537

1538 The Stalemate Fracture Zone delineates the western extent of the Kula plate  
1539 (Figure 6) and tracks the motion of the Kula plate from N-S adjacent to  
1540 Anomalies 34/31 (83.5-71 Ma) to 25 (~56Ma) to NW from Anomalies 24 (~55-  
1541 53 Ma) to 20/19 (~44-41 Ma). Additionally, Lonsdale (1988) interpreted an  
1542 extinct spreading ridge adjacent to Anomalies 20/19 (~44-41 Ma) as well as a  
1543 short sequence of Anomalies 21-20 (47-44 Ma) on the western side of this  
1544 extinct ridge. The study of Lonsdale (1988) therefore suggests a spreading  
1545 history for the Kula plate involving N-S spreading from 32-25 (~71-56 Ma)  
1546 followed by a major change in plate motion by 20-25° at Chron 24 (~55-53 Ma).  
1547 The cessation of spreading along the Pacific-Kula ridge was initially believed to  
1548 have occurred at Chron 25 (~56 Ma) (Byrne, 1979) and later to 43-47 Ma  
1549 corresponding to the major Pacific plate reorganization event (Engebretson et  
1550 al., 1985). The identification of an extinct spreading ridge in the far northwest  
1551 corner of the plate by Lonsdale (1988) further refined the cessation of spreading

1552 to around Chron 18 (~40 Ma). However, the identification of this ridge was  
1553 based on a small number of ship tracks and seismic profiles.

1554

1555 To the east, the Kula plate is delineated by the Great Magnetic Bight, which traces  
1556 the Pacific-Kula-Farallon triple junction in a ridge-ridge-ridge configuration from  
1557 Chron 34/31 (~84-71 Ma) to 25 (~56 Ma) (Figure 7). This is followed by a “T”  
1558 anomaly corresponding to Chron 24 (55-53 Ma), which likely formed during a  
1559 reorganization of the Pacific-Kula-Farallon triple junction (Atwater, 1990;  
1560 Lonsdale, 1988a).

1561

1562 The Great Magnetic Bight traces the location of the Kula-Farallon-Pacific triple  
1563 junction (Figure 7 and 8). Previous models have predicted the location and  
1564 orientation of the resultant Kula-Farallon ridge (for which there is no preserved  
1565 evidence in the seafloor spreading record) based on triple junction closure and  
1566 tracking evidence of a slab window beneath western North American margin  
1567 (e.g. (Atwater, 1990; Breitsprecher et al., 2003; Engebretson et al., 1985; Madsen  
1568 et al., 2006)). Most models lead to a reasonably consistent result of a NE-SW  
1569 trending spreading ridge intersecting the North American margin and forming a  
1570 slab window somewhere near the present-day Pacific Northwest (Atwater, 1990;  
1571 Breitsprecher et al., 2003; Engebretson et al., 1985; Madsen et al., 2006).

1572

1573 Our interpretation for the Kula plate closely follows the model of Lonsdale  
1574 (1988). However, we have interpreted Anomaly 33 (~79 Ma) north of the  
1575 Chinook Trough as the oldest identified magnetic anomaly based on the  
1576 interpretation in Atwater (1990) and our own analysis of the magnetic  
1577 anomalies in the area. Most authors have only been able to interpret anomalies  
1578 back to 32 (~71Ma) as it is the last clearly identified magnetic anomaly, however  
1579 the new gridded magnetic anomaly datasets such as WDMAM, EMAG2 and our  
1580 own gridded compilation (Figure 6-7) shows E-W trending magnetic lineations  
1581 south of Anomaly 32 (~71 Ma). There is space south of our interpreted Anomaly  
1582 33 (~79 Ma) to accommodate a very small portion of older crust (possibly back  
1583 to Anomaly 34 (~84 Ma)), but we believe that the establishment of the stable  
1584 Pacific-Kula-Farallon triple junction in a ridge-ridge-ridge configuration must

1585 have occurred at 33 (~79 Ma) and not earlier. Importantly, our model has  
1586 contemporaneous Pacific-Izanagi and Pacific-Kula spreading (see Section 3.2.1  
1587 Izanagi plate) joined by a NNW-SSE transform. In our model, we have continuing  
1588 N-S directed Pacific-Kula spreading until Anomaly 25 (~56 Ma) followed by an  
1589 anticlockwise change in spreading direction starting at Anomaly 24 (~55-53  
1590 Ma), as suggested by Lonsdale (1988) and expressed in the Stalemate Fracture  
1591 Zone. The magnetic anomaly grids clearly show the NE-SW trending magnetic  
1592 lineations corresponding to the youngest part of Pacific-Kula spreading (Figure  
1593 6). We follow the interpretation of Lonsdale (1988) for the cessation of Pacific-  
1594 Kula spreading to be around 41-40 Ma. We compute finite rotations based on  
1595 the half-stage pole method between Chrons 33-22 (~79-49 Ma) as only the  
1596 Pacific flank of the spreading system is preserved. We use the magnetic  
1597 lineations of Lonsdale (1988) and the Stalemate Fracture Zone to compute finite  
1598 rotations between Chrons 21-20 (~47-44 Ma) using the traditional method.

1599

1600 The factor leading to the abrupt change in plate motion between the Kula and  
1601 Pacific plates was suggested to be a result of the temporary elimination of  
1602 northward slab pull when subduction shifted from the Siberian margin to the  
1603 Aleutian Trench (Lonsdale, 1988). In our model, we argue that the subduction of  
1604 the Izanagi-Pacific ridge at 55-50 Ma resulted in the temporary cessation of  
1605 subduction and slab break-off along the east Asian margin leading to a change in  
1606 motion of the Kula plate to the northwest. The intersection of the Pacific-Izanagi  
1607 ridge with subduction under East Asia eliminated the ridge push force thus  
1608 enabling the Kula plate to move to the west. The change in spreading direction  
1609 in the Kula plate identified by Lonsdale (1988) matches with the change in the  
1610 Pacific plate driven by the subduction of the Izanagi ridge (see Section 3.2.1  
1611 Izanagi plate) and changes that were occurring along the Pacific-Farallon  
1612 spreading system (see Section 3.2.2 Farallon plate).

1613

1614 To the east, we model the Kula-Farallon ridge based on triple junction closure  
1615 and the finite difference method resulting in a stable NE-SW orientation of the  
1616 Kula-Farallon ridge, consistent with previous studies. The Yellowstone hotspot  
1617 located offshore the North American margin in the Paleocene/Eocene (Figure 8)

1618 was used as a further constraint to guide the position of the NE-SW trending  
1619 Kula-Farallon ridge, as mid-ocean ridges are known to preferentially evolve near  
1620 hotspots (Müller et al., 1998b). As a result our modelled position of the Kula-  
1621 Farallon ridge with respect to the North American margin correlates with  
1622 onshore geological and geochemical evidence of a northward migrating slab  
1623 window near the northern US/Canadian margin (Atwater, 1990; Breitsprecher et  
1624 al., 2003; Madsen et al., 2006). Additionally, our position of the Kula-Farallon  
1625 ridge is supported by seismic tomography (Bunge and Grand, 2000).

1626

### 1627 3.2.2.2 Vancouver/Juan De Fuca Plate

1628 The recognition of a difference in trend by about 11° between the fracture zones  
1629 north of the Murray fracture zone in the northeast Pacific and those to the south  
1630 (Figure 1), led Menard (1978) to suggest that the Farallon plate broke into two  
1631 plates around 47-49 Ma (Chron 22-21). Menard (1978) termed the new  
1632 plate north of the Murray Fracture Zone, the Vancouver plate. Differential  
1633 motion between the Vancouver and Farallon plate was confirmed and dated to  
1634 Chron 21 (~47 Ma) with the spacing of magnetic anomalies in the area between  
1635 the Murray and Pioneer fracture zone possibly indicating either asymmetric  
1636 spreading or a ridge jump between Anomalies 21 (~47 Ma) and 13 (~33 Ma)  
1637 (Rosa and Molnar, 1988). The model of Rosa and Molnar (1988) implies slow  
1638 transpressional motion across the plate boundary, which lies between the  
1639 Murray and Pioneer fracture zones as a “set of curving, tooth-like disjunctures”  
1640 (Atwater, 1990) clearly seen between Anomalies 19-13 (~41-33 Ma) (Figure 7)  
1641 possibly indicative of diffuse deformation.

1642

1643 The intersection of the Murray transform fault with the North American  
1644 subduction zone around 30 Ma led to the establishment of the San Andreas Fault  
1645 and corresponds to the establishment of the Juan De Fuca plate at the expense of  
1646 the Vancouver plate. The spreading history of the Juan De Fuca plate is very  
1647 complex (Wilson, 1988; Wilson et al., 1984) most likely due to its proximity to  
1648 the Cascadia subduction zone. Spreading involved counter-clockwise motion  
1649 followed by progressive clockwise rotation starting at Chron 5D (~17 Ma)  
1650 (Atwater, 1990) and a series of propagating rifts and microplate formation

1651 (Wilson, 1988; Wilson et al., 1984). Currently, the Juan De Fuca plate is limited  
1652 at its southern end by the Mendocino Fracture Zone and is subducting slowly  
1653 along the Cascadia subduction zone (Figure 7).

1654

1655 Our reconstructions of the Vancouver/Juan De Fuca plates are largely based on  
1656 the detailed tectonic maps of Atwater and Severinghaus (1990) unchanged from  
1657 the model used by Müller et al. (1997). We implement the break-up of the  
1658 Farallon plate into the Farallon and Vancouver plates along the Pioneer Fracture  
1659 Zone at Chron 22 (~50-49 Ma) (Figure 8). We use the finite rotations from  
1660 Müller et al. (1997) for the Vancouver plate and the rotations in this study for the  
1661 Farallon plate. Our rotations result in transpressional motion along the  
1662 transform fault connecting the Farallon and Vancouver plates. The Juan de Fuca  
1663 plate is modeled as a simple two-plate system and do not include the detailed  
1664 interpretation of Wilson (1988) as there are no rotations associated with the  
1665 isochrons making it difficult to incorporate into our tectonic model. On the  
1666 broad scale, our seafloor spreading isochrons match well with the magnetic  
1667 lineations from our magnetic grid compilation (Figure 7), however there are  
1668 some inconsistencies, particularly approaching the trench as we do not include  
1669 small scale block rotations.

1670

### 1671 3.2.2.3 Nazca and Cocos Plates

1672 The East Pacific Rise is currently the site of very fast seafloor spreading between  
1673 the Pacific and Nazca and Cocos plates and dominates the seafloor of the SE  
1674 Pacific (Figure 9). Other active seafloor spreading ridges are the Chile Ridge  
1675 (active spreading between the Nazca and Antarctic plates) and the Galapagos  
1676 Spreading Centre (Nazca-Cocos spreading) (Figure 9). The Nazca plate  
1677 incorporates oceanic crust that formed as a result of Pacific-Nazca, Pacific-  
1678 Farallon, Nazca-Cocos and Nazca-Antarctic spreading as well as the Bauer  
1679 microplate (Figure 9). The Cocos plate includes oceanic crust that formed as a  
1680 result of Cocos-Pacific and Cocos-Nazca as well as spreading in the Rivera and  
1681 Mathematician microplates.

1682

1683 Both the Nazca and Cocos plates formed as a result of the break-up of the  
1684 southern part of the Farallon plate at approximately 23 Ma (Hey, 1977; Lonsdale,  
1685 2005) or Chron 6By (~23 Ma) (Barckhausen et al., 2008) . The break-up of the  
1686 Farallon plate is believed to have been driven by a combination of increased  
1687 northward pull after the earlier break-up of the Farallon plate to the north  
1688 (Lonsdale, 2005), an increase in slab pull at the Middle America subduction zone  
1689 due to an increase in its length (Lonsdale, 2005) and/or the weakening of the  
1690 plate along the point of break-up due to the influence of the Galapagos hotspot  
1691 (Barckhausen et al., 2008; Hey, 1977; Lonsdale, 2005). In addition, plate break-  
1692 up was preceded by a major plate reorganization in the Southeast Pacific at 24  
1693 Ma leading to a change in motion of the Farallon plate 1-2 million years before  
1694 break-up (Barckhausen et al., 2008; Lonsdale, 2005; Tebbens and Cande, 1997).  
1695 Although the Nazca and Cocos plates are now independent plates, an  
1696 interpretation of their history must consider the evolution of the Farallon plate  
1697 (see Section 3.2.2 Farallon plate) to understand the nature of the oceanic  
1698 lithosphere in this region older than 23 Ma.

1699

1700 The oldest portion of the Nazca plate, adjacent to the South American margin  
1701 includes the crust that formed due to Farallon-Pacific spreading. Magnetic  
1702 anomalies up to Anomaly 23 (~51 Ma) have been tentatively identified on the  
1703 Nazca plate (Cande and Haxby, 1991) but most models confidently identify  
1704 magnetic anomalies only back to Anomaly 13 (~33 Ma) (Handschumacher, 1976;  
1705 Pardo-Casas and Molnar, 1987; Tebbens and Cande, 1997). Pardo-Casas and  
1706 Molnar (1987) and Rosa and Molnar (1988) computed finite rotations and their  
1707 uncertainties to describe the motion of Pacific-Farallon spreading by assuming  
1708 symmetrical spreading where both flanks were not presently preserved. These  
1709 rotations were used as a basis for the rotation model of Tebbens and Cande  
1710 (1997) for the Nazca-Pacific-Antarctic triple junction. A South Pacific-wide study  
1711 by Mayes et al. (1990) computed rotations for the Pacific-Farallon and Pacific-  
1712 Nazca ridges.

1713

1714 The crust that formed between the Pacific-Nazca plates subsequent to plate  
1715 break-up at 23 Ma has a complex spreading history. Spreading occurred as a

1716 northward “step-wise triple junction migration” (see (Tebbens and Cande, 1997)  
1717 for a description of this process) between the Pacific-Nazca-Antarctic ridges,  
1718 leaving behind a record of ridge jumps and microcontinent formation  
1719 particularly at Anomalies 6 (~20 Ma) and 5A (~12 Ma) (Tebbens and Cande,  
1720 1997) including the Friday microplate south of the Chile Fracture Zone (Figure  
1721 9). This complexity in the spreading pattern has hindered the interpretation of  
1722 magnetic anomalies post-Oligocene. Although most of the crust created during  
1723 this spreading phase is preserved in the present day record, it has been  
1724 suggested that isolated sections of Nazca-Pacific spreading have been captured  
1725 by the Cocos plate to the north and subsequently subducted under the Middle  
1726 America trench (Tebbens and Cande, 1997). Finite rotations and their  
1727 uncertainties to describe the post break-up phase of Nazca-Pacific and Nazca-  
1728 Antarctic motion were computed using a combination of the Hellinger technique  
1729 (Tebbens and Cande, 1997), existing rotations (Pardo-Casas and Molnar, 1987)  
1730 and the interpretation of South Pacific magnetic anomalies (Mayes et al. 1990).  
1731  
1732 A major component of the seafloor spreading history of the Nazca plate involves  
1733 the formation of the Bauer Microplate (Figure 9). The Bauer microplate formed  
1734 along the northern East Pacific Rise and grew by crustal accretion and counter-  
1735 clockwise rotation between Pacific and Nazca spreading (Eakins and Lonsdale,  
1736 2003; Goff and Cochran, 1996) shortly after a major plate reorganization event at  
1737 20 Ma (Figure 9). The formation of the Bauer microplate is unlike the step-wise  
1738 triple junction migration models used to explain the formation of the microplates  
1739 associated with the Pacific-Nazca-Antarctic triple junction. Spreading is believed  
1740 to have initiated at 17 Ma via northward propagation of the East Pacific Rise and  
1741 southward propagation of the Galapagos Rise during counter clockwise rotation  
1742 of the spreading axes (Eakins and Lonsdale, 2003). Rotation and spreading  
1743 continued about a pole proximal to the spreading axis creating fan-shaped  
1744 anomalies until 6 Ma when the spreading ridge realigned with the dominant East  
1745 Pacific Rise spreading ridge and the Bauer microplate was captured by the Nazca  
1746 plate (Eakins and Lonsdale, 2003) (Figure 10).  
1747

1748 The other smaller microplates within the Nazca/Cocos/Pacific realm are the  
1749 presently active Easter and Juan Fernandez microplates, which form small  
1750 pseudo-circular plates along the actively spreading East Pacific Rise. These  
1751 plates are believed to have become active at around Chron 3o (~5 Ma) during a  
1752 major plate reorganization event in the SE Pacific (Tebbens and Cande, 1997)  
1753 and have rotated about an axis close to the centre of the plate by between 80-90°  
1754 (Searle et al., 1993a). The mechanism for the formation of these plates is  
1755 believed to be the same process responsible for the development of the Hudson  
1756 and Friday microplates related to the northward migrating Nazca-Pacific-  
1757 Antarctic ridge (Bird et al., 1998 ).

1758

1759 To the north, the Cocos-Pacific spreading ridge was only established in its  
1760 present form from Chron 2A (~3 Ma) (Atwater, 1990). Between 23 Ma and  
1761 Chron 2A (~3 Ma), spreading was being accommodated along the Mathematician  
1762 and Rivera Ridges to the north and the Cocos-Pacific to the south (Atwater, 1990;  
1763 Eakins and Lonsdale, 2003). Spreading in this area included many block  
1764 rotations and ridge jumps possibly due to the proximity of the Cocos-Pacific  
1765 spreading centre to the Middle America trench and Galapagos hotspot. The  
1766 magnetic lineations that formed due to Cocos-Pacific spreading are fan-shaped  
1767 with strongly curved fracture zones observed in the satellite gravity anomalies  
1768 indicating a pole of rotation close to the northern end of the plate (Figure 1 and  
1769 9).

1770

1771 The present day Cocos-Nazca ridge strides the Galapagos hotspot and intersects  
1772 the Middle America convergent margin at the Bulboa Fracture Zone (Figure 9).  
1773 This E-W directed spreading ridge was established around 23 Ma, coinciding  
1774 with the break-up of the Farallon plate. The early spreading history is quite  
1775 complex, requiring several ridge jumps during its formation (Barckhausen et al.,  
1776 2008), the most significant of which is the Malpelo Ridge, which became extinct  
1777 around 15-10 Ma (Meschede et al., 1998a). In addition, numerous pseudo-faults  
1778 indicating rift propagation to the east have been identified in the seafloor fabric,  
1779 the majority in the vicinity of the Galapagos hotspot (Atwater, 1990). Further  
1780 complications occur close to the Middle America trench where several ridge

1781 jumps have isolated spreading systems, particularly in the Panama Basin  
1782 (Lonsdale and Klitgord, 1978).  
1783  
1784 We incorporate the magnetic anomaly identifications from Munschy et al. (1996)  
1785 to derive a set of finite rotations and seafloor spreading isochrons between the  
1786 Pacific and Nazca plates and also extend our analysis to include the parts of  
1787 Pacific-Farallon spreading that are currently preserved on the Nazca plate. The  
1788 magnetic anomaly identifications of Munschy et al. (1996) do not extend to the  
1789 easternmost Nazca plate where we would expect to find the oldest preserved  
1790 oceanic lithosphere corresponding to Pacific-Farallon spreading, mainly due to a  
1791 lack of data and signal intensity. Instead, we predict the age of the oceanic  
1792 lithosphere in this area by reconstructing the conjugate Pacific-Nazca isochrons.  
1793 We find that the resultant location of isochrons closely corresponds to the  
1794 interpretation of magnetic anomalies from Cande and Haxby (1991) and matches  
1795 well with the magnetic lineations observed on our magnetic anomaly grid  
1796 (Figure 9). Thus, our model predicts that the oldest ocean floor off South  
1797 America corresponds to Anomaly 23 (~51 Ma) (Figure 10). We derive a new set  
1798 of finite rotations to describe Pacific-Nazca spreading largely based on the  
1799 rotations of Mayes et al. (1990) to be consistent with our magnetic pick  
1800 compilation. We do not incorporate the detailed triple junction migration model  
1801 of Tebbens and Cande (1997).  
1802  
1803 The seafloor spreading model we implement for the Bauer microplate and its  
1804 relationship to Pacific-Nazca spreading incorporates the finite rotations of  
1805 Eakins and Lonsdale (2003). We implement spreading in the fan-like pattern  
1806 whereby the pole of rotation is located close to the ridge axis (Figure 10).  
1807 Although magnetic anomalies cannot be clearly discerned, we have implemented  
1808 the timing of Eakins and Lonsdale (2003) with spreading initiating at 17 Ma and  
1809 continuing until 6 Ma. The locus of spreading then jumps back to the Pacific-  
1810 Nazca ridge (Figure 10).  
1811  
1812 The model for the Cocos and Mathematician/Rivera plates incorporates the  
1813 magnetic anomaly identification of Munschy et al. (1996) together with the finite

1814 rotations derived from Eakins and Lonsdale (2003) between 17.3-11.9 Ma and  
1815 newly derived finite rotation for 23 Ma and 10.9 Ma. We reconstruct the shape  
1816 and location of the Cocos Ridge from Meschede et al. (1998b). We model  
1817 spreading along the Galapagos Spreading Centre (Cocos-Nazca) based on the  
1818 finite difference method. We do not include the small-scale ridge jumps that  
1819 occurred along the Cocos-Nazca Ridge, instead we model a simple two plate  
1820 system with an eastward propagating ridge (Figure 9-10).

1821

### 1822 *3.2.3 Phoenix Plate*

1823 Until recently, the prevailing view for the evolution of the Phoenix plate was that  
1824 the Phoenix-Pacific spreading ridge was active since the birth of the Pacific plate  
1825 to at least the mid-late Cretaceous as a simple two-plate system with N-S  
1826 directed spreading (Larson and Chase, 1972). The E-W trending Phoenix  
1827 lineations (so named due to their proximity to the Phoenix Islands) form the  
1828 southern arm of the Pacific triangle (Figure 6) with magnetic anomalies ranging  
1829 from M29 (~156 Ma) to M1 (~123 Ma) (Atwater, 1990; Cande et al., 1978;  
1830 Larson, 1976) and possibly M0 (~120 Ma) (Larson, 1997; Nakanishi and  
1831 Winterer, 1998). Undated, presumably older magnetic lineations can be traced  
1832 north of M29 (~156 Ma) (Nakanishi et al., 1992; Nakanishi and Winterer, 1998)  
1833 close to the inferred centre of the Pacific triangle. The lineations disappear  
1834 under the Ontong Java Plateau to the west and abut against a complex set of fan-  
1835 shaped lineations (Magellan lineations) and NE-SW directed lineations (M21-14;  
1836 ~147-136 Ma) south of the Mid-Pacific Mountains (Nakanishi and Winterer,  
1837 1998) to the east. The complex Magellan and Mid-Pacific lineations suggest the  
1838 existence of several microplates (e.g. Trinidad and Magellan) at the Phoenix-  
1839 Pacific-Farallon triple junction (Atwater, 1990) with patterns similar to the fast  
1840 spreading migrating microplates of the East Pacific Rise (Tebbens and Cande,  
1841 1997).

1842

1843 The ocean floor within the Ellice Basin and directly east of the Tonga-Kermadec  
1844 subduction zone is intrinsically linked to the evolution of the Pacific-Phoenix  
1845 ridge after M0 (~120 Ma) (Figure 6 and 11). Early models predicted that the  
1846 area formed as part of a simple, continuous N-S directed spreading system until

1847 the end on the CNS (Larson and Chase, 1972). However, the anomalously fast  
1848 seafloor spreading rates required to populate the region with crust formed  
1849 during the CNS (Atwater, 1990) as well as the identification of tectonic  
1850 structures and seafloor fabric such as the E-W trending Nova Canton Trough, the  
1851 E-W trending Osbourn Trough and the N-S directed seafloor fabric and side-  
1852 stepping fracture zones in the Ellice Basin suggest a more complex history for  
1853 the area. Based on the interpretation of the seafloor spreading structures, two  
1854 distinct models have been developed to explain the evolution of the Pacific-  
1855 Phoenix ridge after M1/M0 (~123-120 Ma): a successive southward ridge jump  
1856 model (Billen and Stock, 2000; Larson, 1997; Müller et al., 2008b; Winterer,  
1857 1976) and a plateau break-up model (Taylor, 2006).

1858

1859 In the successive ridge jump model the Nova Canton Trough, an E-W gravity low  
1860 located south and parallel to the Mesozoic lineations (Figure 6 and 11), is  
1861 interpreted as an abandoned spreading centre associated with Pacific-Phoenix  
1862 spreading (Müller et al., 2008b; Rosendahl et al., 1975; Winterer, 1976). A zone  
1863 of disrupted seafloor fabric bounded by two prominent E-W trending gravity  
1864 lows in the northern Ellice Basin observed in satellite gravity data led to the idea  
1865 of a rift zone associated with N-S directed spreading along the Pacific-Phoenix  
1866 ridge (Larson, 1997). The abandoned ridge/rift zone model implies that the  
1867 Pacific-Phoenix ridge either became extinct shortly after M0 (~120 Ma) or that  
1868 the spreading ridge jumped to another location, likely to the south subsequent to  
1869 M0 (~120 Ma), during a regional plate reorganization. The timing is constrained  
1870 by the identification of magnetic anomaly M0 (~120 Ma) just north of the Nova-  
1871 Canton Trough (Larson, 1997; Nakanishi and Winterer, 1998). The southern  
1872 ridge jump model is supported by the identification of the E-W trending Osbourn  
1873 Trough (located to the east of the Tonga-Kermadec Trench and north of the  
1874 Louisville Seamount Chain) as an extinct spreading ridge of Cretaceous age  
1875 (Billen and Stock, 2000; Lonsdale, 1997) (Figure 11) rather than a late stage  
1876 crack in the Pacific plate (Small and Abbott, 1998).

1877

1878 The seafloor spreading morphology in the vicinity of the Osbourn Trough  
1879 confirms roughly north-south spreading along a slow-intermediate spreading

1880 centre (Downey et al., 2007; Worthington et al., 2006) whereas the early motion  
1881 appears to be parallel to the Wishbone Ridge (Figure 1 and 2g). Spreading along  
1882 the Osbourn Trough is believed to have initiated right after M0 (~120 Ma) (Davy  
1883 et al. 2008) leading to the separation of the Manihiki and Hikurangi Plateaus.  
1884 The timing cannot be constrained from the seafloor spreading record as the early  
1885 crust would have formed during the CNS. Instead, the timing for the initiation of  
1886 spreading is constrained from the dating of rift-related structures on the  
1887 southern side of the Manihiki Plateau (e.g. Nassau-Suwarrow Scarp) and the  
1888 northern side of the Hikurangi Plateau (e.g. Rapuhia Scarp) (Billen and Stock,  
1889 2000; Lonsdale, 1997; Sutherland and Hollis, 2001a; Davy et al. 2008). The  
1890 cessation of spreading is poorly constrained but most authors tie the termination  
1891 of spreading along the Osbourn Trough with the docking of the Hikurangi  
1892 Plateau to the Chatham Rise. Unfortunately, the timing of collision between the  
1893 Hikurangi Plateau and Chatham Rise is also ill constrained. Some authors favour  
1894 collision at 105-100 Ma (Davy et al., 2008; Lonsdale, 1997; Sutherland and Hollis,  
1895 2001a) based on geological observations and the onset of extension in New  
1896 Zealand whereas others favour collision around 80-86 Ma (Billen and Stock,  
1897 2000; Worthington et al., 2006). The youngest magnetic anomalies associated  
1898 with the Osbourn Trough is as young as Anomalies 33 (~79 Ma) or 32 (~71 Ma)  
1899 (Billen and Stock, 2000) or during Anomaly 34 (~84 Ma) but prior to ~87 Ma  
1900 (Downey et al., 2007). Based on the age range allowed from the magnetic  
1901 anomaly interpretation and the age constraints on the initiation of spreading  
1902 between the Pacific and Antarctic plate to the south, Müller et al. (2008b)  
1903 suggested that the spreading along the Osbourn Trough ceased at 85 Ma, leading  
1904 to a final jump in the plate boundary to the south along the present day Pacific-  
1905 Antarctic ridge.

1906

1907 The plateau break-up model (Taylor, 2006) suggests that the Ontong Java  
1908 Plateau, Manihiki and Hikurangi Plateaus were joined at the time of their  
1909 eruption. This mega-LIP erupted around Aptian time based on the dating of  
1910 sediment overlying pillow basalts (Winterer et al., 1974) and Ar/Ar dating  
1911 (Mahoney et al., 1993). Taylor (2006) based his interpretation on recently  
1912 collected marine geophysical data from the Ellice Basin, which he believes was

1913 formed during the separation of the Ontong Java and Manihiki Plateau and  
1914 confirmed by Chandler et al. (In Review). In the Taylor (2006) model, the Nova-  
1915 Canton Trough is interpreted as an extension of the Clipperton Fracture Zone  
1916 (Joseph et al., 1990; Larson et al., 1972; Taylor, 2006) based on side-scan sonar  
1917 data (Joseph et al., 1992) and not an abandoned spreading ridge. The disturbed  
1918 “rift zone” identified by Larson (1997) is instead interpreted as the northern part  
1919 of an E-W directed spreading system with stair-stepped, large offset E-W  
1920 trending fracture zones and N-S abyssal hill fabric (Taylor, 2006) separating the  
1921 Ontong Java and Manihiki Plateaus. This model suggests that after M0 (~120  
1922 Ma), the tectonic regime changed from N-S directed Pacific-Phoenix spreading to  
1923 E-W directed spreading between the Pacific plate and a new Manihiki plate.  
1924 Coincidentally, N-S directed spreading was occurring between the Manihiki and  
1925 Hikurangi plateaus, as suggested in the previous model. The differential motion  
1926 between the two spreading systems requires a triple junction between the  
1927 Pacific, Manihiki and Hikurangi plates (Taylor, 2006). The timing of plateau  
1928 break-up is unconstrained from the seafloor spreading record as no magnetic  
1929 anomalies can be interpreted. However, rift structures on the eastern side of the  
1930 Ontong Java plateau and western margin of the Manihiki plateau suggest that this  
1931 occurred around 120 Ma, matching well with the dated break-up of the Manihiki  
1932 and Hikurangi plateaus. Further supporting the common origin of the Ontong  
1933 Java, Manihiki and Hikurangi Plateaus is similar geochemical compositions  
1934 between the three plateaus suggested a related source (Hoernle et al., 2010;  
1935 Mahoney et al., 1993)

1936

1937 The other main feature on the seafloor attributed to Pacific-Phoenix spreading is  
1938 the Tongareva triple junction trace in the SW Pacific (Larson et al., 2002; Viso et  
1939 al., 2005; (Pockalny et al., 2002). The Tongareva triple junction trace is a roughly  
1940 NNW-SSE linear feature which starts at the northeastern corner of the Manihiki  
1941 Plateau in the Pernyn Basin and extends to west of the Cook Islands before it  
1942 changes trend to NW-SE until it reaches spreading associated with Pacific-  
1943 Antarctic Ridge (Figure 11). The western side of the triple junction trace  
1944 consists of ENE trending abyssal hill topography and directly east, the  
1945 morphology is NNW-SSE trending (Larson et al., 2002; Pockalny et al., 2002).

1946 This lineament is believed to record the migration of a ridge-ridge-ridge triple  
1947 junction between the Pacific-Farallon-Phoenix plates (Larson et al., 2002)  
1948 whereas more detailed analysis revealed that the triple junction likely flipped  
1949 between ridge-ridge-ridge and ridge-ridge-transform configurations throughout  
1950 its evolution (Pockalny et al., 2002). Sutherland and Hollis (2001) suggested that  
1951 this lineament was a rift but this has been refuted by subsequent studies (e.g.  
1952 (Larson et al., 2002). The eastern margin of the Manihiki Plateau comprises a  
1953 dramatic transtensional scarp (Stock et al., 1998; Winterer et al., 1974)  
1954 suggesting that the easternmost portion of a presumably larger Manihiki Plateau  
1955 was rifted off the margin and was controlled by the plate motions related to the  
1956 triple junction. Larson et al. (2002) hypothesized that a piece travelled across  
1957 Panthalassa on the Farallon plate and another piece rifted to the south with the  
1958 Phoenix plate. The timing for activity along the triple junction is poorly  
1959 constrained. Spreading is believed to have initiated around 120 Ma, based on the  
1960 dating of carbonate sedimentation on the Manihiki Plateau (Larson et al., 2002)  
1961 with termination around 84 Ma (Larson et al., 2002).

1962

1963 Our model for the evolution of the Phoenix plate incorporates simple N-S  
1964 directed spreading in the Mesozoic followed by a major plate reorganization at  
1965 ~120 Ma (M0) coincident with the eruption of the Ontong Java-Manihiki-  
1966 Hikurangi plateau as one mega-LIP, as suggested by Taylor (2006) and Chandler  
1967 et al. (In Review) (Figure 10). This spreading system shuts down at 86 Ma, after  
1968 which spreading was accommodated along the Pacific-Farallon and Pacific-  
1969 Antarctic Ridges (Figure 10 and 12).

1970

1971 The Mesozoic lineations are constrained by magnetic anomaly identification  
1972 from Munsch et al. (1996), with geophysical data (including satellite derived  
1973 gravity data) constraining the location of the Osbourn Trough, Nova Canton  
1974 Trough and Tongareva triple junction trace. Our seafloor spreading isochrons  
1975 match the magnetic anomaly grid quite well for the central and western part of  
1976 the Mesozoic lineations but there is a poor match to the east corresponding to  
1977 the fan-shaped Magellan and Mid-Pacific Mountain lineations (Figure 6 and 11).  
1978 We do not reconstruct these complex lineation sets due to a lack of age

1979 constrains on initiation and cessation of the microplates at the Pacific-Phoenix-  
1980 Farallon triple junction that would have formed these lineations. In addition, our  
1981 aim is to model the broad scale development/larger plates of the area rather  
1982 than the smaller scale microplates. Finite rotations are derived for the E-W  
1983 trending M-series anomalies by using the half-stage pole methodology and  
1984 following the fracture zones traced from satellite gravity data (Sandwell and  
1985 Smith 2009).

1986

1987 Our reconstructions are based on the model of Taylor (2006) and Chandler et al.  
1988 (In Review) with roughly E-W directed spreading forming the crust underlying  
1989 the Ellice Basin between the Ontong Java and Manihiki Plateaus and  
1990 simultaneous rifting of the Manihiki and Hikurangi plateaus from a N-S directed  
1991 spreading system along the Osbourn Trough. We initiate this spreading system  
1992 at 120 Ma, corresponding to the timing of the LIP eruption and the dating of rift-  
1993 related sequences along the margin. The oceanic crust between these plateaus  
1994 formed during the CNS so no correlations can be observed in the magnetic  
1995 anomaly grids (Figure 11). However, the satellite derived gravity data indicates  
1996 fracture zone trends and limited abyssal hill fabric. We derive our own finite  
1997 rotations for the opening of the Osbourn Trough region by following fracture  
1998 zone traces. The separation of the mega-LIP requires that a triple junction was  
1999 active accommodating motion between the Ontong Java and Hikurangi Plateaus  
2000 during its formation. We reconstruct the arm of the triple junction based on the  
2001 finite difference method.

2002

2003 We suggest a further two triple junctions were located to the east of the Manihiki  
2004 Plateau, one of which formed the Tongareva triple junction trace. However,  
2005 unlike previous interpretations (Larson et al., 2002; Viso et al., 2005), we suggest  
2006 that the triple junction represented spreading between the Manihiki, Hikurangi  
2007 and a new plate we term the Chasca plate to the east of the Manihiki and  
2008 Hikurangi plates (Figure 10). The Chasca plate, which was located off the South  
2009 American margin, is named after the Incan goddess of dawn and twilight. Our  
2010 finite rotations we derived by using a combination of fracture zone and triple  
2011 junction traces and the finite difference method. A second triple junction

2012 between the Hikurangi, Manihiki and a new plate we term the Catequil plate was  
2013 required to account for the trends in the seafloor fabric to the west of the  
2014 Tongareva triple junction trace. The Catequil plate is named after the Incan god  
2015 of thunder and lightning.

2016

2017 The fracture zone traces between the Manihiki and Hikurangi Plateau show a  
2018 change in direction but this change has never been dated. We hypothesize that  
2019 the date of the change in spreading direction occurred at 100 Ma as this  
2020 corresponds to a time when the fracture zones in other parts of the Pacific  
2021 change direction as well as a change in the bend of Pacific hotspots. In addition,  
2022 a clockwise change in spreading direction between the Manihiki and Hikurangi  
2023 plates at 100 Ma leads to a change in the plate boundary east of Australia from  
2024 convergence to strike-slip, coincident with a change from subduction related  
2025 tectonics to passive margin formation and extension. A further refinement of the  
2026 plate kinematic model for the plateau break-up using improved gravity and  
2027 vertical gravity gradient grids is presented in Chandler et al. (In Review).

2028

2029 The cessation of spreading along all arms of our triple junctions has been dated  
2030 based on the timing of collision between the Hikurangi Plateau and the Chatham  
2031 Rise. As stated previously, there are two competing models for the timing of  
2032 collision. We implement the docking of the Hikurangi Plateau to the Chatham  
2033 Rise at 86 Ma based on the evidence presented in Worthington et al. (2006)  
2034 related to a major episode of metamorphism and garnet growth in the Alpine  
2035 Schist (Vry et al., 2004) and the seafloor spreading constraints presenting in  
2036 Billen and Stock (2000). The docking led to the shut-down of the seafloor  
2037 spreading system in the South Pacific and a change in the east Australian margin  
2038 from strike-slip to convergence (Figure 12). After the cessation of spreading, the  
2039 spreading ridge jumped to the south to initiate rifting and seafloor spreading  
2040 between the Pacific and Antarctic plates. An earlier timing for docking of the  
2041 Hikurangi Plateau requires that rifting and seafloor spreading between the  
2042 Pacific and Antarctic plates started earlier than observed or that there were two  
2043 contemporaneous spreading ridges located in close proximity in the South  
2044 Pacific. It would also require fast seafloor-spreading rates between the Manihiki

2045 and Hikurangi plateaus not supported by the seafloor morphology. To the east,  
2046 the Pacific-Farallon Ridge extended to the south connecting up with the Pacific-  
2047 Antarctic Ridge at the Pacific-Antarctic-Farallon triple junction.

2048

### 2049 3.2.3.1 Pacific-Antarctic Spreading

2050 The Pacific-Antarctic Ridge and associated ocean floor dominates the South  
2051 Pacific (Figure 13) and forms a crucial link in the global plate circuit. Early  
2052 reconstructions of the South Pacific recognised that spreading between the  
2053 Pacific and the Antarctic/Marie Byrd Land margin involved at least a three-plate  
2054 system, this third plate was named the Bellinghausen plate and located east of  
2055 the Marie Byrd Land seamounts (Eagles et al., 2004a, b; Stock and Molnar, 1987).  
2056 Rifting between the Chatham Rise and Antarctica/Marie Byrd Land is believed to  
2057 have occurred at 90 Ma (Eagles et al., 2004a; Larter et al., 2002) with the  
2058 initiation of spreading between the Pacific and Bellinghausen plates at Anomaly  
2059 33r (83.0 - 79.1 Ma) (Larter et al., 2002; Stock and Molnar, 1987)  
2060 contemporaneous with Pacific-Antarctic/Marie Byrd Land spreading (Cande et  
2061 al., 1982; Cande et al., 1995; Croon et al., 2008; Larter et al., 2002; Mayes et al.,  
2062 1990; Molnar et al., 1975; Stock and Molnar, 1987) or 80 Ma for Bellinghausen  
2063 spreading (Eagles et al., 2004a, b). Spreading between the Campbell Plateau and  
2064 Marie Byrd Land occurred from Anomaly 33r (83.0 - 79.1 Ma) (Eagles et al.,  
2065 2004a; Larter et al., 2002). The cessation of the Bellinghausen plate as an  
2066 independent plate and its accretion onto the Pacific plate was initially believed to  
2067 have occurred at Anomaly 25 (~56 Ma) (Stock and Molnar, 1987), but this was  
2068 revised to Anomaly 27 (~61 Ma) during a time of major plate reorganization  
2069 (Cande et al., 1995). Cande et al. (1995) also found that any relative motion  
2070 between the Bellinghausen and Antarctic plates was much smaller than  
2071 previously thought.

2072

2073 New finite rotations based on the improved South Pacific dataset were computed  
2074 for spreading between the Pacific and Antarctic plates from Anomaly 27 (~61  
2075 Ma) to the present day (Cande et al., 1995) and were used in the detailed model  
2076 of Eagles et al. (2004). Spreading between the Pacific and Antarctic plates  
2077 occurred as a two-plate system with major changes in spreading direction

2078 recorded between Chron 27 (~61 Ma) and 20 (~43 Ma), between Chrons 13  
2079 (~33 Ma) and 6C (~24 Ma) and at Chron 3a (~6 Ma) (Cande et al., 1995; Croon et  
2080 al., 2008). A recent update of the seafloor spreading history between the Pacific  
2081 and Antarctic plates (Croon et al., 2008) is in general agreement with the model  
2082 of Cande et al. (1995) for times 61 Ma to 12.3 Ma, but the model and rotations  
2083 differ slightly for younger times.

2084

2085 To construct our seafloor spreading isochrons between the Pacific and Antarctic  
2086 plates, we used the magnetic anomaly pick identifications and finite rotations of  
2087 Cande et al. (1995) for times from 61 Ma to the present day, which are also used  
2088 in the model of Eagles et al. (2004). Croon et al. (2008) provides updated  
2089 rotations for times younger than 12.3 Ma but they are not incorporated into our  
2090 model. As noted by Croon et al. (2008) the effect of using these rotations on  
2091 motion between the Pacific and western North America is small and hence will  
2092 not significantly alter Pacific plate motion. We anticipate that these rotations  
2093 will be included in the next generation of our global plate tectonic model. For  
2094 times between 61 Ma and 83.5 Ma, we followed the magnetic anomaly  
2095 interpretation and finite rotations of Larter et al. (2002) for Pacific-  
2096 Antarctic/Marie Byrd Land spreading and Pacific-Bellinghausen spreading. We  
2097 assigned an age of 90 Ma for the Antarctic margin conjugate to the Chatham  
2098 Plateau to reflect the initiation of rifting and an age of 80 Ma for the onset of  
2099 spreading between the Campbell Plateau and Antarctic margins. Validating the  
2100 shape and location of our seafloor spreading isochrons in this region using the  
2101 magnetic grid compilation is difficult due to the paucity of data available in this  
2102 region (Figure 13). Some magnetic lineations can be identified adjacent to the  
2103 Campbell Plateau and clearly reflect a clockwise change in spreading direction  
2104 between Anomalies 31 (~68 Ma) and 25 (~56 Ma) consistent with our  
2105 isochrons.

2106

### 2107 ***3.3 Tethys/Indian Ocean***

2108 The present day Indian Ocean comprises five main plates: the Indo-Australian,  
2109 Antarctic, African, Somali and Arabian plates (Figure 1 and 14). In addition, the  
2110 Indo-Australian plate is often subdivided into three plates: the Australian, Indian

2111 and Capricorn plates along a zone of diffuse deformation in the East Indian  
2112 Ocean (Demets et al., 1994; Royer et al., 1997; Weissel et al., 1980) (Figure 1 and  
2113 14). Several smaller plates exist along the East African margin associated with  
2114 continental rifting and diffuse deformation, including the proposed Nubian and  
2115 Lake Victoria plates (Bird, 2003; Lemaux et al., 2002). Prior to Gondwana break-  
2116 up and the opening of the Indian Ocean, a now entirely vanished ocean basin, the  
2117 Tethys Ocean, existed between Gondwana and Laurasia. The evidence for this  
2118 ocean basin is primarily preserved in the terranes and ophiolite complexes along  
2119 southern Eurasia and the Mediterranean. The Indian Ocean preserves a record  
2120 of the early break-up history of Gondwana along the East African, Antarctic and  
2121 West Australian passive margins. An extensive mid ocean ridge network  
2122 developed separating India, Antarctica, Australia, Madagascar and Africa. In  
2123 addition, a long-lived subduction zone to the north consumed oceanic  
2124 lithosphere from the Tethys Ocean eventually leading to the uplift of the  
2125 Himalayas resulting from the collision of the Indian continent with southern  
2126 Eurasia.

2127

2128 Detailed reconstructions of the Indian Ocean as they currently stand are  
2129 problematic, leading to gaps and overlaps in full-fit reconstructions, motions of  
2130 continental blocks that are inconsistent with independently modeled motions of  
2131 neighboring plates and not strongly constrained by geological observations. A  
2132 concerted international collaborative effort is currently underway to update  
2133 reconstructions for the entire Indian Ocean with completion expected by early  
2134 2013. Our current model is an amalgamation of a number of published models  
2135 for different portions of the Indian Ocean. We will begin by describing the early  
2136 break-up history of Gondwana and formation of the Indian Ocean followed by  
2137 the Cenozoic-recent opening. Lastly we will discuss our current model for the  
2138 inferred opening and closure history of the Tethys Ocean.

2139

### 2140 *3.3.1 East African Margins*

2141 The break-up of Gondwana initiated in the early Jurassic between West  
2142 Antarctica, Africa and Madagascar following a long period of rifting along the  
2143 Permo-Triassic Karoo Rift and eruption of the Karoo Volcanics during the early

2144 Jurassic (around 185-180 Ma) (Cox, 1992; Forster, 1975; Jourdan et al., 2005;  
2145 Reeves, 2000; Storey et al., 2001) (Figure 14). The cessation of volcanism along  
2146 the Karoo Rift led to a seaward jump in the locus of rifting, initiating  
2147 contemporaneously between Africa and Antarctica in the Mozambique Basin and  
2148 Riiser-Larson Sea (Eagles and König, 2008; Marks and Tikku, 2001; Simpson et  
2149 al., 1979) and Africa and Madagascar in the West Somali Basin (Hankel, 1994;  
2150 Smith and Hallam, 1970) and either contemporaneously or earlier between  
2151 Africa and West Antarctica in the Weddell Sea (König and Jokat, 2006; Livermore  
2152 and Hunter, 1996).

2153

2154 Separation between Africa and Antarctica/Madagascar forming the Mozambique  
2155 Basin, Riiser-Larson Sea and West Somali Basin is believed to have initiated in  
2156 the early-mid Jurassic supported by the stratigraphy and pre-rift structures  
2157 along the conjugate margins (Bunce and Molnar, 1977; Coffin and Rabinowitz,  
2158 1987; Lawver and Scotese, 1987; Müller et al., 2008b; Norton and Sclater, 1979;  
2159 Reeves, 2000; Scrutton et al., 1981; Ségoufin and Patriat, 1980; Smith and  
2160 Hallam, 1970). The transition from continental rifting to seafloor spreading is  
2161 believed to have occurred either at 183-177 Ma based on Eagles and König  
2162 (2008) full-fit reconstruction, 170 Ma (Müller et al., 1997; Reeves and de Wit,  
2163 2000), 167 Ma (König and Jokat, 2006) or 165 Ma based on matching tectonic  
2164 sequences in Africa and East Antarctica (Coffin and Rabinowitz, 1987; Livermore  
2165 and Hunter, 1996; Marks and Tikku, 2001). Early full-fit reconstructions place  
2166 Madagascar west of the Gunnerus Ridge (Royer and Coffin, 1992) whereas most  
2167 recent studies place Madagascar to the east (Eagles and König, 2008; Marks and  
2168 Tikku, 2001) thereby eliminating overlap issues between Antarctica and  
2169 Madagascar.

2170

2171 The oldest identified magnetic anomalies interpreted in the Mozambique and  
2172 West Somali Basins and Riiser-Larson Sea are Anomalies M25-M24 (~154-152  
2173 Ma) (Coffin and Rabinowitz, 1987; Jokat et al., 2003a; Marks and Tikku, 2001;  
2174 Rabinowitz et al., 1983; Roeser et al., 1996; Ségoufin and Patriat, 1980).  
2175 However, some have inferred Jurassic Quiet Zone crust between the oldest  
2176 magnetic anomalies and the continental slope (Coffin and Rabinowitz, 1987)

2177 possibly as old as M40 (~166 Ma) (Gaina et al., 2010). Spreading in all basins  
2178 was directed N-S for most of the opening history, confirmed through the  
2179 interpretation of fracture zones, (Heirtzler and Burroughs, 1971), but a NNE-  
2180 SSW direction can also be seen in the older oceanic crust fabric. Paleomagnetic  
2181 (McElhinny et al., 1976), seismic and gravity anomaly data (e.g. (Bunce and  
2182 Molnar, 1977; Coffin and Rabinowitz, 1987; Coffin and Rabinowitz, 1988;  
2183 Rabinowitz, 1971; Storey, 1995) support the southward motion of Madagascar  
2184 relative to Africa during the Jurassic and Early Cretaceous.

2185

2186 The spreading histories of the Mozambique/Riiser-Larson Sea and the West  
2187 Somali Basin diverge at about M10 (~130-132 Ma). Spreading in the West  
2188 Somali Basin ceased either at M10 (~130-132 Ma) (Coffin and Rabinowitz, 1987;  
2189 Eagles and König, 2008; Rabinowitz et al., 1983) or M0 (~120 Ma) (Cochran,  
2190 1988; Marks and Tikku, 2001; Müller et al., 1997; Müller et al., 2008a; Ségoufin  
2191 and Patriat, 1980) depending on the magnetic anomaly identification used. After  
2192 the cessation of spreading, the mid-ocean ridge jumped southward initiating  
2193 spreading in between Madagascar and Antarctica. The timing of the southern  
2194 ridge jump and seafloor spreading history in the surrounding Enderby Basin and  
2195 Weddell Sea has major implications for the plate boundary configurations in the  
2196 Mesozoic Indian Ocean. For example, the model of Eagles and König (2008)  
2197 infers a southward ridge jump from the West Somali Basin at M10 (~130-132  
2198 Ma) transferred Madagascar to the African plate and initiated spreading in the  
2199 Enderby Basin. In this model Madagascar did not act as an independent plate  
2200 throughout any of its Mesozoic-Cenozoic history. Other models propose that  
2201 Madagascar must have acted independently, at least for part of its history (e.g.  
2202 (Marks and Tikku, 2001)). The mid-ocean ridge which formed the Mesozoic  
2203 magnetic lineations in the Mozambique Basin/Riiser-Larson Sea continued  
2204 throughout the Cenozoic eventually becoming the Southwest Indian Ridge where  
2205 highly oblique, ultra-slow seafloor spreading is occurring (Patriat and Ségoufin,  
2206 1988; Royer et al., 1988).

2207

2208 The final break-up of Gondwana continental blocks occurred with the separation  
2209 of Madagascar and India forming the Mascarene Basin. Previous interpretations

2210 of the area suggest that rifting initiated in the late Cretaceous (Norton and  
2211 Sclater 1979; Masson 1984; (Bernard and Munschy, 2000) with the oldest  
2212 magnetic anomaly identified being Anomaly 34 (~84 Ma) or 33 (~79 Ma). A  
2213 major change to NE-SW spreading is recorded in the fracture zones and magnetic  
2214 lineations around Anomaly 31 (~68 Ma) (Bernard and Munschy, 2000). Part of  
2215 the Mascarene Ridge jumped northward isolating the Seychelles microcontinent  
2216 (Masson, 1984). The model of Bernard and Munschy (2000) suggests  
2217 contemporaneous spreading between the easternmost part of the Mascarene  
2218 Basin and spreading to the north between the Seychelles and Laxmi Ridge,  
2219 implying a cessation of spreading in the Mascarene Basin as late as Anomaly 27  
2220 (~61 Ma). The oldest identified magnetic lineation between the Seychelles and  
2221 Laxmi Ridge in the East Somali and West Arabian Basin is Anomaly 28 (~63 Ma)  
2222 (Collier et al., 2008; Masson, 1984) based on the dating of syn-rift volcanics  
2223 offshore from the Seychelles (Collier et al., 2008) or Anomaly 27 (~61 Ma)  
2224 (Chaubey et al., 1998) defining the initiation of spreading along the Carlsberg  
2225 Ridge.

2226

2227 We have adopted a model for East Africa whereby pre-breakup margin extension  
2228 was initiated at 180 Ma as a response to thermal weakening by the eruption of  
2229 the Karoo flood basalts. We initiate seafloor spreading at 160 Ma along the  
2230 entire East Africa margin after the cessation of rifting in the Karoo Rift, about 5  
2231 million years before the last confidently dated magnetic anomaly, M25 (~154  
2232 Ma) (Figure 15). We connect the rift to the mid-ocean ridge that developed  
2233 between Patagonia and Southern Africa (Torsvik et al., 2009) and Weddell Sea to  
2234 the southwest and to a transform in the Tethys to the northeast (Figure 14 and  
2235 15). The identification of magnetic anomalies and fracture zone trends is  
2236 difficult in the area due to thick sediment cover and volcanic overprinting.

2237 Weakly trending magnetic lineations observed in the magnetic anomaly grid  
2238 confirm the N-S directed spreading direction (Figure 14). We adopt the model  
2239 for the cessation of spreading in the West Somali Basin shortly after M0 (~120  
2240 Ma) and not at M10 (~131 Ma) as suggested by Eagles and Konig (2008). The  
2241 cessation of spreading at M10 (~131 Ma) results in the position of Africa relative  
2242 to Madagascar and Antarctica that is incompatible with newly interpreted

2243 aeromagnetic data in the area (König and Jokat, 2010). After the cessation of  
2244 spreading, we implement a southward ridge jump towards the site of  
2245 Madagascar Ridge and Conrad Rise eruption. Our model implies that  
2246 Madagascar operated as an independent plate from 144-115 Ma, based on our  
2247 interpretation of the West Somali Basin. Spreading in the Mozambique/Riiser-  
2248 Larson Sea continued unabated throughout the Mesozoic and along the  
2249 Southwest Indian Ridge to the present day.

2250

2251 Our model for the separation of Madagascar and India is similar to that  
2252 presented in Masson (1984) and Müller et al. (1997). Although the oldest  
2253 magnetic anomaly identified is Anomaly 34 (~84 Ma), we initiate rifting at 87  
2254 Ma, preceded by a period of strike-slip motion between India and Madagascar. A  
2255 major change in spreading direction occurred at Anomaly 31 (~68 Ma) to NE-SW  
2256 spreading based on an interpretation of the fracture zone trends in the basin.  
2257 Spreading in the Mascarene Basin ceased at 64 Ma resulting in a northward ridge  
2258 jump and initiation of spreading between India and the Seychelles  
2259 microcontinent forming the crust in the East Somali and West Arabian Basins.  
2260 However, spreading may have continued to at least Anomaly 27 (~61 Ma) in the  
2261 eastern Mascarene Basin (Bernard and Munsch, 2000). The spreading ridge  
2262 between the Seychelles to the south and Laxmi ridge to the north (Carlsberg  
2263 Ridge) is modeled based on triple junction closure with India and Arabia. The  
2264 Carlsberg Ridge connected with the Central Indian Ridge to the southeast and the  
2265 Sheba Ridge via a series of large offset transform faults to the northwest. The  
2266 Sheba Ridge separates Arabia from Africa/Somalia, which we initiate at 20 Ma to  
2267 coincide with the initiation of the East African Rift. The Sheba Ridge propagated  
2268 into the Red Sea at 15 Ma.

2269

### 2270 *3.3.2 Antarctic Margin*

2271 The Antarctic margin bordering the Indian Ocean involves at least four distinct  
2272 spreading phases, including (from west to east): the Weddell Sea opening  
2273 between West Antarctica and South America, the Riiser-Larson Sea between  
2274 Antarctica and Africa (conjugate to the Mozambique Basin), the Enderby Basin

2275 between Antarctica and India/Elan Bank and the Southern Ocean between  
2276 Antarctica and Australia (Figure 13 and 14).  
2277  
2278 The opening of the Weddell Sea is believed to have initiated as a three-plate  
2279 system between Antarctica, South America and Africa (Marks and Tikku, 2001),  
2280 or initially as a two-plate system with N-S directed spreading between South  
2281 America and Antarctica (Kovacs et al., 2002). The transition from seafloor  
2282 spreading to incipient spreading is believed to have occurred at ~167 Ma (König  
2283 and Jokat, 2006), 165 Ma (Livermore and Hunter, 1996; Marks and Tikku, 2001)  
2284 and 160 Ma (Ghidella et al., 2002; Müller et al., 2008a). The M-series magnetic  
2285 anomalies are difficult to identify but a recent study by König and Jokat (2006)  
2286 identified magnetic anomalies as old as M17 (~140 Ma) with seafloor spreading  
2287 believed to have initiated around M20 (~146 Ma), suggesting 15-20 million  
2288 years of rifting and continental stretching before the establishment of seafloor  
2289 spreading. Seafloor spreading was initially very slow, directed north-south  
2290 (König and Jokat, 2006). The Cenozoic magnetic anomalies are well-identified  
2291 (Kovacs et al., 2002; LaBrecque and Barker, 1981) eventually leading to the  
2292 establishment of the American-Antarctic Ridge (Figure 13). Due to subduction  
2293 starting in the Cretaceous, the entire northern plate involved in Weddell Sea  
2294 spreading has been subducted including parts of the Cenozoic crust from the  
2295 Antarctic (southern) plate.  
2296  
2297 Spreading in the Riiser-Larson Sea (conjugate to Mozambique Basin, west of the  
2298 Gunnerus Ridge), has been dated with a well-defined sequence from at least M24  
2299 (~152-153 Ma) (Jokat et al., 2003a; Roeser et al., 1996), although a recent  
2300 reinterpretation of magnetic anomalies suggest that magnetic anomalies as old  
2301 as M40 (~166 Ma) exist in both the Riiser-Larson and Mozambique Basins  
2302 (Gaina et al., 2010). The spreading system here continued into the Cenozoic to  
2303 the west and north of the Conrad Rise where Anomalies 34 (~83.5 Ma) to 28  
2304 (~63 Ma) have been identified (Goslin and Schlich, 1976; Royer and Coffin,  
2305 1992). This spreading ridge developed into the ultra-slow Southwest Indian  
2306 Ridge (Patriat and Ségoufin, 1988)

2307

2308 East of the Gunnerus Ridge and west of the Bruce Rise lies the Enderby Basin  
2309 (Figure 13) recording the opening and seafloor spreading history between  
2310 Antarctica and India. The paucity of data in the area and the identification of  
2311 magnetic anomalies sequences on the conjugate Indian side in the Bay of Bengal  
2312 and south of Sri Lanka has led to two alternative theories for the break-up of  
2313 Antarctica and India: 1. Break up and seafloor spreading during the CNS  
2314 (Banerjee et al., 1995; Jokat et al., 2010; Müller et al., 2000; Royer and Coffin,  
2315 1992), or 2. Break-up and seafloor spreading in the Mesozoic at 135 Ma with the  
2316 oldest identified magnetic anomaly being M11 (~132 Ma) (Desa et al., 2006;  
2317 Ramana et al., 2001; Ramana et al., 1994) or M9 (~129 Ma) (Gaina et al., 2007).  
2318 The model of Marks and Tikku (2001) tentatively identified anomalies M10Ny–  
2319 M1 (~132-121 Ma) in the West Enderby Basin, whereas the most recent model  
2320 of Jokat et al. (2010) for the West Enderby Basin suggests break-up between  
2321 India and Antarctica during the CNS (~90-118 Ma).

2322

2323 The Mesozoic spreading model implies contemporaneous opening with the well-  
2324 documented M-sequence anomalies (M10–M0; ~132-120 Ma) off the Perth  
2325 Abyssal Plain (Müller et al., 1998a; Powell et al., 1988). The model of Gaina et al.  
2326 (2007) further incorporates microcontinent formation (Elan Bank) due to one or  
2327 several ridge jumps associated with the Kerguelen Plume (Gaina et al., 2003;  
2328 Müller et al., 2000).

2329

2330 The area east of the Bruce Rise and Vincennes Fracture Zone and south of  
2331 Australia involves rifting, break-up and seafloor spreading between Antarctica  
2332 and Australia forming the Southern Ocean (Figure 13 and 14). The conjugate  
2333 Australia and Antarctic margins consist of a wide zone of highly extended  
2334 continental crust adjacent to a narrow zone of incipient oceanic crust formed by  
2335 slow to ultra-slow seafloor spreading. Continental rifting is believed to have  
2336 initiated at 165 Ma based on the dating of syn-rift sedimentary sequences within  
2337 the Australian rift basins and increased tectonic subsidence rates (Totterdell et  
2338 al., 2000) or 160 Ma (Powell et al., 1988). However, the nature of break-up and  
2339 transition to true seafloor spreading along the margin remains controversial

2340 (Sayers et al., 2001; Tikku and Cande, 1999). The timing of break-up is inferred  
2341 to be around 100 Ma based on the identification of seafloor spreading magnetic  
2342 anomalies adjacent to the margin (Cande & Mutter, 1982) or by extrapolation of  
2343 the spreading rate (Veevers et al., 1990), 135-125 Ma based on the relationship  
2344 between continental margin sequences and the oceanic crust from seismic data  
2345 (Stagg and Willcox, 1992) or 83.5 Ma based on the dating of the oldest magnetic  
2346 anomaly (Tikku and Cande, 1999; Whittaker et al., 2007), depending on how the  
2347 crust in the transition zone is defined. The oldest magnetic anomaly that can be  
2348 identified Anomaly 34 (~84 Ma) (Cande and Mutter, 1982; Tikku and Cande,  
2349 1999; Whittaker et al., 2007) but Anomalies 34 (~84 Ma) and 33 (~79 Ma) are  
2350 located in a zone of transitional crust (i.e. morphology not typical of abyssal hill  
2351 fabric), therefore Anomaly 32 (71 Ma) is often quoted as the oldest magnetic  
2352 anomaly to indicate true seafloor spreading. The direction of spreading has  
2353 previously been modeled as N-S, however a recent reanalysis of gravity and  
2354 magnetic anomaly profiles (Whittaker et al., 2007) suggests early seafloor  
2355 spreading (Anomalies 34-27; ~84-61 Ma) via NW-SE directed spreading.  
2356 Spreading developed into a N-S configuration and has continued to the present  
2357 day with a dramatic increase in spreading rate from Anomaly 13 (~33 Ma)  
2358 (Tikku and Cande, 1999).

2359

2360 We adopt a model for the Antarctic margins, which suggests contemporaneous  
2361 rifting in the Weddell Sea, Riiser-Larson Sea and the East African margins  
2362 starting in the late Jurassic, at 180 Ma, after the cessation of Karoo volcanism and  
2363 seaward jump in the locus of rifting. We model the opening of the Weddell Sea  
2364 based on Konig and Jokat (2006), with M20 (~146 Ma) corresponding to the  
2365 oldest oceanic crust in the area. Comparison of our seafloor spreading isochrons  
2366 with our magnetic anomaly compilation is difficult (Figure 13 and 14) due to the  
2367 lack of data coverage and weak magnetic anomaly signatures. Spreading  
2368 continued until the end of the CNS (83.5 Ma) when there was a reorganization of  
2369 the spreading ridge system leading to the establishment of spreading along the  
2370 American-Antarctic Ridge. This ultra-slow spreading system is currently  
2371 intersecting the Sandwich subduction zone, one of the few regions of the world  
2372 where an active mid ocean ridge is intersecting a subduction zone. The Mesozoic

2373 Weddell spreading centre connected with spreading in the Riiser-Larson  
2374 Sea/Mozambique Basin in a triple junction configuration.  
2375  
2376 Further east, we initiate rifting between Antarctica and India in the Enderby  
2377 Basin (central and eastern part) at 160 Ma to coincide with the initiation of  
2378 rifting between Australia and Antarctic, which has been well dated. We adopt  
2379 the Mesozoic seafloor spreading model in Gaina et al. (2007) using the finite  
2380 rotations that describe motion between Antarctica and the Elan Bank from Gaina  
2381 et al. (2003) for the central and eastern Enderby Basin. Here, seafloor spreading  
2382 initiated at 132 Ma with M9 (~129 Ma) corresponding to the oldest identified  
2383 magnetic anomaly. The initiation of spreading in the Enderby Basin results in  
2384 strike-slip motion between India and Madagascar of over 1000 km. A ridge jump  
2385 isolating the Elan Bank microcontinent occurred at 120 Ma coincident with the  
2386 eruption of the Kerguelen Plateau. For the Western Enderby Basin, we initiate  
2387 break-up during the CNS at around 118 Ma, consistent with the model of Jokat et  
2388 al. (2010).  
2389  
2390 We model a simple scenario for the rifting, break-up and seafloor spreading  
2391 history between Australia and Antarctica with rifting initiating at 165 Ma based  
2392 on the evidence presented in Totterdell et al. (2000) and break-up at 99 Ma  
2393 (Müller et al., 2000; Müller et al., 2008a). The rift boundary extended into the  
2394 Enderby Basin from 165 Ma and extended eastward to connect with the Western  
2395 Panthalassic subduction zone along eastern Australia. We incorporate the oldest  
2396 magnetic anomaly as Anomaly 34 (~83.5 Ma) based on the model of Tikku and  
2397 Cande (2000) with a N-S direction of spreading. We do not incorporate the NW-  
2398 SE early separation motion of Australia and Antarctica (Whittaker et al., 2007)  
2399 but anticipate that this will be incorporated in a future model. We use the  
2400 rotations and magnetic anomaly identifications of Muller et al. (1997) for  
2401 Anomalies 31-18 (~68-40 Ma) and Royer & Chang (1991) from Anomaly 18  
2402 (~40 Ma) to the present day. Our resultant seafloor spreading isochrons match  
2403 very well with the trends observed in our magnetic anomaly grid (Figure 13 and  
2404 14).  
2405

### 2406 3.3.3 *West Australian margins*

2407 The West Australian continental margin is an old, sediment-starved volcanic  
2408 continental margin, which formed as a result of multistage rifting and seafloor-  
2409 spreading during a late Paleozoic and early Mesozoic phase of East Gondwana  
2410 break-up (Baillie and Jacobson, 1995; Bradshaw et al., 1988; Veevers, 1988). The  
2411 area can be separated into four distinct zones: the Argo Abyssal Plain, alongside  
2412 the Browse and Roebuck (former offshore Canning Basin) basins, the Gascoyne  
2413 Abyssal Plain, alongside the Exmouth Plateau and the Northern Carnarvon Basin,  
2414 the Cuvier Abyssal Plain delimited by the Cape Range Fracture Zone (CRFZ) and  
2415 Wallaby-Zenith Fracture Zones (WZfZ), and includes the Southern Carnarvon  
2416 Basin, the Exmouth Sub-basin and the Wallaby and Zenith plateaus and the Perth  
2417 Abyssal Plain extending from the WZfZ to the Naturaliste Plateau in the south  
2418 (Figure 14).

2419

2420 Rifting in the Argo Abyssal Plain started around 230 Ma (e.g. (Müller et al.,  
2421 2005)) eventually leading to the separation of the West Burma block/Argoland  
2422 from the Australian continental margin. The transition from rifting to seafloor  
2423 spreading has been constrained by the dating of magnetic anomalies in the Argo  
2424 Abyssal Plain and through tectonic subsidence analysis along the margin. The  
2425 interpretation of magnetic lineations resolve that seafloor spreading initiated  
2426 immediately prior to Anomaly M26 (~155 Ma) (Fullerton et al., 1989; Heine and  
2427 Müller, 2005; Müller et al., 1998a; Sager et al., 1992) with NW-SE directed  
2428 spreading. Previous models have invoked a southward propagating ridge along  
2429 the Western Australian margin, which started in the Argo Abyssal Plain  
2430 progressing southward. Spreading in the Gascoyne and Cuvier Abyssal Plains  
2431 initiated at M10 (~132 Ma) (Falvey and Mutter, 1981; Fullerton et al., 1989;  
2432 Johnson et al., 1976, 1980; Larson, 1977; Müller et al., 1998a; Powell et al., 1988;  
2433 Sager et al., 1992) and marked the break-up between Australia and Greater  
2434 India. The model for the opening of the Argo Abyssal Plain presented in Heine et  
2435 al. (2005) differs from previous models and that of Robb et al. (2005) in that  
2436 spreading between the Argo and Gascoyne Abyssal Plains initiated almost  
2437 simultaneously with the same orientation. The model also invoked a landward  
2438 ridge jump at M13 (~136 Ma). Further southward, spreading in the Perth

2439 Abyssal Plain which records break-up between Australia and India occurred  
2440 around 132 Ma based on the mapping of magnetic anomalies (Müller et al.,  
2441 1998a; Veevers et al., 1985) and involved several seaward ridge jumps towards  
2442 the Kerguelan plume (Müller et al., 2000). However, the majority of the crust  
2443 may have formed during the CNS.

2444

2445 We adopt the model for the formation of the Argo and Gascoyne Abyssal Plains  
2446 following Heine and Müller (2005) which involves NW-SE oriented rifting of  
2447 West Burma from the northwestern margin of Australia at around 156 Ma  
2448 (Figure 16). The continent-ocean boundary along Australia's western margin is  
2449 from Heine and Müller (2005). Spreading continued until a landward ridge jump  
2450 at M13 (~136 Ma). We infer that the plate boundary connected with a Tethyan  
2451 spreading ridge located to the north of India/Greater India to the west and a  
2452 transform fault to the north (Figure 16). Our model invokes a southward  
2453 propagating ridge into the Cuvier and Perth Abyssal Plain at 132 Ma following  
2454 the models presented in Müller et al. (1998a) and Müller et al. (2000). The mid-  
2455 ocean ridge associated with spreading in the Perth Abyssal Plain formed a triple  
2456 junction with mid-ocean ridge opening the Enderby Basin (between East  
2457 Antarctica and India) (e.g. Gaina et al., 2007) and the Australia-Antarctic mid-  
2458 ocean ridge (Figure 16). The NW-SE directed spreading along the Western  
2459 Australian margin persisted until around 99 Ma. The fracture zones record a  
2460 dramatic change in trend from NW-SE to roughly N-S at around 99 Ma (Mihut  
2461 and Müller, 1998). The change to N-S spreading forms the oldest crust  
2462 associated with the Wharton Ridge/Wharton Basin. Seafloor spreading in the  
2463 Wharton Basin ceased at 43 Ma (Singh et al., 2010).

2464

### 2465 *3.3.4 Tethys Ocean*

2466 The Tethys Ocean represents a now largely subducted ocean basin that existed  
2467 between Gondwanaland and Laurasia and involves a history of successive  
2468 continental rifting events along the northern Gondwana margin, oceanic basin  
2469 formation and accretion of Gondwana-derived continental blocks onto the  
2470 southern Laurasian margin and Indochina/SE Asia. The majority of Tethyan  
2471 oceanic crust no longer exists due to long-lived subduction along the southern

2472 Eurasian margin, except in the Argo Abyssal Plain off NW Australia where a  
2473 fragment of in-situ oceanic crust recording the youngest Tethyan spreading  
2474 system is preserved (Fullerton et al., 1989; Heine and Müller, 2005). In addition,  
2475 the Ionian Sea and several basins in the eastern Mediterranean (e.g. Levant  
2476 Basin) may be floored by Mesozoic Tethyan oceanic crust (Müller et al., 2008b;  
2477 Stampfli and Borel, 2002), however identification of magnetic anomalies is  
2478 difficult. The limited amount of preserved in-situ oceanic crust of Tethyan origin  
2479 hampers our knowledge and understanding of the evolution and structure of the  
2480 Tethys ocean. Instead we primarily rely on the accreted terranes and sutures in  
2481 SE Asia, southern Eurasia, Arabia and throughout the Mediterranean and  
2482 southern and central Europe (e.g. (Metcalf, 1996; Stampfli and Borel,  
2483 2002)(Sengor, 1987) as they record the timing of continental block collision,  
2484 ophiolite emplacement, back-arc basin development and provide paleo-  
2485 latitudinal estimates of continental material derived from the northern  
2486 Gondwana margin.

2487

2488 Successive rifting events from the Gondwana margin have led to the subdivision  
2489 of the Tethys Ocean into several oceanic domains: the paleo- and neo- Tethys  
2490 (e.g. (Stampfli and Borel, 2002)) or the paleo-, meso- and neo-Tethys (Heine et  
2491 al., 2004; Metcalfe, 1996) (Figure 3a-d). The additional subdivision by Heine et  
2492 al. (2004) and Metcalfe (1996) stems from an alternative rift history for crust  
2493 that formed after the paleo-Tethys, which affects whether the Argo Abyssal Plain  
2494 is classified as part of the Tethys or Indian Ocean domains.

2495

2496 The paleo-Tethys formed after the initiation of rifting and seafloor spreading  
2497 between the European and Asian Hunic superterrane (e.g. North China,  
2498 Indochina, Tarim, Serindia, Bohemia) and the northern Gondwana margin  
2499 (Blakely, 2008; Metcalfe, 1996; Stampfli and Borel, 2002). The timing of passive  
2500 margin formation is dependent on the margin segment and ranges from  
2501 Ordovician/Silurian based on subsidence analysis in the western Tethys  
2502 (Stampfli, 2000; Stampfli and Borel, 2002) or the late/early Devonian based on  
2503 the Gondwana affinity of Devonian vertebrate faunas in the Hun superterrane  
2504 (Metcalf, 1996), Devonian to Triassic passive margin sequences along the

2505 southern margin of South China (Metcalf, 1996) and the dating of oceanic deep-  
2506 marine ribbon bedded cherts in the Chang-Rai region of Thailand (Metcalf,  
2507 1996; Sashida et al., 1993). The direction of spreading is uncertain due to the  
2508 lack of in-situ preserved crust, however the seafloor spreading model of Stampfli  
2509 and Borel (2002) invokes NE-SW directed spreading orthogonal to the inferred  
2510 margin. The passage of the Hunic superterrane from south to north was  
2511 facilitated by northward-dipping subduction along the southern Eurasian  
2512 margin. The Hunic superterrane accreted to the southern Laurasian margin  
2513 diachronously in the Carboniferous-Permian (Stampfli and Borel, 2002). The  
2514 cessation of spreading in the paleo-Tethys is difficult to establish, however most  
2515 modelers agree the paleo-Tethys spreading ridge jumped southward along the  
2516 northern Gondwana margin and initiated the rifting of a new continental sliver  
2517 from the Gondwana margin (e.g. (Blakely, 2008; Metcalf, 1996; Stampfli and  
2518 Borel, 2002)) after the accretion of the Hunic superterrane.

2519

2520 The second main phase of rifting isolated the Cimmerian terrane from the  
2521 Gondwana margin some time in the Pennsylvanian-early Permian (Metcalf,  
2522 1996; Stampfli and Borel, 2002), constrained by changes in biota (Shi and  
2523 Archbold, 1998) and evidence of rifting on the northwest shelf of Australia  
2524 (Falvey and Mutter, 1981; Müller et al., 2005), northern Pakistan and  
2525 Afghanistan (Boulin, 1988; Pogue et al., 1992) and Iran (Stocklin, 1974). The  
2526 Cimmerian terrane comprises elements including Sibumasu (Sino-Burma-  
2527 Malaya-Sumatra continental sliver), Qiangtang (North Tibet), Helmand  
2528 (Afghanistan), Iran and possibly Lhasa/South Tibet (Figure 18a). The ocean  
2529 basin that formed between the Gondwana margin to the south and the  
2530 Cimmerian terrane is labeled as the meso-Tethys in the models of Metcalf  
2531 (1996) and Heine et al. (2004) but the neo-Tethys for most other models.  
2532 Continued northward-dipping subduction of paleo-Tethys oceanic lithosphere  
2533 along southern Laurasia carried the Cimmerian terrane northward, leading to its  
2534 accretion and closure of the paleo-Tethys ocean starting in the late Triassic  
2535 (Blakely, 2008; Golonka et al., 2006; Metcalf, 1996; Stampfli and Borel, 2002).  
2536 Accretion is constrained by the Cimmerian orogeny in present-day Iran, which  
2537 initiated in the late Triassic (Hassanzadeh et al., 2008; Sengor, 1987; Stampfli

2538 and Borel, 2002), the collision of Sibumasu/Malaya to Indochina by 250-220 Ma  
2539 (Golonka, 2007; Metcalfe, 1999; Stampfli and Borel, 2002) and 200-160 Ma for  
2540 other elements including Qiangtang (North Tibet) and Helmand (Stampfli and  
2541 Borel, 2002). The accretion of South Tibet varies from 200-160 Ma (Stampfli and  
2542 Borel, 2002), 150 Ma (Golonka et al., 2006) and 120 Ma related to a separate  
2543 episode of accretion (Metcalfe, 1996).

2544

2545 Following closure of the paleo-Tethys and accretion of the Cimmerian terrane,  
2546 several back-arc basins opened as a response to slab-pull forces along the  
2547 Tethyan subduction zone. The major back-arc complexes include the Pindos,  
2548 Maliac, Meliata, Küre, Sangpan, Kudi, Vardar (Stampfli and Borel, 2002) and the  
2549 early Cretaceous Taurus, Troodos, Hatay and Baer-Bassit ophiolite complexes  
2550 (Whitechurch et al., 1984). The closure of these back-arc basins varied along the  
2551 margin from Triassic to Cenozoic (Stampfli and Borel, 2002), with a date of ~70-  
2552 65 Ma for the obduction of the Taurus, Troodos, Hatay and Baer-Bassit ophiolite  
2553 complexes (Whitechurch et al., 1984) and an early Cenozoic age of obduction for  
2554 the Pindos and Vardar back-arc basins (Stampfli and Borel, 2002). As these  
2555 back-arc basins opened and closed, inferred NE-SW directed spreading  
2556 continued in the meso-Tethys (or neo-Tethys ocean) orthogonal to the  
2557 Gondwana rifted margin (Stampfli and Borel, 2002). The cessation of spreading  
2558 in the meso- or neo-Tethys is difficult to ascertain. However, Stampfli and Borel  
2559 (2002) postulate that the subduction of the mid-ocean ridge diachronously  
2560 across the margin can be tied to the initiation of rifting of the Argoland  
2561 Block/West Burma from the northwest shelf of Australia, thus timing the  
2562 cessation of spreading in the meso-/neo-Tethys ocean.

2563

2564 The initiation of a third phase of rifting along the northern Gondwana margin  
2565 initiated along the northwest shelf of Australia in the late Triassic (Müller et al.,  
2566 2005). The models of Heine et al. (2004) and Metcalfe (1996) label the resultant  
2567 ocean basin as the neo-Tethys as their models extend the Argo Abyssal Plain  
2568 mid-ocean ridge north of Greater India. Hence, this ocean basin forms part of the  
2569 Tethys ocean domain. However, most other studies associate the Argo Abyssal  
2570 Plain with the Indian Ocean because they follow the Argo spreading ridge

2571 southward between India and Australia, thus representing earliest Indian Ocean  
2572 spreading. The preserved seafloor spreading record in the Argo Abyssal Plain  
2573 confirms that spreading initiated around 156 Ma leading to the separation of the  
2574 West Burma Block from the northwest Australian margin (Heine and Müller,  
2575 2005). The model of Metcalfe (1996) suggests that Lhasa (South Tibet) also  
2576 rifted off the northern margin of Greater India at the time. Spreading in the Argo  
2577 Abyssal Plain is described in the Indian Ocean section of this paper. The West  
2578 Burma Block was carried northward due to continuing subduction along the  
2579 northern Tethyan margin and sutured to Sibumasu in the Cretaceous around 80  
2580 Ma (Heine and Müller, 2005; Lee and Lawver, 1995; Metcalfe, 1996)

2581

2582 The termination of spreading in the Tethys Ocean is controversial. The model of  
2583 Stampfli and Borel (2002) suggests cessation of spreading in the early  
2584 Cretaceous when the meso- or neo-Tethys spreading ridge intersected the  
2585 Tethyan subduction zone. However, other models (Heine and Müller, 2005;  
2586 Heine et al., 2004; Metcalfe, 1996) suggests that neo-Tethyan spreading  
2587 continued through the Cretaceous, merging into the Wharton Basin spreading  
2588 ridge from the end of the CNS to 43 Ma (Heine et al., 2004). The final closure of  
2589 the Tethys Ocean started with the collision of Greater India to the southern  
2590 Eurasian margin either around 55 Ma (Lee and Lawver, 1995) or 35 Ma  
2591 (Aitchison et al., 2007; Hafkenscheid et al., 2001; Van der Voo et al., 1999b)  
2592 marked by the Indus-Tsangpo Suture zone and ended with the closure of the  
2593 Tethyan seaway between Arabia and Iran forming the Zagros Mountains  
2594 (Hessami et al., 2001). Several fragments of Tethyan ocean floor are postulated  
2595 to underlay some of the basins in the eastern Mediterranean (see (Müller et al.,  
2596 2008a)).

2597

2598 In the Mediterranean region, several Cenozoic back-arc basins formed due to the  
2599 convergence between Eurasia and Africa (Rosenbaum et al., 2002). The Liguro-  
2600 Provençal basin opened from around early Oligocene (~35 Ma) due to the  
2601 eastward rollback of Apennines subduction (e.g. (Carminati et al., 2004)) and the  
2602 rotation of Corsica and Sardinia (Speranza et al., 2002) and the accretion of the  
2603 Kabylies blocks to the African margin (e.g. (Rosenbaum et al., 2002)). Additional

2604 extensional basins such as the Pannonian basin were associated with Africa-  
2605 Eurasia collision and associated with the Carpathian, Ionian and Hellenic  
2606 subduction zones (Faccenna et al., 2001).

2607

2608 Our model for the evolution of the Tethys Ocean closely follows that of Heine et  
2609 al. (2004), which is largely based on Stampfli and Borel (2002) except in the  
2610 Jurassic-Cretaceous. We agree with the separation of the Tethys into three  
2611 oceanic domains, as first suggested by Metcalfe (1996) and adopted by Heine et  
2612 al. (2004). We define the paleo-Tethys as the ocean basin that formed after the  
2613 separation of the Hunic superterrane from the northern Gondwana margin, the  
2614 meso-Tethys as the ocean basin that formed after the separation of the  
2615 Cimmerian terrane from the northern Gondwana margin and the neo-Tethys as  
2616 the ocean basin that formed when West Burma/Argoland separated from  
2617 northwest Australia. Finite rotations describing the opening of all three basins  
2618 as well as associated seafloor spreading isochrons are mostly derived by  
2619 following the model of Stampfli and Borel (2002) and Heine et al. (2004).

2620

2621 We follow a Devonian opening model for the paleo-Tethys (Metcalfe, 1996) but  
2622 do not discount that opening may have been diachronous and occurred as  
2623 early as the Silurian (Stampfli and Borel, 2002) in the western Tethys. As the  
2624 reconstructions presented in this paper do not extend beyond 200 Ma, we will  
2625 not describe the accretionary history of the Hunic superterrane. We agree with  
2626 Stampfli and Borel (2002) that the cessation of spreading in the paleo-Tethys led  
2627 to southern ridge jump, initiating opening of the meso-Tethys around 280 Ma,  
2628 coincident with the collision of the Hunic terrane to the southern Laurasian  
2629 margin and the initiation of rifting of the Cimmerian terrane from the northern  
2630 Gondwana margin in the early-mid Permian (Metcalfe, 1996). We invoke NE-SW  
2631 directed spreading for the meso-Tethys consistent with Stampfli and Borel  
2632 (2002). The accretion of the Cimmerian terrane to the southern Laurasian  
2633 margin also marks the closure of the paleo-Tethys ocean. We broadly follow the  
2634 timing of accretion based on Golonka (2006) and Golonka (2007). The  
2635 uncertainty in the southern extent of the Laurasian margin means that the timing  
2636 of accretion may change significantly depending on the southern extent of the

2637 Laurasian continental margin. Following the closure of the paleo-Tethys, a  
2638 margin-wide episode of back-arc opening occurred along the southern Eurasian  
2639 margin – from China to western Europe. This back-arc system was responsible  
2640 for the crust that now forms part of the Cretaceous aged ophiolite complexes  
2641 through southern Europe, Cyprus (Troodos), Iran and Oman. Although these  
2642 basins are known to have existed after the closure of the paleo-Tethys, we do not  
2643 include their formation (e.g. (Robertson, 2000; Stampfli and Borel, 2002;  
2644 Whitechurch et al., 1984) as we focused on the broad-scale development of the  
2645 Tethys Ocean. However, these back-arc basins have played a vital role in the  
2646 development of the region and we anticipate that a thorough review of ophiolite  
2647 complexes and back-arc basins correlatives will be included in the next  
2648 generation of the plate motion model.

2649

2650 Our model invokes continuous seafloor spreading in the meso-Tethys from 280  
2651 Ma to 145-140 Ma. The neo-Tethys ocean forms with rifting and seafloor  
2652 spreading in the Argo Abyssal Plain, following the model of Heine and Müller  
2653 (2005), isolating the West Burma Block from the Gondwana margin. We initiate  
2654 seafloor spreading at 156 Ma and extend the mid-ocean ridge westward, north of  
2655 Greater India where it intersects with a Tethyan transform fault. The accretion  
2656 of West Burma to Sibumasu occurred at 80 Ma, following Heine and Müller  
2657 (2005). Seafloor spreading in the neo-Tethyan ocean continued unabated  
2658 eventually transforming into the Wharton basin spreading ridge system in the  
2659 eastern Indian Ocean until 43 Ma (Singh et al., 2010).

2660

2661 In the western Mediterranean, we reconstruct the continental blocks that  
2662 comprise southern Europe and the Middle East in the same manner as in Müller  
2663 et al. (2008a). The basins floored by oceanic crust in the Mediterranean fall into  
2664 two types. The Mesozoic basins in the eastern Mediterranean (e.g. Levant basin  
2665 and Ionian Sea) represent the oldest preserved in-situ ocean floor, ranging in age  
2666 from about 270 Ma (Late Permian) to 230 Ma (Middle Triassic) according to our  
2667 model. The Cenozoic basins in the western Mediterranean (e.g. Liguro-  
2668 Provençal Basin) are reconstructed based on the tectonic model and rotations  
2669 from Speranza et al. (2002), describing a Miocene counterclockwise rotation of

2670 Corsica-Sardinia relative to Iberia and France, thereby creating accommodation  
2671 space for back-arc opening.

2672

### 2673 ***3.4 Marginal and Back-arc Basins***

2674 The present day distribution of the continents and oceans includes many smaller  
2675 ocean basins that formed either in a back-arc setting behind a retreating  
2676 subduction zone (Faccenna et al., 2001; Karig, 1971; Sdrolias and Müller, 2006;  
2677 Sleep and Toksoz, 1971; Taylor and Karner, 1983; Uyeda and Kanamori, 1979)  
2678 or as a result of continental rifting without the influence of a subduction zone  
2679 forming marginal seas. The presence of ophiolites embedded within accreted  
2680 terranes provide evidence for the opening and closing of marginal seas and back-  
2681 arc basins in the past, most notably along the Tethyan margin and in the western  
2682 North American margin. We have modeled some of the major marginal and  
2683 back-arc basins observed in the seafloor spreading record today. We have also  
2684 modeled the opening of three critical marginal and back-arc basins that existed  
2685 in the past but have been subsequently destroyed. These include the Mongol-  
2686 Okhotsk Ocean in Central Asia, the marginal basins that formed in the Caribbean,  
2687 off the coast of western North America and the proto-South China Sea. We also  
2688 model the opening of the Caribbean, which includes a combination of marginal  
2689 seas and back-arc basins.

2690

#### 2691 ***3.4.1 Caribbean***

2692 The Caribbean resides between the North American and South American plates  
2693 and contains Jurassic-Cretaceous ocean floor in the Gulf of Mexico and Venezuela  
2694 Basin, Cenozoic ocean basins such as the Cayman Trough, Gernada and Yucatan  
2695 Basins, numerous continental blocks, accreted terranes, volcanic arcs and the  
2696 Caribbean Large Igneous Province (CLIP) (Figure 3 and 9). The sedimentary  
2697 basins surrounding the Gulf of Mexico are some of the world's most productive  
2698 hydrocarbon bearing basins, prompting quite detailed studies of the tectonic  
2699 evolution of the region (Burke, 1988; Pindell and Kennan, 2009; Pindell, 1987;  
2700 Ross and Scotese, 1988). The development of the Caribbean is tied to break-up  
2701 of Pangea and rifting in the Central Atlantic, which extended into the Caribbean  
2702 during the Triassic to earliest Cretaceous. This early phase formed rift basins,

2703 stretched continental crust and salt basins in areas such as the South Florida  
2704 Basin, Great Bank of the Bahamas, Yucatan and along northern South America  
2705 (Pindell and Kennan, 2009). To the west, a continuous subduction zone along  
2706 the eastern margin on Panthalassa was consuming oceanic lithosphere beneath  
2707 the western margin of the proto-Caribbean/trans-American region.

2708

2709 The Gulf of Mexico is bounded by predominately Triassic-Jurassic syn-rift  
2710 structures and salt bearing basins and is partly floored by Jurassic-Cretaceous  
2711 oceanic crust. The timing of seafloor spreading in the Gulf of Mexico is not well  
2712 constrained with ages ranging from 158-170 Ma based on the timing of salt  
2713 deposition and regional changes in structural trend and block rotations (Buffler  
2714 and Sawyer, 1983; Pindell and Kennan, 2009; Ross and Scotese, 1988). The  
2715 cessation of extensional faulting in the SE Gulf of Mexico and the dating of a post-  
2716 rift unconformity (Marton and Buffler, 1999; Pindell and Kennan, 2009; Ross and  
2717 Scotese, 1988), places the cessation of seafloor spreading in the latest Jurassic-  
2718 earliest Cretaceous between 145-135 Ma. The opening of the Gulf of Mexico led  
2719 to a two-stage anticlockwise rotation of the Yucatan Block away from North  
2720 America into its present day location (Pindell and Kennan, 2009).

2721

2722 The existence of a proto-Caribbean Basin has been hypothesized based on the  
2723 accommodation space created by the relative motion between the North and  
2724 South American plates. The development of this basin (its orientation and  
2725 timing) is therefore purely dependent on the chosen plate tectonic model.  
2726 Opening of the basin was either coincident with spreading in the Gulf of Mexico  
2727 (Meschede and Frisch, 1998; Pindell and Kennan, 2009) or initiated only after a  
2728 southward ridge jump in the early Cretaceous (Ross and Scotese, 1988). Models  
2729 that propose the encroachment of proto-Pacific oceanic lithosphere into the  
2730 Caribbean (e.g. (Pindell and Kennan, 2009; Ross and Scotese, 1988)) imply that  
2731 all evidence of the proto-Caribbean Basin was subducted by the late-Cretaceous-  
2732 early Cenozoic, whereas models that do not invoke an advancing trench relate  
2733 NE-SW trending magnetic lineations in the Venezuela Basin (Ghosh et al., 1984)  
2734 to the proto-Caribbean Basin (Meschede and Frisch, 1998).

2735

2736 One of the major features that controlled the broad-scale development of the  
2737 Caribbean is the nature of the plate boundary between the Caribbean and  
2738 Panthalassa/Pacific Ocean. Most models agree that east-dipping trans-America  
2739 subduction was consuming proto-Pacific oceanic lithosphere during the Triassic-  
2740 Cretaceous (Meschede and Frisch, 1998; Pindell and Kennan, 2009; Ross and  
2741 Scotese, 1988). However, models subsequently diverge into either “Pacific  
2742 origin” (Burke, 1988; Malfait and Dinkelman, 1972; Pindell and Kennan, 2009;  
2743 Ross and Scotese, 1988) or “intra-American origin” scenarios (James, 2006;  
2744 Meschede and Frisch, 1998). “Pacific-origin” scenarios propose a switch in the  
2745 polarity of the trans-American plate boundary from east-dipping to southwest-  
2746 dipping in the late Cretaceous along the Caribbean/Greater Antilles Arc, causing  
2747 the subduction of the proto-Caribbean Basin and encroachment of oceanic  
2748 lithosphere from the Pacific domain into the Caribbean. The timing of this  
2749 polarity flip is believed to be around 100-90 Ma (Pindell and Kennan, 2009; Ross  
2750 and Scotese, 1988) and constrained to 90 Ma in the south on Aruba and within  
2751 the Bonaire Block (van der Lelij et al., 2010). Continued northeastward rollback  
2752 of the subduction hinge eventually caused collision with Yucatan and accretion of  
2753 the arc along the Bahamas Platform. In the model of Ross and Scotese (1988)  
2754 this accretion led to a jump in the locus of subduction westward, initiating  
2755 subduction along the Panama-Costa Rica Arc around 60 Ma. However, other  
2756 models place the initiation of Panama-Costa Rica Arc to 80-88 Ma (Pindell and  
2757 Kennan, 2009) before the accretion of the Caribbean Arc to the Bahamas  
2758 Platform. Recent tectonostratigraphic and geochemical data from exposed rocks  
2759 in southern Costa Rica and western Panama indicate protoarc initiation on top of  
2760 CLIP basement occurred between 75-73 Ma (Buchs et al., 2010). Irrespective of  
2761 timing, in the “Pacific origin” model, the initiation of the Panama-Costa Rica Arc  
2762 trapped Pacific-derived oceanic lithosphere (now underlying the Venezuela  
2763 Basin) as well as the CLIP onto the Caribbean plate. “Intra-American origin”  
2764 models assume a continuous trans-America east-dipping subduction zone, which  
2765 provided a permanent barrier between the Pacific/Panthalassa and Caribbean.  
2766 Concurrently, southwest-dipping subduction to the east of the proto-Caribbean  
2767 Basin led to the docking of tectonic elements along the Bahaman Platform. In the  
2768 “intra-American” model, the origin of the oceanic lithosphere underlying the

2769 Venezuela Basin and the CLIP are both derived in-situ. This model implies that  
2770 the Panama-Costa Rica Arc was built upon a much older arc sequence.  
2771  
2772 After ~60 Ma, most models for the Caribbean are largely similar on a broad scale.  
2773 After the establishment of subduction along the Panama-Costa Rica Arc, the  
2774 Caribbean plate became a stationary feature influenced only by the relative  
2775 motions between the North and South American plates (Ross and Scotese, 1988).  
2776 The southern margin of the Bahaman platform changed from convergence to  
2777 sinistral strike-slip after the accretion of arc terranes with E-W transform faults  
2778 dominating the region. To the east, west-dipping subduction and arc volcanism  
2779 along the Aves Ridge was still occurring. To the south, thermochronological and  
2780 sedimentological analyses suggest that the Bonaire Block collided with the South  
2781 American margin at ~50 Ma thereby constraining the change from convergence  
2782 to strike-slip along South America (van der Lelij et al., 2010). The new tectonic  
2783 regime led to opening of the Yucatan and Grenada-Tobago Basins in the  
2784 Paleogene, Cayman Trough since the Eocene (Pindell and Kennan, 2009; Ross  
2785 and Scotese, 1988) and the Puerto Rico Basin in the Oligocene (Ross and Scotese,  
2786 1988).  
2787  
2788 The Yucatan Basin currently resides between Cuba and the Cayman Ridge and is  
2789 believed to have formed prior to the collision of the Caribbean Arc as a passive  
2790 response to the rollback of the northward rollback of the trench (Pindell et  
2791 al., 2006). The cessation of spreading is correlated with the docking of the arc  
2792 terranes along Cuba and the Bahaman Platform. The Grenada-Tobago Basin  
2793 formed as a back-arc due between the Aves Ridge and Lesser Antilles Ridge due  
2794 to the eastward rollback of the Lesser Antilles Trench. The timing of spreading is  
2795 unconstrained by magnetic anomaly interpretations but initiation is believed to  
2796 have occurred sometime in the Paleogene based on the cessation of plutonism on  
2797 the Aves Ridge (Pindell et al., 1988) and from seismic stratigraphy and heatflow  
2798 measurements within the basin (Pindell and Kennan, 2009; Speed, 1985).  
2799 Spreading is believed to have ceased in the Oligocene coincident with the  
2800 collision of the Lesser Antilles forearc with the Venezuelan margin (Pindell and  
2801 Kennan, 2009). The Cayman Trough formed as a left-lateral pull-apart basin

2802 between two major transform faults starting at Chron 19 (~41 Ma) (Rosencrantz  
2803 et al., 1988; Ross and Scotese, 1988) based on the interpretation of magnetic  
2804 anomalies. The Puerto Rico Basin opened in the Oligocene-early Miocene as a  
2805 result of relative motion between Hispaniola and the Caribbean plate (Ross and  
2806 Scotese, 1988).

2807

2808 Our model largely follows the hierarchical model of Ross and Scotese (1988)  
2809 (with an updated timescale) and elements of Pindell and Kennan (2009), with  
2810 minor adjustments based on recent geological information and an updated  
2811 spreading model in the Central and Equatorial Atlantic. Rifting in the Caribbean  
2812 since the Triassic connected to the Central Atlantic rift zone through Florida and  
2813 Gulf of Mexico and extended westward to the trans-America subduction zone,  
2814 which was actively consuming Panthalassic ocean floor. In our model, we follow  
2815 the initiation of spreading in the Gulf of Mexico at 170 Ma based on Ross and  
2816 Scotese (1988) coincident with accelerated seafloor spreading rates in the  
2817 Central Atlantic (Labails et al., 2010) (Figure 8). We update the cessation of  
2818 spreading to 145 Ma based on evidence presented in Pindell and Kennan (2009).  
2819 After the cessation of spreading in the Gulf Of Mexico, we model a ridge jump to  
2820 the south initiating the opening of the proto-Caribbean Basin through the  
2821 accommodation space created due to the relative motion between the North and  
2822 South American plates (Figure 8). Spreading was NW-SE directed and initiated  
2823 around 145 Ma forming a triple junction to the east between the mid ocean ridge  
2824 of the Central Atlantic and rift axis of the Equatorial/South Atlantic. To the west,  
2825 the mid ocean ridge of the proto-Caribbean Basin formed a ridge-ridge-  
2826 transform triple junction with the spreading ridge of the Andean back-arc basin  
2827 and the trans-American subduction zone.

2828

2829 We favor the “Pacific-origin” model for the formation of the Caribbean plate with  
2830 a subduction polarity flip of the trans-America subduction zone to west-dipping  
2831 along the eastern boundary of the Caribbean Arc at 100 Ma (Figure 8). The  
2832 rollback of this subduction zone led to the consumption of the actively spreading  
2833 proto-Caribbean ocean floor and encroachment of the Farallon plate into the  
2834 Caribbean domain. Our model predicts that the oceanic lithosphere intruding

2835 into the Caribbean (and currently underlying the Venezuela Basin) formed along  
2836 the Pacific-Farallon ridge between Chrons M16-M4 (~139-127 Ma) at a latitude  
2837 of around 10-15°S, agreeing well with paleomagnetic constraints, which suggest  
2838 an equatorial formation for the oceanic crust of the Nicoya Complex (Duncan and  
2839 Hargraves, 1984). The continued roll-back of the Caribbean Arc subduction zone  
2840 led to the formation of the Yucatan Basin as a back-arc in the late Cretaceous  
2841 with cessation occurring at 70 Ma when the Caribbean Arc accreted to the  
2842 Bahaman Platform. The accretion led to a jump in the locus of subduction  
2843 westward along the newly developed Panama-Costa Rica to accommodate the  
2844 continued eastward motion of the Farallon plate, trapping Farallon oceanic  
2845 lithosphere onto the Caribbean plate in the process. The eruption of the  
2846 Caribbean flood basalt province occurred around 90 Ma on top of the oceanic  
2847 lithosphere that now underlies much of the Caribbean ocean floor (Sinton et al.,  
2848 1998). The Caribbean flood basalt province (or CLIP) has been suggested to be  
2849 the product of the Galapagos hotspot (Pindell and Kennan, 2009), however in our  
2850 model the CLIP erupted on Farallon oceanic lithosphere over 2000 km away  
2851 from the present day position of the Galapagos hotspot precluding this as a  
2852 source, even assuming the motion of hotspots relative to each other (Figure 10).

2853

2854 Coincident with subduction along the proto-middle America trench was west-  
2855 dipping subduction to the east along the Aves/Lesser Antilles Ridge, consuming  
2856 Atlantic ocean floor (Figure 8). The rollback of this subduction zone led to the  
2857 formation of the Grenada Basin between the Aves and Lesser Antilles Arcs in the  
2858 Paleogene. In the middle Eocene (41 Ma), relative motion between North  
2859 America and Caribbean began to form the Cayman Trough along sinistral faults  
2860 that later merge with the Lesser Antilles trench. In early Miocene (20 Ma), the  
2861 Cayman Trough continued to expand and develop, and the Chortis Block moved  
2862 over the Yucatan promontory. Westward motion of the North American plate  
2863 relative to the slow moving Caribbean plate was accommodating the opening of  
2864 the Cayman Trough. The Puerto Rico Basin formed in the Oligocene-early  
2865 Miocene due to a similar process. Currently, opening is continuing within the  
2866 Cayman Trough accommodated by the motion along the bounding transforms.  
2867 Active subduction of Atlantic oceanic lithosphere is occurring along the Lesser

2868 Antilles Trench, which connects up to the Mid-Atlantic Ridge along the  
2869 Researcher Ridge and Royal Trough (Müller et al., 1999).

2870

### 2871 *3.4.2 Mongol-Okhotsk Basin*

2872 The Mongol-Okhotsk Basin is a Mesozoic ocean basin that existed between the  
2873 Siberian craton to the north and the Amuria/Mongolia block to the south. The  
2874 Mongol-Okhotsk suture zone defines basin closure (Apel et al., 2006; Cocks and  
2875 Torsvik, 2007; Golonka et al., 2006). Evidence for the existence of the Mongol-  
2876 Okhotsk Basin is found in a series of remnant island arc volcanics and ophiolites  
2877 adjacent to the suture zone as well as a large area of seismically fast material in  
2878 the lower mantle underlying Siberia imaged in seismic tomography (Van der Voo  
2879 et al., 1999a).

2880

2881 The opening of the Mongol-Okhotsk Basin is not well constrained, ages range  
2882 from 610-570 Ma (Sengör et al., 1993), Ordovician (Cocks and Torsvik, 2007),  
2883 Cambrian (Harland et al., 1989) and Permian (Kravchinsky et al., 2002; Zorin,  
2884 1999). The large age range stems from the associations made between  
2885 geological units in the Siberia, Mongolia and North China realm and the  
2886 definition of the ocean basins that existed between these geological units. A  
2887 zircon age of 325 Ma from a leucogabbro pegmatite has been associated with  
2888 oceanic crust from the Mongol-Okhotsk Ocean (Tomurtogoo et al., 2005)  
2889 indicating that seafloor spreading was active from at least the late Carboniferous.  
2890 In addition, paleomagnetic data suggests that Siberia and Mongolia were  
2891 separated by 10-15° (Zorin, 1999) by the Permian. The presence of continental  
2892 volcano-sedimentary sequences and granitoid magmatism proximal to the  
2893 suture zone indicates that the basin was being subducted northward during the  
2894 Permian (Zorin, 1999), Triassic and Jurassic (Golonka et al., 2006; Stampfli and  
2895 Borel, 2002). It is difficult to ascertain when seafloor spreading ceased in the  
2896 Mongol-Okhotsk Basin. Triassic MORB basalts in the eastern part of the Mongol-  
2897 Okhotsk belt (Golonka et al., 2006) provide a minimum age for seafloor  
2898 spreading. Continued subduction along the Siberian margin led to initial closure  
2899 of the Mongol-Okhotsk Ocean sometime in the Jurassic (Golonka, 2007; Golonka  
2900 et al., 2006; Kravchinsky et al., 2002; Stampfli and Borel, 2002; Van der Voo et al.,

2901 1999a; Zorin, 1999) based on collision followed by folding and intrusion of  
2902 granitic batholiths in Mongolia and the trans-Baikal area (Golonka et al., 2006)  
2903 and the formation of the Mongol-Okhotsk Suture (Tomurtogoo et al., 2005).  
2904 Complete closure may have ended as late as the early Cretaceous (Zorin, 1999)  
2905 based on the cessation of compression in the area (Zorin, 1999). Alternative  
2906 models exist that predict an older initial closure age of late Carboniferous  
2907 (Badarch et al., 2002; Cocks and Torsvik, 2007), but again, this may be due to a  
2908 difference in the definition of the Mongol-Okhotsk Ocean.

2909

2910 We have modeled the opening of the Mongol-Okhotsk Basin in the late  
2911 Carboniferous to account for the zircon data of Tomurtogoo et al. (2005),  
2912 followed by the onset of subduction along the Siberian margin in the late  
2913 Permian. We continue seafloor spreading in the Mongol-Okhotsk Basin until the  
2914 Permo-Triassic boundary (250 Ma). Based on our initiation and termination of  
2915 spreading, we suggest that the Mongol-Okhotsk Ocean had a maximum width of  
2916 about 4000 km. We model the closure of the Mongol-Okhotsk Basin to 150 Ma  
2917 (late Jurassic) based on the overwhelming evidence in the literature for the  
2918 dating of the Mongol-Okhotsk Suture.

2919

### 2920 *3.4.3 North American Margins*

2921 The western North American margin is characterized by the accretion of native  
2922 and exotic terranes throughout the late Paleozoic and Mesozoic. The timing of  
2923 formation of the numerous terranes with island arc affinities, their accretion  
2924 onto the continental margin and other subduction-related structures provide  
2925 constraints for the age, orientation and tectonics associated with the oceanic  
2926 basins that formed adjacent to the margin. The Laurentian peri-continental  
2927 margin was a passive Atlantic-style margin until the early Mesozoic (Nokleberg  
2928 et al., 2001). Many accretion events have been recorded along this margin but  
2929 we simplify them into three main sectors: the Yukon-Tanana/Quesnellia/Stikina  
2930 terrane, the East Klamath terrane and the Wrangellia superterrane separated by  
2931 major fault systems. There are many alternative interpretations for the source of  
2932 the terranes, their age of formation, timing and location of accretion and their  
2933 field relationships. Our model relies heavily on the reconstructions represented

2934 in Nokleberg et al. (2001) and Colpron et al. (2007) but note that other  
2935 alternative scenarios exist.

2936

2937 Arc magmatism occurred along the western Laurentian margin ~390-380 Ma  
2938 forming many of the rocks of the Yukon-Tanana Terrane (YTT) and western  
2939 Kootenay terranes (Nokleberg et al., 2001) currently located in Yukon and  
2940 southern Alaska (Figure 7). The base of the YTT has isotopic, geochemical  
2941 characteristics indicating a Laurentian source for the terrane (Nokleberg et al.,  
2942 2001). Following a period of arc magmatism was a period with coeval rift-  
2943 related magmatism leading to the rifting of the YTT from the Laurentian margin  
2944 around 360-320 Ma (Colpron et al., 2002; Mortensen, 1992; Nelson et al., 2006;  
2945 Nokleberg et al., 2001). The separation of the YTT was driven by N-NE dipping  
2946 subduction and led to the opening of the Slide Mountain Ocean. The Slide  
2947 Mountain ophiolite, which is currently emplaced onto the YTT and Cassier  
2948 Terranes (Nokleberg et al., 2001) preserves evidence of this paleo-ocean basin.  
2949 The Slide Mountain Ocean is less commonly referred to as the Anvil Ocean  
2950 (Hansen, 1990). Some of the rocks related to arc magmatism were left on the  
2951 margin (in the parautochthonous rocks of east-central Alaska and the Kootenay  
2952 terrane) before the opening of the Slide Mountain Ocean while the majority of  
2953 the YTT formed the base of the frontal arc (Nokleberg et al., 2001).

2954

2955 The Slide Mountain Ocean opened due to west-southwest slab roll-back, reaching  
2956 a maximum width in the early Permian (Nelson et al., 2006) of around 1300 km  
2957 (Nokleberg et al., 2001). Spreading in the back-arc basin ceased at around 280-  
2958 260 Ma coincident with a subduction polarity reversal (Mortensen, 1992;  
2959 Nokleberg et al., 2001) recorded in west-facing coeval calc-alkalic and alkalic  
2960 plutons (Nokleberg et al., 2001). The subduction polarity reversal led to the  
2961 formation of two adjacent arcs, the Stikinia and Quesnellia Arcs, overlying the  
2962 YTT via a southwest-dipping subduction zone along the eastern side of the YTT.  
2963 This subduction led to the closure of the Slide Mountain Ocean and the accretion  
2964 of the YTT/Quesnellia Arc to the Laurentian margin by the middle Triassic (240-  
2965 230 Ma) (Hansen, 1990; Nelson et al., 2006; Nokleberg et al., 2001). The Stikinia  
2966 Arc was still intraoceanic when the YTT/Quesnellia Arc accreted to the margin as

2967 it trends outboard of the Cache Creek Terrane (Figure 7). The Cache Creek  
2968 Terrane is a mid-Paleozoic to mid Jurassic oceanic terrane with exotic Permian  
2969 Tethyan faunas in limestone blocks and long-lived island edifices (Mihalynuk et  
2970 al., 1994; Nelson and Mihalynuk, 1993). The Cache Creek Terrane, which is very  
2971 distinct from the Slide Mountain Terrane implies that another ocean basin, the  
2972 Cache Creek Ocean, formed in between the Stikinia Arc to the west and the  
2973 rapidly retreating YTT/Quesnellia Arc to the east. Based on trend-surface  
2974 analysis of the distribution of Permian coral genera, taxonomic diversity and  
2975 paleomagnetic data, Belasky and Runnegar (1994) predict that the Stikinia Arc  
2976 was located up to 6700 km from the Laurentian margin in the early Permian and  
2977 that the Eastern Klamath terrane was located proximal to the Stikinia Arc.  
2978

2979 To address the field relationships of the YTT, Quesnellia Arc, Cache Creek  
2980 Terrane and Stikinia Arc, Colpron et al. (2007) invoke an “oroclinal” model  
2981 whereby the Stikinia Arc segment rotated counterclockwise consuming the  
2982 Cache Creek Ocean along a west-southwest-dipping subduction zone. The  
2983 rotation of the Stikinia Arc may have initiated as early as ~230 Ma. The timing of  
2984 accretion of the Stikinia Arc to the North American margin and therefore the  
2985 closure of the Cache Creek Ocean is tightly constrained to around 172-174 Ma  
2986 (Colpron et al., 2007) and references therein. However, collision may have  
2987 started in the early Jurassic coincident with a phase of cooling (Nokleberg et al.,  
2988 2001).

2989

2990

2991 The next major event to affect the margin was the accretion of the exotic  
2992 Wrangellia superterrane. The basement of the Wrangellia superterrane consists  
2993 of Triassic flood basalts (285-297 Ma) that formed at equatorial latitudes and  
2994 overlain by a carbonate platform (Greene et al., 2008; Richards et al., 1991).  
2995 Although recent data suggests initial collision with the North American margin at  
2996 about 175 Ma (Colpron et al., 2007; Gehrels, 2001, 2002), the main accretion  
2997 event occurred at 145-130 Ma (Nokleberg et al., 2001; Trop et al., 2002). There  
2998 is controversy over whether the allochthonous terranes (including Wrangellia)  
2999 of southern Alaska and western Canada were originally accreted (a)  $\leq$  1000km of  
3000 their existing location, offshore present day British Columbia, Oregon, and

3001 Washington, during the late Mesozoic and early Cenozoic or (b) were located  
3002 1000-5000 km along the western coast of the North American Craton and  
3003 subsequently transported northwards during the Late Cretaceous and Cenozoic,  
3004 (Keppie and Dostal, 2001; Stamatakos et al., 2001). After collision, the  
3005 Wrangellia terrane underwent margin-parallel dextral motion but the amount of  
3006 dextral motion is a matter of debate.

3007

3008 We model the evolution of the marginal and back-arc basins that formed along  
3009 the western North American margin as described above. We create a set of  
3010 synthetic seafloor spreading isochrons to depict the opening of the Slide  
3011 Mountain Ocean starting at 340 Ma based on a margin parallel opening and a  
3012 maximum opening width of 1300 km, suggested by Nokleberg et al. (2001).  
3013 Break-up may have been at least partially driven by a mantle plume as our  
3014 reconstructions show that the plume associated with the present day Azores  
3015 hotspot closely corresponds to the break-up location. Osmium isotopes suggest  
3016 that Azores has a deep origin (Schaefer et al., 2002) suggesting that this plume  
3017 may have been long-lived but whether hotspots are active and can be traced as  
3018 far back as 340 Ma remains open to debate. We terminate spreading in the Slide  
3019 Mountain Ocean at 280 Ma followed by a subduction polarity flip along the YTT  
3020 and the establishment of an eastward retreating subduction zone. Subduction  
3021 led to the consumption of the Slide Mountain Ocean along this southwest-west  
3022 dipping subduction zone.

3023

3024 We form the Cache Creek Ocean in between the retreating YTT and the Stikinia  
3025 Arc and East Klamath at 280 Ma with a cessation of spreading in the Cache Creek  
3026 Ocean simultaneous with the accretion of the YTT along the Laurentian margin at  
3027 230 Ma. This is followed by the subduction of the Cache Creek Ocean behind a  
3028 rapidly retreating west-dipping subduction zone along the eastern side of the  
3029 Stikinia Arc and East Klamath (Figure 17). The Stikinia Arc and East Klamath  
3030 accrete to the North American margin at 172 Ma (Figure 17), resulting in the  
3031 emplacement of the Cache Creek ophiolite between the Stikinia Arc and the  
3032 Quesnellia Arc. We accrete the Wrangellia superterrane to the margin at 140 Ma  
3033 following the northern accretion model. The accretion of the Wrangellia Terrane

3034 marks the true establishment of the boundary between North America and the  
3035 Pacific.

3036

#### 3037 *3.4.4 Proto-South China Sea*

3038 A Mesozoic-Cenozoic back-arc basin situated adjacent to the Eurasian passive  
3039 margin, named the proto-South China Sea, is incorporated into many regional  
3040 models of SE Asia (Hall, 2002; Hamilton, 1979; Holloway, 1982; Hutchison, 1989;  
3041 Lee and Lawver, 1994; Williams et al., 1988). Rifting is believed to have initiated  
3042 along the South China margin in the late Cretaceous (Lee and Lawver, 1994; Ru  
3043 and Pigott, 1986) although a rift-related unconformity is dated to the early  
3044 Cretaceous (Lee and Lawver, 1994). This rift event led to the separation of  
3045 northern Borneo from the South China margin resulting in the formation of NE-  
3046 SW trending structures and sedimentary basins (Lee and Lawver, 1994). The  
3047 provenance of ophiolitic igneous rocks in northwest Borneo from late Jurassic-  
3048 late Cretaceous (based on the dating of sediments overlying pillow basalts) is  
3049 tied to the proto-South China Sea (Hutchison, 2005), further constraining the  
3050 timing of formation of the basin.

3051

3052 The cessation of spreading in the proto-South China Sea and its lateral extent is  
3053 unknown. Most models invoke the initiation of closure in the early  
3054 Cenozoic/early Neogene beneath Kalimantan/northern Borneo and Palawan  
3055 (Hall, 2002; Lee and Lawver, 1994; Ludwig, 1979; Williams et al., 1988). The  
3056 closure is believed to have been triggered either by the counterclockwise  
3057 rotation of Borneo (Hall, 2002) or by the southeast extrusion of Indochina (Lee  
3058 and Lawver, 1994).

3059

3060 We model the opening of the proto-South China Sea during rifting between the  
3061 stable Eurasian margin and northern Borneo during the late Cretaceous (~90  
3062 Ma) with spreading orthogonal to the Eurasian margin. The cessation of  
3063 spreading occurred at 50 Ma coincident with the clockwise rotation of the  
3064 neighboring Philippine Sea plate. The dramatic change in motion of the  
3065 Philippine Sea plate reorganized the plate boundaries in the area leading to the  
3066 establishment of a subduction zone between Palawan and the proto-South China

3067 Sea, which began actively consuming the proto-South China Sea since 50 Ma with  
3068 an increase in convergence rate from 25 Ma. We model complete closure of the  
3069 proto-South China Sea at around 10 Ma behind a subduction zone located along  
3070 Palawan and the north Borneo/Kalimantan margin.

3071

#### 3072 *3.4.5 Western Pacific and SE Asian Back-arc Basins*

3073 The continental blocks and basins in SE Asia comprise one of the most complex  
3074 regions in the world. Most models focus on the Cenozoic interpretation of  
3075 onshore geology, including: Rangin et al. (1990), Lee and Lawver (1995), Hall  
3076 (2002). Other models couple the seafloor spreading history in the back-arc  
3077 basins of both SE Asia and the Western Pacific for a continent and ocean basin  
3078 evolution (Gaina and Müller, 2007). The model we use in our plate motion  
3079 model is based on Gaina and Müller (2007) and additionally incorporate the  
3080 rotation of the Philippine Sea plate based on Hall et al. (1995) and the seafloor  
3081 spreading model of Sdrolias et al. (2003b) for spreading in the Parece Vela and  
3082 Shikoku Basins. For further details of the model, we refer to Gaina and Muller  
3083 (2007) and Sdrolias et al. (2003b).

3084

#### 3085 *3.4.6 SW Pacific Back-arc Basins and Marginal Seas*

3086 The SW Pacific is characterized by a series of marginal basins (Tasman and Coral  
3087 Seas), submerged continental slivers (Lord Howe Rise, Mellish Rise, Louisiade,  
3088 Papuan, Kenn, Dampier and Chesterfield Plateaus), island arcs (Norfolk, Three-  
3089 Kings, Loyalty, New Hebrides, Vitiaz and Lau-Colville Ridges), back-arc basins  
3090 (South Loyalty, North Loyalty, Norfolk, South Fiji, North Fiji and Lau Basins and  
3091 Havre Trough) as well as numerous features with an uncertain origin (e.g.  
3092 D'Entrecasteaux Zone and Basin and Rennell Trough and Basin) (Figure 11). In a  
3093 broad sense, these features developed behind the eastward migrating Australia-  
3094 Pacific plate boundary from the late Mesozoic to the present day (Crawford et al.,  
3095 2002; Karig, 1971; Müller et al., 2000; Sdrolias et al., 2003a; Symonds et al.,  
3096 1996). Our plate motion model incorporates the opening model for the Tasman  
3097 and Coral Seas based on Gaina et al. (1998) and Gaina et al. (1999). We  
3098 incorporate the model of Sdrolias et al. (2003a) and Sdrolias et al. (2004) for the

3099 formation of the back-arc basin and island arc systems seaward of the Lord  
3100 Howe Rise. For further details, we refer to the abovementioned publications.

3101

#### 3102 **4 Global plate reconstructions**

3103 Our regional kinematic models fit within a hierarchical global plate circuit tied to  
3104 a hybrid moving hotspot/true polar wander corrected absolute reference frame  
3105 through Africa. We create a set of dynamic plate polygons since the time of  
3106 Pangea break-up with the assumption that the plates themselves are rigid. The  
3107 birth of a plate (the establishment of relative motion after a break in the  
3108 lithosphere), can be defined in two ways: either the initiation of rifting due to  
3109 weakening of the lithosphere by basal heating forming a series of faults and rift-  
3110 related structures (sometimes called incipient spreading), or the initiation of  
3111 seafloor spreading, when there is a complete break of the lithosphere and  
3112 extrusion of the mantle. Our plate boundary set distinguishes between the two  
3113 modes via a continental/oceanic rift or mid-ocean ridge coding of the plate  
3114 boundaries, which allows for the construction of a plate polygon dataset using  
3115 either mode. The plate polygons presented in this study follow the former  
3116 definition but an ancillary set can be produced to follow the later definition.  
3117 Below we describe tectonic events every 20 million years with accompanying  
3118 maps (Figure 18-28) and also provide the plate polygon and plate boundary files.  
3119 These files can be directly loaded into *GPlates* software for reconstructions in  
3120 one million year time intervals.

3121

#### 3122 **4.1 200-180 Ma (Figure 18-19)**

3123 Prior to the Mesozoic, the continents were amalgamated into one big  
3124 supercontinent, Pangea, surrounded by two ancient oceans, Panthalassa and the  
3125 smaller Tethys Ocean. By the early-mid Mesozoic, Pangea was undergoing slow  
3126 continental break-up centered along a rift zone extending from the Arctic, North  
3127 Atlantic (adjacent to the Norwegian shelf and Iberia-Newfoundland margins),  
3128 Central Atlantic and along the Jacksonville Fracture Zone through Florida and the  
3129 Gulf of Mexico in the Caribbean region. The Caribbean rift zone, defined by a  
3130 series of Mesozoic rift basins, connected with east-dipping trans-America  
3131 subduction, which was consuming oceanic lithosphere from Panthalassa. At 190

3132 Ma, there was a change from rift to drift along the early Atlantic rift, restricted to  
3133 the Central Atlantic. Contemporaneously, dextral motion was occurring along  
3134 the early Atlas Rift, isolating Morocco.

3135

3136 The Panthalassic Ocean was entirely surrounded by subduction during the mid-  
3137 early Mesozoic. We model seafloor spreading as a simple three-plate system  
3138 between the Izanagi, Farallon and Phoenix plates. The three arms of the triple  
3139 junction extended outward intersecting with the circum-Panthalassic margins  
3140 with minor margin migration: east of Australia (Izanagi-Phoenix ridge), along the  
3141 Amurian margin (Izanagi-Farallon ridge) and southern North America (Farallon-  
3142 Phoenix ridge). At 190 Ma, the birth of the Pacific plate established a more  
3143 complex spreading ridge system involving three triple junctions and six  
3144 spreading centers (Izanagi-Farallon, Izanagi-Phoenix, Izanagi-Pacific, Phoenix-  
3145 Farallon, Phoenix-Pacific, Farallon-Pacific). Initially spreading along the Pacific  
3146 ridges was slow/moderate (70-80 mm/yr) with a progressive increase in  
3147 spreading rates to a peak in the mid Cretaceous. In northeast Panthalassa,  
3148 closure of the Cache Creek Ocean (back-arc basin which formed between the  
3149 Yukon-Tanana Terrane and the Stikinia Arc) was occurring along a southwest  
3150 dipping subduction zone on the eastern side of the Stikinia Arc. In northwestern  
3151 Panthalassa, the Mongol-Okhotsk Ocean (an ancient ocean basin which formed  
3152 between Amuria and Siberia) continued its closure via northeast directed  
3153 subduction along the southern Siberia margin. This Mongol-Okhotsk subduction  
3154 zone connected with the landward-facing northern Panthalassic subduction zone  
3155 to its northeast and the Tethyan subduction zone to its southwest.

3156

3157 In the Tethys Ocean, the remnant paleo-Tethys was separated from the actively  
3158 spreading meso-Tethys ocean by the continental blocks of the Cimmerian  
3159 terrane (e.g. Iran, Afghanistan, Pakistan, South Tibet, Sibumasu). The Tethyan  
3160 subduction zone located along the southern Laurasian margin was driving the  
3161 opening of the Meso-Tethys and consumption of the paleo-Tethys ocean. Active  
3162 rifting was occurring along the Argo Abyssal Plain (NW Australia) that we  
3163 suggest extended to the north of Greater India and westward to the East  
3164 Africa/Karoo Rift, marking the break-up of Gondwanaland into West Gondwana

3165 (including South America, most of Africa and Arabia) and East Gondwana  
3166 (including Antarctica, Australia, India, eastern Africa, Madagascar). We continue  
3167 the Karoo Rift southward to connect with extension along the Agulhas-Falkland  
3168 transform. This plate boundary between West Gondwana and Patagonia  
3169 connected with east-dipping subduction along the South American/Panthalassa  
3170 margin.

3171

3172 An extensive seaway between the Tethys Ocean and Panthalassa existed in the  
3173 mid-Mesozoic. We envisage that the confluence of these two oceanic domains  
3174 occurred north of Australia at the so-called Junction region/plate (Seton and  
3175 Müller, 2008). The differential motion between the meso-Tethys and Izanagi  
3176 plates results in convergence and we model the subduction of Izanagi  
3177 lithosphere beneath a westward verging subduction zone.

3178

#### 3179 **4.2 180-160 Ma (Figure 19-20)**

3180 At 180 Ma, early opening by ultra-slow seafloor spreading continued in the  
3181 Central Atlantic with ongoing rifting in the northern Atlantic and Caribbean. A  
3182 readjustment of the plate-mantle system occurred at 170 Ma, coincident with a  
3183 doubling of seafloor spreading rates in the Central Atlantic (Labails et al., 2010)  
3184 and the establishment of seafloor spreading in the Gulf of Mexico. Evidence for  
3185 changes in plate motion and accretion events in the Tethys Ocean and  
3186 Panthalassa at 170 Ma (see below) may indicate a global plate reorganization  
3187 event at this time.

3188

3189 This time period saw the accelerated growth of the Pacific plate at the expense of  
3190 the Izanagi, Farallon and Phoenix plates. In northeast Panthalassa, closure of the  
3191 Cache Creek Ocean, obduction of the Cache Creek Terrane and accretion of the  
3192 Stikinia Arc occurred along the Laurentian margin between 175-172 Ma. The  
3193 accretion of the Stikinia Arc forced a jump in the locus of subduction and reversal  
3194 of subduction polarity from southwest to northeast along the new Laurentian  
3195 margin, establishing the Farallon subduction zone. The northwest Panthalassa  
3196 margin interacted with the Mongol-Okhotsk Ocean, which continued its closure  
3197 along the southern Siberia subduction zone.

3198

3199 Rifting continued along the southern Tethyan margin, adjacent to  
3200 Argoland/West Burma and northern Greater India to the east African rifts. In the  
3201 western Tethys, volcanism ceased along the Karoo Rift at 180 Ma leading to a  
3202 jump in the locus of rifting from the Karoo Rift to the area between Africa and  
3203 Madagascar/Antarctica, later forming the Weddell and Riiser-Larson Sea and  
3204 Mozambique and West Somali Basins. Incipient spreading in the Mozambique  
3205 and West Somali Basins connected with both the Weddell Sea rift and the  
3206 Agulhas-Falkland transform in the south. In the northern Tethys, closure of the  
3207 paleo-Tethys and accretion of the Cimmerian terrane occurred along the  
3208 southern Laurasian margin at 170 Ma. Spreading in the meso-Tethys continued  
3209 with an acceleration in spreading rate after the complete accretion of the  
3210 Cimmerian terrane at 170 Ma. At 165 Ma, rifting extended southward from  
3211 Argoland to the area between Australia and India (adjacent to the Gascoyne,  
3212 Cuvier and Perth Abyssal Plains) thereby initiating a plate boundary between  
3213 India and Australia. This connected with the newly established rift margin  
3214 between Australia and Antarctica at 165 Ma and extended into the Enderby  
3215 Basin from 165 Ma to the west connected with the Western Panthalassic  
3216 subduction zone along eastern Australia to the east.

3217

#### 3218 **4.3 160-140 Ma (Figure 20-21)**

3219 The Central Atlantic continued spreading between 160-140 Ma, connecting with  
3220 the Gulf of Mexico ridge system to the south. After the cessation of spreading in  
3221 the Gulf of Mexico, the mid-ocean ridge jumped southward initiating the opening  
3222 of the proto-Caribbean Basin through the accommodation space created due to  
3223 the relative motion between the North and South American plates. Spreading  
3224 was NW-SE directed and initiated around 145 Ma forming a triple junction to the  
3225 east between the mid ocean ridge of the Central Atlantic and rift axis of the  
3226 Equatorial/South Atlantic. To the west, the spreading ridge of the proto-  
3227 Caribbean Basin formed a ridge-ridge-transform triple junction with the  
3228 spreading ridge of the Andean back-arc basin and the trans-American subduction  
3229 zone. In the South Atlantic, extension began within continental South America at  
3230 150 Ma, partitioning the southern part of the continent into the Parana and

3231 Colorado subplates and inducing a rift zone between South America and Africa,  
3232 which connected to the Agulhas-Falkland transform to the south.  
3233

3234 The Agulhas-Falkland transform extended eastward connecting to the mid-ocean  
3235 ridge in the Weddell Sea, which was established at 160 Ma. The Weddell Sea  
3236 ridge joined with mid-ocean ridges along East Africa, including between Africa  
3237 and Antarctica in the Mozambique Basin/Riiser-Larson Sea and Africa and  
3238 Madagascar in the West Somali Basin. This newly established ridge system led to  
3239 an acceleration of break-up between East and West Gondwana. From 144 Ma  
3240 onwards, Madagascar operated as an independent plate. In the eastern Tethys,  
3241 rifting extended along the Argo Gascoyne, Cuvier and Perth Abyssal Plains  
3242 forming a triple junction between the Australia/Antarctic rift margin and the  
3243 Enderby rift. By 156 Ma, NW-SE oriented seafloor spreading begun in the Argo  
3244 Abyssal Plain, rifting West Burma/Argoland and establishing the mid-ocean  
3245 ridge system that resulted in the formation of the neo-Tethys ocean. Spreading  
3246 in the meso-Tethys continued the meso-Tethys ridge intersected the Tethyan  
3247 subduction zone around 140-145 Ma resulting in a southern ridge jump and  
3248 continuation of seafloor spreading in the meso-Tethys.  
3249

3250 Spreading and growth of the Pacific plate continued in Panthalassa, with a  
3251 gradual increase in spreading rate. The eruption of the Shatsky Rise at the  
3252 Pacific-Izanagi-Farallon triple junction led to a major readjustment of the triple  
3253 junction centre and was coincident with a major clockwise change in spreading  
3254 direction, by 24°, between the Pacific and Izanagi plates at M21 (~147 Ma). This  
3255 resulted in an increased clockwise rotation and a change in configuration of the  
3256 Pacific-Izanagi, Izanagi-Phoenix and Izanagi-Farallon ridges. The Mongol-  
3257 Okhotsk Ocean closed at 150 Ma forming the Mongol-Okhotsk Suture.  
3258

3259 In the Arctic Ocean, the Canada Basin initiated opening at 145 Ma via  
3260 counterclockwise rotation of North Slope of Alaska with seafloor spreading  
3261 starting at 142 Ma. The Canada Basin spreading ridge connected with the North  
3262 Atlantic rift zone, which extended as far south as the Kings Trough adjacent to  
3263 the Newfoundland/Iberia margin. The plate boundary follows the Kings Trough

3264 through the Pyrenees connecting with the northern Tethyan subduction zone  
3265 and to the south connects with the Central Atlantic mid-ocean ridge.

3266

#### 3267 **4.4 140-120 Ma (Figure 21-22)**

3268 The Central Atlantic and Iberia-Newfoundland spreading ridge continued and  
3269 connected via a series of rift zones to the Canada Basin in the Arctic and to the  
3270 south Atlantic spreading centre to the south. In addition, rifting between North  
3271 America and Greenland initiated around 135 Ma, establishing Greenland as an  
3272 independent plate and marking the end of the Laurentian continental landmass.

3273 The proto-Caribbean Sea continued its growth via differential motion between  
3274 South and North America. Seafloor spreading initiated in the southern South  
3275 Atlantic by 132 Ma coinciding with a peak in magmatism (Parana-Etendeka  
3276 Large Igneous Province) and the initiation of rifting in the African continental  
3277 interior via the West and Central African rift zones. At this time, we break the  
3278 African continent into three discrete plates: South, NW and NE Africa. Seafloor  
3279 spreading between Madagascar and the East African margin ceased around 120  
3280 Ma. In the South Atlantic, seafloor spreading propagated northward to the  
3281 central segment of this ocean by 125 Ma.

3282

3283 The early-mid Cretaceous marks a significant increase in seafloor spreading  
3284 rates in Panthalassa corresponding to the mid-Cretaceous seafloor spreading  
3285 pulse. Spreading was occurring between the Pacific, Farallon, Izanagi and  
3286 Phoenix plates. In northern Panthalassa, North Slope of Alaska was continuing  
3287 its counterclockwise rotation and opening of the Canada Basin.

3288 The southwest Panthalassic margin, along eastern Australia involved the opening  
3289 of the South Loyalty Basin, due to roll-back of the southwest Panthalassic  
3290 subduction zone from 140 Ma. The South Loyalty Basin was actively opening  
3291 until 120 Ma until a major change in the plate configurations in the SW  
3292 Panthalassic Ocean.

3293

3294 Seafloor spreading in the meso-Tethys continued after its southern ridge jump at  
3295 140 Ma. Coincidentally, spreading along the neo-Tethys ridge extending from the  
3296 Argo Abyssal Plain to north of Greater India. After a landward ridge jump of the

3297 neo-Tethys ridge at 135 Ma, the mid-ocean ridge propagated southward to open  
3298 the Gascoyne, Cuvier and Perth Abyssal Plains between India and Australia. The  
3299 West Australian spreading ridge system joined with the Enderby Basin spreading  
3300 ridge, separating Antarctica from the Elan Bank/India, to the west and to the rift  
3301 between Australia and Antarctica to the east. The initiation of seafloor spreading  
3302 in the Enderby Basin accommodated strike-slip motion between India and  
3303 Madagascar of over 1000 km and connected to the West Somali Basin spreading  
3304 ridge. The East African and Weddell Sea spreading ridges were active during this  
3305 time period and connected to the South Atlantic via the Agulhas-Falkland  
3306 transform.

3307

#### 3308 **4.5 120-100 Ma (Figure 22-23)**

3309 Spreading along the Central Atlantic ridge continued into the proto-Caribbean  
3310 Sea until 100 Ma. Spreading extended southward along the South Atlantic ridge  
3311 with a northward propagation leading to seafloor spreading in the “Central”  
3312 segment by 120 Ma and in the “Equatorial” segment by 110 Ma. Extension along  
3313 the West and Central African rifts, including the Benue Trough continued during  
3314 this time period. Further north, spreading between Iberia and Newfoundland  
3315 connected to a rift zone adjacent to the Rockall and Porcupine Plateaus and  
3316 continued to the Labrador Sea/Baffin Bay (between Greenland and North  
3317 America) and between Greenland and Eurasia. Break-up between Porcupine and  
3318 North America occurred from 110 Ma. These North Atlantic rift zones connected  
3319 with the Canada Basin spreading centre until about 118 Ma when spreading  
3320 ceased in the Canada Basin. Spreading terminated when the rotation of North  
3321 Slope Alaska ceased, coincident with a change in the southern North Slope  
3322 margin from largely strike-slip to convergence due to a change in spreading  
3323 direction in Panthalassa.

3324

3325 Ultra fast seafloor spreading rates were occurring in Panthalassa together with  
3326 the eruption of a suite of Large Igneous Provinces, most notably the eruption of  
3327 the Ontong-Java, Manihiki and Hikurangi Plateaus at 120 Ma. The eruption of  
3328 this mega-LIP led directly to the break-up of the Phoenix plate into four plates:  
3329 the Hikurangi, Manihiki, Chasca and Catequil plates. The separation occurred at

3330 120 Ma in an E-W direction in the Ellice Basin between the Ontong Java and  
3331 Manihiki Plateaus with simultaneous rifting of the Manihiki and Hikurangi  
3332 plateaus from a N-S directed spreading system along the Osbourn Trough. An  
3333 additional two triple junctions were active in the region leading to the break-up  
3334 of the Eastern Manihiki Plateau and the development of the Tongareva triple  
3335 junction. The eastern triple junction represented spreading between the  
3336 Manihiki, Phoenix and Chasca plate and the southern triple junction represented  
3337 spreading between the Hikurangi, Catequil and Manihiki plates. The initiation of  
3338 the Pacific-Manihiki-Hikurangi triple junction led to change in the tectonic  
3339 regime along eastern Australia. Prior to 120 Ma, the Phoenix plate was  
3340 subducting beneath the east Australia margin, which changed to the Hikurangi  
3341 plate and a small portion of the Catequil plate but with a decreased rate of  
3342 convergence after 120 Ma.

3343

3344 In the Tethys Ocean, spreading was continuing along the western Australian  
3345 margin, connecting to spreading in the Enderby Basin and rifting between  
3346 Australia and Antarctica. A ridge jump at 120 Ma isolated the Elan Bank  
3347 microcontinent, roughly coincident with the eruption of the Kerguelen Plateau.  
3348 A strike-slip margin between India and Madagascar joined to a transform in the  
3349 Tethys Ocean and not to the West Somali Basin spreading ridge which had  
3350 become extinct at 120 Ma. Spreading continued in the Mozambique Basin/Riiser  
3351 Larson Sea and continued to the Weddell Sea and north to the South Atlantic  
3352 spreading ridge.

3353

#### 3354 ***4.6 100-80 Ma (Figure 23-24)***

3355 The Mid and South Atlantic Ridges were well established from 100 Ma. As  
3356 spreading occurred, rifting in the interior of Africa ceased at about 85 Ma. The  
3357 Mid-Atlantic ridge propagated northward to between the Porcupine margin and  
3358 between North America and the Rockall margin at 50 Ma. Rifts were still active  
3359 surrounding Greenland. The south of the Mid Atlantic Ridge connected to the  
3360 actively opening proto-Caribbean Sea along a major transform fault. The  
3361 western margin of the Caribbean plate underwent a change in subduction  
3362 polarity from east-dipping to west-dipping at 100 Ma. The rollback of this

3363 subduction zone along the Caribbean Arc led to the consumption of the actively  
3364 spreading proto-Caribbean ocean floor and encroachment of the Farallon plate  
3365 into the Caribbean domain (Figure 9). The continued roll-back of the Caribbean  
3366 Arc subduction zone led to the formation of the Yucatan Basin as a back-arc in  
3367 the late Cretaceous. The eruption of the Caribbean flood basalt province  
3368 occurred around 90 Ma overlying oceanic lithosphere that formed on the  
3369 Farallon plate and later migrated to the Caribbean region.

3370

3371 In Panthalassa, spreading was occurring along the Pacific-Izanagi, Pacific-  
3372 Farallon, Farallon-Izanagi and along the ridges associated with the plateau  
3373 break-up region. A change in spreading direction is recorded in the Mendocino,  
3374 Molokai and Clarion fracture zones (associated with Pacific-Farallon spreading),  
3375 which we date to 103-100 Ma coincident with an observed bend in the hotspot  
3376 trails on the Pacific plate, suggesting a plate reorganization at this time. In  
3377 addition, we model a clockwise change in spreading direction in the Osbourn  
3378 Trough region based on our age estimate for a bend in observed fracture zones  
3379 between the Manihiki and Hikurangi plateaus. The change in spreading direction  
3380 modified the nature of the boundary east of Australia from convergence to  
3381 dominantly strike-slip. At 86 Ma, we model the docking of the Hikurangi Plateau  
3382 with the Chatham Rise triggering a cessation in spreading associated the Ontong-  
3383 Java, Manihiki and Hikurangi plateaus. After the cessation of spreading along  
3384 these ridges axes, the locus of extension jumped southward between Antarctica  
3385 and the Chatham Rise, establishing the Pacific-Antarctic spreading ridge. To the  
3386 east, the Pacific-Farallon Ridge extended to the south connecting with the  
3387 Pacific-Antarctic Ridge at the Pacific-Antarctic-Farallon triple junction.

3388

3389 After the cessation of the spreading centers associated with the LIP break-up, the  
3390 Pacific plate became the dominant plate in Panthalassa and it is at this time that  
3391 we switch to the Pacific Ocean. In the western Pacific, the Tasman Sea was  
3392 opening from 84 Ma leading to the establishment of the Lord Howe Rise plate.  
3393 Further north, the proto-South China Sea initiated its opening between the South  
3394 China margin and Borneo/Kalimantan.

3395

3396 In the Tethys/Indian Ocean, spreading was occurring along the West Australian  
3397 margins continuing the separation of India and West Burma from Australia. A  
3398 major change direction is recorded in the fracture zone trends at 99 Ma, led to a  
3399 change in the motion of the Indian plate. Spreading became dominantly N-S  
3400 directed establishing spreading in the Wharton Basin. The West Australian mid  
3401 ocean ridge system formed a triple junction with the Australian-Antarctic ridge  
3402 at 99 Ma (initiation of ultra-slow seafloor spreading) and spreading between  
3403 India and Antarctica north of Elan Bank. The Indian-Antarctic ridge (or  
3404 Southeast Indian Ridge) connected with the African-Antarctic ridge (or  
3405 Southwest Indian Ridge) from 100 Ma. Rifting between India and Madagascar in  
3406 the Mascarene Basin initiated at 87 Ma. The Southwest Indian Ridge connected  
3407 with spreading in the Malvinas plate in the southernmost Atlantic at 83.5 Ma and  
3408 the American-Antarctic ridge (established after the cessation of spreading in the  
3409 Weddell Sea). The West Burma continental sliver reached the Eurasian margin  
3410 and accreted starting at 87 Ma and sutured to Sibumasu at 73 Ma.

3411

#### 3412 ***4.7 80-60 Ma (Figure 24-25)***

3413 The South and Mid-Atlantic ridges continued spreading. The Mid-Atlantic Ridge  
3414 propagated northward into the North Atlantic with the initiation of seafloor  
3415 spreading in the Labrador Sea (between North America and Greenland) and  
3416 between Rockall and Greenland at 79 Ma. Spreading propagated from the  
3417 Labrador Sea to Baffin Bay by 63 Ma across the Davis Straits via left-lateral  
3418 transform faults and connected to the Arctic via the Nares Strait. In the  
3419 Caribbean, spreading in the proto-Caribbean Sea ceased at 80 Ma whereas the  
3420 Caribbean Arc subduction zone continued its northeastward rollback. The  
3421 Yucatan Basin opened as a back-arc in the late Cretaceous with cessation  
3422 occurring at 70 Ma when the Caribbean Arc accreted to the Bahaman Platform.  
3423 The accretion led to a jump in the locus of subduction westward along the newly  
3424 developed Panama-Costa Rica to accommodate the continued eastward motion  
3425 of the Farallon plate, trapping Farallon oceanic lithosphere onto the Caribbean  
3426 plate.

3427

3428 The Pacific was dominated by the break-up of the Farallon plate into the Kula  
3429 plate at 79 Ma initiating spreading along the E-W trending Kula-Pacific ridge and  
3430 the NE-SW trending Kula-Farallon ridge. The Kula-Farallon Ridge follows the  
3431 location of the Yellowstone hotspot and intersects the North American margin in  
3432 Washington/British Columbia before migrating northward along the margin.  
3433 The break up of the Farallon plate into the Kula plate coincides with a major  
3434 change in spreading direction observed in all northeast Pacific fracture zones. In  
3435 our model spreading continued along the Pacific-Izanagi ridge after the  
3436 establishment of the Kula-Pacific ridge to the east connected via a large offset  
3437 transform fault. The Pacific-Izanagi ridge was rapidly approaching the East  
3438 Asian margin and was proximal by 60 Ma. In the southern Pacific, spreading was  
3439 occurring along the Pacific-Antarctic ridge, extending eastward to connect with  
3440 the Pacific-Farallon and Farallon-Antarctic spreading ridges. At 67 Ma, a change  
3441 in spreading direction is recorded in the fracture zones of the South Pacific.

3442

3443 In the Indian Ocean, spreading was occurring along the Wharton Ridge,  
3444 Southeast Indian Ridge, Southwest Indian Ridge and in the Mascarene Basin.  
3445 Spreading in the Mascarene Basin ceased at 64 Ma jumping northward, isolating  
3446 the Seychelles microcontinent and initiating spreading between India and the  
3447 Seychelles along the Carlsberg Ridge. The Southwest Indian Ridge connected  
3448 with spreading in the Malvinas plate until 66 Ma. After this, the Southwest  
3449 Indian Ridge connected directly with the American-Antarctic and South Atlantic  
3450 Ridge.

3451

#### 3452 ***4.8 60-40 Ma (Figure 25-26)***

3453 Seafloor spreading propagated into the Eurasia-Greenland margin along the  
3454 Reykjanes Ridge by 58 Ma, forming a triple junction between North America,  
3455 Greenland and Eurasia. The Jan Mayen microcontinent rifted off the margin  
3456 forming the fan-shaped Norway Basin along the Aegir Ridge. The Aegir Ridge  
3457 connected to the Mohns Ridge to the north and Reykjanes Ridge to the south via  
3458 a series of transform faults. Spreading in the Eurasian Basin to the north  
3459 initiated around 55 Ma along the Gakkel/Nansen Ridge. This ridge connected to  
3460 the Baffin Bay ridge axis through the Nares Strait and the Mohns Ridge to the

3461 south via major strike-slip faults with minor compression between Greenland  
3462 and Svalbard. In our model the Lomonosov Ridge is coupled to North America.  
3463 The initiation of spreading in the Eurasian Basin also coincides with the  
3464 initiation of independent motion of the Porcupine Plate, resulting in a small  
3465 clockwise rotation of Eurasia and counter-clockwise rotation of Iberia relative to  
3466 the Porcupine Plate. A change in spreading direction is also observed in the  
3467 Labrador Sea.

3468

3469 The Mid-Atlantic Ridge connects with the west-dipping subduction zone  
3470 bordering the Caribbean via a transform fault. By the middle Eocene, relative  
3471 motion between North America and the Caribbean began to form the Cayman  
3472 Trough along sinistral faults that later merge with the Lesser Antilles trench.  
3473 East-dipping subduction was still occurring along the Middle America margin  
3474 bordering the Pacific.

3475

3476 In the Pacific, the Pacific-Izanagi ridge started to subduct under the East Asian  
3477 margin between 55-50 Ma, signaling the death of the Izanagi plate coincident  
3478 with a dramatic change in spreading direction from N-S to NW-SE between Kula-  
3479 Pacific spreading. The Kula-Pacific Ridge connected with the Pacific-Farallon  
3480 Ridge and Kula-Farallon Ridge from 60-55 Ma. After 55 Ma, the eastern Pacific  
3481 was dominated by the rupture of the Farallon plate close to the Pioneer Fracture  
3482 Zone, forming the Vancouver plate. The break-up resulted in minor relative  
3483 motion along the Pioneer fracture zone. Further south, spreading was  
3484 continuing along the Pacific-Farallon, Pacific-Antarctic, Farallon-Antarctic and  
3485 Pacific-Aluk Ridges. The fracture zones associated with the Pacific-Antarctic  
3486 Ridge close to the Campbell Plateau record a change in spreading direction at 55  
3487 Ma, coincident the other events that occurred in the Pacific at this time.

3488

3489 In the western Pacific, spreading in the proto-South China Sea ceased at 50 Ma  
3490 coincident with the clockwise rotation of the neighboring Philippine Sea plate.  
3491 The dramatic change in motion of the Philippine Sea plate reorganized the plate  
3492 boundaries in the area leading to the establishment of a subduction zone  
3493 between Palawan and the proto-South China Sea, which led to the subduction of

3494 the proto-South China Sea after 50 Ma. Spreading was occurring in the West  
3495 Philippine Basin and Celebes Sea. Further south, spreading initiated in the North  
3496 Loyalty Basin behind the proto-Tonga-Kermadec Trench.

3497

3498 The Indian Ocean was dominated by a series of mid ocean ridges such as the  
3499 Wharton Ridge, Southeast Indian Ridge, Southwest Indian Ridge and Carlsberg  
3500 Ridge. Prior to 55 Ma, subduction was occurring along the Tethyan subduction  
3501 zone, consuming crust that formed during meso and neo Tethys spreading. At 55  
3502 Ma, the northern tip of Greater India marks the start of collision between India  
3503 and Eurasia and the uplift of the Himalayas. Closure of the Tethys Ocean in this  
3504 area occurred by about 43 Ma. Full closure of the neo-Tethys between India and  
3505 Eurasia also corresponds to the cessation of spreading in the Wharton Basin,  
3506 which describes Australia-India motion.

3507

#### 3508 **4.9 40-20 Ma (Figure 26-27)**

3509 At 40 Ma, the Atlantic Ocean consisted of a continuous mid-ocean ridge system  
3510 that extended from the South America-Antarctica-Africa triple junction to the  
3511 Eurasian Basin in the north. The cessation of independent Porcupine motion  
3512 occurred at 33 Ma coinciding with the cessation of seafloor spreading in the  
3513 neighboring Labrador Sea and Baffin Bay and the establishment of a simple two-  
3514 plate system to describe the plate motions in the North Atlantic. From 33 Ma  
3515 onwards, Greenland and North America have been fused into one plate. At about  
3516 30 Ma, spreading jumped from the Aegir Ridge in the Norway Basin to the  
3517 Kolbeinsey Ridge connecting up with the Mohns Ridge via a series of transform  
3518 faults. Further south, adjacent to the Iberian margin, a southern jump of the  
3519 plate boundary at 28 Ma from the Kings Tough to the Azores transform fault and  
3520 along the Straits of Gibraltar led to the capture of Iberia by the Eurasian plate.

3521

3522 In the Pacific, spreading between the Kula-Pacific and Kula-Farallon ceased at 40  
3523 Ma, leading to the Pacific plate consisting of the Pacific, Vancouver, Farallon, Aluk  
3524 and Antarctic plates. The intersection of the Murray transform fault with the  
3525 North American subduction zone around 30 Ma led to the establishment of the  
3526 San Andreas Fault and corresponds to the establishment of the Juan De Fuca

3527 plate at the expense of the Vancouver plate. A further rupture of the Farallon  
3528 plate occurred at 23 Ma leading to the establishment of the Cocos and Nazca  
3529 plates and initiation of the East Pacific Rise, Galapagos Spreading Centre and  
3530 Chile Ridge.

3531

3532 In the Western Pacific, spreading in the West Philippine Basin ceased at 38 Ma  
3533 whereas spreading continued in the Celebes Sea. The formation of the Caroline  
3534 Sea occurred behind a rapidly southward migrating subduction zone. By 30 Ma,  
3535 spreading initiated in the Shikoku and Parece Vela Basins behind the west-  
3536 dipping Izu-Bonin-Mariana Arc. Spreading terminated in the Celebes Sea. In the  
3537 SW Pacific, spreading initiated in the Solomon Sea at 40 Ma and in the South Fiji  
3538 Basin at 35 Ma. Cessation of spreading in the South Fiji Basin occurred at 25 Ma.

3539

3540 In the Indian Ocean, spreading continued along the Southwest Indian Ridge,  
3541 Southeast Indian Ridge, Central Indian Ridge and Carlsberg Ridge. Extension  
3542 along the East Africa rifts was established at 30 Ma leading to the break-up of  
3543 Africa into Somalia plate. Rifting along the Sheba Ridge, separating Arabia from  
3544 Africa/Somalia initiated at 30 Ma.

3545

#### 3546 **4.10 20-0 Ma (Figure 27-28)**

3547 Spreading in the South, Central and North Atlantic continued unabated since 20  
3548 million years ago. In the Caribbean, the Cayman Trough continued to expand and  
3549 develop, and the Chortis Block moved over the Yucatan promontory. Westward  
3550 motion of the North American plate relative to the slow moving Caribbean plate  
3551 was accommodating the opening of the Cayman Trough. Active subduction of  
3552 Atlantic oceanic lithosphere has been occurring along the Lesser Antilles Trench,  
3553 which connects to the Mid-Atlantic Ridge along the Researcher Ridge and Royal  
3554 Trough.

3555

3556 In the Pacific, spreading was occurring along the Pacific-Juan De Fuca, Pacific-  
3557 Nazca, Pacific-Cocos, Cocos-Nazca, Pacific-Antarctic and Nazca-Antarctic ridges.  
3558 The Bauer microplate formed along the East Pacific Rise at 17 Ma and continued  
3559 until 6 Ma. The locus of spreading then jumped back to the East Pacific Rise

3560 (between the Pacific and Nazca plates). The East Pacific Rise is the fastest  
3561 spreading ridge system (excluding back-arc opening) and currently encompasses  
3562 microplate formation at the Easter, Juan Fernandez and Galapagos plates.  
3563 Currently, the Juan De Fuca plate is limited at its southern end by the Mendocino  
3564 Fracture Zone and is subducting slowly along the Cascadia subduction zone.

3565

3566 The western Pacific is dominated by the opening of a series of back-arc basins  
3567 due to the roll-back of the subduction hinge of the Tonga-Kermadec and Izu-  
3568 Bonin-Mariana trenches. Spreading in the Shikoku and Parece Vela Basins and  
3569 South China Sea ceased at 15 Ma. By 9 Ma, spreading initiated in the Mariana  
3570 Trough. We model complete closure of the proto-South China Sea at around 10  
3571 Ma behind a subduction zone located along Palawan and the north  
3572 Borneo/Kalimantan margin. In the SW Pacific, spreading in the Lau Basin  
3573 initiated by 7 Ma with back-arc extension occurring in the Havre Trough.

3574

3575 In the Indian Ocean, diffuse deformation occurring in the middle of the Indo-  
3576 Australian plate led to the development of the Capricorn plate in the central-east  
3577 Indian Ocean at 20 Ma. Further west, we initiate spreading along the Sheba  
3578 Ridge at 20 Ma. The Sheba Ridge propagated into the Red Sea at 15 Ma.

3579

## 3580 **5. Discussion**

### 3581 ***5.1 Comparison with other models***

3582 Our plate motion model offers an alternative approach to traditional global plate  
3583 reconstructions. Tectonic features that reside on the surface of the Earth are not  
3584 modeled as discrete features but rather the plates themselves are modeled as  
3585 dynamically evolving features. The nature of the plate boundaries that combine  
3586 to form a plate will necessarily change based on the magnitude and direction of  
3587 motion of each plate. Therefore, one of the supplementary outcomes of this  
3588 approach is the ability to directly compare competing tectonic models, most  
3589 easily expressed through plate velocity vectors for a common set of points on the  
3590 surface of the Earth. We directly compare the plate motion model presented in  
3591 Gurnis et al. (2012) to the model presented in this study (Figure 29).

3592

3593 In this study we have adopted a new absolute plate motion model for Africa for  
3594 times prior to 100 Ma based on a true-polar wander corrected paleomagnetic  
3595 reference frame (Steinberger and Torsvik, 2008). This new reference frame  
3596 allows us to extend our plate reconstructions back to 200 Ma, the time of Pangea  
3597 break-up, with the potential to model processes occurring during supercontinent  
3598 break-up and dispersal. The Gurnis et al. (2012) dataset was restricted to the  
3599 past 140 million years. Adjusting the absolute reference frame causes a global  
3600 shift in the absolute positioning of the continents but in theory, should not affect  
3601 the relative motion and therefore the nature of the plate boundary between  
3602 plates. However prior to 83.5 Ma, the Pacific plate can no longer link to the  
3603 African plate circuit via seafloor spreading (see Section 2 Methodology)  
3604 requiring a distinct absolute reference frame for the Pacific realm. As a result, a  
3605 change in the absolute reference frame for either the African or Pacific realms  
3606 will change the nature of the plate boundaries that border the  
3607 Pacific/Panthalassic ocean (Figure 29).

3608  
3609 Relative motions between most of the plates in Panthalassa have been updated  
3610 compared to the Gurnis et al. (2012) model. We reinterpreted the M-series  
3611 Japanese magnetic lineations leading to a dramatic change in spreading direction  
3612 by about 24° and an updated orientation of the Izanagi-Farallon and Izanagi-  
3613 Phoenix ridges. The change in the Izanagi plate motion results in an increase in  
3614 the convergence rate and more orthogonal convergence in northern Panthalassa  
3615 bordering eastern Laurasia but more oblique convergence in the area further  
3616 south adjacent to the Junction plate (Figure 29).

3617  
3618 Another major addition to the model presented in this study is the  
3619 implementation of the plateau break-up model of Taylor (2006) for the Ontong-  
3620 Java, Manihiki and Hikurangi plateaus (Figure 29). Incorporating the plateau  
3621 break-up has consequences for the evolution of the Phoenix plate and the  
3622 eastern Gondwana margin. Most Mesozoic models for eastern Gondwana  
3623 propose a long-lived convergent plate margin along the eastern edge of Australia  
3624 (Cluzel et al., 2010; Matthews et al., 2010; Veevers, 2006), expressed through  
3625 andesitic volcanism that occurred along the Queensland margin north to Papua

3626 New Guinea (Jones and Veevers, 1983) and Aptian-Albian andesitic volcanogenic  
3627 detritus in east Australian continental basins (e.g. Eromanga and Surat Basins)  
3628 (Hawllader, 1990; Veevers, 2006). Plate velocity vectors using either Gurnis et al.  
3629 (2012) or the this study, predict a convergent margin between the Phoenix plate  
3630 and eastern Gondwana during this time (Figure 29). There is ambiguity as to  
3631 whether the margin continued as a convergent margin or whether there was a  
3632 major tectonic regime change after ~120 Ma, coincident with the eruption of the  
3633 Ontong-Java, Manihiki and Hikurangi plateaus and subsequent change in the mid  
3634 ocean ridge configuration in southern Panthalassa. Extensive magmatism  
3635 recorded in the Whitsunday Volcanic Province is attributed to continental  
3636 margin break-up rather than from a convergent margin setting (Bryan et al.,  
3637 1997) while others invoke a rift-related volcanics associated with west-dipping  
3638 subduction (Veevers, 2006). New Caledonia and parts of New Zealand, which  
3639 were located at the easternmost boundary of the Australian continent record  
3640 subduction related magmatism until at least 99 Ma (Veevers, 2006) or 95 Ma  
3641 (Cluzel et al. 2010) suggesting convergence was occurring along eastern  
3642 Gondwana. Although the plate motion model of Gurnis et al. (2012) does not  
3643 include the rotations associated with the plateau break-up, both models predict  
3644 continuing convergence until 100 Ma (Figure 29).

3645

3646 At 100-99 Ma, a major tectonic regime change is recorded in eastern Australia  
3647 (Veevers, 2006). Sedimentation in the east Australian basins changed from  
3648 volcanogenic dominated to quartzose sandstone (Veevers, 2006), the basins  
3649 themselves changed from a prolonged period of subsidence to uplift (Matthews  
3650 et al., 2010) and volcanism became alkalitic (Veevers, 2006). In addition, the  
3651 eastern margin changed to a period of extension and passive margin formation  
3652 (e.g. extension in the Lord Howe Rise and New Caledonia Basins), which are  
3653 believed to have formed adjacent to a strike-slip margin defining the boundary  
3654 between Panthalassa and eastern Gondwana (Jones and Veevers, 1983; Veevers,  
3655 2006). A hiatus in subduction-related volcanism in Eastern Australia, New  
3656 Caledonia and New Zealand is recorded between 95-83 Ma (Cluzel et al., 2010).  
3657 This major tectonic regime change is coincident with a change in spreading  
3658 direction in the plates associated with the plateau break-up and bordering the

3659 eastern Gondwana margin at this time. The result is that the eastern Gondwana  
3660 margin changes from convergent to strike-slip, as predicted by geological  
3661 observations. This is in contrast to the model of Gurnis et al. (2012) which  
3662 suggests oblique convergence after 100-99 Ma (Figure 29). In our current plate  
3663 motion model, a strike-slip dominated margin is predicted from 100-86 Ma,  
3664 which marks the timing of Hikurangi plateau collision with the Chatham Rise and  
3665 the cessation of mid ocean ridge subduction related to the plateau break-up. The  
3666 plate adjacent to eastern Australia became the Pacific plate and all subsequent  
3667 motions have been between the Pacific and Australian or Lord Howe Rise plates.  
3668

3669 Additional differences between the relative plate motions presented in Gurnis et  
3670 al. (2012) and this study include an updated northern Atlantic based on Gaina et  
3671 al. (2009) and the Arctic based on Alvey et al. (2008). The changes here are  
3672 minor adjustments and do not substantially change plate motion directions or  
3673 the nature of the plate boundaries in the area.

3674

## 3675 ***5.2 Future Directions***

3676 Our global plate motion model presents the development of the continents and  
3677 oceans on a global scale within a rigid plate framework, underpinned by a  
3678 combination of marine geophysical data, onshore geological data and plate  
3679 tectonic principles. Although we have presented our preferred interpretations  
3680 for each region based on available data, there are regions that could benefit from  
3681 re-analysis of the seafloor spreading and break-up history, which will have a  
3682 significant flow-on affect further down the global plate circuit. These include:

- 3683 1. The early break-up history between Africa and South America to account  
3684 for significant overlaps and gaps between the two margins. Refining the  
3685 history between these two plates will lead to a revision of the Mesozoic  
3686 history of the Caribbean region (i.e. the accommodation space created to  
3687 form the proto-Caribbean Sea and the rift basins associated with  
3688 hydrocarbon-bearing basins in the Gulf of Mexico), a more tightly  
3689 constrained equatorial Atlantic and also the plate boundaries surrounding  
3690 the Weddell Sea, which are very ill-constrained due to a paucity of data.

- 3691 2. The early break-up history and Mesozoic spreading between Africa and  
3692 Antarctica. A further refinement of the opening history of this area will  
3693 affect the motions of Antarctica, India and Australia and the interaction  
3694 (plate boundary processes) along the eastern Gondwana margin  
3695 bordering Panthalassa.
- 3696 3. The break-up history of the Pacific-Marie Byrd Land margin (~100-83  
3697 Ma), which has consequences for the motion of the Pacific plate and  
3698 associated plates, such as the Izanagi, Phoenix, Farallon, Hikurangi,  
3699 Manihiki, Catequil and Casca plates. The Pacific plate can only be linked  
3700 to the plate circuit, through Africa, when there is a mid-ocean ridge (or  
3701 rift) between the Pacific and Antarctica/Marie Byrd Land. Greater  
3702 constraints on the timing of break-up between the Campbell Plateau and  
3703 Antarctica and a revised set of finite rotations to describe the opening will  
3704 potentially mean we can confidently extend the Pacific plate's link to the  
3705 plate circuit further back in time and decrease the uncertainty in Pacific  
3706 plate motion during this time interval.

3707

3708 A major improvement that is essential for global plate motion models that extend  
3709 into the Mesozoic is a more robust Pacific absolute plate motion model. The  
3710 latest models available with associated published rotation poles for Pacific  
3711 hotspots (Wessel et al. 2006; Wessel and Kroenke 2008) result in major shifts  
3712 and rotations of the Pacific plate, which are inconsistent with geological  
3713 observations; for example their Pacific hotspot models, combined with a relative  
3714 plate motion model for motion between the Farallon and Pacific plates, results in  
3715 transform motion between the Farallon and North American plates, while  
3716 geological observations indicate subduction being active (DeCelles, 2004). This  
3717 model also leads to an anomalous amount of material entering the mantle in the  
3718 southern hemisphere (Shephard et al., 2012). This inconsistency may result  
3719 from the assumption of Pacific hotspot fixity and poor sampling of Pacific  
3720 seamount chains due to a paucity of available data. A new approach using a  
3721 combination of methods, for example moving hotspot models, paleomagnetism  
3722 and coupled geodynamic-plate motion models, may result in a more robust

3723 model for the Pacific plate prior to ~83 Ma and may potentially extend the  
3724 Pacific absolute reference frame to the earliest Mesozoic.

3725  
3726 A further limitation of the present model is that the entire surface of the earth is  
3727 represented as rigid blocks, which is clearly not true for some plate interiors and  
3728 plate boundaries (Bird, 2003; Gordon and Stein, 1992). Deforming regions within  
3729 plate interiors or straddling plate boundaries will clearly be required for  
3730 reconstructions beyond those presented here. For future models, deforming  
3731 regions can now be encompassed within the domain of an evolving, closed  
3732 polygon and consequently incorporated as an extension of the CCP algorithm  
3733 (see Gurnis et al 2012). We expect that such deforming regions will be  
3734 represented as deforming meshes within continuously closing polygons as the  
3735 lowest level of a global hierarchy. Such functionality has now been incorporated  
3736 in experimental versions of *GPlates* and will be a part of a new generation of  
3737 global plate reconstructions. The first region to be addressed within a deforming  
3738 plate network is the opening of the rift basins within the interior of Africa as the  
3739 accounting of this extension will have flow-on effects for all the plates that hang-  
3740 off the African-centered plate circuit.

3741

## 3742 **6. Conclusions**

3743 There are currently three main types of plate motion models that enable us to  
3744 place features on the surface of the earth into their spatio-temporal context.  
3745 Geologically-current plate motion models are ideal because they provide a set of  
3746 plate velocity vectors and delineate the boundaries between tectonic plates in a  
3747 self-consistent way (i.e. the combined area of the plates equals the area of the  
3748 Earth). However, they are restricted to the Pliocene, making analysis of  
3749 supercontinent break-up and accretion, the linkages between the deep earth and  
3750 surface processes and larger-scale tectonic cycles unrealistic. Traditional plate  
3751 motion models do not treat plates in a self-consistent way but rather reconstruct  
3752 discrete features on the surface of the Earth without regard to the evolving  
3753 nature of plate boundaries. Coupled geodynamic models are prone to large  
3754 uncertainties and have not been successful at replicating past plate motions  
3755 consistently in deep time.

3756

3757 In this paper, we have presented a new type of global plate motion model, which  
3758 extends into deep time and involves a continuously evolving and self-consistent  
3759 set of plate polygons and plate boundaries from the time of Pangea break-up.

3760 Our model is underpinned by a detailed analysis of the seafloor spreading record  
3761 for the major tectonic plates. Our regional models are built within a hierarchical  
3762 plate circuit framework linked to a hybrid absolute reference frame that includes  
3763 moving Indian/Atlantic hotspots and a true polar wander corrected  
3764 paleomagnetic-based model.

3765

3766 The plate motion model presented in this study will be of particular use to  
3767 geodynamicists who require surface boundary conditions for the motions of the  
3768 plates through time to link to models of the convecting mantle. However, our  
3769 hope is that it can also be used as a framework for further detailed work so that  
3770 we may converge towards an ever-improved set of global plate reconstructions.

3771 We provide all data freely in digital form, welcome feedback to improve our  
3772 models and anticipate that refinements to the plate model will be published in  
3773 the future. The plate polygon data files with associated rotation file and an  
3774 accompanying coastline and continent-ocean boundary file can be downloaded  
3775 from the following location:

3776 [ftp://ftp.earthbyte.org/earthbyte/GlobalPlateModel/Seton\\_etal\\_Data.zip](ftp://ftp.earthbyte.org/earthbyte/GlobalPlateModel/Seton_etal_Data.zip).

3777

### 3778 **Acknowledgements**

3779 We thank Roi Granot and an anonymous reviewer for agreeing to review such a  
3780 lengthy manuscript and for their thoughtful and careful review, which greatly  
3781 improved the manuscript. We would also like to thank members of the  
3782 EarthByte Group and the group at Caltech led by Michael Gurnis who have  
3783 contributed over many years towards the continuous improvement of the global  
3784 plate motion model and associated files. This project was funded through  
3785 Australian Research Council grants FL0992245 and DP0987713.

3786

### 3787 **Figure Captions**

3788

3789 **Figure 1**

3790 Global gravity anomalies from satellite altimetry (Sandwell and Smith 2009).  
3791 Red lines denote present day plate boundaries from the plate boundary set  
3792 presented in this study. AFR = Africa, ANT = Antarctica, ARA = Arabia, AUS =  
3793 Australia, C = Cocos, CAP = Capricorn, CAR = Caribbean, EUR = Eurasia, IND =  
3794 India, NAM = North America, NAZ = Nazca, PAC = Pacific, PH = Philippine, SAM =  
3795 South America, SOM = Somalia.

3796

3797 **Figure 2**

3798 a. Gridded magnetic anomalies for the South Atlantic. Seafloor spreading  
3799 isochrons used in this study plotted as thin black lines. Due to poor data  
3800 coverage, correlations between the gridded data and isochrons are difficult. AB  
3801 = Agulhas Basin, BT = Benue Trough, P-E = Parana Flood Basalts, RG = Rio-  
3802 Grande Rise, WR = Walvis Ridge.

3803 b. Seafloor spreading isochron map coloured by spreading system or plate pair.  
3804 Map abbreviations are same as a. Legend abbreviations are: AFR = South Africa,  
3805 BB = Back-arc Basins, EANT = East Antarctica/Antarctica, MAL = Malvinas, NWA  
3806 = Northwest Africa, OTH = Other spreading systems outside area of interest, SAM  
3807 = South America.

3808

3809 **Figure 3**

3810 a. Gridded magnetic anomalies for the Central and North Atlantic. Seafloor  
3811 spreading isochrons used in this study plotted as thin black lines. BB = Bay of  
3812 Biscay, CG = Charlie-Gibbs Fracture Zone, CLIP = Caribbean Large Igneous  
3813 Province, DS = Davis Strait, JFZ = Jacksonville Fracture Zone, KT = Kings Trough,  
3814 MM = Morocco Maeseta, NF = Newfoundland, RR = Rekyjanes Ridge, RP = Rockall  
3815 Plateau, RT = Rockall Trough.

3816 b. Seafloor spreading isochron map coloured by spreading system or plate pair.  
3817 Map abbreviations are same as a. Legend abbreviations are: AFR = Africa, BB =  
3818 Back-arc Basins, EUR = Eurasia, GRN = Greenland, IBR = Iberia, NAM = North  
3819 America, NWA = Northwest Africa, OTH = Other spreading systems outside area  
3820 of interest, POR = Porcupine, SAM = South America.

3821

3822 **Figure 4**

- 3823 a. Agegrid reconstructions of the Central and North Atlantic at 120, 90, 60,  
3824 30, 0 Ma highlighting the age-area distribution of oceanic lithosphere at  
3825 the time of formation and the extent of continental crust (grey polygons).  
3826 Plate boundaries from our continuously closing plate polygon dataset are  
3827 denoted as thick white lines, hotspot locations as yellow stars, large  
3828 igneous provinces and flood basalts as brown polygons and coastlines as  
3829 thin black lines.
- 3830 b. Reconstructions showing the outlines of the plates in the Central and  
3831 North Atlantic for each reconstruction time listed above. Feature  
3832 descriptions as in Figure 4a. Abbreviations are: NAM = North American  
3833 plate, GRN = Greenland plate, EUR = Eurasian plate, IBR = Iberian plate,  
3834 AFR = African plate, NWA = Northwest African plate, NEA = Northeast  
3835 African plate, POR = Porcupine plate.

3836

3837 **Figure 5**

- 3838 a. Gridded magnetic anomalies for the Arctic. Seafloor spreading isochrons used  
3839 in this study plotted as thin black lines. AL = Alpha Ridge, AR = Aegir Ridge, CR =  
3840 Chukchi Ridge, DS = Davis Strait, GR = Gakkel Ridge, JM = Jan Mayen, KR =  
3841 Kolbeinsey Ridge, LR = Lomonosov Ridge, MB = Makarov Basin, MD = Mendeleev  
3842 Ridge, MR = Mohs Ridge, NR = Northwind Ridge, NS = Nares Strait, PB =  
3843 Podvodnikov Basin.
- 3844 b. Seafloor spreading isochron map coloured by spreading system or plate pair.  
3845 Map abbreviations are same as a. Legend abbreviations are: BB = Back-arc  
3846 Basins, EUR = Eurasia, GRN = Greenland, JAM = Jan Mayen, MDR = Mendeleev,  
3847 NAM = North America, NOR = Norway, NSA = North Slope Alaska, OTH = Other  
3848 spreading systems outside area of interest.

3849

3850 **Figure 6**

- 3851 a. Gridded magnetic anomalies for the Western Pacific, based on isotropic  
3852 gridding of a combination of public domain and in-house data. Seafloor  
3853 spreading isochrons used in this study plotted as thin black lines. Numbers

3854 correspond to magnetic anomaly chron. HR = Hess Rise, OJP = Ontong Java  
3855 Plateau, SR = Shatsky Rise.  
3856 b. Seafloor spreading isochron map coloured by spreading system or plate pair.  
3857 Map abbreviations are same as a. Legend abbreviations are: BB = Back-arc  
3858 Basins, FAR = Farallon, IZA = Izanagi, KUL = Kula, MAN = Manihiki, OTH = Other  
3859 spreading systems outside area of interest, PAC = Pacific, PHX = Phoenix.

3860

3861 **Figure 7**

3862 a. Gridded magnetic anomalies for the northeast Pacific. Seafloor spreading  
3863 isochrons used in this study plotted as thin black lines. Numbers correspond to  
3864 magnetic anomaly chron. QT = Quesnellia Terrane, ST = Stikinia Arc, W =  
3865 Wrangellia, YTT = Yukon/Tanana Terrane.

3866 b. Seafloor spreading isochron map coloured by spreading system or plate pair.  
3867 Map abbreviations are same as a. Legend abbreviations are: COC = Cocos, FAR =  
3868 Farallon, JDF = Juan De Fuca, KUL = Kula, PAC = Pacific, RIV = Rivera/Guadalupe,  
3869 VAN = Vancouver.

3870

3871 **Figure 8**

3872 a. Agegrid reconstructions of the northeast Pacific at 120, 100, 50, 30, 10, 0  
3873 Ma highlighting the age-area distribution of oceanic lithosphere at the  
3874 time of formation and the extent of continental crust (grey polygons).  
3875 Plate boundaries from our continuously closing plate polygon dataset are  
3876 denoted as thick white lines, hotspot locations as yellow stars, large  
3877 igneous provinces and flood basalts as brown polygons and coastlines as  
3878 thin black lines.

3879 b. Reconstructions showing the outlines of the plates in the northeast Pacific  
3880 for each reconstruction time listed above. Feature descriptions as in  
3881 Figure 8a. Abbreviations are: AFR = African plate, CAR = Caribbean plate,  
3882 COC = Cocos plate, EUR = Eurasian plate, FAR = Farallon plate, GRN =  
3883 Greenland plate, IBR = Iberian plate, IZA = Izanagi plate, JDF = Juan de  
3884 Fuca plate, KUL = Kula plate, NAM = North American plate, NAZ = Nazca  
3885 plate, PAC = Pacific plate, POR = Porcupine plate, RIV = Rivera plate, SAM  
3886 = South American plate, VAN = Vancouver plate.

3887

3888 **Figure 9**

- 3889 a. Gridded magnetic anomalies for the southeast Pacific. Seafloor spreading  
3890 isochrons used in this study plotted as thin black lines. Numbers correspond to  
3891 magnetic anomaly chron. B = Bauer Microplate, CR = Chile Ridge, E = Easter  
3892 Microplate, EPR = East Pacific Rise, F = Friday Microplate, G = Galapagos  
3893 Microplate, GR = Galapagos Ridge, J = Juan Fernandez Microplate, PAR = Pacific-  
3894 Antarctic Ridge.
- 3895 b. Seafloor spreading isochron map coloured by spreading system or plate pair.  
3896 Map abbreviations are same as a. Legend abbreviations are: BAU = Bauer, COC =  
3897 Cocos, FAR = Farallon, NAZ = Nazca, PAC = Pacific, RIV = Rivera/Guadalupe,  
3898 WANT = West Antarctica/Antarctica.

3899

3900 **Figure 10**

- 3901 a. Agegrid reconstructions of the southeast Pacific at 120, 100, 80, 40, 10, 0  
3902 Ma highlighting the age-area distribution of oceanic lithosphere at the  
3903 time of formation and the extent of continental crust (grey polygons).  
3904 Plate boundaries from our continuously closing plate polygon dataset are  
3905 denoted as thick white lines, hotspot locations as yellow stars, large  
3906 igneous provinces and flood basalts as brown polygons and coastlines as  
3907 thin black lines.
- 3908 b. Reconstructions showing the outlines of the plates in the southeast Pacific  
3909 for each reconstruction time listed above. Feature descriptions as in  
3910 Figure 10a. Abbreviations are: AFR = African plate, ANT = Antarctic plate,  
3911 BAU = Bauer plate, CAR = Caribbean plate, CAZ = Casca plate, COC = Cocos  
3912 plate, CQL = Catquil plate, ESC = East Scotia Sea plate, FAR = Farallon  
3913 plate, HIK = Hikurangi plate, IZA = Izanagi plate, MAN = Manihiki plate,  
3914 NAM = North American plate, NAZ = Nazca plate, NSC = North Scotia Sea  
3915 plate, PAC = Pacific plate, SAM = South American plate, SND = Sandwich  
3916 plate, SSC = South Scotia Sea plate.

3917

3918 **Figure 11**

3919 a. Gridded magnetic anomalies for the southwest Pacific. Seafloor spreading  
3920 isochrons used in this study plotted as thin black lines. Numbers correspond to  
3921 magnetic anomaly chron. CP = Campbell Plateau, CR = Chatham Rise, CS = Coral  
3922 Sea, EB = Ellice Basin, HP = Hikurangi Plateau, HT = Havre Trough, LB = Lau  
3923 Basin, LHR = Lord Howe Rise, MP = Manihiki Plateau, NFB = North Fiji Basin, NLB  
3924 = North Loyalty Basin, OJP = Ontong Java Plateau, OT = Osbourn Trough, SFB =  
3925 South Fiji Basin, SS = Solomon Sea.

3926 b. Seafloor spreading isochron map coloured by spreading system or plate pair.  
3927 Map abbreviations are same as a. Legend abbreviations are: BB = Back arc  
3928 Basins, CHS = Chasca, FAR = Farallon, HIK = Hikurangi, MAN = Manihiki, OTH =  
3929 Other, PAC = Pacific, PHX = Phoenix, SEM = Southeast Manihiki, WANT = West  
3930 Antarctica/Antarctica.

3931

3932 **Figure 12**

3933 a. Agegrid reconstructions of the southwest Pacific at 140, 120, 80, 40, 20, 0  
3934 Ma highlighting the age-area distribution of oceanic lithosphere at the  
3935 time of formation and the extent of continental crust (grey polygons).  
3936 Plate boundaries from our continuously closing plate polygon dataset are  
3937 denoted as thick white lines, hotspot locations as yellow stars, large  
3938 igneous provinces and flood basalts as brown polygons and coastlines as  
3939 thin black lines.

3940 b. Reconstructions showing the outlines of the plates in the southwest  
3941 Pacific for each reconstruction time listed above. Feature descriptions as  
3942 in Figure 12a. Abbreviations are: ANT = Antarctic plate, AUS = Australian  
3943 plate, CAR = Caroline plate, ENK = East Norfolk Basin plate, EUR =  
3944 Eurasian plate, HIK = Hikurangi plate, IZA = Izanagi plate, JUN = Junction  
3945 plate, LAU = Lau Basin plate, LHR = Lord Howe Rise plate, NBR = New  
3946 Britain plate, NFB = North Fiji Basin plate, NTY = Neo-Tethys plate, PAC =  
3947 Pacific plate, PHL = Philippine Sea plate, PHX = Phoenix plate, SLY = South  
3948 Loyalty Basin plate, SOL = Solomon Sea plate, WNK = West Norfolk Basin  
3949 plate.

3950

3951 **Figure 13**

3952 a. Gridded magnetic anomalies for the circum-Antarctic. Seafloor spreading  
3953 isochrons used in this study plotted as thin black lines. AAB Australia-Antarctic  
3954 Basin, AAR = American-Antarctic Ridge, AT = Adare Trough, CP = Campbell  
3955 Plateau, EB = Enderby Basin, EM = Emerald Basin, GR = Gunnerus Ridge, KP =  
3956 Kerguelan Plateau, RLS = Riiser-Larson Sea, SEIR = Southeast Indian Ridge, SWIR  
3957 = Southwest Indian Ridge, WS = Weddell Sea.

3958 b. Seafloor spreading isochron map coloured by spreading system or plate pair.  
3959 Map abbreviations are same as a. Legend abbreviations are: AFR = Africa, ALK =  
3960 Aluk, AUS = Australia/Lord Howe Rise, BB = Back arc Basins, EANT = East  
3961 Antarctica/Antarctica, END = Enderby, FAR = Farallon, FLK = Falkland, IND =  
3962 India, MAL = Malvinas, OTH = Other (Adare Trough and Emerald Basin), PAC =  
3963 Pacific, SAM = South America, WANT = West Antarctica/Antarctica.

3964

3965 **Figure 14**

3966 a. Gridded magnetic anomalies for the Indian Ocean. Seafloor spreading  
3967 isochrons used in this study plotted as thin black lines. A = Argo Abyssal Plain,  
3968 AAB Australia-Antarctic Basin, BR = Broken Ridge, C = Cuvier Abyssal Plain, CIR  
3969 = Central Indian Ridge, CR = Carlsberg Ridge, EFR = East Africa Rift, G = Gascoyne  
3970 Abyssal Plain, KP = Kerguelan Plateau, MB = Mascarene Basin, MP = Madagascar  
3971 Plateau, MR = Mascarene Ridge, MZB = Mozambique Basin, P = Perth Abyssal  
3972 Plain, SEIR = Southeast Indian Ridge, SR = Sheba Ridge, SWIR = Southwest Indian  
3973 Ridge, WB = Wharton Basin.

3974 b. Seafloor spreading isochron map coloured by spreading system or plate pair.  
3975 Map abbreviations are same as a. Legend abbreviations are: AFR = Africa, ALK =  
3976 Aluk, AUS = Australia/Lord Howe Rise, BB = Back arc Basins, EANT = East  
3977 Antarctica/Antarctica, END = Enderby, FAR = Farallon, FLK = Falkland, IND =  
3978 India, MAL = Malvinas, OTH = Other (Adare Trough and Emerald Basin), PAC =  
3979 Pacific, SAM = South America, WANT = West Antarctica/Antarctica.

3980

3981 **Figure 15**

3982 a. Agegrid reconstructions of the east African basins at 160, 140, 120, 80, 40,  
3983 0 Ma highlighting the age-area distribution of oceanic lithosphere at the  
3984 time of formation and the extent of continental crust (grey polygons).

3985 Plate boundaries from our continuously closing plate polygon dataset are  
3986 denoted as thick white lines, hotspot locations as yellow stars, large  
3987 igneous provinces and flood basalts as brown polygons and coastlines as  
3988 thin black lines.

3989 b. Reconstructions showing the outlines of the plates in the east African  
3990 basins for each reconstruction time listed above. Feature descriptions as  
3991 in Figure 15a. Abbreviations are: AFR = African plate, ANT = Antarctic  
3992 plate, EGD = east Gondwana plate, IND = Indian plate, NEA = northeast  
3993 African plate, NTY = Neo-Tethys plate, NWA = northwest African plate,  
3994 SOM = Somali plate, WGD = west Gondwana plate.

3995

3996 **Figure 16**

3997 a. Agegrid reconstructions of the west Australian margin at 150, 130, 100,  
3998 80, 50, 0 Ma highlighting the age-area distribution of oceanic lithosphere  
3999 at the time of formation and the extent of continental crust (grey  
4000 polygons). Plate boundaries from our continuously closing plate polygon  
4001 dataset are denoted as thick white lines, hotspot locations as yellow stars,  
4002 large igneous provinces and flood basalts as brown polygons and  
4003 coastlines as thin black lines.

4004 b. Reconstructions showing the outlines of the plates in the west Australian  
4005 margins for each reconstruction time listed above. Feature descriptions  
4006 as in Figure 16a. Abbreviations are: ANT = Antarctic plate, AUS =  
4007 Australian plate, CAP = Capricorn plate, EGD = east Gondwana plate, EUR  
4008 = Eurasian plate, IND = Indian plate, JUN = Junction plate, NEA = northeast  
4009 African plate, NJU = north Junction plate, NTY = Neo-Tethys plate, NWA =  
4010 northwest African plate, SOM = Somali plate.

4011

4012 **Figure 17**

4013 a. Agegrid reconstructions of Mesozoic North America at 200, 180, 170, 150,  
4014 140 Ma highlighting the age-area distribution of oceanic lithosphere at  
4015 the time of formation and the extent of continental crust (grey polygons).  
4016 Plate boundaries from our continuously closing plate polygon dataset are  
4017 denoted as thick white lines, hotspot locations as yellow stars, large

4018 igneous provinces and flood basalts as brown polygons and coastlines as  
4019 thin black lines.

4020 b. Reconstructions showing the outlines of the plates around Mesozoic  
4021 North America for each reconstruction time listed above. Feature  
4022 descriptions as in Figure 17a. Abbreviations are: CAR = Caribbean plate,  
4023 EUR = Eurasian plate, FAR = Farallon plate, IZA = Izanagi plate, NAM =  
4024 North American plate, PAC = Pacific plate, SAM = South American plate.

4025

4026 **Figure 18-28**

4027 Global plate reconstructions from 200 Ma to the present day in 20 million year  
4028 time intervals. Basemap shows the age-area distribution of oceanic lithosphere  
4029 at the time of formation. Red lines denote subduction zones, black lines denote  
4030 mid-ocean ridges and transform faults. Brown polygons indicate products of  
4031 plume-related excessive volcanism. Yellow stars are present day hotspot  
4032 locations. Absolute plate velocity vectors are denoted as black arrows.

4033 Abbreviations for the plates are the same as in previous figures. Additional  
4034 abbreviations include: ALA = Alaska, CA = Central Atlantic, CAP = Capricorn, CAR  
4035 = Caribbean, CAT = Catequil, CCO = Cache Creek Ocean, COL = Colorado, CS =  
4036 Caroline Sea, JUN = Junction, MOO = Mongol-Okhotsk Ocean, NL = North Loyalty  
4037 Basin, NMT = North Meso-Tethys, NNT = North Neo-Tethys, PAR = Parana, PAT =  
4038 Patagonia, PS = Philippine Sea, PSC = Proto-South China Sea, SCO = Scotia Sea,  
4039 SLB = South Loyalty Basin, SMT = South Meso-Tethys, TS = Tasman Sea.

4040

4041 **Figure 29**

4042 Global comparison between the Gurnis et al. (2012) plate motion model and the  
4043 one presented in this study, centered on Australia and the western Panthalassic  
4044 margin. Reconstructions are shown at 120 and 90 Ma with red plate velocity  
4045 vectors denoting the Gurnis et al. (2012) model and blue plate velocity vectors  
4046 from this study. Dark green line indicates the east Australian margin.

4047

4048 **Table 1**

4049 Summary table of magnetic chrons used in this study and referred to in text with  
4050 ages based on alternative timescales. CK94, G94, T06 refers to a merged Cande

4051 and Kent (1994) (Chronos 0-34), Gradstein et al. (1995) (Chronos M0-M33) and  
4052 Tivey et al. (2006) (M34-M44) timescale. GTS2004 from Gradstein et al. (2004).  
4053 GK07 refers to the timescale presented in Gee and Kent (2007).

4054

## 4055 **References**

4056

4057 Aitchison, J.C., Ali, J.R., and Davis, A.M., 2007, When and where did India and Asia  
4058 collide: *Journal of Geophysical Research*, v. 112, p. B05423.

4059 Alvey, A., Gaina, C., Kusznir, N., and Torsvik, T., 2008, Integrated crustal thickness  
4060 mapping and plate reconstructions for the high Arctic: *Earth and Planetary  
4061 Science Letters*, v. 274, p. 310-321.

4062 Apel, E., Bergmann, R., Steblov, G., Vasilenko, N., King, R., and Prytkov, A., 2006,  
4063 Independent active microplate tectonics of northeast Asia from GPS velocities  
4064 and block modeling: *Geophysical Research Letters*, v. 33, p. L11303.

4065 Argus, D.F., Gordon, R.G., Heflin, M.B., Ma, C., Eanes, R.J., Willis, P., Peltier,  
4066 W.R., and Owen, S.E., 2010, The angular velocities of the plates and the  
4067 velocity of Earth's centre from space geodesy: *Geophysical Journal  
4068 International*, v. 180, p. 913-960.

4069 Argus, D.F., and Heflin, M.B., 1995, Plate motion and crustal deformation estimated  
4070 with geodetic data from the Global Positioning System: *Geophys. Res. Lett.*,  
4071 v. 22, p. 1973-1976.

4072 Atwater, T., 1970, Implications of Plate Tectonics for the Cenozoic Tectonic  
4073 Evolution of Western North America: *Geological Society of America Bulletin*,  
4074 v. 81, p. 3513-3536.

4075 —, 1990, Plate tectonic history of the northeast Pacific and western North America, *in*  
4076 Winterer, E.L., Hussong, D.M., and Decker, R.W., eds., *The Eastern Pacific  
4077 Ocean and Hawaii, Volume N: The Geology of North America: Boulder,  
4078 Colorado, Geological Society of America*, p. 21-72.

4079 Atwater, T., Sclater, J., and Sandwell, D., 1993, Fracture zone traces across the North  
4080 Pacific Cretaceous Quiet Zone and their tectonic implications, *in* Pringle,  
4081 M.S., and et al., eds., *Mesozoic Pacific: Geology, Tectonics, and Volcanism  
4082 (Series: Geophysical Monograph Series, Volume 77: Geophysical Monograph  
4083 Series: Washington, D.C., AGU*, p. 137-154.

4084 Atwater, T., and Severinghaus, J., 1990, Tectonic maps of the northeast Pacific, *in*  
4085 Winterer, E.L., Hussong, D.M., and Decker, R.W., eds., *The Eastern Pacific  
4086 Ocean and Hawaii, Volume N: The Geology of North America: Boulder,  
4087 Colorado, Geological Society of America*, p. 15-20.

4088 Atwater, T.a.J.S., 1989, *Magnetic Anomalies in the North Pacific: Geological Society  
4089 of America*, v. *Geology of North America*.

4090 Badarch, G., Dickson Cunningham, W., and Windley, B.F., 2002, A new terrane  
4091 subdivision for Mongolia: implications for the Phanerozoic crustal growth of  
4092 Central Asia: *Journal of Asian Earth Sciences*, v. 21, p. 87-110.

4093 Banerjee, B., Sengupta, B., and Banerjee, P., 1995, Signals of Barremian (116 Ma) or  
4094 younger oceanic crust beneath the Bay of Bengal along 14 N latitude between  
4095 81 E and 93 E: *Marine geology*, v. 128, p. 17-23.

4096 Banks, N., Bardwell, K., and Musiwa, S., 1995, Karoo rift basins of the Luangwa  
4097 Valley, Zambia: *Geological Society London Special Publications*, v. 80, p.  
4098 285.

- 4099 Barckhausen, U., Ranero, C.R., Cande, S.C., Engels, M., and Weinrebe, W., 2008,  
4100 Birth of an intraoceanic spreading center: *Geology*, v. 36, p. 767.
- 4101 Beauchamp, W.H., 1998, Tectonic evolution of the Atlas Mountains, North Africa.
- 4102 Belasky, P., and Runnegar, B., 1994, Permian longitudes of Wrangellia, Stikinia, and  
4103 Eastern Klamath terranes based on coral biogeography: *Geology*, v. 22, p.  
4104 1095-1098.
- 4105 Bernard, A., and Munsch, M., 2000, Were the Mascarene and Laxmi Basins  
4106 (western Indian Ocean) formed at the same spreading centre?: *Comptes*  
4107 *Rendus de l'Academie des Sciences Series IIA Earth and Planetary Science*, v.  
4108 330, p. 777-783.
- 4109 Billen, M.I., and Stock, J., 2000, Morphology and origin of the Osbourn Trough:  
4110 *Journal of Geophysical Research-Solid Earth*, v. 105, p. 13481-13489.
- 4111 Bird, D., Hall, S., Burke, K., Casey, J., and Sawyer, D., 2007, Early Central Atlantic  
4112 Ocean seafloor spreading history: *Geosphere*, v. 3, p. 282.
- 4113 Bird, P., 2003, An updated digital model of plate boundaries: *Geochemistry,*  
4114 *Geophysics, Geosystems*, v. 4, p. 1027, doi:10.1029/2001GC000252.
- 4115 Bird, R.T., and Naar, D.F., 1994, Intra-transform origins of mid-ocean ridge  
4116 microplates: *Geology*, v. 22, p. 987-990.
- 4117 Bird, R.T., Naar, D.F., Larson, R.L., Searle, R.C., and Scotese, C.R., 1998 Plate  
4118 tectonic reconstructions of the Juan Fernandez microplate: Transformation  
4119 from internal shear to rigid rotation *J Geophys Res Solid Earth* v. 103 p. 7049-  
4120 7067
- 4121 Boillot, G., and Winterer, E., 1988, Drilling on the Galicia margin: retrospect and  
4122 prospect, Volume 103, p. 809-828.
- 4123 Boulin, J., 1988, Hercynian and Eocimmerian events in Afghanistan and adjoining  
4124 regions: *Tectonophysics*, v. 148, p. 253-278.
- 4125 Boyden, J.A., Müller, R.D., Gurnis, M., Torsvik, T.H., Clark, J.A., Turner, M., Ivey-  
4126 Law, H., Watson, R.J., and Cannon, J.S., 2011, Next-generation plate-tectonic  
4127 reconstructions using GPlates, *in* Keller, G.R., and Baru, C, ed.,  
4128 *Geoinformatics: Cyberinfrastructure for the Solid Earth Sciences*, Cambridge  
4129 University Press, p. 95-114.
- 4130 Bradley, D., 2008, Passive margins through Earth history: *Earth-Science Reviews*, v.  
4131 91, p. 1-26.
- 4132 Brekke, H., 2000, The tectonic evolution of the Norwegian Sea continental margin  
4133 with emphasis on the Voring and More basins: *Geological Society London*  
4134 *Special Publications*, v. 167, p. 327.
- 4135 Brozena, J., Childers, V., Lawver, L., Gahagan, L., Forsberg, R., Faleide, J., and  
4136 Eldholm, O., 2003, New aerogeophysical study of the Eurasia Basin and  
4137 Lomonosov Ridge: Implications for basin development: *Geology*, v. 31, p.  
4138 825.
- 4139 Bryan, S.E., Constantine, A.E., Stephens, C.J., Ewart, A., Schon, R.W., and Parianos,  
4140 J., 1997, Early Cretaceous Volcano-Sedimentary Successions Along the  
4141 Eastern Australian Continental Margin - Implications for the Break-up of  
4142 Eastern Gondwana: *Earth and Planetary Science Letters*, v. 153, p. 85-102.
- 4143 Buchs, D.M., Arculus, R.J., Baumgartner, P.O., Baumgartner-Mora, C., and Ulianov,  
4144 A., 2010, Late Cretaceous arc development on the SW margin of the  
4145 Caribbean Plate: Insights from the Golfito, Costa Rica, and Azuero, Panama,  
4146 complexes: *Geochemistry Geophysics Geosystems*, v. 11, p. Q07S24.

- 4147 Bunge, H., and Grand, S., 2000, Mesozoic plate-motion history below the northeast  
4148 Pacific Ocean from seismic images of the subducted Farallon slab: *Nature*, v.  
4149 405, p. 337-340.
- 4150 Byrne, T., 1979, Late Paleocene demise of the Kula-Pacific spreading center:  
4151 *Geology*, v. 7, p. 341.
- 4152 Cande, S., LaBrecque, J., and Haxby, W., 1988, Plate kinematics of the South  
4153 Atlantic: Chron C34 to present: *Journal of Geophysical Research*, v. 93, p.  
4154 13479-13,492.
- 4155 Cande, S.C., and Haxby, W.F., 1991, Eocene propagating rifts in the Southwest  
4156 Pacific and their conjugate features on the Nazca Plate: *Journal of*  
4157 *Geophysical Research*, v. 96, p. 19609.
- 4158 Cande, S.C., and Kent, D.V., 1992, A new geomagnetic polarity time scale for Late  
4159 Cretaceous and Cenozoic: *Journal of Geophysical Research*, v. 97, p. 13917-  
4160 13951.
- 4161 —, 1995, Revised calibration of the geomagnetic polarity timescale for the Late  
4162 Cretaceous and Cenozoic: *Journal of Geophysical Research*, v. 100, p. 6093-  
4163 6095.
- 4164 Cande, S.C., Raymond, C.A., Stock, J., and Haxby, W.F., 1995, Geophysics of the  
4165 Pitman Fracture Zone and Pacific-Antarctic Plate Motions During the  
4166 Cenozoic: *Science*, v. 270, p. 947-953.
- 4167 Carminati, E., Doglioni, C., and Scrocca, D., 2004, Alps vs Apennines: Special  
4168 volume of the Italian Geological Society for the IGC, v. 32, p. 141ñ151.
- 4169 Catuneanu, O., Wopfner, H., Eriksson, P., Cairncross, B., Rubidge, B., Smith, R., and  
4170 Hancox, P., 2005, The Karoo basins of south-central Africa: *Journal of*  
4171 *African Earth Sciences*, v. 43, p. 211-253.
- 4172 Chalmers, J., and Pulvertaft, T., 2001, Development of the continental margins of the  
4173 Labrador Sea: a review: *Geological Society London Special Publications*, v.  
4174 187, p. 77.
- 4175 Chalmers, J.A., 1991, New evidence on the structure of the Labrador Sea/Greenland  
4176 continental margin: *Journal of the Geological Society, London*, v. 148, p. 899-  
4177 908.
- 4178 Chalmers, J.A., and Laursen, K.H., 1995, Labrador Sea: The extent of continental and  
4179 oceanic crust and the timing of the onset of seafloor spreading: *Marine and*  
4180 *Petroleum Geology*, v. 12, p. 205-217.
- 4181 Channell, J.E.T., 1995, Recalibration of the geomagnetic polarity timescale: *Reviews*  
4182 *of Geophysics*, v. 33, p. 161-168.
- 4183 Chaubey, A.K., Bhattacharya, G.C., Murty, G.P.S., Srinivas, K., Ramprasad, T., and  
4184 Rao, D.G., 1998, Early Tertiary Seafloor Spreading Magnetic Anomalies and  
4185 Paleo-Propagators in the Northern Arabian Sea: *Earth and Planetary Science*  
4186 *Letters*, v. 154, p. 41-52.
- 4187 Churkin, M., and Trexler, J., J.H., 1980, Circum-Arctic plate accretion-isolating part  
4188 of a Pacific plate to form the nucleus of the Arctic Basin: *Earth and Planetary*  
4189 *Science Letters*, v. 49, p. 356-362.
- 4190 Cluzel, D., Adams, C., Meffre, S., Campbell, H., and Maurizot, P., 2010, Discovery  
4191 of Early Cretaceous rocks in New Caledonia; new geochemical and U-Pb  
4192 zircon age constraints on the transition from subduction to marginal breakup  
4193 in the Southwest Pacific.
- 4194 Cocks, L.R.M., and Torsvik, T.H., 2007, Siberia, the wandering northern terrane, and  
4195 its changing geography through the Palaeozoic: *Earth-Science Reviews*, v. 82,  
4196 p. 29-74.

- 4197 Coffin, M.F., and Rabinowitz, P.D., 1987, Reconstruction of Madagascar and Africa:  
4198 evidence from the Davie Fracture Zone and western Somali Basin: *Journal of*  
4199 *Geophysical Research*, v. 92, p. 9385-9406.
- 4200 Cole, J., and Peachey, J., 1999, Evidence for pre-Cretaceous rifting in the Rockall  
4201 Trough: an analysis using quantitative plate tectonic modelling, *Geological*  
4202 *Society Pub House*, p. 359.
- 4203 Collier, J., Sansom, V., Ishizuka, O., Taylor, R., Minshull, T., and Whitmarsh, R.,  
4204 2008, Age of Seychelles-India break-up: *Earth and Planetary Science Letters*,  
4205 v. 272, p. 264-277.
- 4206 Colpron, M., Logan, J.M., and Mortensen, J.K., 2002, U-Pb zircon age constraint for  
4207 late Neoproterozoic rifting and initiation of the lower Paleozoic passive  
4208 margin of western Laurentia: *Canadian Journal of Earth Sciences*, v. 39, p.  
4209 133-143.
- 4210 Colpron, M., Nelson, J.A.L., and Murphy, D.C., 2007, Northern Cordilleran terranes  
4211 and their interactions through time: *GSA Today*, v. 17, p. 4-10.
- 4212 Crawford, T., Meffre, S., and Symonds, P.A., 2002, Tectonic Evolution of the SW  
4213 Pacific: Lessons for the Geological Evolution of the Tasman Fold Belt System  
4214 in eastern Australia from 600 to 220 Ma., *in* Hillis, R., and Müller, R.D., eds.,  
4215 *Evolution and Dynamics of the Australian Plate*.
- 4216 Croon, M.B., Cande, S.C., and Stock, J.M., 2008, Revised Pacific-Antarctic plate  
4217 motions and geophysics of the Menard Fracture Zone: *Geochemistry,*  
4218 *Geophysics, Geosystems*, v. 9, p. 7.
- 4219 Daly, M., Chorowicz, J., and Fairhead, J., 1989, Rift basin evolution in Africa: the  
4220 influence of reactivated steep basement shear zones: *Geological Society*  
4221 *London Special Publications*, v. 44, p. 309.
- 4222 De Graciansky, P., POAG, C., CUNNINGHAM JR, R., LOUBERE, P., MASSON,  
4223 D., MAZZULLO, J., MONTADERT, L., MULLER, C., OTSUKA, K., and  
4224 REYNOLDS, L., 1985, The Goban Spur transect: Geologic evolution of a  
4225 sediment-starved passive continental margin: *Bulletin of the Geological*  
4226 *Society of America*, v. 96, p. 58.
- 4227 DeCelles, P., 2004, Late Jurassic to Eocene evolution of the Cordilleran thrust belt  
4228 and foreland basin system, western USA: *American Journal of Science*, v.  
4229 304, p. 105.
- 4230 DeMets, C., Gordon, R.G., and Argus, D.F., 2010, Geologically current plate  
4231 motions: *Geophysical Journal International*, v. 181, p. 1-80.
- 4232 DeMets, C., Gordon, R.G., Argus, D.F., and Stein, S., 1990, Current plate motions:  
4233 *Geophysical Journal International*, v. 101, p. 425-478.
- 4234 Downey, N.J., Stock, J.M., Clayton, R.W., and Cande, S.C., 2007, History of the  
4235 Cretaceous Osborn spreading center: *Journal of Geophysical Research*, v.  
4236 112, p. B04102.
- 4237 Dunbar, J., and Sawyer, D., 1989, Patterns of continental extension along the  
4238 conjugate margins of the central and North Atlantic Ocean and Labrador Sea:  
4239 *Tectonics*, v. 8.
- 4240 Duncan, R., and Hargraves, R., 1984, Plate tectonic evolution of the Caribbean region  
4241 in the mantle reference frame: *The Caribbean-South American Plate Boundary*  
4242 *and Regional Tectonics*, p. 81-93.
- 4243 Eagles, G., 2007, New angles on South Atlantic opening: *Geophysical Journal*  
4244 *International*, v. 168, p. 353-361.

- 4245 Eagles, G., Gohl, K., and Larter, R.D., 2004a, High-resolution animated tectonic  
4246 reconstruction of the South Pacific and West Antarctic margin - art. no.  
4247 Q07002: *Geochemistry, Geophysics, Geosystems*, v. 5, p. 7002-7002.
- 4248 —, 2004b, Life of the Bellingshausen plate: *Geophysical Research Letters*, v. 31, p.  
4249 7603-7603.
- 4250 Eagles, G., and König, M., 2008, A model of plate kinematics in Gondwana breakup:  
4251 *Geophysical Journal International*, v. 173, p. 703-717.
- 4252 Eakins, B.W., and Lonsdale, P.F., 2003, Structural patterns and tectonic history of the  
4253 Bauer microplate, Eastern Tropical Pacific: *Marine Geophysical Researches*,  
4254 v. 24, p. 171-205.
- 4255 Engebretson, D.C., Cox, A., and Gordon, R.G., 1985, Relative motions between  
4256 oceanic and continental plates in the Pacific Basin, *Geol. Soc. of Am.*
- 4257 Faccenna, C., Becker, T.W., Lucente, F.P., Jolivet, L., and Rossetti, F., 2001, History  
4258 of subduction and back arc extension in the Central Mediterranean:  
4259 *Geophysical Journal International*, v. 145, p. 809-820.
- 4260 Falvey, D.A., and Mutter, J.C., 1981, Regional plate tectonics and the evolution of  
4261 Australia's passive margins: *Journal of Australian Geology and Geophysics*, v.  
4262 6, p. 1-29.
- 4263 Fullerton, L.G., Sager, W.W., and Handschumacher, D.W., 1989, Late Jurassic-Early  
4264 Cretaceous evolution of the eastern Indian Ocean adjacent to northwest  
4265 Australia: *Journal of Geophysical Research*, v. 94, p. 2937-2953.
- 4266 Gaina, C., Gernigon, L., and Ball, P., 2009, Palaeocene-Recent plate boundaries in the  
4267 NE Atlantic and the formation of the Jan Mayen microcontinent: *Journal of*  
4268 *the Geological Society*, v. 166, p. 601.
- 4269 Gaina, C., Labails, C., and Reeves, C., 2010, The Early Opening of the Indian Ocean:  
4270 An African Perspective, 2010 Fall Meeting, Volume Abstract T13C-2222: San  
4271 Francisco, California, 13-17 Dec, AGU.
- 4272 Gaina, C., Müller, D.R., Royer, J.Y., Stock, J., Hardebeck, J., and Symonds, P., 1998,  
4273 The tectonic history of the Tasman Sea: a puzzle with 13 pieces: *Journal of*  
4274 *Geophysical Research*, v. 103, p. 12413-33.
- 4275 Gaina, C., and Müller, R.D., 2007, Cenozoic tectonic and depth/age evolution of the  
4276 Indonesian gateway and associated back-arc basins: *Earth-Science Reviews*, v.  
4277 83, p. 177-203.
- 4278 Gaina, C., Müller, R.D., Brown, B., and Ishihara, T., 2003, Micro-continent formation  
4279 around Australia, *in* Hillis, R., and Müller, R.D., eds., *The Evolution and*  
4280 *Dynamics of the Australian Plate*, Volume 22: *Geol. Soc. Aust. Spec. Publ.*,  
4281 *Geological Society of Australia*.
- 4282 Gaina, C., Müller, R.D., Brown, B., Ishihara, T., and Ivanov, S., 2007, Breakup and  
4283 early seafloor spreading between India and Antarctica: *Geophysical Journal*  
4284 *International*, v. 170, p. 151-169.
- 4285 Gaina, C., Müller, R.D., Royer, J.-Y., and Symonds, P., 1999, The tectonic evolution  
4286 of the Louisiade Triple Junction: *Journal of Geophysical Research*, v. 104, p.  
4287 12973-12939.
- 4288 Gaina, C., Roest, W.R., and Muller, R.D., 2002, Late Cretaceous-Cenozoic  
4289 deformation of northeast Asia: *Earth and Planetary Science Letters*, v. 197, p.  
4290 273-286.
- 4291 Gee, J., and Kent, D., 2007, Source of Oceanic magnetic anomalies and the  
4292 geomagnetic polarity timescale: *Treatise Geophys*, v. 5, p. 455-507.

- 4293 Gehrels, G.E., 2001, Geology of the Chatham Sound region, southeast Alaska and  
4294 coastal British Columbia: *Canadian Journal of Earth Sciences*, v. 38, p. 1579-  
4295 1599.
- 4296 —, 2002, Detrital zircon geochronology of the Taku terrane, southeast Alaska:  
4297 *Canadian Journal of Earth Sciences*, v. 39, p. 921-931.
- 4298 Gerstell, M., and Stock, J., 1994, Testing the Porcupine Plate Hypothesis: *Marine*  
4299 *Geophysical Researches*, v. 16, p. 315-323.
- 4300 Ghosh, N., Hall, S., and Casey, J., 1984, Seafloor spreading magnetic anomalies in  
4301 the Venezuelan Basin: *The Caribbean-South American Plate Boundary and*  
4302 *Regional Tectonics*, p. 65-80.
- 4303 Goff, J.A., and Cochran, J.R., 1996, The Bauer scarp ridge jump: A complex tectonic  
4304 sequence revealed in satellite altimetry: *Earth and Planetary Science Letters*, v.  
4305 141, p. 21-33.
- 4306 Golonka, J., 2007, Late Triassic and Early Jurassic palaeogeography of the world:  
4307 *Palaeogeography, Palaeoclimatology, Palaeoecology*, v. 244, p. 297-307.
- 4308 Golonka, J., and Ford, D., 2000, Pangean (Late Carboniferous-Middle Jurassic)  
4309 paleoenvironment and lithofacies: *Palaeogeography, Palaeoclimatology,*  
4310 *Palaeoecology*, v. 161, p. 1-34.
- 4311 Golonka, J., Gahagan, L., Krobicki, M., Marko, F., Oszczytko, N., and Slaczka, A.,  
4312 2006, Plate-tectonic evolution and paleogeography of the circum-Carpathian  
4313 region: The Carpathians and their foreland: *Geology and hydrocarbon*  
4314 *resources. AAPG Mem*, v. 84, p. 11646.
- 4315 Gordon, R.G., and Stein, S., 1992, Global tectonics and space geodesy: *Science*, v.  
4316 256, p. 333.
- 4317 Goslin, J., and Schlich, R., 1976, Structural limits of the South Crozet Basin; relations  
4318 to Enderby Basin and the Kerguelen-Heard Plateau.: *International Geological*  
4319 *Congress, Abstracts*, v. 25 (3), p. 884-885.
- 4320 Gradstein, F., Ogg, J., Smith, A., Agterberg, F., Bleeker, W., Cooper, R., Davydov,  
4321 V., Gibbard, P., Hinnov, L., and House, M., 2004, *A geologic time scale 2004*,  
4322 Cambridge University Press.
- 4323 Gradstein, F.M., Agterberg, F.P., Ogg, J.G., Hardenbol, S., Vanveen, P., Thierry, J.,  
4324 and Huang, Z.H., 1994, A Mesozoic time scale: *Journal of Geophysical*  
4325 *Research-Solid Earth*, v. 99, p. 24051-24074.
- 4326 Granot, R., Cande, S.C., and Gee, J.S., 2009, The implications of long-lived  
4327 asymmetry of remanent magnetization across the North Pacific fracture zones:  
4328 *Earth and Planetary Science Letters*, v. 288, p. 551-563.
- 4329 Grantz, A., Clark, D., Phillips, R., Srivastava, S., Blome, C., Gray, L., Haga, H.,  
4330 Mamet, B., McIntyre, D., and McNeil, D., 1998, Phanerozoic stratigraphy of  
4331 Northwind Ridge, magnetic anomalies in the Canada basin, and the geometry  
4332 and timing of rifting in the Amerasia basin, Arctic Ocean: *Geological Society*  
4333 *of America Bulletin*, v. 110, p. 801.
- 4334 Greene, A.R., Scoates, J.S., and Weis, D., 2008, Wrangellia flood basalts in Alaska: A  
4335 record of plume-lithosphere interaction in a Late Triassic accreted oceanic  
4336 plateau: *Geochemistry, Geophysics, Geosystems*, v. 9, p. 12004.
- 4337 Gurnis, M., Turner, M., Zahirovic, S., DiCaprio, L., Spasojevic, S., Muller, R.,  
4338 Boyden, J., Seton, M., Manea, V., and Bower, D., 2012, Plate Tectonic  
4339 Reconstructions with Continuously Closing Plates: *Computers and*  
4340 *Geosciences*, v. 38, p. 35-42.

- 4341 Haeussler, P.J., Bradley, D., Goldfarb, R., Snee, L., and Taylor, C., 1995, Link  
4342 between ridge subduction and gold mineralization in southern Alaska:  
4343 *Geology*, v. 23, p. 995.
- 4344 Hafkenscheid, E., Buitter, S.J.H., Wortel, M.J.R., Spakman, W., and Bijwaard, H.,  
4345 2001, Modelling the seismic velocity structure beneath Indonesia: a  
4346 comparison with tomography: *Tectonophysics*, v. 333, p. 35-46.
- 4347 Halgedahl, S., and Jarrard, R., 1987, Paleomagnetism of the Kugaruk River formation  
4348 from oriented drill core: Evidence for rotation of the North Slope block, *in*  
4349 Tailleux, I.L., and Weimer, P., eds., *Alaskan North Slope Geology*: Los  
4350 Angeles, Soc. Econ. Paleont. and Min., Pacific Section, p. 581-617.
- 4351 Hall, R., 2002, Cenozoic geological and plate tectonic evolution of Southeast Asia  
4352 and the SW Pacific: computer-based reconstructions, models and animations:  
4353 *Journal of Asian Earth Sciences*, v. 20, p. 353-431.
- 4354 Hall, R., Fuller, M., Ali, J.R., and Anderson, C.D., 1995, The Philippine Sea plate:  
4355 Magnetism and reconstructions, *in* Taylor, B., and Natland, J.H., eds., *Active*  
4356 *margins and marginal basins: A synthesis of western Pacific drilling results*,  
4357 *Volume 88*, American Geophysical Union, p. 371-404.
- 4358 Hamilton, W., 1979, *Tectonics of the Indonesian Region*: USGS Professional Paper,  
4359 v. 1078, p. 345.
- 4360 Hankel, O., 1994, Early Permian to middle Jurassic rifting and sedimentation in East  
4361 Africa and Madagascar: *Geologische Rundschau*, v. 83, p. 703-710.
- 4362 Hansen, V.L., 1990, Yukon-Tanana terrane: A partial acquittal: *Geology*, v. 18, p.  
4363 365.
- 4364 Hassanzadeh, J., Stockli, D.F., Horton, B.K., Axen, G.J., Stockli, L.D., Grove, M.,  
4365 Schmitt, A.K., and Walker, J.D., 2008, U-Pb zircon geochronology of late  
4366 Neoproterozoic-Early Cambrian granitoids in Iran: Implications for  
4367 paleogeography, magmatism, and exhumation history of Iranian basement:  
4368 *Tectonophysics*, v. 451, p. 71-96.
- 4369 Hawlader, H., 1990, Diagenesis and reservoir potential of volcanogenic sandstones--  
4370 Cretaceous of the Surat Basin, Australia: *Sedimentary Geology*, v. 66, p. 181-  
4371 195.
- 4372 Heine, C., and Müller, R.D., 2005, Late Jurassic rifting along the Australian  
4373 Northwest Shelf: margin geometry and spreading ridge configuration:  
4374 *Australian Journal of Earth Science*.
- 4375 Heine, C., Müller, R.D., and Gaina, C., 2004, Reconstructing the lost Eastern Tethys  
4376 Ocean Basin: Constraints for the convergence history of the SE Asian margin  
4377 and marine gateways, *in* Clift, P., Hayes, D., Kuhnt, W., and Wang, P., eds.,  
4378 *Continent-Ocean Interactions in Southeast Asia*, Volume 1149: *Geophys.*  
4379 *Monogr. Ser.*: Washington, American Geophysical Union.
- 4380 Heirtzler, J., and Burroughs, R., 1971, Madagascar's Paleoposition: New Data from  
4381 the Mozambique Channel: *Science (New York, NY)*, v. 174, p. 488.
- 4382 Heirtzler, J.R., G.O. Dickson, E.M. Herman, W.C. Pitman III and X. LePichon, 1968,  
4383 Marine Magnetic Anomalies, Geomagnetic Field Reversals, and Motions of  
4384 the Ocean Floor and Continents: *Journal of Geophysical Research*, v. 73, p.  
4385 2119-2136.
- 4386 Hessami, K., Koyi, H.A., Talbot, C.J., Tabishi, H., and Shabanian, E., 2001,  
4387 Progressive unconformities within an evolving foreland fold-thrust belt,  
4388 Zagros Mountains: *Journal of the Geological Society*, v. 158, p. 969.
- 4389 Hey, R., 1977, Tectonic evolution of the Cocos-Nazca spreading center: *Geological*  
4390 *Society of America Bulletin*, v. 88, p. 1404-1420.

- 4391 Hillier, J., 2007, Pacific seamount volcanism in space and time: *Geophysical Journal*  
4392 *International*, v. 168, p. 877-889.
- 4393 Hoernle, K., Hauff, F., van den Bogaard, P., Werner, R., Mortimer, N., Geldmacher,  
4394 J., Garbe-Schönberg, D., and Davy, B., 2010, Age and Geochemistry of  
4395 Volcanic Rocks from the Hikurangi and Manihiki Oceanic Plateaus:  
4396 *Geochimica et Cosmochimica Acta*.
- 4397 Holloway, N., 1982, North Palawan block, Philippines-its relation to Asian mainland  
4398 and role in evolution of South China Sea: *American Association of Petroleum*  
4399 *Geologists Bulletin*, v. 66, p. 1355-1383.
- 4400 Hutchison, C.S., 1989, *Geological evolution of South-east Asia*, p. 368.  
4401 —, 2005, *Geology of north-west Borneo: Sarawak, Brunei and Sabah*, Elsevier  
4402 Science Ltd.
- 4403 Jackson, H., and Gunnarsson, K., 1990, Reconstructions of the Arctic: Mesozoic to  
4404 present: *Tectonophysics*, v. 172, p. 303-322.
- 4405 James, K., 2006, Arguments for and against the Pacific origin of the Caribbean Plate:  
4406 *Geologica acta*, v. 4, p. 279.
- 4407 Jokat, W., Nogi, Y., and Leinweber, V.T., 2010, New aeromagnetic data from the  
4408 western Enderby Basin and consequences for Antarctic-India break-up:  
4409 *Geophysical Research Letters*, 37, L21311.
- 4410 Jokat, W., Ritzmann, O., Schmidt-Aursch, M.C., Drachev, S.S., Gauger, S., and  
4411 Snow, J.H., 2003, Geophysical evidence for reduced melt production on the  
4412 Arctic ultraslow Gakkel mid-ocean ridge: *Nature*, v. 423, p. 962-965.
- 4413 Jokat, W., Uenzelmann-Neben, G., Kristoffersen, Y., and Rasmussen, T., 1992,  
4414 Lomonosov Ridge--A double-sided continental margin: *Geology*, v. 20, p.  
4415 887.
- 4416 Jones, J.G., and Veevers, J.J., 1983, Mesozoic origins and antecedents of Australia's  
4417 Eastern Highlands: *Journal of the Geological Society of Australia*, v. 30, p.  
4418 305-322.
- 4419 Joseph, D., Taylor, B., and Shor, A.N., 1992, New sidescan sonar and gravity  
4420 evidence that the Nova-Canton Trough is a fracture zone: *Geology*, v. 20, p.  
4421 435-438.
- 4422 Karig, D.E., 1971, Origin and Development of Marginal Basins in the Western  
4423 Pacific: *Journal of Geophysical Research*, v. 76, p. 2542.
- 4424 Keppie, J.D., and Dostal, J., 2001, Evaluation of the Baja controversy using  
4425 paleomagnetic and faunal data, plume magmatism, and piercing points:  
4426 *Tectonophysics*, v. 339, p. 427-442.
- 4427 Klitgord, K., and Schouten, H., 1986, Plate kinematics of the central Atlantic, *in* Vogt,  
4428 P.R., and Tucholke, B.E., eds., *The Western North Atlantic Region, DNAG,*  
4429 *Volume M: The geology of North America, Geol. Soc. Am., Boulder, CO,*  
4430 *United States*, p. 351-378.
- 4431 Knott, S., Burchell, M., Jolley, E., and Fraser, A., 1993, Mesozoic to Cenozoic plate  
4432 reconstructions of the North Atlantic and hydrocarbon plays of the Atlantic  
4433 margins, Volume 4, *Geological Society of London*, p. 953.
- 4434 König, M., and Jokat, W., 2006, The Mesozoic breakup of the Weddell Sea: *Journal*  
4435 *of Geophysical Research*, v. 111, p. B12102.  
4436 —, 2010, Advanced insights into magmatism and volcanism of the Mozambique  
4437 Ridge and Mozambique Basin in the view of new potential field data:  
4438 *Geophysical Journal International*, v. 180, p. 158-180.

- 4439 Kovacs, L.C., Morris, P., Brozena, J., and Tikku, A., 2002, Seafloor spreading in the  
4440 Weddell Sea from magnetic and gravity data: *Tectonophysics*, v. 347, p. 43-  
4441 64.
- 4442 Kravchinsky, V.A., CognÈ, J.P., Harbert, W.P., and Kuzmin, M.I., 2002, Evolution of  
4443 the MongolĭOkhotsk Ocean as constrained by new palaeomagnetic data from  
4444 the MongolĭOkhotsk suture zone, Siberia: *Geophysical Journal International*,  
4445 v. 148, p. 34-57.
- 4446 Kuzmichev, A.B., 2009, Where does the South Anyui suture go in the New Siberian  
4447 islands and Laptev Sea?: Implications for the Amerasia basin origin:  
4448 *Tectonophysics*, v. 463, p. 86-108.
- 4449 Labails, C., Olivet, J., Aslanian, D., and Roest, W., 2010, An alternative early opening  
4450 scenario for the Central Atlantic Ocean: *Earth and Planetary Science Letters*.
- 4451 LaBrecque, J.L., and Hayes, D.E., 1979, Seafloor spreading history of the Agulhas  
4452 Basin: *Earth and Planetary Science Letters*, v. 45, p. 411-428.
- 4453 Lancelot, Y., Larson, R.L., and et al, 1990, Proc. ODP Initial Reports 129, Ocean  
4454 Drilling Program: College Station, TX.
- 4455 Lane, L.S., 1997, CANADA BASIN, ARCTIC OCEAN - EVIDENCE AGAINST A  
4456 ROTATIONAL ORIGIN [Review]: *Tectonics*, v. 16, p. 363-387.
- 4457 Larson, R., Smith, S., and Chase, C., 1972, Magnetic lineations of Early Cretaceous age in the  
4458 western equatorial Pacific Ocean: *Earth and Planetary Science Letters*, v. 15, p. 315-  
4459 319.
- 4460 Larson, R.L., 1995, The mid-Cretaceous superplume episode: *Scientific American*, v.  
4461 272, p. 66-70.
- 4462 —, 1997, Superplumes and ridge interactions between Ontong Java and Manihiki  
4463 plateaus and the Nova-Canton trough: *Geology*, v. 25, p. 779-782.
- 4464 Larson, R.L., and Chase, C.G., 1972, Late Mesozoic Evolution of the Western  
4465 Pacific: *Geological Society of America Bulletin*, v. 83, p. 3627-3644.
- 4466 Larson, R.L., and Pitman, W.C.I., 1972, World-wide correlation of Mesozoic  
4467 magnetic anomalies, and its implications: *Geological Society of America*  
4468 *Bulletin*, v. 83, p. 3645-3662.
- 4469 Larson, R.L., Pockalny, R.A., Viso, R.F., Erba, E., Abrams, L.J., Luyendyk, B.P.,  
4470 Stock, J.M., and Clayton, R.W., 2002, Mid-Cretaceous tectonic evolution of  
4471 the Tongareva triple junction in the southwestern Pacific Basin: *Geology*, v.  
4472 30, p. 67-70.
- 4473 Larter, R.D., Cunningham, A.P., Barker, P.F., Gohl, K., and Nitsche, F.O., 2002,  
4474 Tectonic evolution of the Pacific margin of Antarctica 1. Late Cretaceous  
4475 tectonic reconstructions: *Journal of Geophysical Research-Solid Earth*, v. 107,  
4476 p. 2345-2345.
- 4477 Lawver, L.A., and Muller, R.D., 1994, Iceland hotspot track: *Geology*, v. 22, p. 311.
- 4478 Lawver, L.A., Müller, R.D., Srivastava, S.P., and Roest, W., 1990, Opening of the  
4479 Arctic Ocean, *in* Bleil, U., and Thiede, J., eds., *Geological History of the Polar*  
4480 *Oceans: Arctic Versus Antarctic*, p. 29-62.
- 4481 Lee, T.-Y., and Lawver, L.A., 1994, Cenozoic plate reconstruction of the South China  
4482 Sea region: *Tectonophysics*, v. 235, p. 149-180.
- 4483 —, 1995, Cenozoic plate reconstruction of Southeast Asia: *Tectonophysics*, v. 251, p.  
4484 85-138.
- 4485 Lemaux, J., Gordon, R.G., and Royer, J.Y., 2002, Location of the Nubia-Somalia  
4486 boundary along the Southwest Indian Ridge: *Geology*, v. 30, p. 339-342.
- 4487 Lemoine, M., 1983, Rifting and early drifting: Mesozoic central Atlantic and Ligurian  
4488 Tethys: *Initial Reports of the Deep Sea Drilling Project*, v. 76, p. 885ñ895.

- 4489 Liu, L., Gurnis, M., Seton, M., Saleeby, J., Miller, R., and Jackson, J., 2010, The role  
4490 of oceanic plateau subduction in the Laramide orogeny: *Nature Geoscience*, v.  
4491 3, p. 353-357.
- 4492 Livermore, R., and Hunter, R., 1996, Mesozoic seafloor spreading in the southern  
4493 Weddell Sea: *Geological Society London Special Publications*, v. 108, p. 227.
- 4494 Lonsdale, P., 1988, Paleogene history of the Kula plate: Offshore evidence and  
4495 onshore implications: *Geological Society of America Bulletin*, v. 100, p. 733.
- 4496 —, 1997, An incomplete geologic history of the southwest Pacific basin: *GSA*  
4497 *Abstracts with Programs*, v. 29, p. 25.
- 4498 —, 2005, Creation of the Cocos and Nazca plates by fission of the Farallon plate:  
4499 *Tectonophysics*, v. 404, p. 237-264.
- 4500 Lonsdale, P., and Klitgord, K.D., 1978, Structure and tectonic history of the eastern  
4501 Panama Basin: *Geological Society of America Bulletin*, v. 89, p. 981-999.
- 4502 Lowrie, W., and Kent, D., 2004, Geomagnetic polarity timescales and reversal  
4503 frequency regimes: *Timescales of the Paleomagnetic Field*, *Geophys. Monogr.*  
4504 *Ser.*, v. 145, p. 117-129.
- 4505 Ludwig, W.J., N. Kumar, and R.E. Houtz, 1979, Profiler-Sonobuoy Measurements in  
4506 the South China Sea Basin: *Journal of Geophysical Research*, v. 84, p. 3505-  
4507 3518.
- 4508 Mahoney, J., Duncan, R., Tejada, M., Sager, W., and Bralower, T., 2005, Jurassic-  
4509 Cretaceous boundary age and mid-ocean-ridge-type mantle source for Shatsky  
4510 Rise: *Geology*, v. 33, p. 185.
- 4511 Mahoney, J.J., Storey, M., Duncan, R.A., Spencer, K.J., and  
4512 Pringle, M., 1993, Geochemistry and geochronology of  
4513 Leg 130 basement lavas: nature and origin of the  
4514 Ontong Java Plateau, *in* Berger, W.H., Kroenke, L.W., and Mayer,  
4515 L.A., eds., *Proceedings of the Ocean Drilling Program, Scientific Results*,  
4516 *Volume 130*: College Station, TX, Ocean Drilling Program, Texas A&M  
4517 University, p. 3-22.
- 4518 Mammerickx, J., and Klitgord, K., 1982, Northern East Pacific Rise: Evolution from  
4519 25 my BP to the present: *Journal of Geophysical Research*, v. 87, p. 6751-  
4520 6759.
- 4521 Mammerickx, J., and Sharman, G.F., 1988, Tectonic evolution of the North Pacific  
4522 during the Cretaceous quiet period: *Journal of Geophysical Research*, v. 93, p.  
4523 3009-3024.
- 4524 Marks, K.M., and Stock, J.M., 2001, Evolution of the Malvinas Plate south of Africa:  
4525 *Marine Geophysical Researches*, v. 22, p. 289-302.
- 4526 Marks, K.M., and Tikku, A.A., 2001, Cretaceous reconstructions of East Antarctica,  
4527 Africa and Madagascar: *Earth and Planetary Science Letters*, v. 186, p. 479-  
4528 495.
- 4529 Masson, D.G., 1984, Evolution of the Mascarene basin, western Indian Ocean, and  
4530 the significance of the Amirante arc: *Marine Geophysical Researches*, v. 6, p.  
4531 365-382.
- 4532 Matthews, K.J., Hale, A.J., Gurnis, M., Miller, R.D., and DiCaprio, L., 2010,  
4533 Dynamic subsidence of Eastern Australia during the Cretaceous: *Gondwana*  
4534 *Research*.
- 4535 Maus, S., Barckhausen, U., Berkenbosch, H., Bournas, N., Brozena, J., Childers, V.,  
4536 Dostaler, F., Fairhead, J., Finn, C., and von Frese, R., 2009, EMAG2: A 2-arc  
4537 min resolution Earth Magnetic Anomaly Grid compiled from satellite,

- 4538 airborne, and marine magnetic measurements: *Geochemistry Geophysics*  
4539 *Geosystems*, v. 10, p. Q08005.
- 4540 Maus, S., Sazonova, T., Hemant, K., Fairhead, J.D., and Ravat, D., 2007, National  
4541 Geophysical Data Center candidate for the World Digital Magnetic Anomaly  
4542 Map: *Geochemistry, Geophysics, Geosystems*, v. 8, p. Q06017,  
4543 doi:10.1029/2007GC001643.
- 4544 Mayes, C.L., Lawver, L.A., and Sandwell, D.T., 1990, Tectonic history and new  
4545 isochron chart of the South Pacific: *Journal of Geophysical Research*, v. 95, p.  
4546 8543-8567.
- 4547 McElhinny, M.W., Embleton, B.J.J., Daly, L., and Pozzi, J.P., 1976, Paleomagnetic  
4548 Evidence for the Location of Madagascar in Gondwanaland: *Geology*, v. 4, p.  
4549 455-457.
- 4550 McKenzie, D.P., and Morgan, J., 1969, The Evolution of Triple Junctions: *Nature*, v.  
4551 224, p. 125-133.
- 4552 Menard, H.W., 1978, Fragmentation of the Farallon plate by pivoting subduction:  
4553 *Journal of Geology*, v. 86, p. 99-110.
- 4554 Meschede, M., Barckhausen, U., and Worm, H.U., 1998a, Extinct spreading on the  
4555 Cocos Ridge: *Terra Nova*, v. 10, p. 211-216.
- 4556 —, 1998b, Extinct spreading on the Cocos Ridge: *Terra Nova. The European Journal*  
4557 *of Geosciences*, v. 10, p. 211-216.
- 4558 Meschede, M., and Frisch, W., 1998, A plate-tectonic model for the Mesozoic and  
4559 Early Cenozoic history of the Caribbean plate: *Tectonophysics*, v. 296, p. 269-  
4560 291.
- 4561 Metcalfe, I., 1996, Gondwanaland Dispersion, Asian Accretion and Evolution of  
4562 Eastern Tethys: *Australian Journal of Earth Sciences*, v. 43, p. 605-623.
- 4563 —, 1999, Gondwana dispersion and Asian accretion: An overview, *in* Metcalfe, I.,  
4564 ed., *Gondwana dispersion and Asian accretion*: Rotterdam, A.A. Balkema, p.  
4565 9-29.
- 4566 Mihalynuk, M.G., Nelson, J.A., and Diakow, L.J., 1994, Cache Creek terrane  
4567 entrapment: oroclinal paradox within the Canadian Cordillera: *Tectonics*, v.  
4568 13, p. 575-595.
- 4569 Mihut, D., and Müller, R.D., 1998, Revised seafloor spreading history of the Argo  
4570 Abyssal Plain, West Australian Basins Symposium 98: Perth.
- 4571 Moran, K., Backman, J., Brinkhuis, H., Clemens, S.C., Cronin, T., Dickens, G.R.,  
4572 Eynaud, F., Gattacceca, J., Jakobsson, M., and Jordan, R.W., 2006, The  
4573 Cenozoic palaeoenvironment of the Arctic Ocean: *Nature*, v. 441, p. 601-605.
- 4574 Morgan, W.J., 1972, Plate motions and deep mantle convection: *GSA Memoir*, v.  
4575 132, p. 7-22.
- 4576 Mortensen, J., 1992, Pre-mid-Mesozoic tectonic evolution of the Yukon-Tanana  
4577 terrane, Yukon and Alaska: *Tectonics*, v. 11, p. 836-853.
- 4578 Moulin, M., Aslanian, D., and Unternehr, P., 2010, A new starting point for the South  
4579 and Equatorial Atlantic Ocean: *Earth-Science Reviews*, v. 98, p. 1-37.
- 4580 Müller, R., Goncharov, A., and Kritski, A., 2005, Geophysical evaluation of the  
4581 enigmatic Bedout basement high, offshore northwestern Australia: *Earth and*  
4582 *Planetary Science Letters*, v. 237, p. 264-284.
- 4583 Müller, R.D., Cande, S.C., Royer, J.-Y., Roest, W.R., and Maschenkov, S., 1999,  
4584 New constraints on the Late Cretaceous/Tertiary plate tectonic evolution of the  
4585 Caribbean, *in* Mann, P., ed., *Caribbean Basins, Volume 4: Sedimentary basins*  
4586 *of the world*: Amsterdam, Elsevier, p. 39-55.

- 4587 Müller, R.D., Gaina, C., Tikku, A., Mihut, D., Cande, S., and Stock, J.M., 2000,  
4588 Mesozoic/Cenozoic tectonic events around Australia, *in* Richards, M., and  
4589 Gordon, R., eds., *The History and Dynamics of Global Plate Motions*, Volume  
4590 121: American Geophysical Union Monograph, American Geophysical Union,  
4591 p. 161-188.
- 4592 Müller, R.D., Mihut, D., and Baldwin, S., 1998a, A new kinematic model for the  
4593 formation and evolution of the Northwest and West Australian margin, *in* R.R.,  
4594 P.P.G.a., ed., *The sedimentary basins of western Australia 2: Perth*, Petroleum  
4595 Exploration Society of Australia, p. 55-72.
- 4596 Müller, R.D., Roest, W.R., and Royer, J.-Y., 1998b, Asymmetric seafloor spreading  
4597 expresses ridge-plume interactions: *Nature*, v. 396, p. 455-459.
- 4598 Müller, R.D., Roest, W.R., Royer, J.-Y., Gahagan, L.M., and Sclater, J.G., 1997,  
4599 Digital isochrons of the world's ocean floor: *Journal of Geophysical Research*,  
4600 v. 102, p. 3211-3214.
- 4601 Müller, R.D., Sdrolias, M., Gaina, C., and Roest, W.R., 2008a, Age, spreading rates  
4602 and spreading asymmetry of the world's ocean crust: *Geochemistry,*  
4603 *Geophysics, Geosystems*, v. 9.
- 4604 Müller, R.D., Sdrolias, M., Gaina, C., Steinberger, B., and Heine, C., 2008b, Long-  
4605 Term Sea-Level Fluctuations Driven by Ocean Basin Dynamics: *Science*, v.  
4606 319, p. 1357-1362.
- 4607 Munschy, M., Antoine, C., and Gachon, A., 1996, Tectonic evolution in the Tuamotu  
4608 Islands Region, Central Pacific Ocean: *C R Acad Sci Ser II A*, v. 323, p. 941-  
4609 948.
- 4610 Nakanishi, M., Sager, W.W., and Klaus, A., 1999, Magnetic lineations within Shatsky  
4611 Rise, northwest Pacific Ocean: Implications for hot spot-triple junction  
4612 interaction and oceanic plateau formation: *Journal of Geophysical Research-*  
4613 *Solid Earth*, v. 104, p. 7539-7556.
- 4614 Nakanishi, M., and Winterer, E.L., 1998, Tectonic history of the Pacific-Farallon-  
4615 Phoenix triple junction from late Jurassic to early Cretaceous: An abandoned  
4616 Mesozoic spreading system in the central Pacific basin: *J Geophys Res Solid*  
4617 *Earth*, v. 103, p. 12453-12468.
- 4618 Nelson, J.A., and Mihalyuk, M., 1993, Cache Creek ocean: Closure or enclosure?:  
4619 *Geology*, v. 21, p. 173.
- 4620 Nelson, J.A.L., Colpron, M., Piercey, S.J., Dusel-Bacon, C., Murphy, D.C., and  
4621 Roots, C.F., 2006, Paleozoic tectonic and metallogenetic evolution of  
4622 pericratonic terranes in Yukon, northern British Columbia and eastern  
4623 Alaska: Paleozoic evolution and metallogeny of pericratonic terranes at the  
4624 ancient pacific margin of North America, Canadian and Alaskan cordillera, p.  
4625 323.
- 4626 Nokleberg, W., Parfenov, L., Monger, J., Norton, I., Chan uk, A., Stone, D., Scotese,  
4627 C., Scholl, D., and Fujita, K., 2001, Phanerozoic tectonic evolution of the  
4628 Circum-North Pacific, US Dept. of the Interior, US Geological Survey.
- 4629 Norton, I., 2007, Speculations on Cretaceous tectonic history of the northwest Pacific  
4630 and a tectonic origin for the Hawaii hotspot: *Geological Society of America*  
4631 *Special Papers*, v. 430, p. 451.
- 4632 Nunns, A.G., 1983, Plate tectonic evolution of the Greenland-Scotland Ridge and  
4633 surrounding regions, *in* Bott, M.H.P., Saxov, S., Talwani, M., and Thiede, J.,  
4634 eds., *Structure and Development of the Greenland-Scotland Ridge*: New York,  
4635 New York, Plenum, p. 11-30.

- 4636 Nürnberg, D., and Müller, R.D., 1991, The tectonic evolution of the South Atlantic  
4637 from Late Jurassic to present: *Tectonophysics*, v. 191, p. 27-53.
- 4638 O'Neill, C., Müller, R.D., and Steinberger, B., 2005, On the Uncertainties in Hotspot  
4639 Reconstructions, and the Significance of Moving Hotspot Reference Frames:  
4640 *Geochemistry, Geophysics, Geosystems*, v. 6, p. doi:10.1029/2004GC000784,  
4641 2005.
- 4642 Pardo-Casas, F., and Molnar, P., 1987, Relative motion of the Nazca (Farallon) and  
4643 South American plates since Late Cretaceous time: *Tectonics*, v. 6, p.  
4644 215-232.
- 4645 Patriat, P., and Ségoufin, J., 1988, Reconstruction of the central Indian Ocean:  
4646 *Tectonophysics*, v. 155, p. 211-234.
- 4647 Pindell, J., and Kennan, L., 2009, Tectonic evolution of the Gulf of Mexico,  
4648 Caribbean and northern South America in the mantle reference frame: an  
4649 update: *Geological Society London Special Publications*, v. 328, p. 1.
- 4650 Pindell, J., Kennan, L.S., and K-P, M., 2006, Foundations of Gulf of Mexico and  
4651 Caribbean evolution: eight controversies resolved: *Geologica acta*, v. 4, p.  
4652 303-341.
- 4653 Pindell, J.L., Cande, S., Pitman III, W.C., Rowley, D.B., Dewey, J.F., Labrecque, J.,  
4654 and Haxby, W., 1988, A plate-kinematic framework for models of Caribbean  
4655 evolution: *Tectonophysics*, v. 155, p. 121-138.
- 4656 Pockalny, R.A., Larson, R.L., Viso, R.F., and Abrams, L.J., 2002, Bathymetry and  
4657 gravity data across a mid-Cretaceous triple junction trace in the southwest  
4658 Pacific basin: *Geophysical Research Letters*, v. 29, p. 1007.
- 4659 Pogue, K.R., DiPietro, J.A., Khan, S.R., Hughes, S.S., Dilles, J.H., and Lawrence,  
4660 R.D., 1992, Late Paleozoic rifting in northern Pakistan: *Tectonics*, v. 11, p.  
4661 871-883.
- 4662 Powell, C.M., Roots, S.R., and Veevers, J.J., 1988, Pre-breakup continental extension  
4663 in East Gondwanaland and the early opening of the eastern Indian Ocean:  
4664 *Tectonophysics*, v. 155, p. 261-283.
- 4665 Rangin, C., Jolivet, L., and Pubellier, M., 1990, A simple model for the tectonic  
4666 evolution of southeast Asia and Indonesia region for the past 43 my: *Bulletin  
4667 de la Société Géologique de France*, v. 8, p. 889-905.
- 4668 Rea, D.K., and Dixon, J.M., 1983, Late Cretaceous and Paleogene tectonic evolution  
4669 of the North Pacific Ocean: *Earth and Planetary Science Letters*, v. 65, p. 145-  
4670 66.
- 4671 Reeves, C., and de Wit, M., 2000, Making ends meet in Gondwana: retracing the  
4672 transforms of the Indian Ocean and reconnecting continental shear zones:  
4673 *Terra Nova*, v. 12, p. 272-280.
- 4674 Richards, M.A., Jones, D.L., Duncan, R.A., and DePaolo, D.J., 1991, A mantle plume  
4675 initiation model for the formation of Wrangellia and other oceanic flood basalt  
4676 plateaus: *Science*, v. 254, p. 263-267.
- 4677 Riisager, P., Hall, S., Antretter, M., and Zhao, X., 2003, Paleomagnetic paleolatitude  
4678 of Early Cretaceous Ontong Java Plateau basalts: implications for Pacific  
4679 apparent and true polar wander: *Earth and Planetary Science Letters*, v. 208, p.  
4680 235-252.
- 4681 Robertson, A.H.F., 2000, Mesozoic-Tertiary tectonic-sedimentary evolution of a  
4682 south Tethyan oceanic basin and its margins in southern Turkey: *Geological  
4683 Society, London, Special Publications*, v. 173, p. 97-138.
- 4684 Roeser, H., Steiner, C., Schreckenberger, B., and Block, M., 2002, Structural  
4685 development of the Jurassic Magnetic Quiet Zone off Morocco and

- 4686 identification of Middle Jurassic magnetic lineations: *Journal of Geophysical*  
4687 *Research*, v. 107, p. 2207.
- 4688 Roest, W., and Srivastava, S., 1991, Kinematics of the plate boundaries between  
4689 Eurasia, Iberia, and Africa in the North Atlantic from the Late Cretaceous to  
4690 the present: *Geology*, v. 19, p. 613.
- 4691 Roest, W.R., and Srivastava, S.P., 1989, Seafloor spreading in the  
4692 Labrador Sea: a new reconstruction: *Geology*, v. 17, p. 1000-  
4693 1004.
- 4694 Rosa, J.W.C., and Molnar, P., 1988, Uncertainties in reconstructions of the Pacific,  
4695 Farallon, Vancouver, and Kula plates and constraints on the rigidity of the  
4696 Pacific and Farallon (and Vancouver) plates between 72 and 35 Ma: *Journal of*  
4697 *Geophysical Research*, v. 93, p. 2997-3008.
- 4698 Rosenbaum, G., Giles, D., Saxon, M., Betts, P.G., Weinberg, R.F., and Duboz, C.,  
4699 2005, Subduction of the Nazca Ridge and the Inca Plateau: Insights into the  
4700 formation of ore deposits in Peru: *Earth and Planetary Science Letters*, v. 239,  
4701 p. 18-32.
- 4702 Rosenbaum, G., Lister, G.S., and Duboz, C., 2002, Relative motions of Africa, Iberia  
4703 and Europe during Alpine orogeny: *Tectonophysics*, v. 359, p. 117-129.
- 4704 Rosendahl, B.R., Moberly, R., Halunen, A.J., Rose, J.C., and Kroenke, L.W., 1975,  
4705 Geological and geophysical studies of the Canton Trough region: *Journal of*  
4706 *Geophysical Research*, v. 80, p. 2565-2574.
- 4707 Ross, M., and Scotese, C., 1988, A hierarchical tectonic model of the Gulf of Mexico  
4708 and Caribbean region: *Tectonophysics*, v. 155, p. 139-168.
- 4709 Rowley, D.B., and Lottes, A.L., 1988, Plate-kinematic reconstructions of the North  
4710 Atlantic and Arctic: Late Jurassic to present: *Tectonophysics*, v. 155, p. 73-  
4711 120.
- 4712 Royer, J.-Y., and Chang, T., 1991, Evidence for relative motions between the Indian  
4713 and Australian plates during the last 20 m.y. from plate tectonic  
4714 reconstructions: implications for the deformation of the Indo-Australian plate:  
4715 *Journal of Geophysical Research*, v. 96, p. 11779-11802.
- 4716 Royer, J.-Y., and Coffin, M.F., 1992, Jurassic to Eocene plate tectonic reconstructions  
4717 in the Kerguelen Plateau region, *in* S.W. Wise, J., Julson, A.P., Schlich, R.,  
4718 and Thomas, E., eds., *Proceedings of the Ocean Drilling Program, Scientific*  
4719 *Results, Volume 120: College Station, TX, Ocean Drilling Program, Texas*  
4720 *A&M University*, p. 917-930.
- 4721 Royer, J.-Y., Patriat, P., Bergh, H., and Scotese, C.R., 1988, Evolution of the  
4722 Southwest Indian Ridge from the Late Cretaceous (anomaly 34) to the middle  
4723 Eocene (anomaly 20): *Tectonophysics*, v. 155, p. 235-260.
- 4724 Ru, K., and Pigott, J.D., 1986, Episodic rifting and subsidence in the South China  
4725 Sea: *American Association of Petroleum Geologists Bulletin*, v. 70, p. 1136-  
4726 1155.
- 4727 Russell, S.M., and Whitmarsh, R.B., 2003, Magmatism at the west Iberia non-  
4728 volcanic rifted continental margin: Evidence from analyses of magnetic  
4729 anomalies: *Geophysical Journal International*, v. 154, p. 706-730.
- 4730 Sager, W., 2005, What built Shatsky Rise, a mantle plume or ridge tectonics?:  
4731 *Geological Society of America Special Papers*, v. 388, p. 721.
- 4732 Sager, W., Handschumacher, D., Hilde, T., and Bracey, D., 1988, Tectonic evolution  
4733 of the northern Pacific plate and Pacific-Farallon Izanagi triple junction in the  
4734 Late Jurassic and Early Cretaceous (M21-M10): *Tectonophysics*, v. 155, p.  
4735 345-364.

- 4736 Sager, W.W., Kim, J., Klaus, A., Nakanishi, M., and Khankishieva, L.M., 1999,  
4737 Bathymetry of Shatsky Rise, northwest Pacific Ocean: Implications for ocean  
4738 plateau development at a triple junction: *Journal of Geophysical Research-*  
4739 *Solid Earth*, v. 104, p. 7557-7576.
- 4740 Sager, W.W., Weiss, C.J., Tivey, M.A., and Johnson, H.P., 1998, Geomagnetic  
4741 polarity reversal model of deep-tow profiles from the Pacific Jurassic Quiet  
4742 Zone: *J Geophys Res Solid Earth*, v. 103, p. 5269-5286.
- 4743 Sagong, H., Kwon, S., and Ree, J., 2005, Mesozoic episodic magmatism in South  
4744 Korea and its tectonic implication: *Tectonics*, v. 24.
- 4745 Sahabi, M., Aslanian, D., and Olivet, J., 2004, A new starting point for the history of  
4746 the central Atlantic: *Comptes Rendus Geoscience*, v. 336, p. 1041-1052.
- 4747 Sandwell, D., and Smith, W., 2009, Global marine gravity from retracked Geosat and  
4748 ERS-1 altimetry: Ridge segmentation versus spreading rate: *J. geophys. Res.*,  
4749 v. 114.
- 4750 Sandwell, D.T., and Smith, W.H.F., 1997, Marine gravity anomaly from Geosat and  
4751 ERS-1 satellite altimetry: *Journal of Geophysical Research-Solid Earth*, v.  
4752 102, p. 10039-10054.
- 4753 —, 2005, Retracking ERS-1 altimeter waveforms for optimal gravity field recovery:  
4754 *Geophysical Journal International*, v. 163, p. 79-89.
- 4755 Sayers, J., Symonds, P.A., Direen, N.G., and Bernadel, G., 2001, Nature of the  
4756 continent-ocean transition on the non-volcanic rifted margin in the central  
4757 Great Australian Bight, *in* Wilson, R.C.L., Whitmarsh, R.B., Taylor, B., and  
4758 Froitzheim, N., eds., *Non-volcanic rifting of continental margins: a  
4759 comparison of evidence from land and sea*, Volume Special Publication,  
4760 Geological Society of London, p. 51-76.
- 4761 Schaefer, B.F., Turner, S., Parkinson, I., Rogers, N., and Hawkesworth, C., 2002,  
4762 Evidence for recycled Archaean oceanic mantle lithosphere in the Azores  
4763 plume: *Nature*, v. 420, p. 304-307.
- 4764 Schettino, A., and Scotese, C.R., 2005, Apparent polar wander paths for the major  
4765 continents (200 Ma to the present day): a palaeomagnetic reference frame for  
4766 global plate tectonic reconstructions: *Geophysical Journal International*, v.  
4767 163, p. 727-759.
- 4768 Schettino, A., and Turco, E., 2009, Breakup of Pangaea and plate kinematics of the  
4769 central Atlantic and Atlas regions: *Geophysical Journal International*, v. 178,  
4770 p. 1078-1097.
- 4771 Scotese, C.R., 1991, Jurassic and cretaceous plate tectonic reconstructions:  
4772 *Palaeogeography, Palaeoclimatology, Palaeoecology*, v. 87, p. 493-501.
- 4773 Scotese, C.R., Gahagan, L.M., and Larson, R.L., 1988, Plate tectonic reconstructions  
4774 of the Cretaceous and Cenozoic ocean basins: *Tectonophysics*, v. 155, p. 27-  
4775 48.
- 4776 Sdrolias, M., Müller, R.D., Mauffret, A., and Bernadel, G., 2004, Enigmatic  
4777 formation of the Norfolk Basin, SW Pacific: A plume influence on back-arc  
4778 extension: *Geochemistry Geophysics Geosystems*, v. 5, p. Q06005.
- 4779 Sdrolias, M., and Müller, R.D., 2006, The Controls on Back-arc Basin Formation:  
4780 *Geochemistry, Geophysics, Geosystems*, v. 7, p. Q04016,  
4781 doi:10.1029/2005GC001090.
- 4782 Sdrolias, M., R.D., M., and Gaina, C., 2003a, Tectonic Evolution of the SW Pacific  
4783 Using Constraints from Back-arc Basins, *in* R.R., H., and R.D., M., eds.,  
4784 *Evolution and Dynamics of the Australian Plate*, Geological Society of

- 4785 Australia Special Publication 22 and Geological Society of America Special  
4786 Paper.
- 4787 Sdrolias, M., Roest, W.R., and Müller, R.D., 2003b, An Expression of Philippine  
4788 Plate Rotation: the Parece Vela and Shikoku Basins: Tectonophysics.
- 4789 Searle, R., Bird, R., Rusby, R., and Naar, D., 1993a, The development of two oceanic  
4790 microplates: Easter and Juan Fernandez microplates, East Pacific Rise: Journal  
4791 of the Geological Society, v. 150, p. 965.
- 4792 Searle, R., Holcomb, R., Wilson, J., Holmes, M., Whittington, R., Kappel, E.,  
4793 McGregor, B., and Shor, A., 1993b, The Molokai fracture zone near Hawaii,  
4794 and the Late Cretaceous change in Pacific/Farallon spreading direction: The  
4795 Mesozoic Pacific: geology, tectonics, and volcanism: a volume in memory of  
4796 Sy Schlanger, p. 155.
- 4797 Sengor, A., 1987, Tectonics of the Tethysides: orogenic collage development in a  
4798 collisional setting: Annual Review of Earth and Planetary Sciences, v. 15, p.  
4799 213-244.
- 4800 Sengör, A.M.C., Cin, A., Rowley, D.B., and S-Y, N., 1993, Space-time patterns of  
4801 magmatism along the Tethysides: t preliminary study: The Journal of  
4802 Geology, v. 101, p. 51-84.
- 4803 Seton, M., Gaina, C., Muller, R., and Heine, C., 2009, Mid-Cretaceous seafloor  
4804 spreading pulse: Fact or fiction?: Geology, v. 37, p. 687.
- 4805 Seton, M., and Müller, R., 2008, Reconstructing the junction between Panthalassa and  
4806 Tethys since the Early Cretaceous: Eastern Australasian Basins III, p.  
4807 263-266.
- 4808 Seton, M., Whittaker, J., Flament, N., Müller, R., and Gurnis, M., In Prep, A case for a  
4809 top-down plate reorganization at 50 Ma: Nature Geosciences, v. In Prep.
- 4810 Shaw, P., and Cande, S.C., 1990, High-Resolution Inversion for South Atlantic Plate  
4811 Kinematics Using Joint Altimeter and Magnetic Anomaly Data: Journal of  
4812 Geophysical Research, v. v. 95, p. p. 2625-2644.
- 4813 Shephard, G.E., Bunge, H.P., Schuberth, B.S.A., Müller, R.D., Talsma, A.S., Moder,  
4814 C., and Landgrebe, T.C.W., 2012, Testing absolute plate reference frames and  
4815 the implications for the generation of geodynamic mantle heterogeneity  
4816 structure: Earth and Planetary Science Letters, v. 317-318, p. 204-217.
- 4817 Shi, G., and Archbold, N., 1998, Permian marine biogeography of SE Asia:  
4818 Biogeography and Geological Evolution of SE Asia. Backhuys, Leiden, p.  
4819 57-72.
- 4820 Sibuet, J., Srivastava, S., and Manatschal, G., 2007, Exhumed mantle-forming  
4821 transitional crust in the Newfoundland-Iberia rift and associated magnetic  
4822 anomalies: Journal of Geophysical Research, v. 112, p. B06105.
- 4823 Sibuet, J., Srivastava, S., and Spakman, W., 2004, Pyrenean orogeny and plate  
4824 kinematics: J. geophys. Res, v. 109, p. B08104.
- 4825 Singh, S.C., Carton, H., Chauhan, A.S., Androvandi, S., Davaille, A., Dymant, J.,  
4826 Cannat, M., and Hananto, N.D., 2010, Extremely thin crust in the Indian  
4827 Ocean possibly resulting from Plume-Ridge Interaction: Geophysical Journal  
4828 International.
- 4829 Sinton, C., Duncan, R., Storey, M., Lewis, J., and Estrada, J., 1998, An oceanic flood  
4830 basalt province within the Caribbean plate: Earth and Planetary Science  
4831 Letters, v. 155, p. 221-235.
- 4832 Skogseid, J., Planke, S., Faleide, J., Pedersen, T., Eldholm, O., and Neverdal, F.,  
4833 2000, NE Atlantic continental rifting and volcanic margin formation:  
4834 Dynamics of the Norwegian Margin, v. 167, p. 295-326.

- 4835 Sleep, N.H., and Toksoz, M.N., 1971, Evolution of marginal seas: *Nature*, v. 233, p.  
4836 548-550.
- 4837 Small, C., and Abbott, D., 1998, Subduction obstruction and the crack-up of the  
4838 Pacific plate: *Geology*, v. 26, p. 795-798.
- 4839 Smith, A.G., and Hallam, A., 1970, The fit of the southern continents: *Nature*, v. 225,  
4840 p. 139-144.
- 4841 Sokolov, S., Ye, B., Morozov, O., Shekhovtsov, V., Glotov, S., Ganelin, A., and  
4842 Kravchenko-Berezhnoy, I., 2002, South Anjui suture, northeast Arctic Russia:  
4843 Tectonic Evolution of the Bering Shelf-Chukchi Sea-Arctic Margin and  
4844 Adjacent Landmasses, p. 209-223.
- 4845 Speed, R.C., 1985, Cenozoic collision of the Lesser Antilles arc and continental South  
4846 America and the origin of the El Pilar fault: *Tectonics*, v. 4, p. 41-69.
- 4847 Speranza, F., Villa, I., Sagnotti, L., Florindo, F., Cosentino, D., Cipollari, P., and  
4848 Mattei, M., 2002, Age of the Corsica-Sardinia rotation and Liguro-Provençal  
4849 basin spreading: new paleomagnetic and Ar/Ar evidence: *Tectonophysics*, v.  
4850 347, p. 231-251.
- 4851 Srivastava, S., Schouten, H., Roest, W., Klitgord, K., Kovacs, L., Verhoef, J., and  
4852 Macnab, R., 1990, Iberian plate kinematics: a jumping plate boundary between  
4853 Eurasia and Africa.
- 4854 Srivastava, S.P., 1985, Evolution of the Eurasian Basin and its implication to the  
4855 motion of Greenland along Nares Strait: *Tectonophysics*, v. 114, p. 29-53.
- 4856 Srivastava, S.P., and Roest, W.R., 1989, Seafloor spreading history II-IV,  
4857 in East Coast Basin Atlas Series: Labrador Sea, J.S. Bell (co-  
4858 ordinator). Atlantic Geoscience Centre, Geologic Survey of  
4859 Canada, Map sheets L17-2 - L17-6.
- 4860 —, 1996, Porcupine Plate Hypothesis - Comment: *Marine Geophysical Researches*, v.  
4861 18, p. 589-593.
- 4862 Srivastava, S.P., Sibuet, J.C., Cande, S., Roest, W.R., and Reid, I.D., 2000, Magnetic  
4863 evidence for slow seafloor spreading during the formation of the  
4864 Newfoundland and Iberian margins: *Earth and Planetary Science Letters*, v.  
4865 182, p. 61-76.
- 4866 Srivastava, S.P., and Tapscott, C.R., 1986, Plate kinematics of the North Atlantic, *in*  
4867 R., V.P., and Tucholke, B.E., eds., *The Western North Atlantic Region*,  
4868 Volume M: *The Geology of North America*, Geol. Soc. Am., p. 379-405.
- 4869 Stagg, H.M.J., and Willcox, J.B., 1992, A case for Australia-Antarctica separation in  
4870 the Neocomian (c.a. 125 Ma): *Tectonophysics*, v. 210, p. 21-32.
- 4871 Stamatakos, J.A., Trop, J.M., and Ridgway, K.D., 2001, Late Cretaceous  
4872 paleogeography of Wrangellia: Paleomagnetism of the MacColl Ridge  
4873 Formation, southern Alaska, revisited: *Geology*, v. 29, p. 947-a-950.
- 4874 Stampfli, G.M., and Borel, G.D., 2002, A plate tectonic model for the Paleozoic and  
4875 Mesozoic constrained by dynamic plate boundaries and restored synthetic  
4876 oceanic isochrons: *Earth and Planetary Science Letters*, v. 196, p. 17-33.
- 4877 Steinberger, B., and Torsvik, T., 2008, Absolute plate motions and true polar wander  
4878 in the absence of hotspot tracks: *Nature*, v. 452, p. 620-623.
- 4879 Stock, J., Luyendyk, B., Clayton, R., and Party, S.S., 1998, Tectonics and structure of  
4880 the Manihiki Plateau, western Pacific Ocean: *Eos Trans. AGU*, v. 79.
- 4881 Stock, J., and Molnar, P., 1987, Revised history of early Tertiary plate motion in the  
4882 southwest Pacific: *Nature*, v. 325, p. 495-499.

- 4883 —, 1988, Uncertainties and implications of the Late Cretaceous and Tertiary position  
4884 of North America relative to the Farallon, Kula, and Pacific plates: *Tectonics*,  
4885 v. 7, p. 1339-1384.
- 4886 Stocklin, J., 1974, Possible ancient continental margins in Iran: The geology of  
4887 continental margins, p. 873-887.
- 4888 Straub, S., Goldstein, S., Class, C., and Schmidt, A., 2009, Mid-ocean-ridge basalt of  
4889 Indian type in the northwest Pacific Ocean basin: *Nature Geoscience*, v. 2, p.  
4890 286-289.
- 4891 Sutherland, R., and Hollis, C., 2001, Cretaceous demise of the Moa Plate and strike-  
4892 slip motion at the Gondwana margin: *Geology*, v. 29, p. 279-282.
- 4893 Symonds, P.A., Colwell, J.B., Struckmeyer, H.I.M., Willcox, J.B., and Hill, P.J.,  
4894 1996, Mesozoic rift basin development off eastern Australia, *Mesozoic  
4895 Geology of the Eastern Australia Plate, Volume 43: Brisbane, Geological  
4896 Society of Australia*, p. 528-542.
- 4897 Talwani, M., and Eldholm, O., 1977, Evolution of the Norwegian-Greenland Sea:  
4898 *Geological Society of America Bulletin*, v. 88, p. 969-999.
- 4899 Tamaki, K., and Larson, R.L., 1988, The Mesozoic tectonic history of the Magellan  
4900 microplate in the western Central Pacific: *Journal of Geophysical Research*, v.  
4901 93, p. 2857-2874.
- 4902 Tankard, A.J., and Welsink, H.J., 1987, Extensional Tectonics and Stratigraphy of  
4903 Hibernia Oil Field, Grand Banks, Newfoundland: *American Association of  
4904 Petroleum Geologists Bulletin*, v. 71, p. 1210 - 1232.
- 4905 Taylor, B., 2006, The single largest oceanic plateau: Ontong Java-Manihiki-  
4906 Hikurangi: *Earth and Planetary Science Letters*, v. 241, p. 372-380.
- 4907 Taylor, B., and Karner, G., 1983, On the evolution of marginal basins: *Reviews of  
4908 Geophysics*, v. 21, p. 1727-1741.
- 4909 Tebbens, S.F., and Cande, S.C., 1997, Southeast Pacific Tectonic Evolution From  
4910 Early Oligocene to Present: *Journal of Geophysical Research-Solid Earth*, v.  
4911 102, p. 12061-12084.
- 4912 Thorkelson, D.J., 1996, Subduction of diverging plates and the principles of slab  
4913 window formation: *Tectonophysics*, v. 255, p. 47-63.
- 4914 Tikku, A.A., and Cande, S.C., 1999, The oldest magnetic anomalies in the Australian-  
4915 Antarctic Basin: Are they isochrons?: *Journal of Geophysical Research*, v. 104,  
4916 p. 661-677.
- 4917 —, 2000, On the fit of Broken Ridge and Kerguelen plateau: *Earth and Planetary  
4918 Science Letters*, v. 180, p. 117-132.
- 4919 Tivey, M., Sager, W., Lee, S., and Tominaga, M., 2006, Origin of the Pacific Jurassic  
4920 quiet zone: *Geology*, v. 34, p. 789.
- 4921 Todd, B., Reid, I., and Keen, C., 1988, Crustal structure across the southwest  
4922 Newfoundland transform margin: *Canadian Journal of Earth Sciences*, v. 25,  
4923 p. 744-759.
- 4924 Tominaga, M., and Sager, W.W., 2010, Revised Pacific M-anomaly geomagnetic  
4925 polarity timescale: *Geophysical Journal International*, v. 182, p. 203-232.
- 4926 Tominaga, M., Sager, W.W., Tivey, M.A., and Lee, S.M., 2008, Deep-tow magnetic  
4927 anomaly study of the Pacific Jurassic Quiet Zone and implications for the  
4928 geomagnetic polarity reversal timescale and geomagnetic field behavior:  
4929 *Journal of Geophysical Research*, v. 113, p. B07110.
- 4930 Tomurtogoo, O., Windley, B., Kroner, A., Badarch, G., and Liu, D., 2005, Zircon age  
4931 and occurrence of the Adaatsag ophiolite and Muron shear zone, central

- 4932 Mongolia: constraints on the evolution of the Mongol-Okhotsk ocean, suture  
4933 and orogen: *Journal of Geological Society*, v. 162, p. 125.
- 4934 Torsvik, T., Rouse, S., Labails, C., and Smethurst, M., 2009, A new scheme for the  
4935 opening of the South Atlantic Ocean and the dissection of an Aptian salt basin:  
4936 *Geophysical Journal International*, v. 177, p. 1315-1333.
- 4937 Torsvik, T., Steinberger, B., Cocks, L., and Burke, K., 2008, Longitude: Linking  
4938 Earth's ancient surface to its deep interior: *Earth and Planetary Science  
4939 Letters*, v. 276, p. 273-282.
- 4940 Totterdell, J., Blevin, J., Bradshaw, B., Colwell, J., and Kennard, J., 2000, A NEW  
4941 SEQUENCE FRAMEWORK FOR THE GREAT AUSTRALIAN BIGHT:  
4942 STARTING WITH A CLEAN SLATE: *The APPEA journal*, p. 95.
- 4943 Trop, J.M., Ridgway, K.D., Manuszak, J.D., and Layer, P., 2002, Mesozoic  
4944 sedimentary-basin development on the allochthonous Wrangellia composite  
4945 terrane, Wrangell Mountains basin, Alaska: A long-term record of terrane  
4946 migration and arc construction: *Geological Society of America Bulletin*, v.  
4947 114, p. 693.
- 4948 Tucholke, B., Sawyer, D., and Sibuet, J., 2007, Breakup of the Newfoundland Iberia  
4949 rift: *Geological Society London Special Publications*, v. 282, p. 9.
- 4950 Tucholke, B., and Whitmarsh, R., 2006, The Newfoundland-Iberia conjugate rifted  
4951 margins: *Principles of Phanerozoic Regional Geology*.
- 4952 Umpleby, D., 1979, *Geology of the Labrador shelf*, Geological Survey of Canada  
4953 Commission géologique du Canada.
- 4954 Uyeda, S., and Kanamori, H., 1979, Back-arc opening and the mode of subduction:  
4955 *Journal of Geophysical Research*, v. 84, p. 1049-1061.
- 4956 van der Lelij, R., Spikings, R., Kerr, A., Kounov, A., Cosca, M., Chew, D., and  
4957 Villagomez, D., 2010, Thermochronology and Tectonics of the Leeward  
4958 Antilles: evolution of the Southern Caribbean Plate Boundary Zone and  
4959 accretion of the Bonaire Block.
- 4960 Van der Voo, R., Spakman, W., and Bijwaard, H., 1999a, Mesozoic subducted slabs  
4961 under Siberia: *Nature*, v. 397, p. 246-249.
- 4962 —, 1999b, Tethyan subducted slabs under India: *Earth and Planetary Science Letters*,  
4963 v. 171, p. 7-20.
- 4964 Veevers, J., 2006, Updated Gondwana (Permian-Cretaceous) earth history of  
4965 Australia: *Gondwana Research*, v. 9, p. 231-260.
- 4966 Veevers, J.J., 2000, Change of tectono-stratigraphic regime in the Australian plate  
4967 during the 99 Ma (mid-Cretaceous) and 43 Ma (mid-Eocene) swerves of the  
4968 Pacific: *Geology*, v. 28, p. 47-50.
- 4969 Veevers, J.J., Stagg, H.M.J., Willcox, J.B., and Davies, H.L., 1990, Pattern of slow  
4970 seafloor spreading (<4mm/year) from breakup (96 Ma) to A20 (44.5 Ma) off  
4971 the southern margin of Australia: *BMR Journal of Australian Geology and  
4972 Geophysics*, v. 11, p. 499-507.
- 4973 Veevers, J.J., Tayton, J.W., and Johnson, B.D., 1985, Prominent magnetic anomaly  
4974 along the continent-ocean boundary between the northwestern margin of  
4975 Australia (Exmouth and Scott plateaus) and the Argo abyssal plain: *Earth and  
4976 Planetary Science Letters*, v. 72, p. 415-426.
- 4977 Vry, J., Baker, J., Maas, R., Little, T., Grapes, R., and Dixon, M., 2004, Zoned  
4978 (Cretaceous and Cenozoic) garnet and the timing of high grade  
4979 metamorphism, Southern Alps: New Zealand. *Journal of Metamorphic  
4980 Geology*, v. 22, p. 137-157.

- 4981 Wessel, P., Harada, Y., and Kroenke, L.W., 2006, Toward a self-consistent, high-  
4982 resolution absolute plate motion model for the Pacific: *Geochemistry*  
4983 *Geophysics Geosystems*, v. 7, p. Q03L12.
- 4984 Wessel, P., and Kroenke, L., 2008, Pacific absolute plate motion since 145 Ma: An  
4985 assessment of the fixed hot spot hypothesis: *Journal of Geophysical Research*,  
4986 v. 113, p. B06101.
- 4987 Whitechurch, H., Juteau, T., and Montigny, R., 1984, Role of the Eastern  
4988 Mediterranean ophiolites (Turkey, Syria, Cyprus) in the history of the Neo-  
4989 Tethys: Geological Society, London, Special Publications, v. 17, p. 301-317.
- 4990 Whitmarsh, R.B., and Miles, P.R., 1995, Models of the Development of the West  
4991 Iberia Rifted Continental Margin at 40-Degrees-30n Deduced from Surface  
4992 and Deep-Tow Magnetic Anomalies: *Journal of Geophysical Research-Solid*  
4993 *Earth*, v. 100, p. 3789-3806.
- 4994 Whittaker, J., Müller, R.D., Leitchenkov, G., Stagg, H., Sdrolias, M., Gaina, C., and  
4995 Goncharov, A., 2007, Major Australian-Antarctica Plate Reorganization at  
4996 Hawaiian-Emperor Bend Time: *Science*, v. 318, p. 83-86.
- 4997 Williams, P., Johnston, C., Almond, R., and Simamora, W., 1988, Late Cretaceous to  
4998 early Tertiary structural elements of West Kalimantan: *Tectonophysics*, v.  
4999 148, p. 279-297.
- 5000 Wilson, D.S., 1988, Tectonic history of the Juan de Fuca Ridge over the last 40  
5001 million years: *Journal of Geophysical Research*, v. 33, p. 11,863-11,876.
- 5002 —, 1996, Fastest known spreading on the Miocene Cocos-Pacific plate boundary:  
5003 *Geophysical Research Letters*, v. 23, p. 3003-3006.
- 5004 Wilson, D.S., Hey, R.N., and Nishimura, C., 1984, Propagation as a mechanism of  
5005 reorientation of the Juan de Fuca Ridge: *Journal of Geophysical Research*, v.  
5006 89, p. 9215-9225.
- 5007 Winterer, E., 1976, Anomalies in the tectonic evolution of the Pacific, *in* Sutton, G.,  
5008 Manghnani, M., and Moberly, R., eds., *The Geophysics of the Pacific Ocean Basin*  
5009 *and its Margins*: Washington, D.C., AGU, p. 269-278.
- 5010 Winterer, E., Lonsdale, P., Matthews, J., and Rosendahl, B., 1974, Structure and acoustic  
5011 stratigraphy of the Manihiki Plateau: *Deep-Sea Res.*, v. 21, p. 793-814.
- 5012 Withjack, M.O., Schlische, R.W., and Olsen, P.E., 1998, Diachronous Rifting,  
5013 Drifting, and Inversion On the Passive Margin of Central Eastern North  
5014 America - an Analog For Other Passive Margins: *AAPG Bulletin-American*  
5015 *Association of Petroleum Geologists*, v. 82, p. 817-835.
- 5016 Woods, M.T., and Davies, G.F., 1982, Late Cretaceous genesis of the Kula plate:  
5017 *Earth and Planetary Science Letters*, v. 58, p. 161-166.
- 5018 Worthington, T.J., Hekinian, R., Stoffers, P., Kuhn, T., and Hauff, F., 2006, Osbourn  
5019 Trough: Structure, geochemistry and implications of a mid-Cretaceous  
5020 paleospreading ridge in the South Pacific: *Earth and Planetary Science Letters*,  
5021 v. 245, p. 685-701.
- 5022 Zorin, Y.A., 1999, Geodynamics of the western part of the Mongolia-Okhotsk  
5023 collisional belt, Trans-Baikal region (Russia) and Mongolia: *Tectonophysics*,  
5024 v. 306, p. 33-56.
- 5025
- 5026

Figure 1

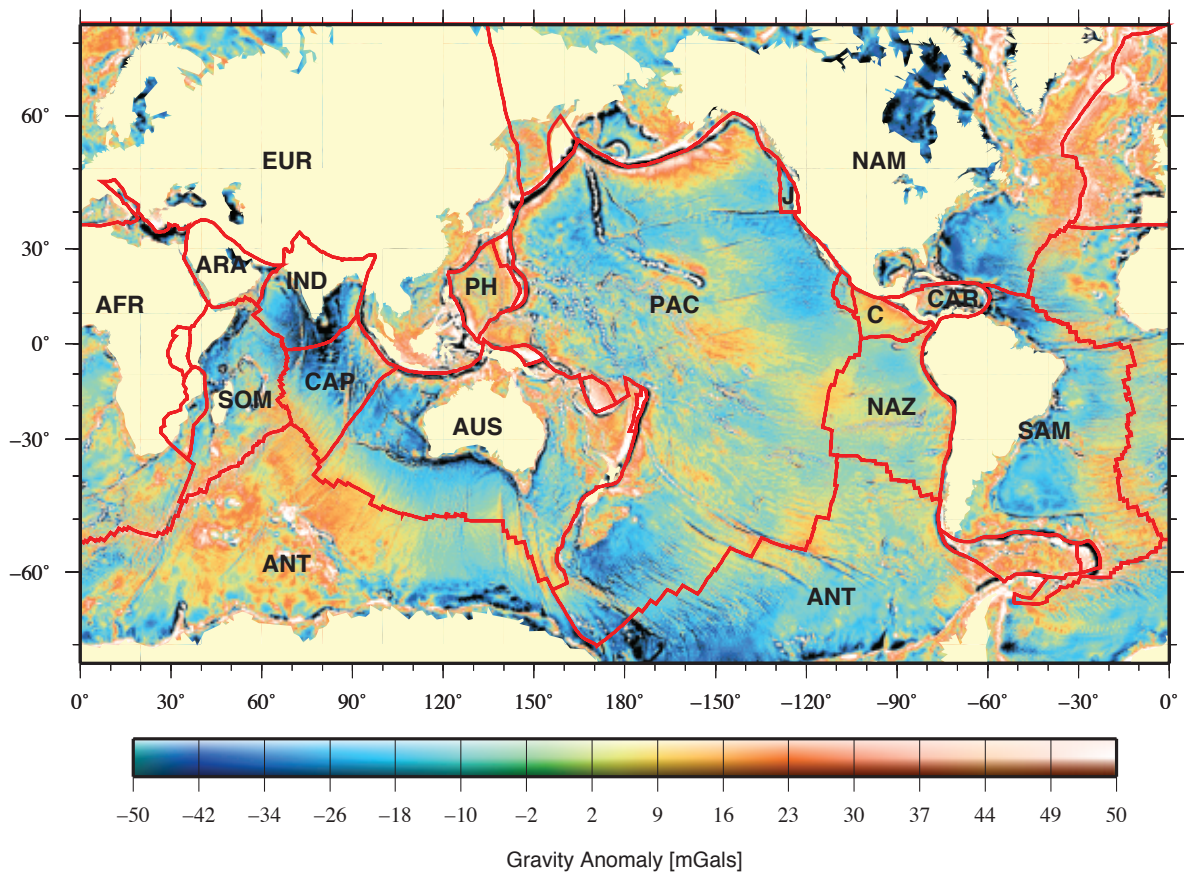


Figure 1: Seton et. al.

Figure 2

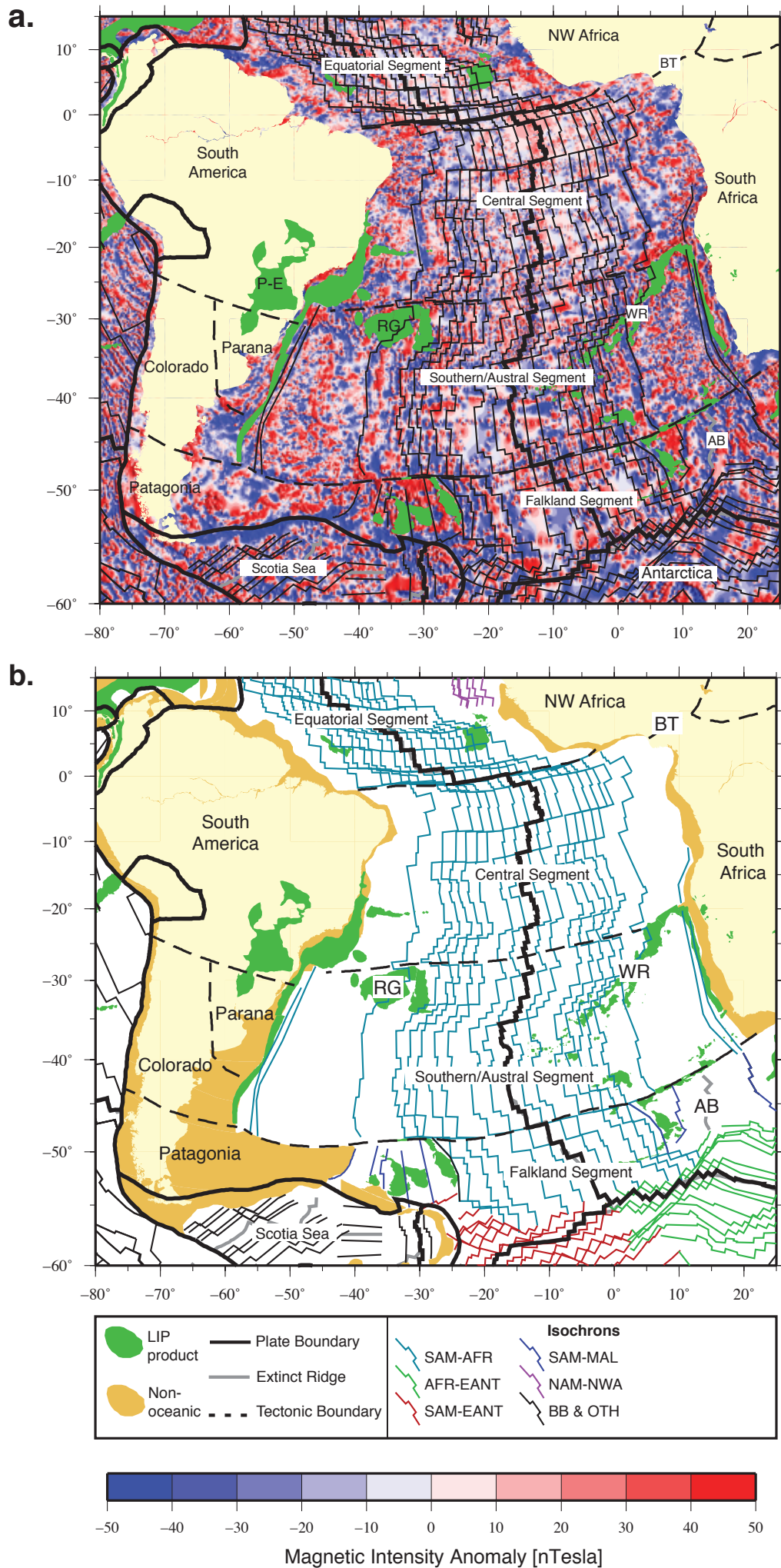


Figure 2: Seton et. al.

Figure 3

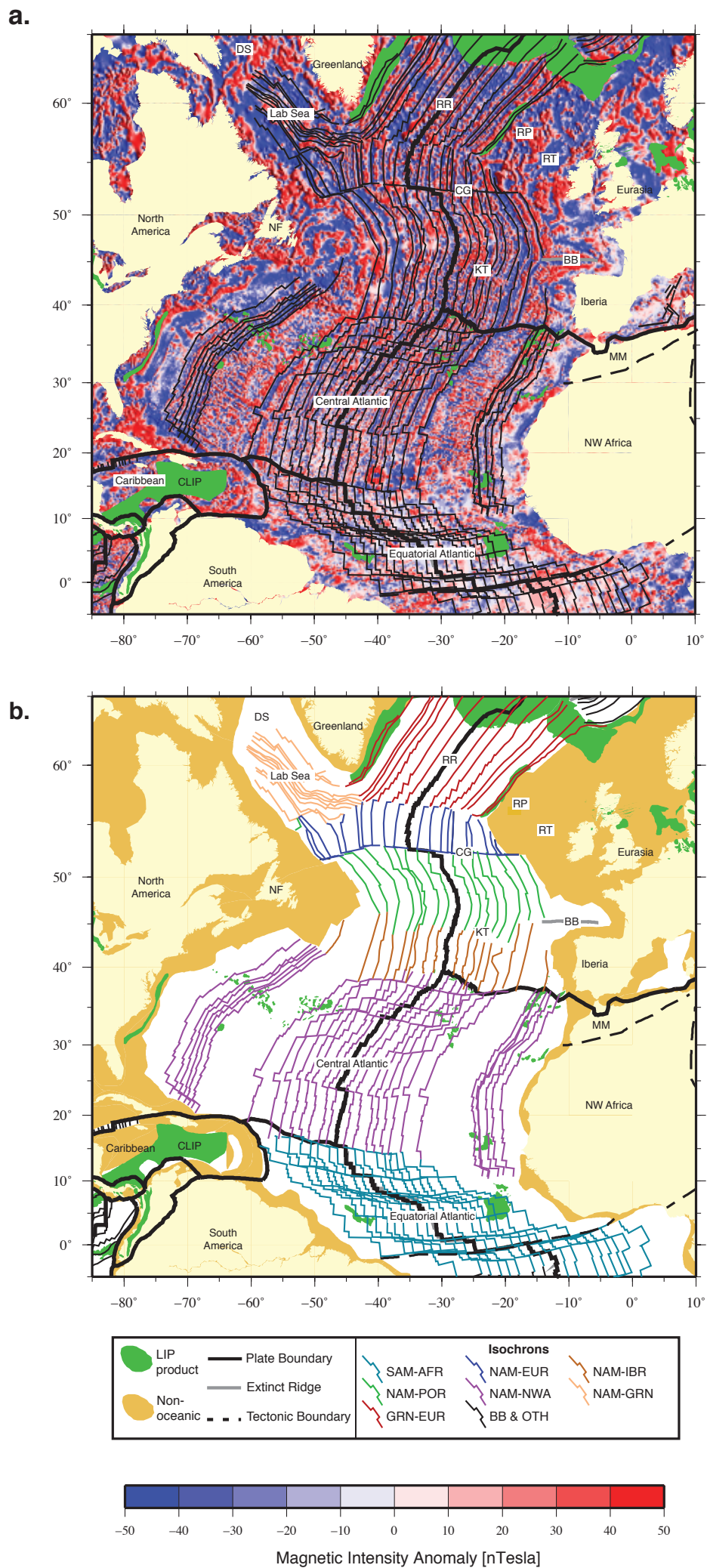


Figure 3: Seton et. al.

Figure 4

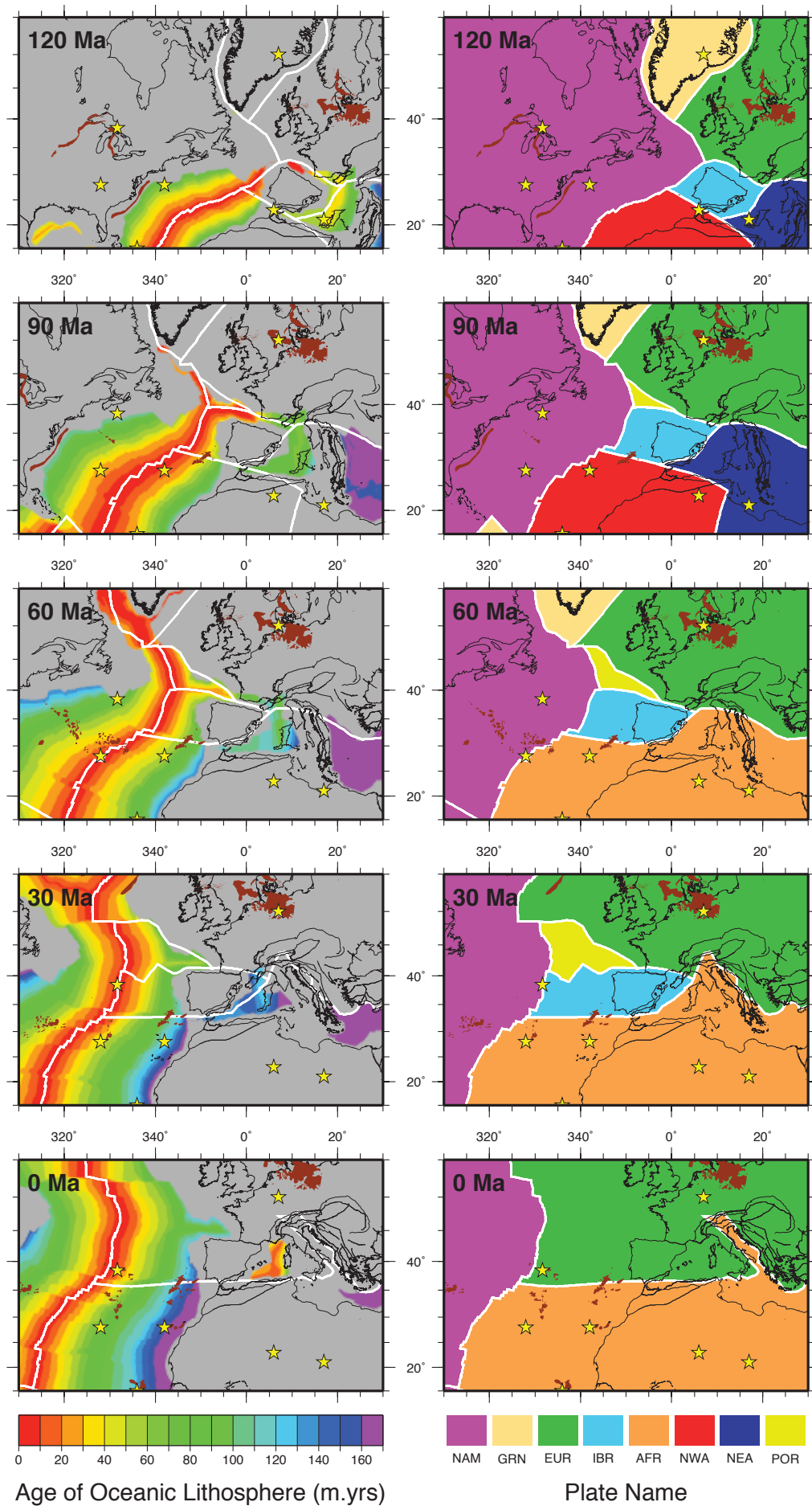


Figure 4: Seton et. al.

Figure 5

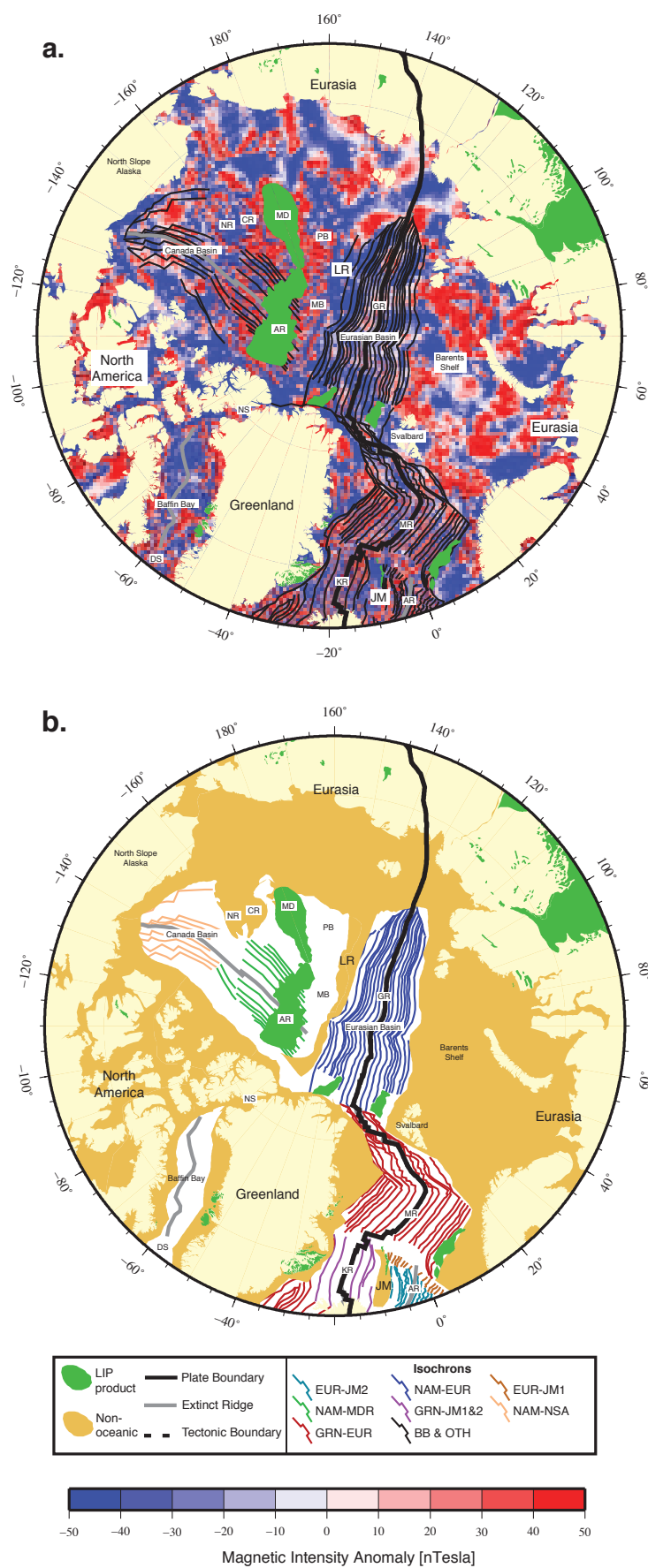


Figure 5: Seton et. al.

Figure 6

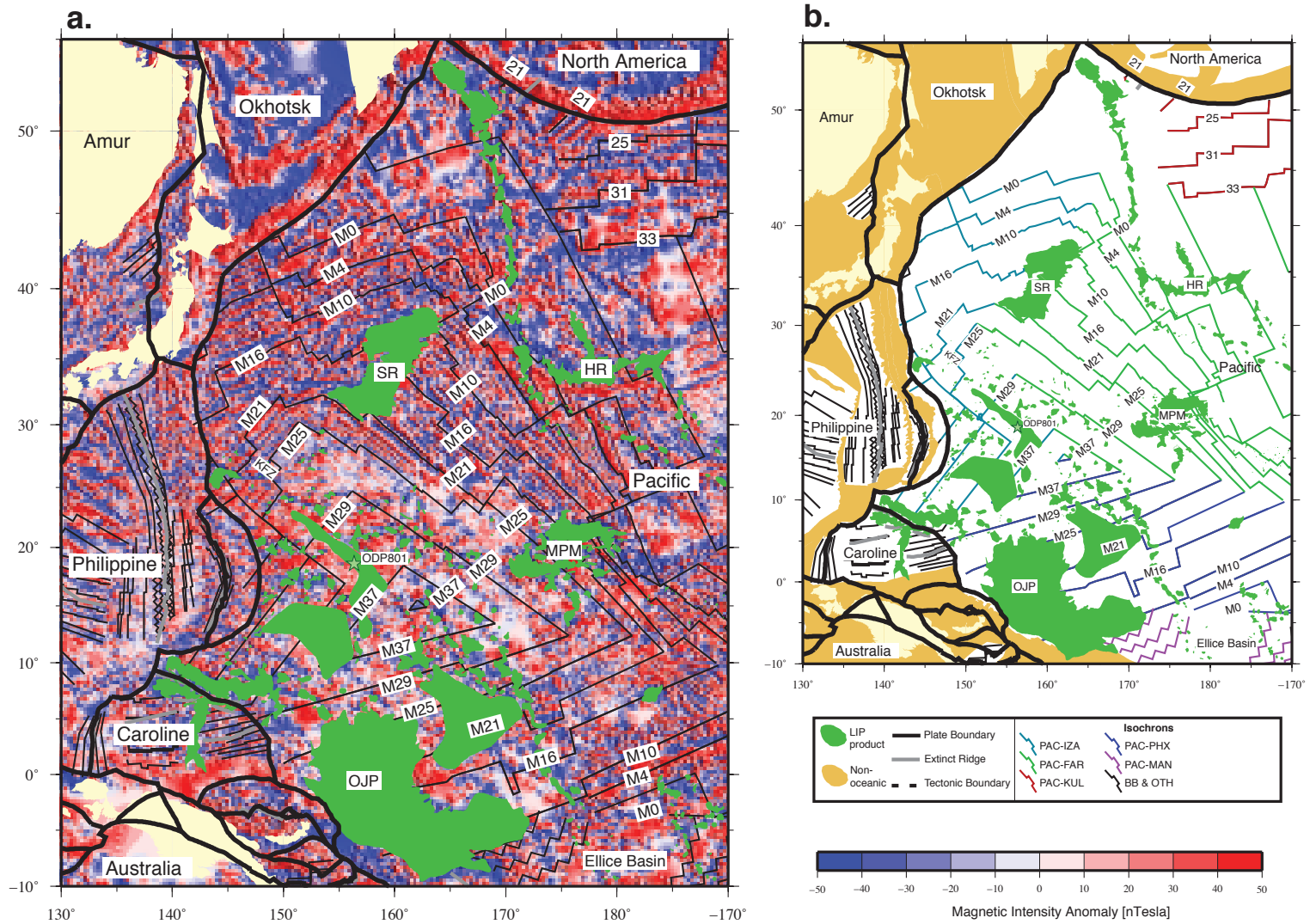


Figure 6: Seton et. al.

Figure 7

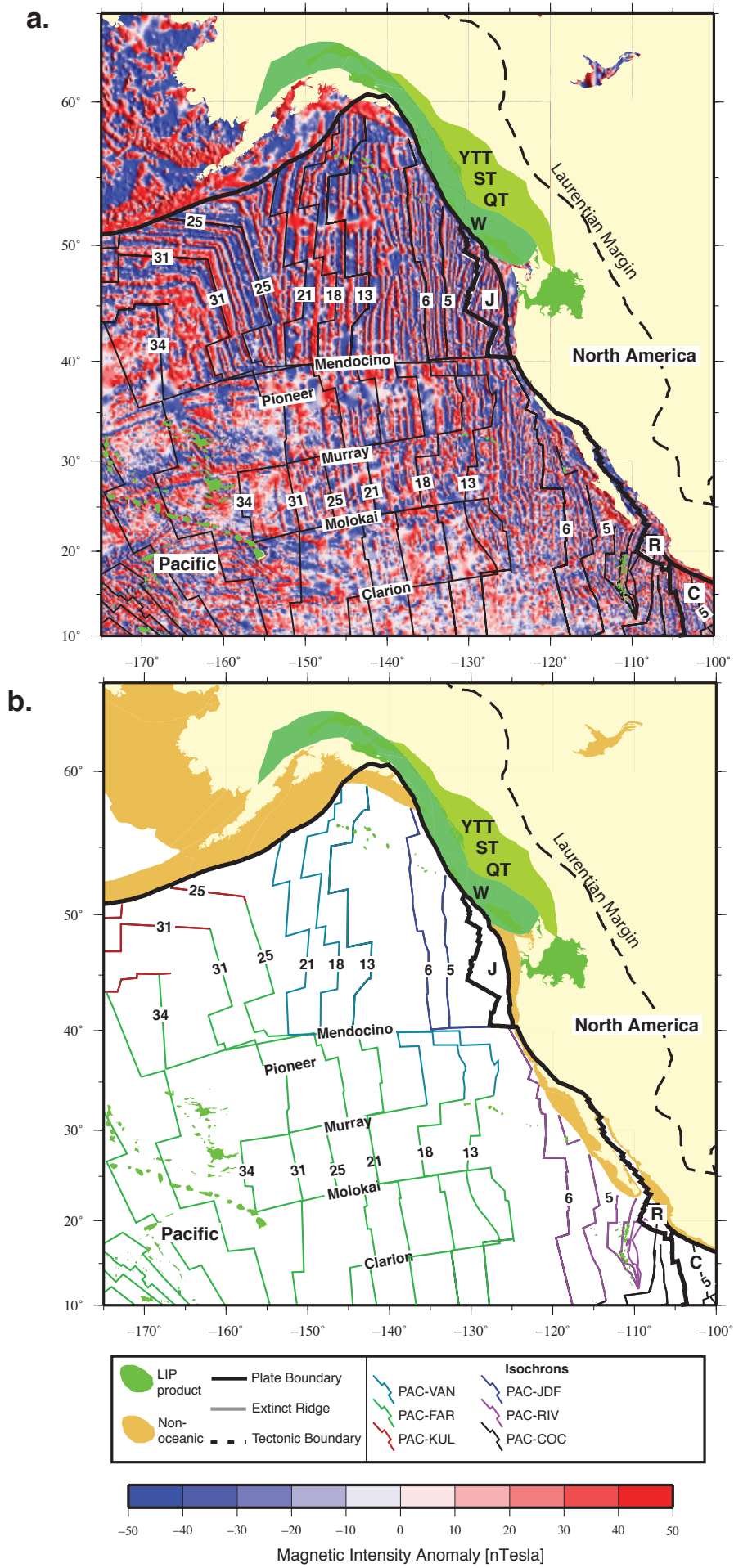


Figure 7: Seton et. al.

Figure 8

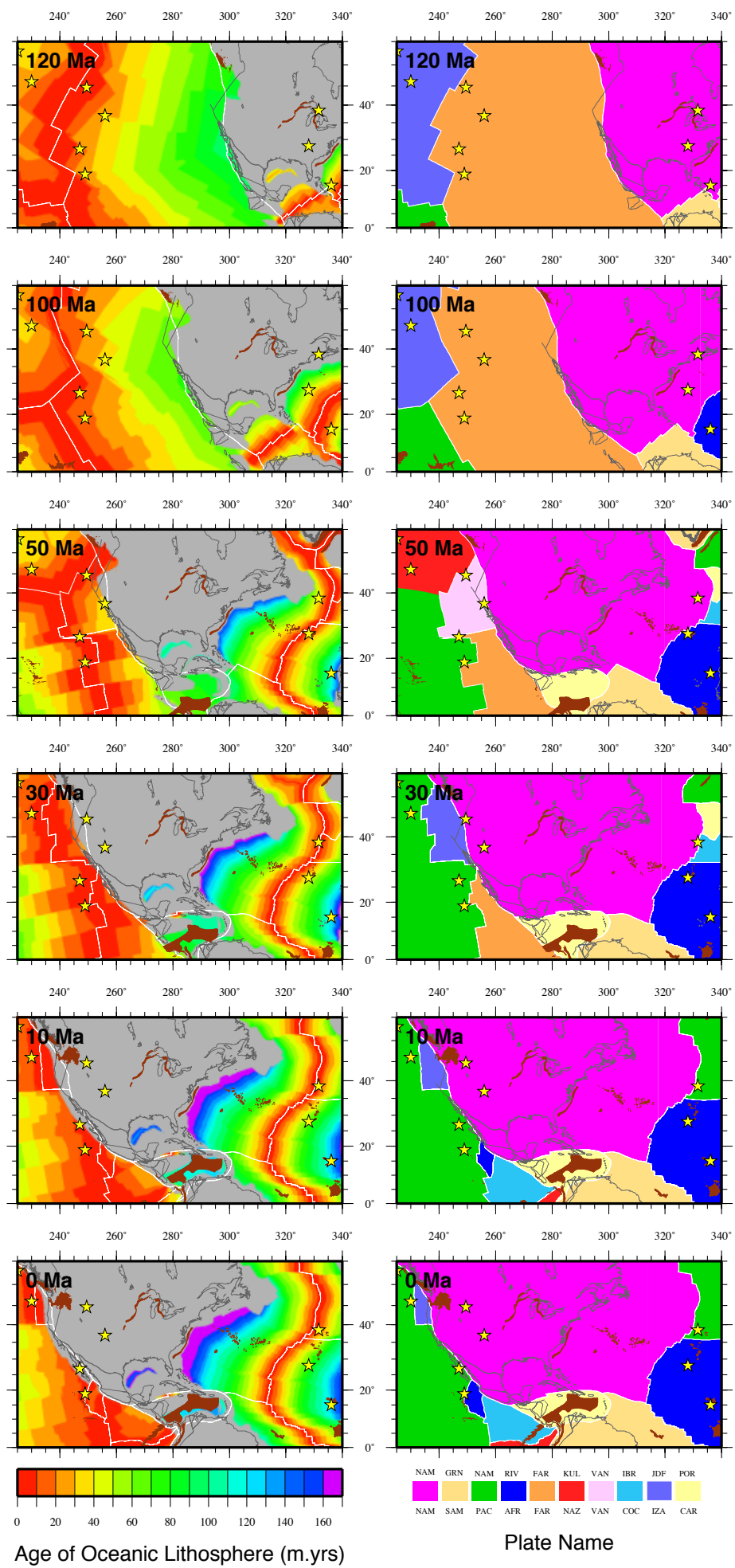
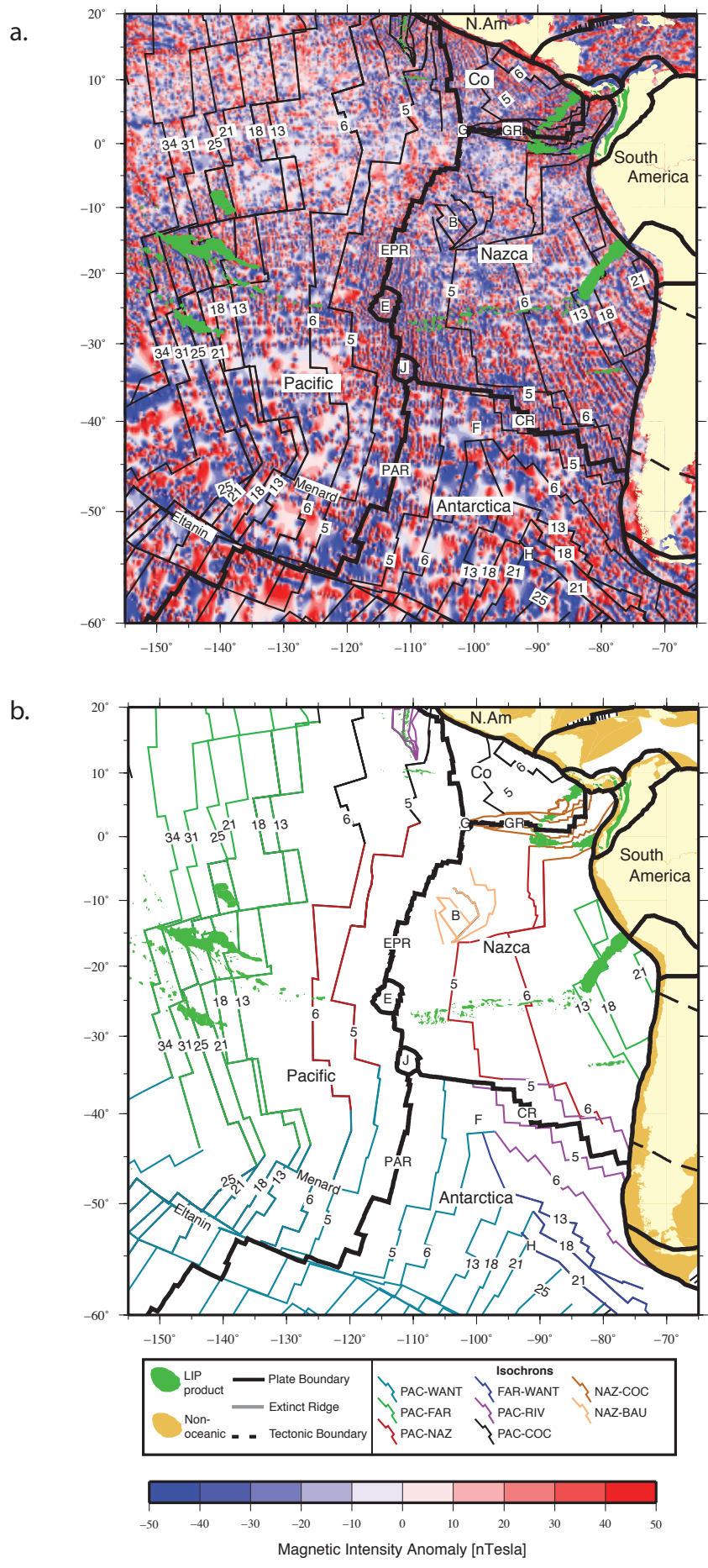


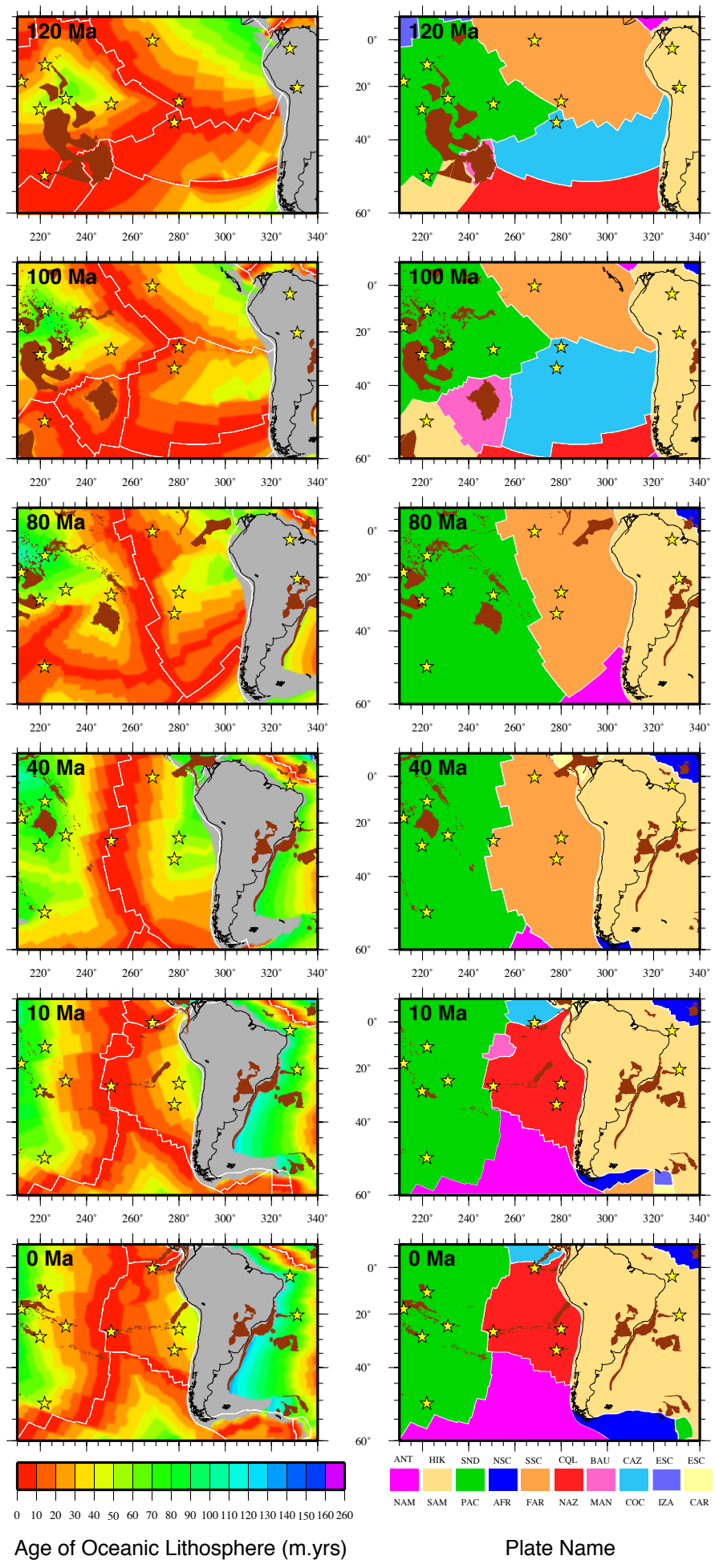
Figure 8: Seton et. al.

Figure 9



Seton et. al. Figure 9

Figure 10



Seton et. al. Figure 10

Figure 11

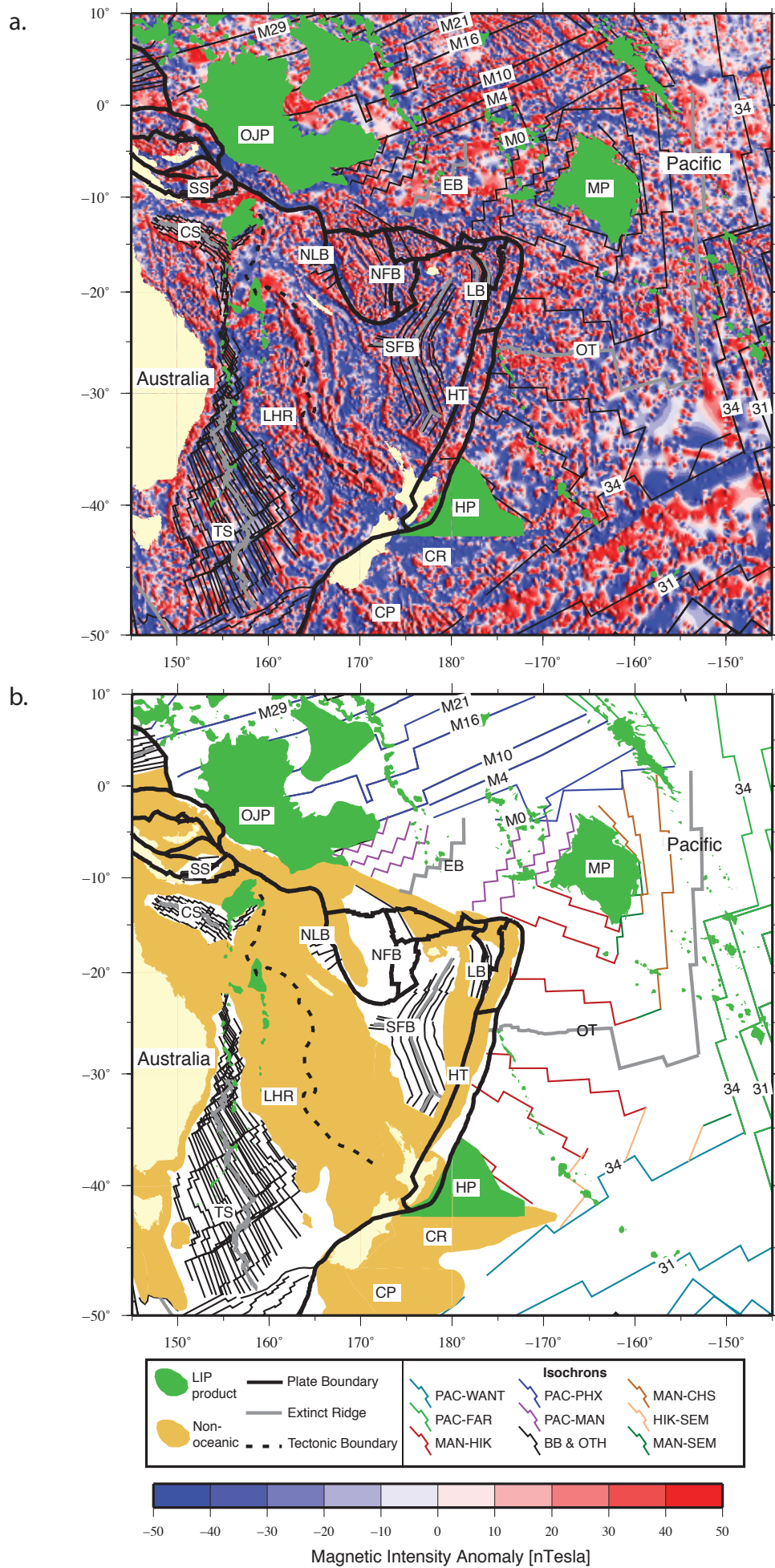


Figure 11: Seton et. al.

Figure 12

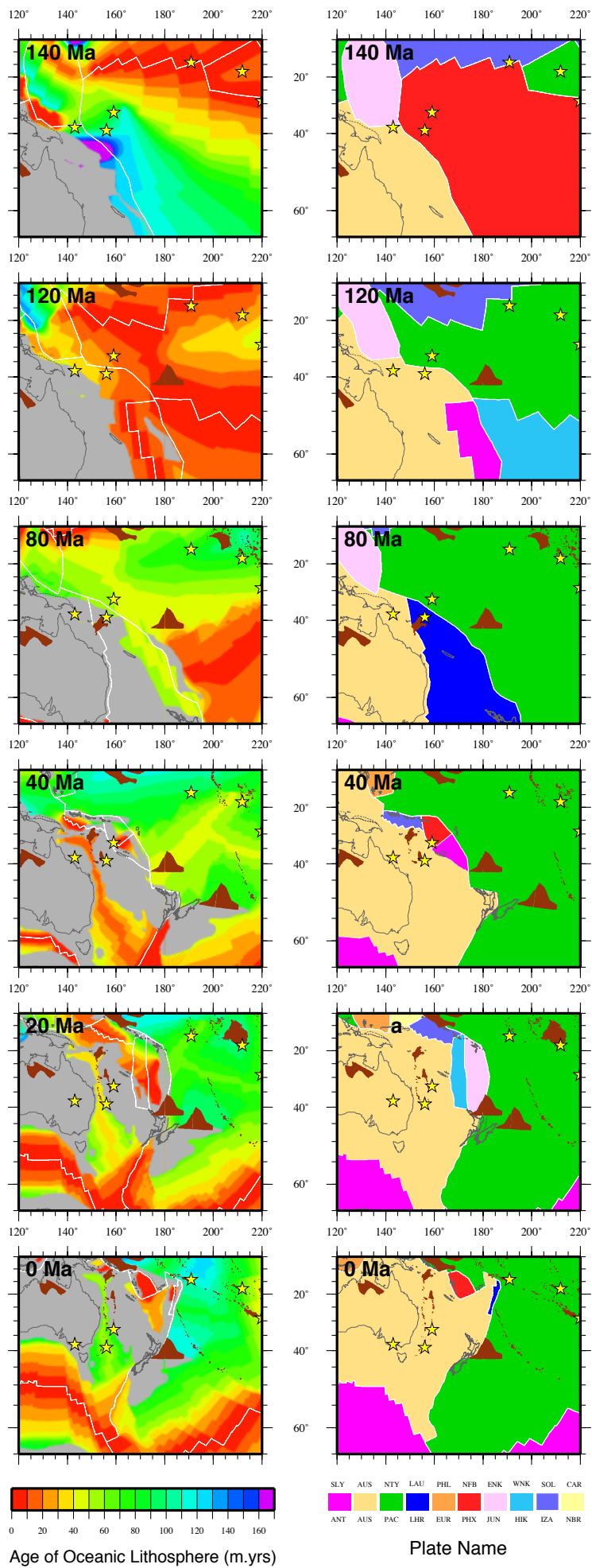


Figure 12: Seton et. al.



Figure 14

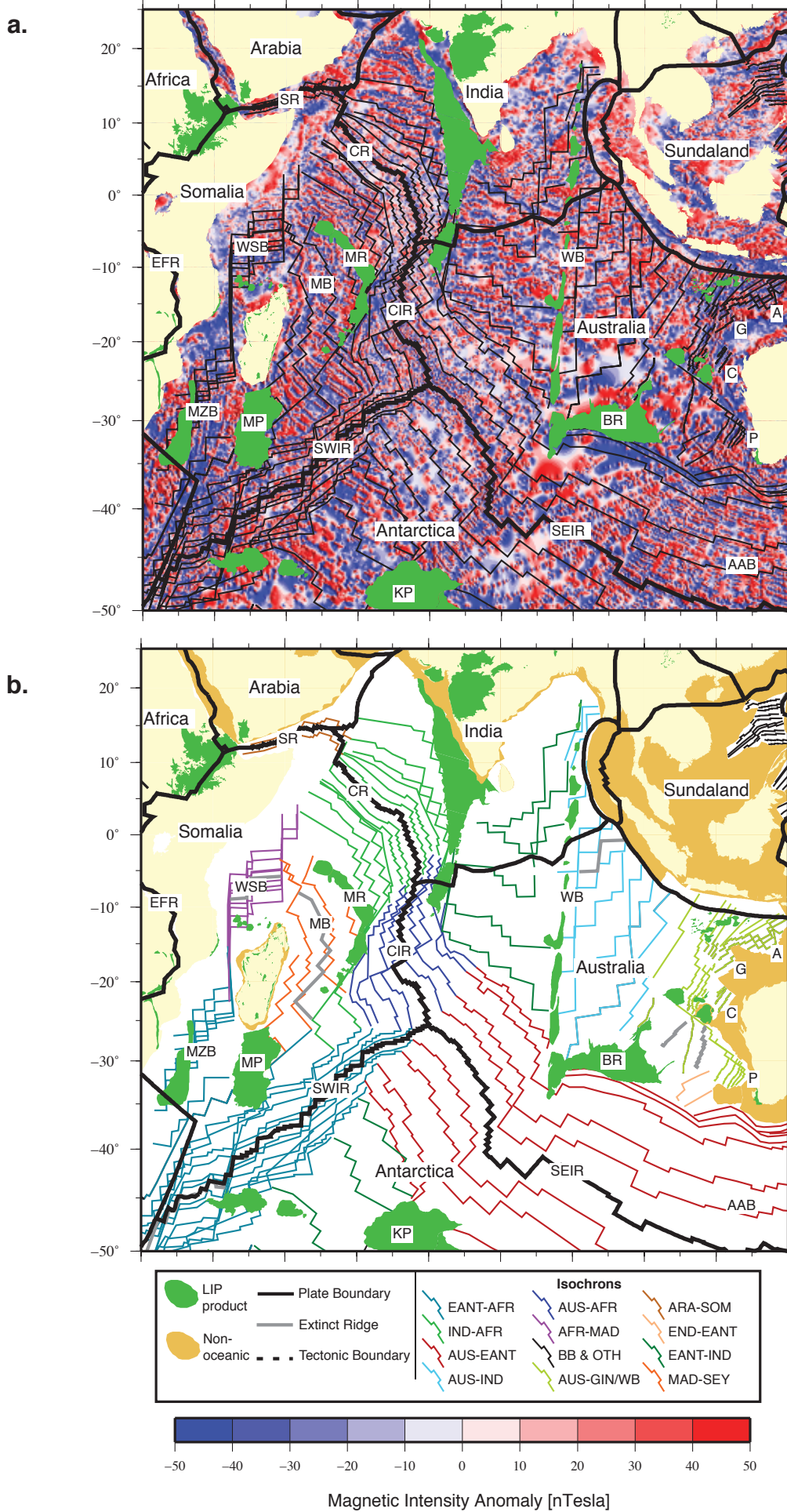
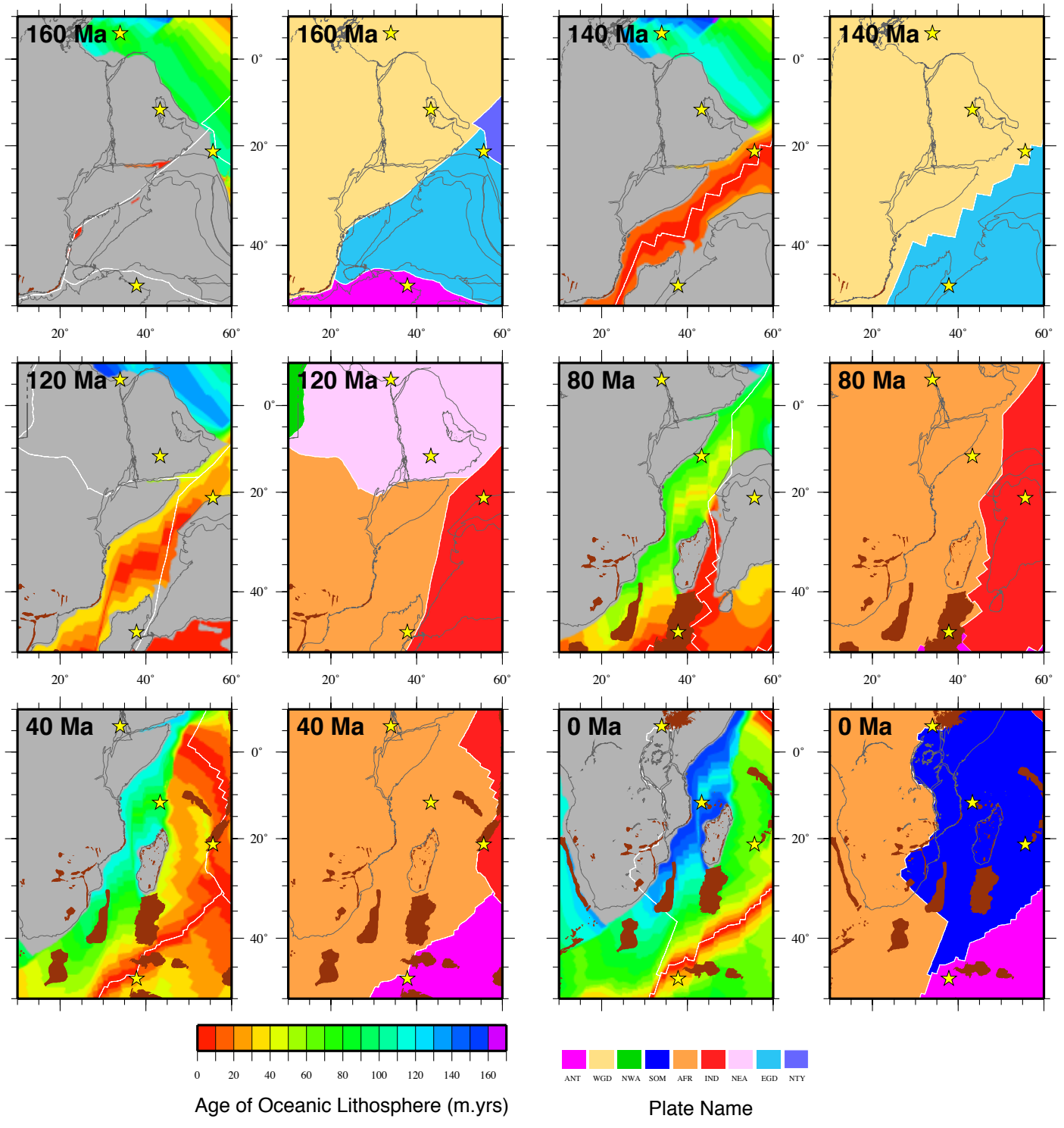


Figure 14: Seton et. al.

Figure 15



Seton et. al.: Figure 15

Figure 16

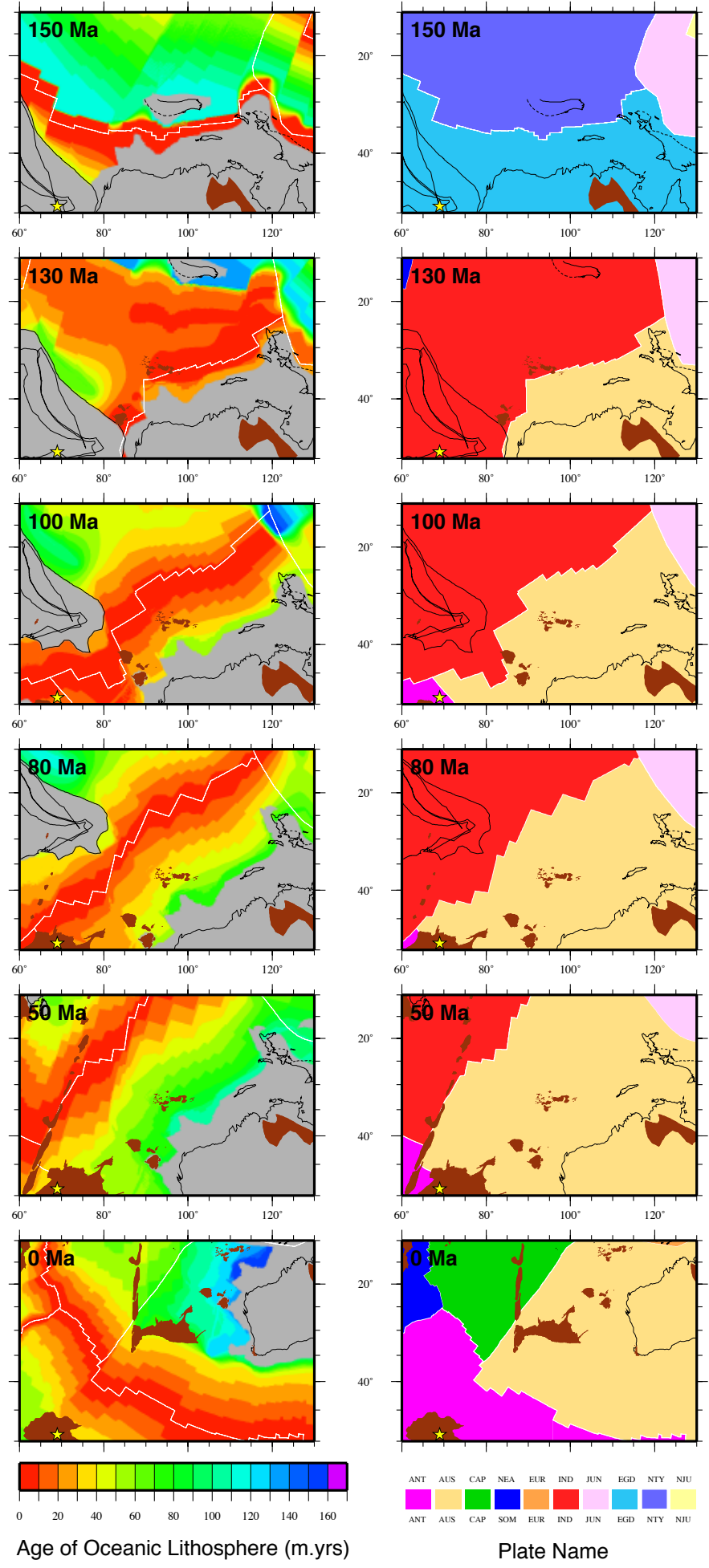


Figure 16: Seton et. al.

Figure 17

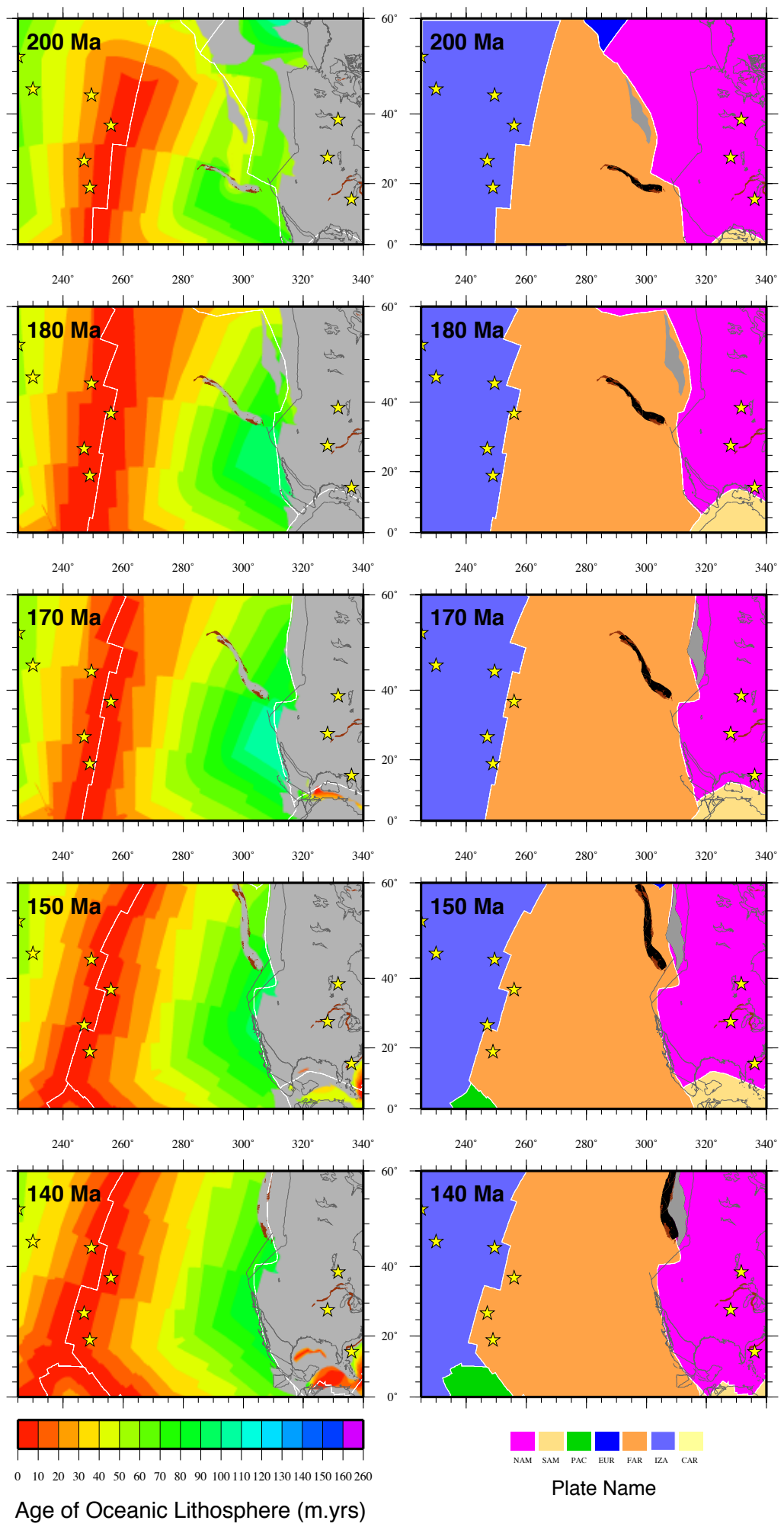


Figure 17: Seton et. al.

Figure 18a

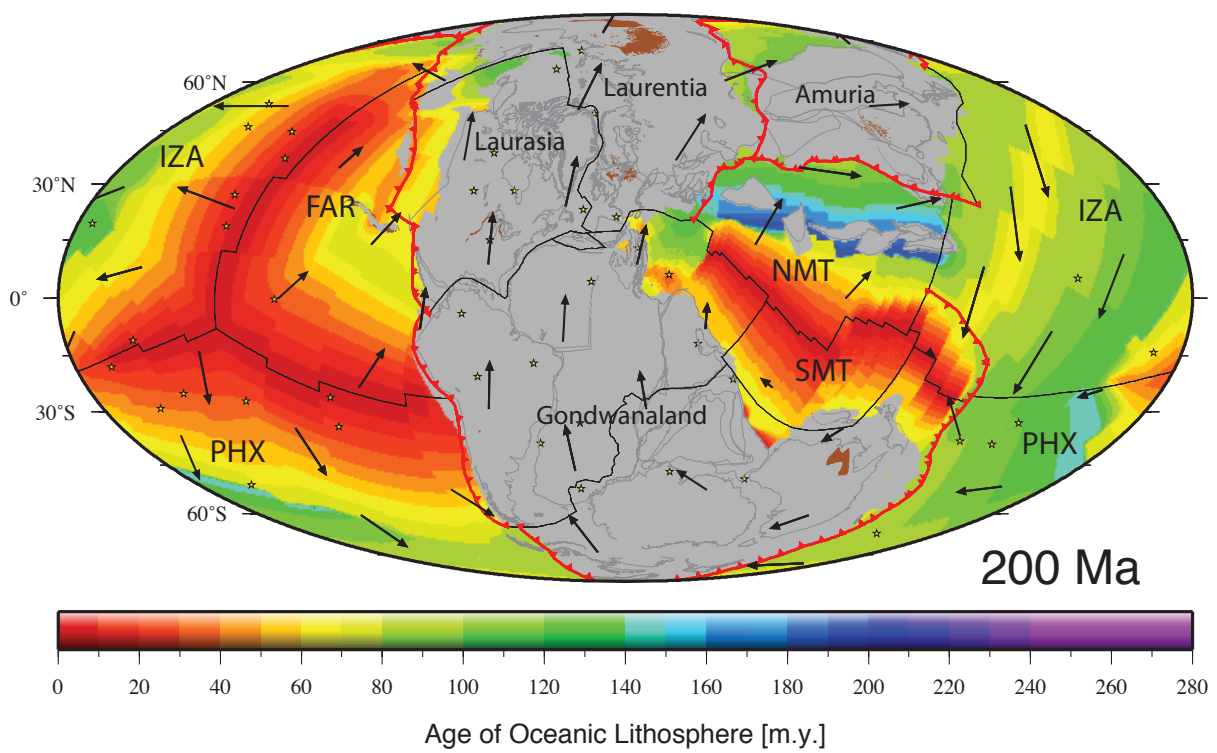


Figure 18a: Seton et. al.

Figure 18b

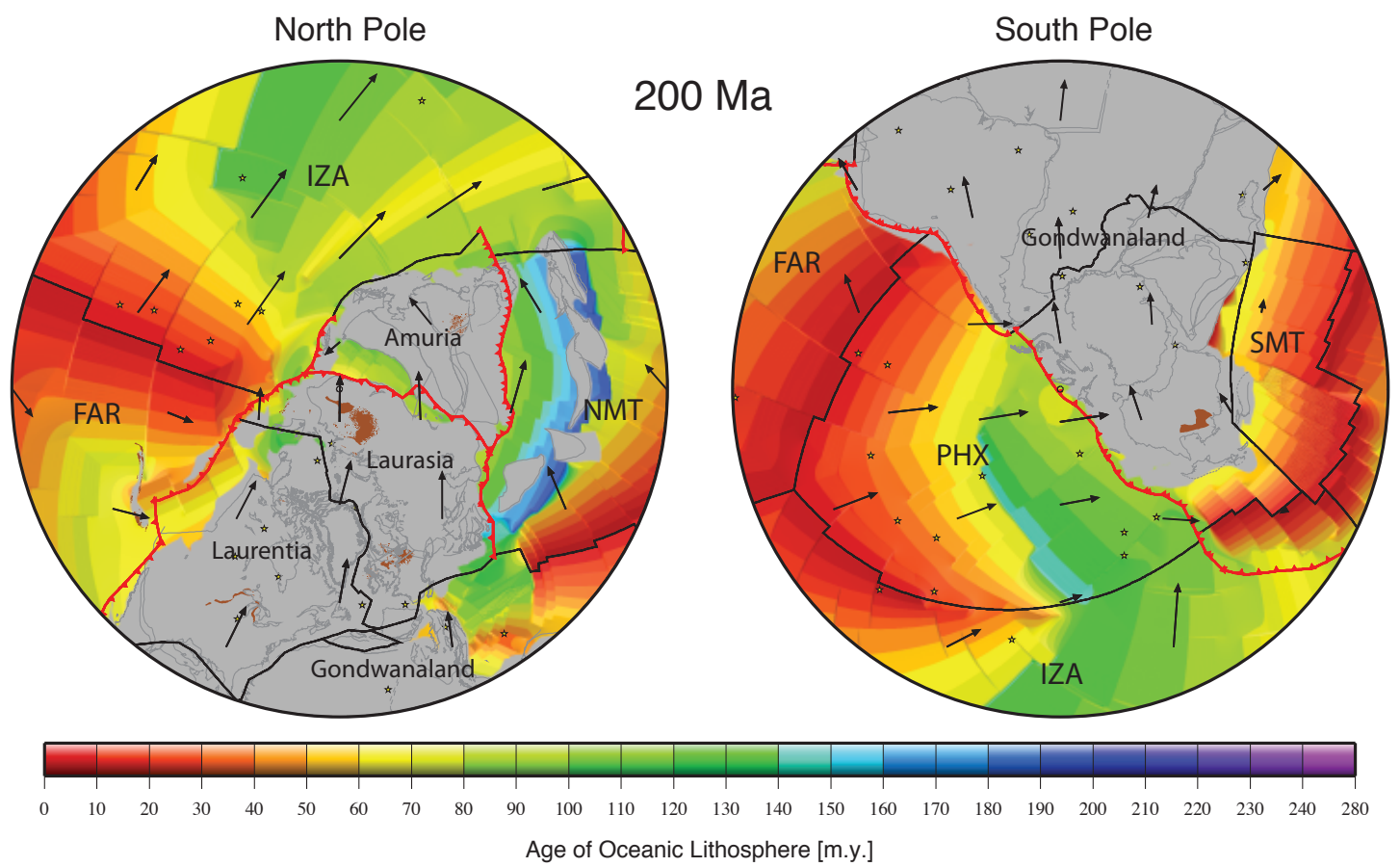


Figure 18b: Seton et. al.

Figure 19a

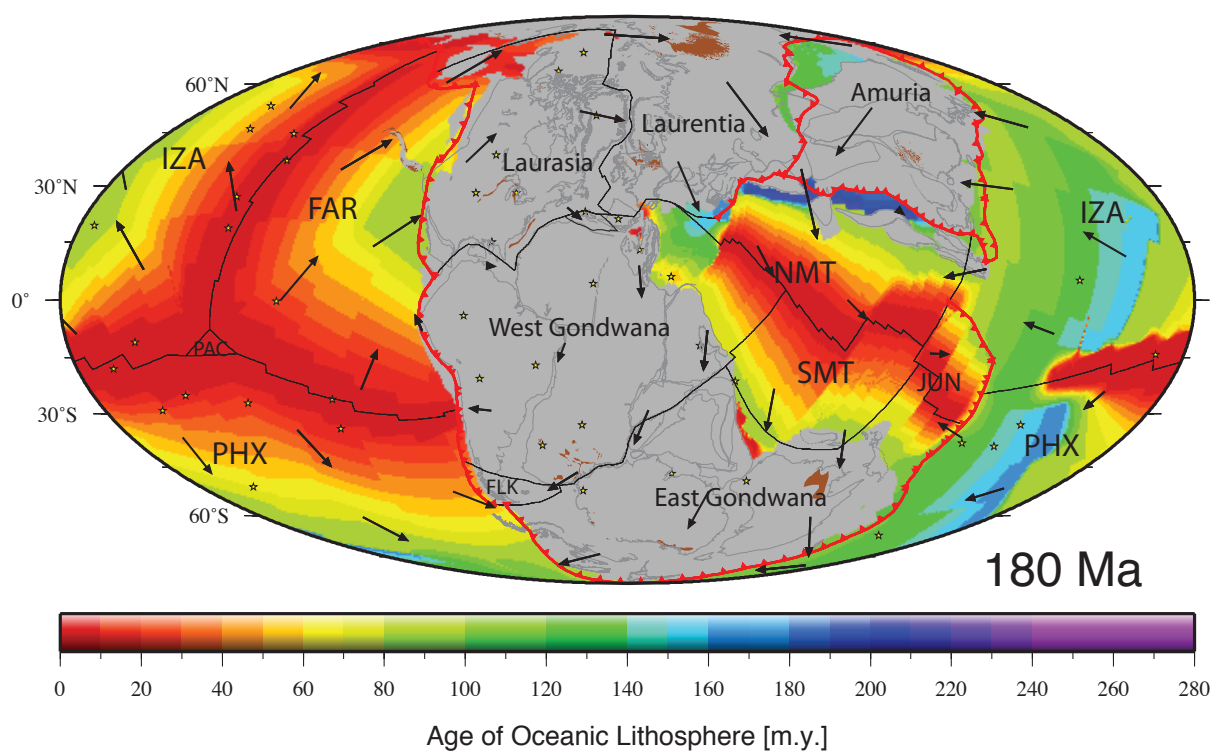


Figure 19a: Seton et. al.

Figure 19b

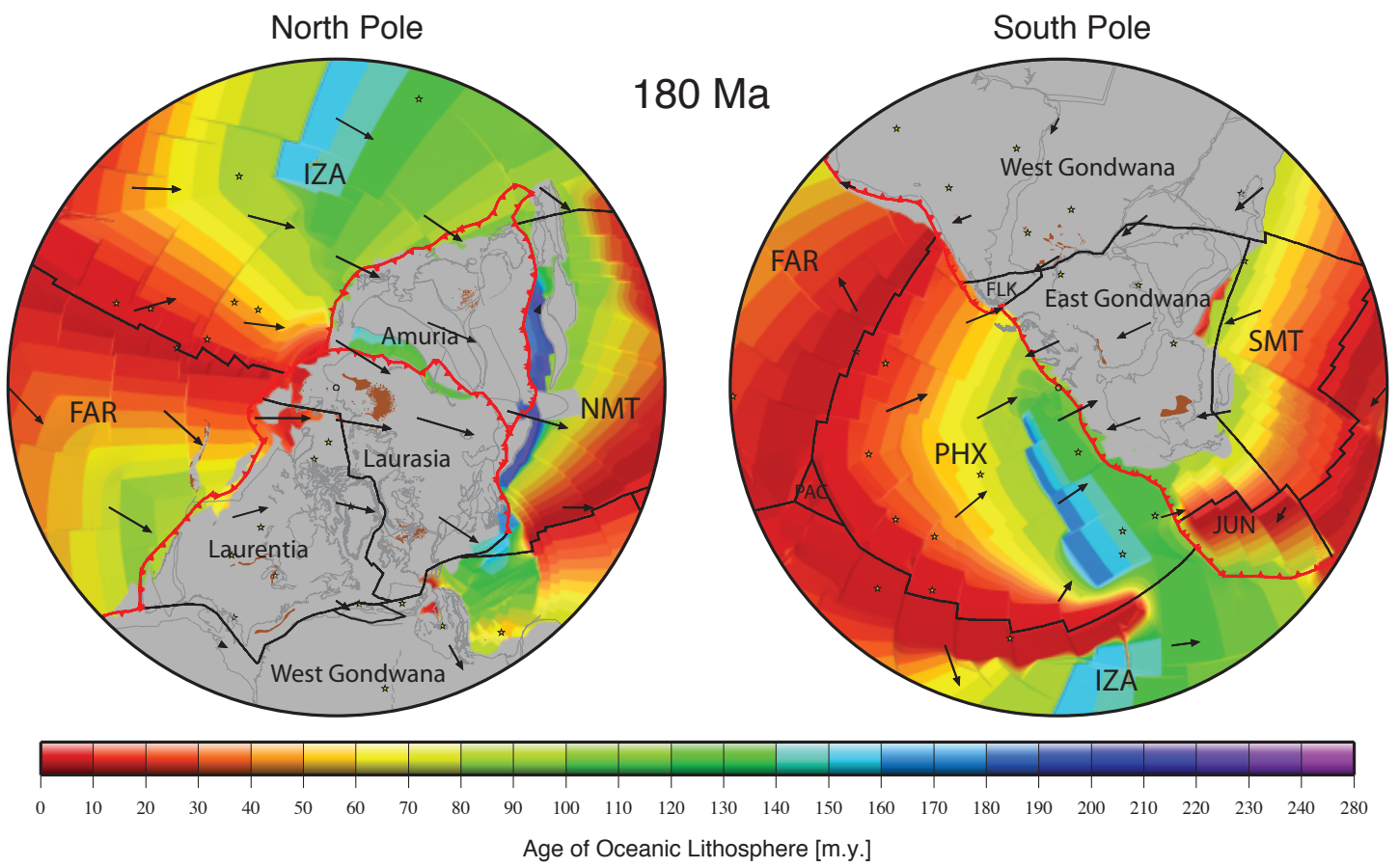


Figure 19b: Seton et. al.

Figure 20a

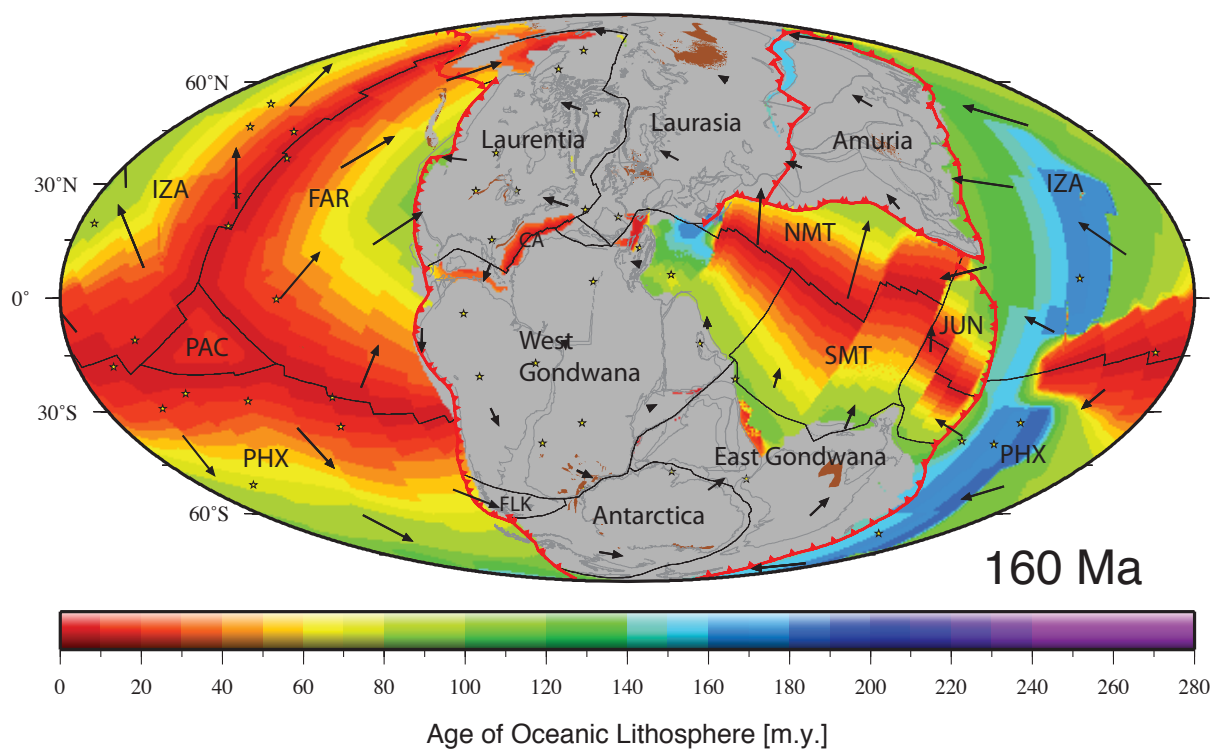


Figure 20a: Seton et. al.

Figure 20b

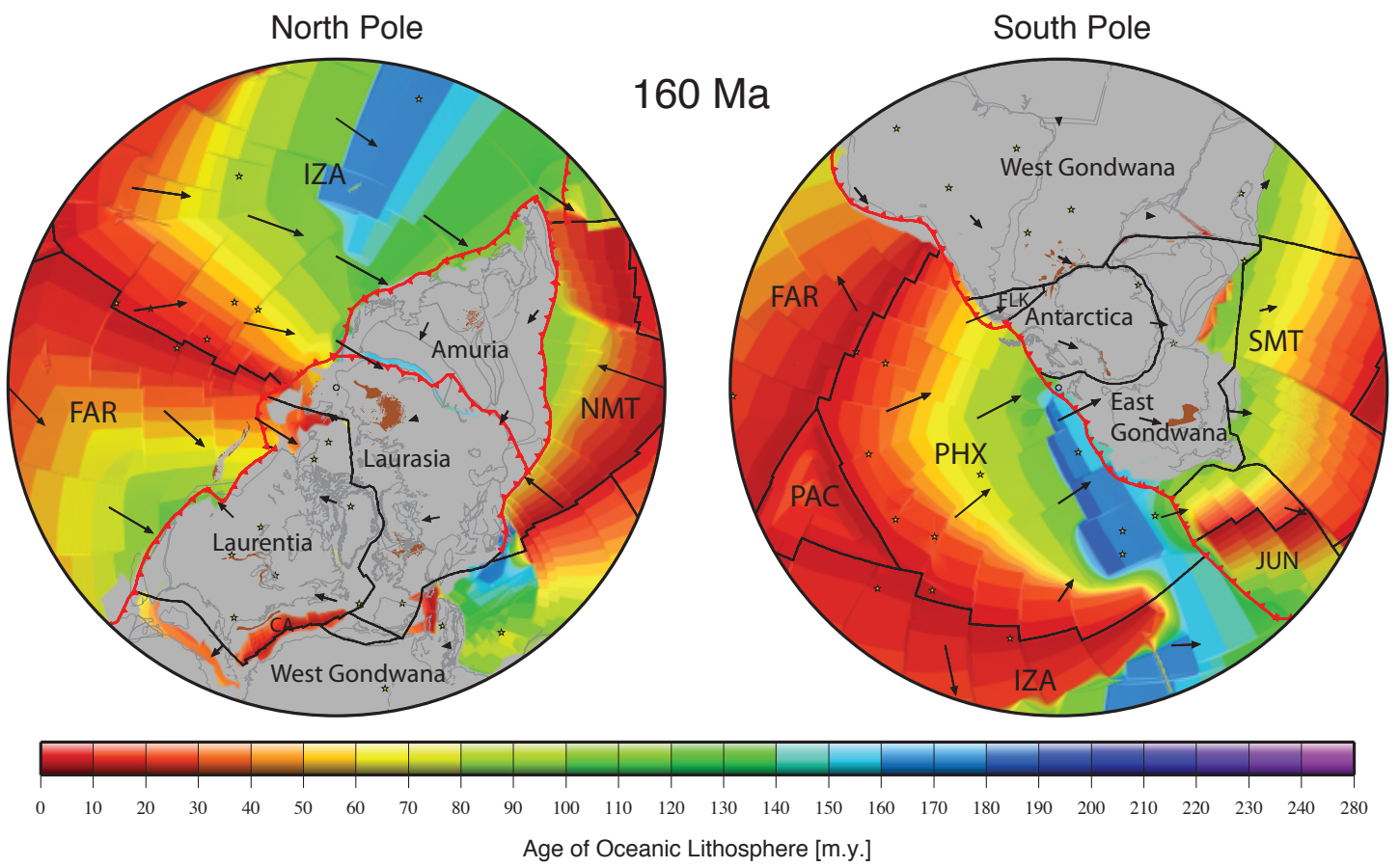


Figure 20b: Seton et. al.

Figure 21a

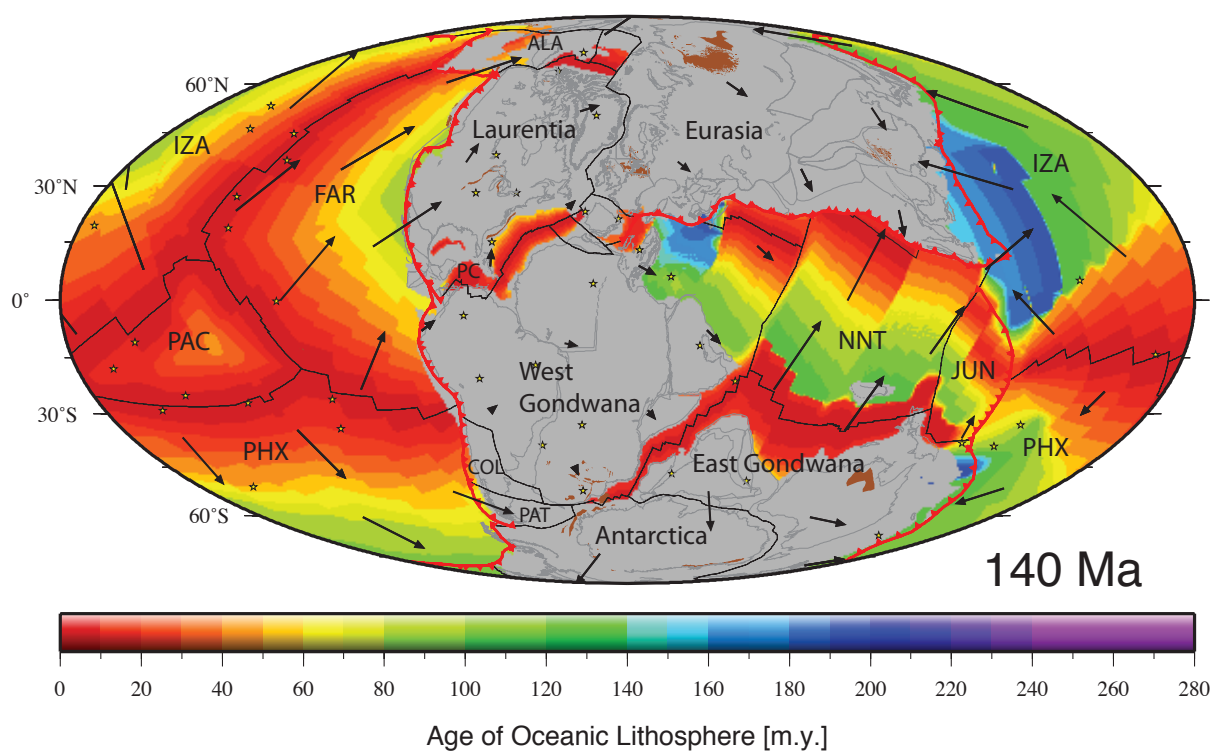


Figure 21a: Seton et. al.

Figure 21b

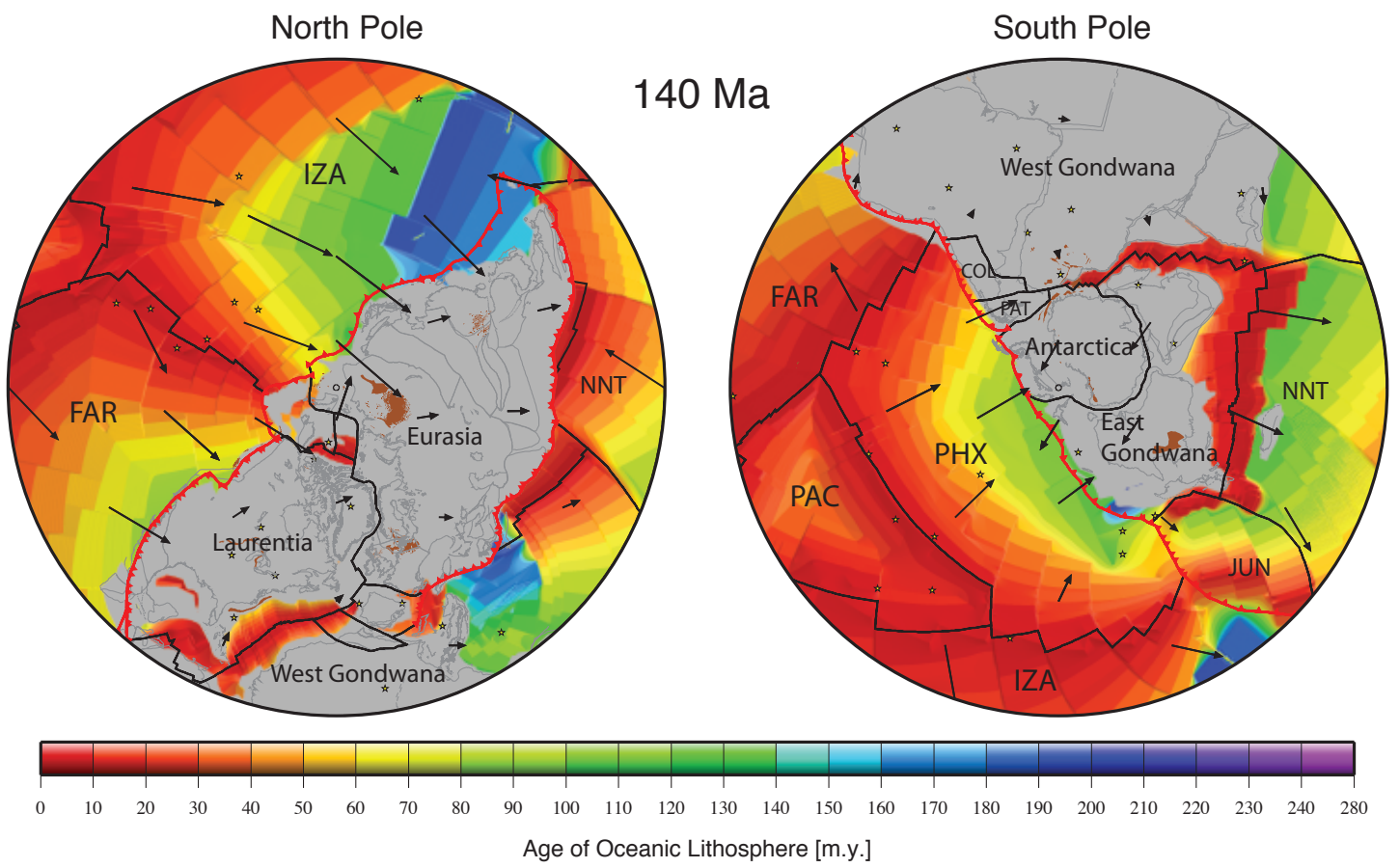


Figure 21b: Seton et. al.

Figure 22a

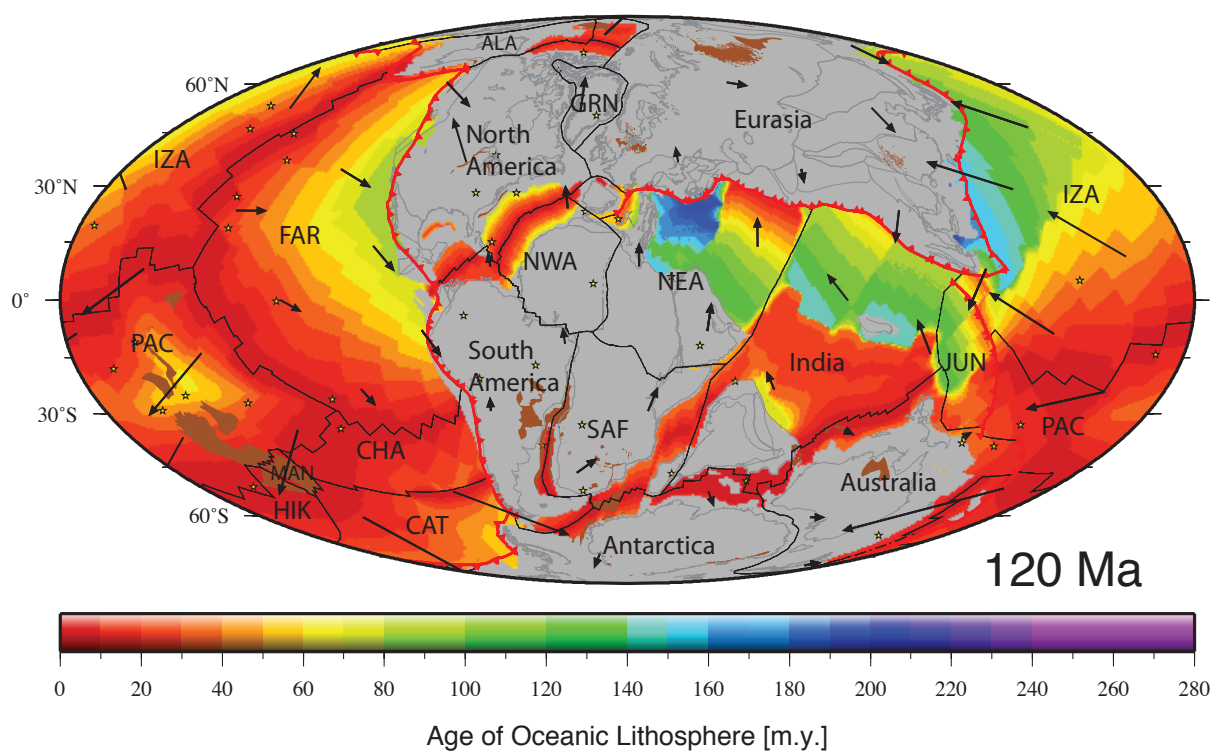


Figure 22a: Seton et. al.

Figure 22b

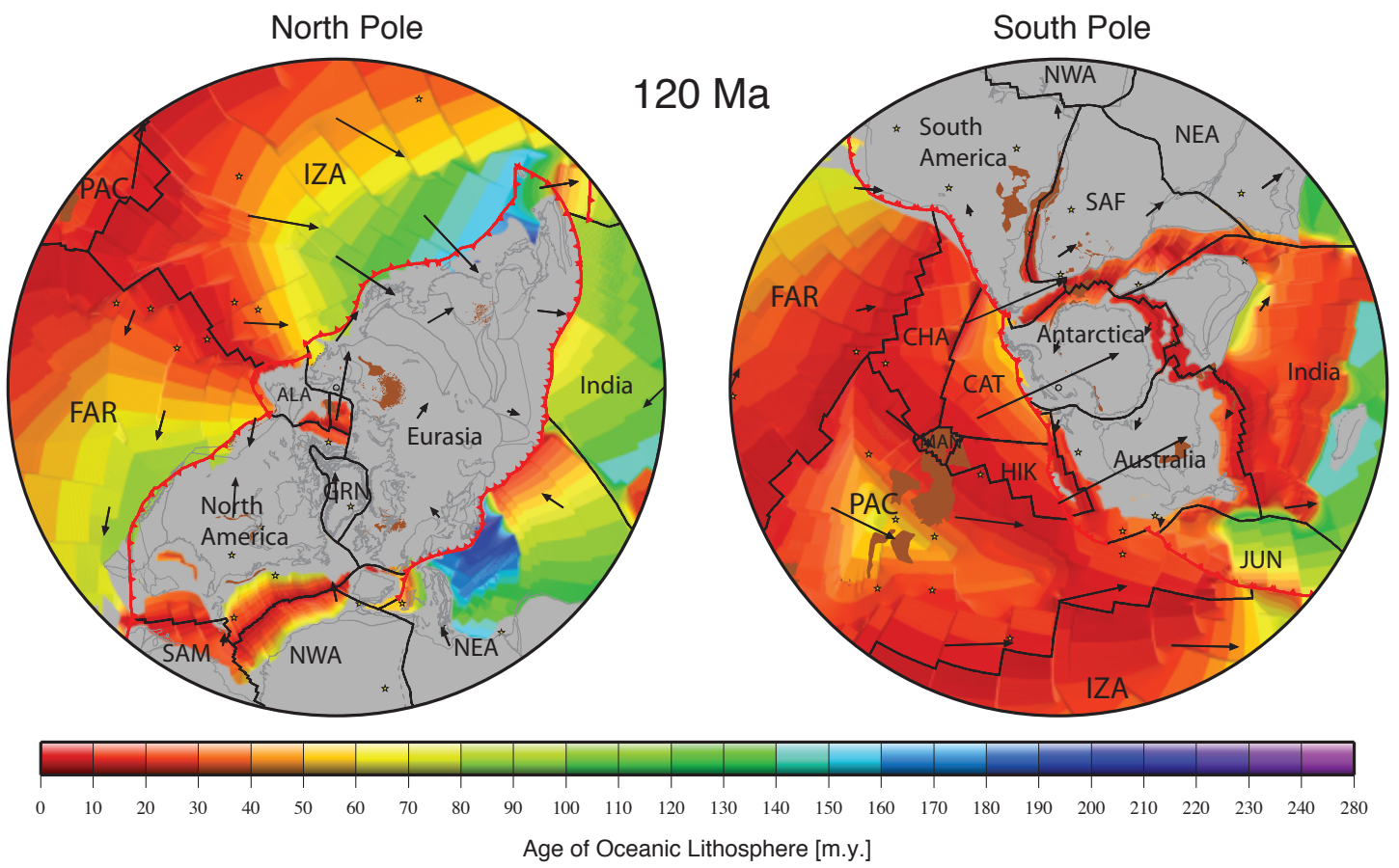


Figure 22b: Seton et. al.

Figure 23a

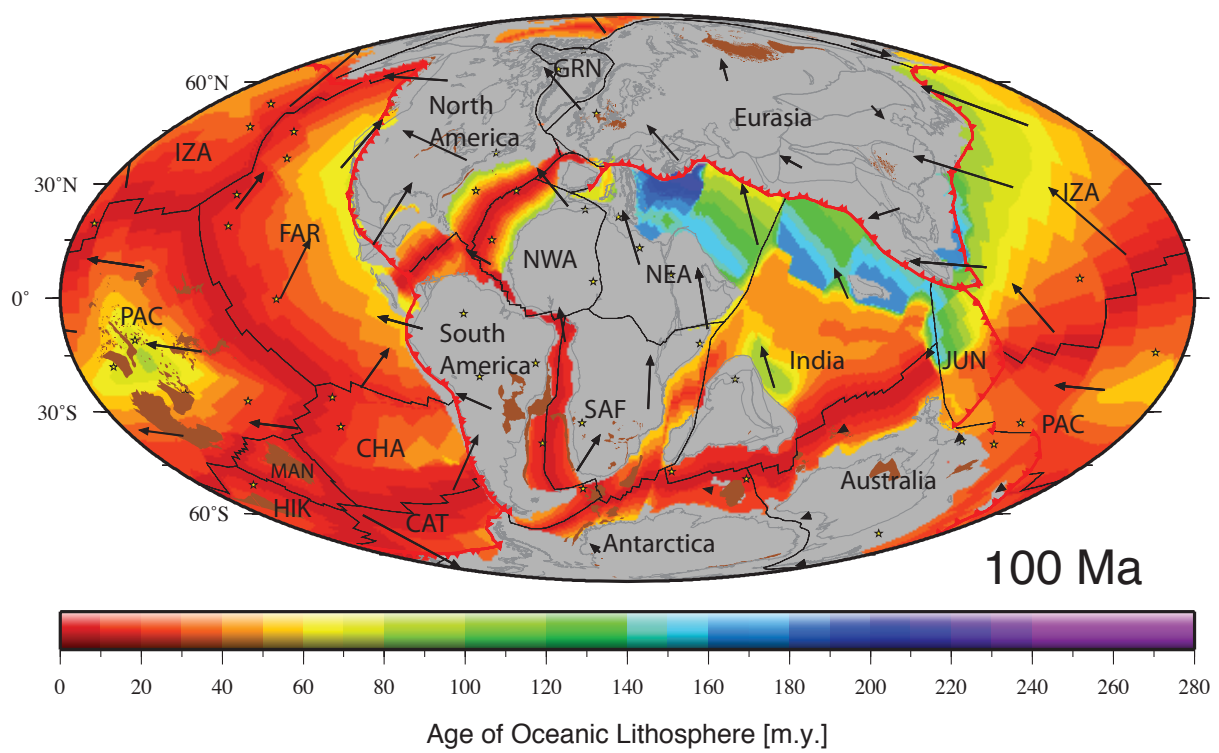


Figure 23a: Seton et. al.

Figure 23b

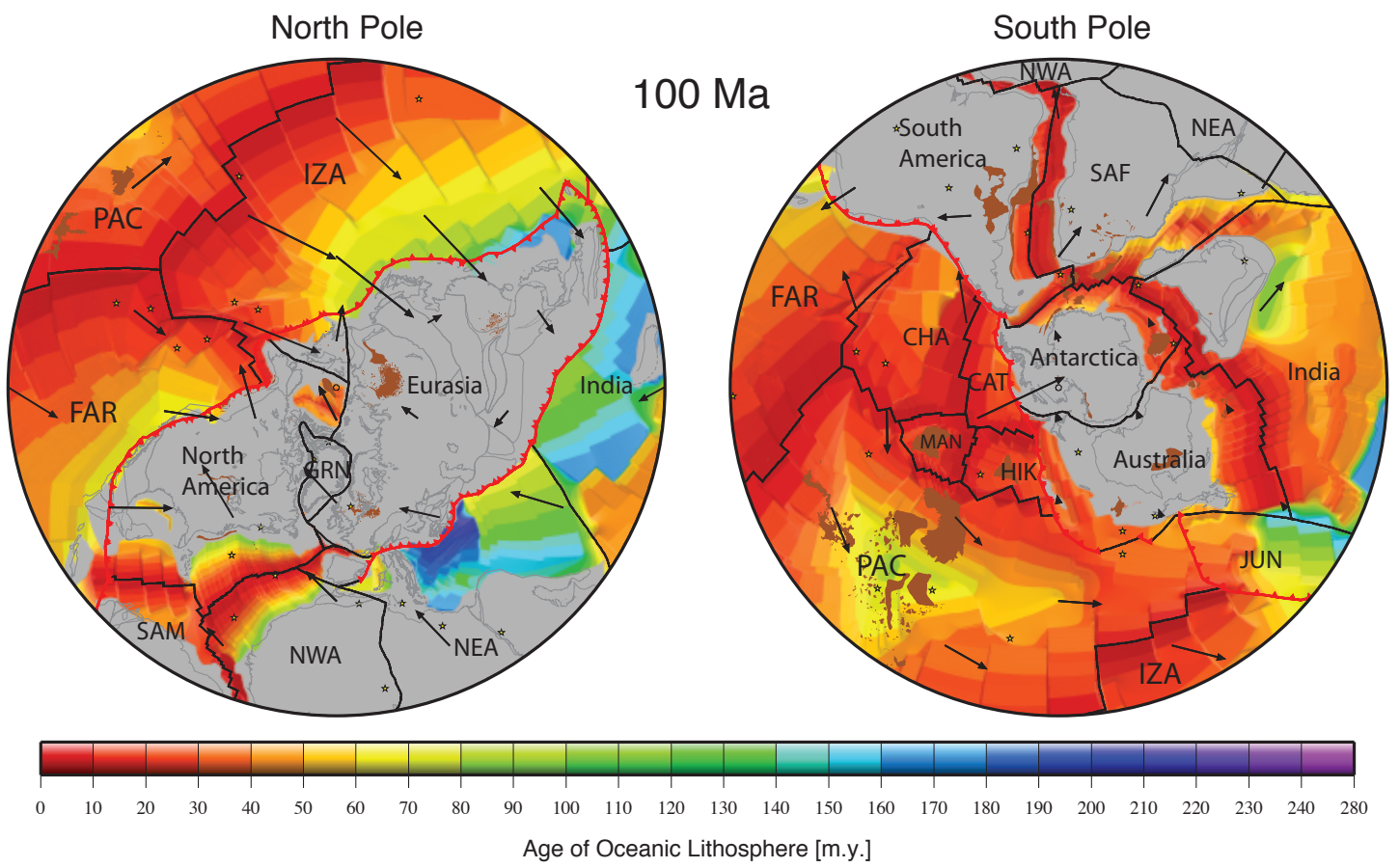


Figure 23b: Seton et. al.

Figure 24a

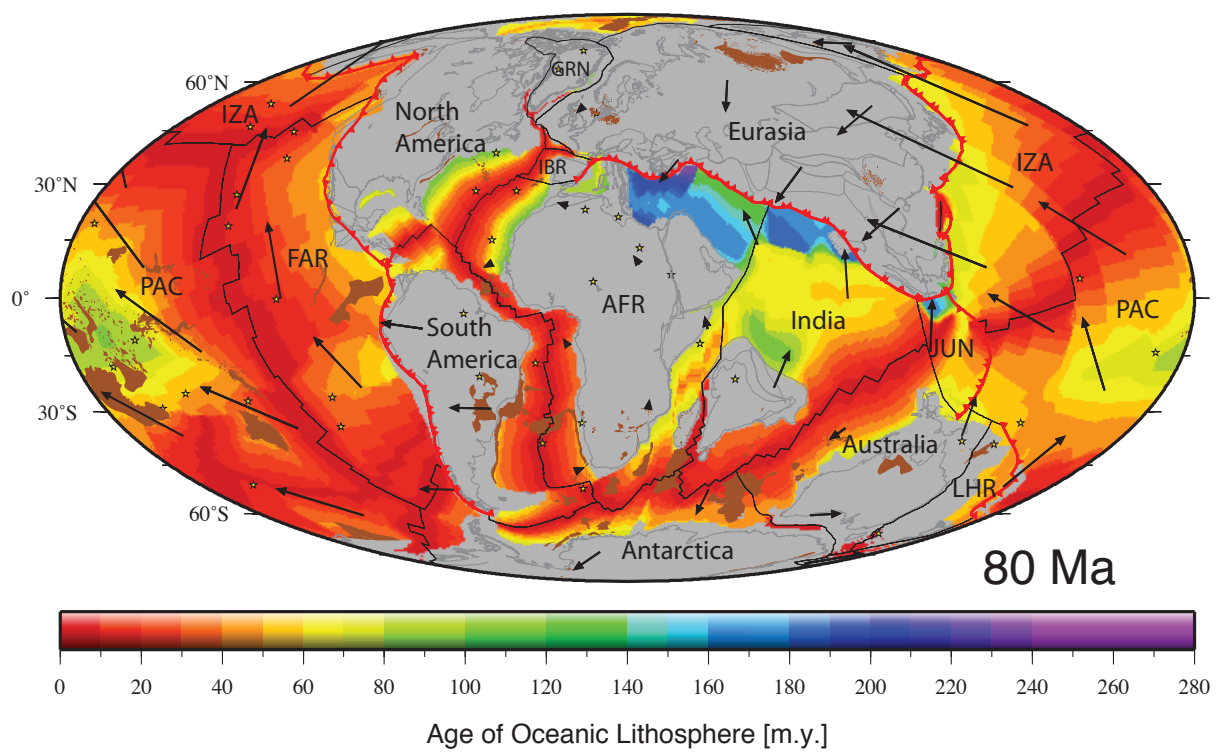


Figure 24a: Seton et. al.

Figure 24b

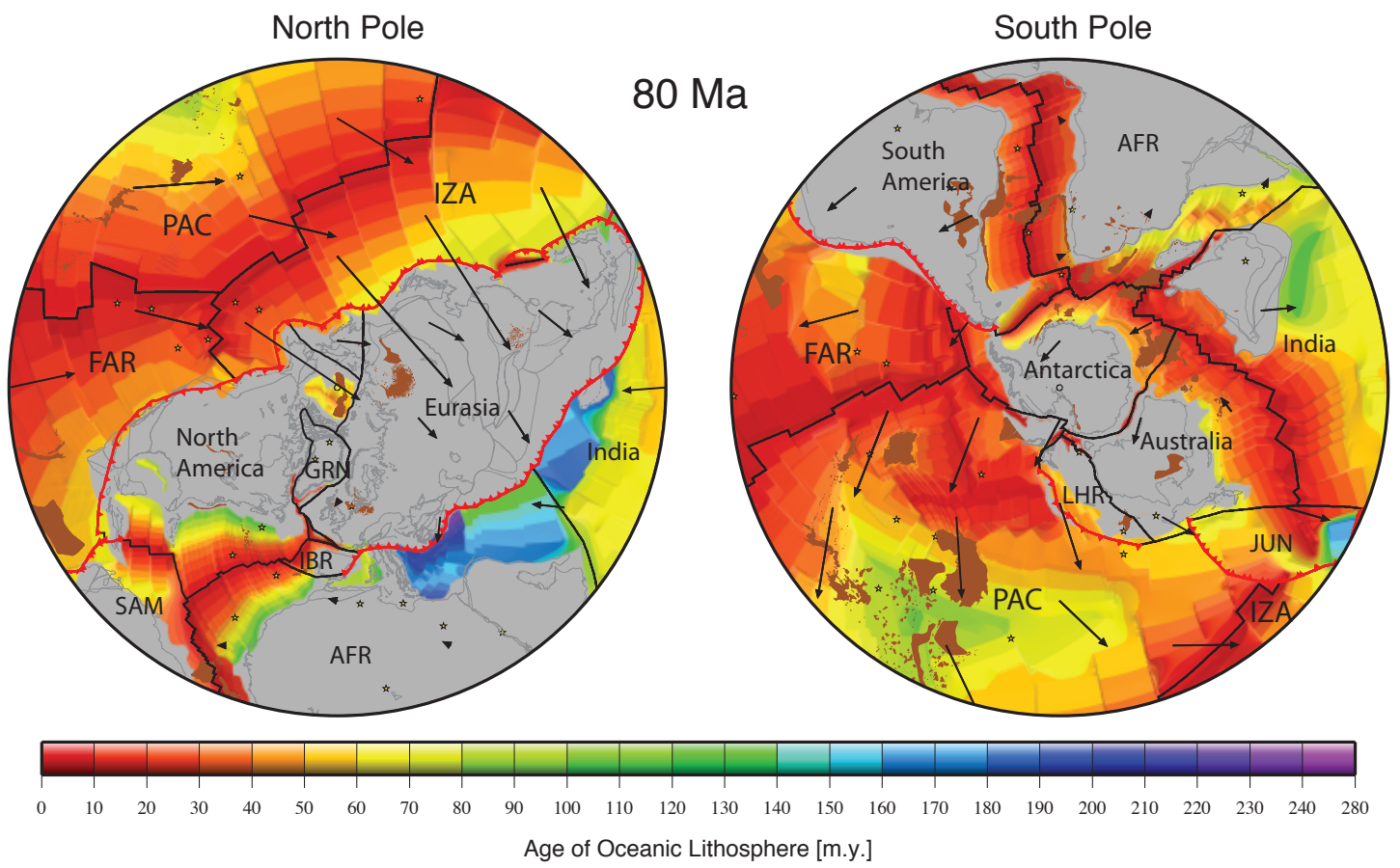


Figure 24b: Seton et. al.

Figure 25a

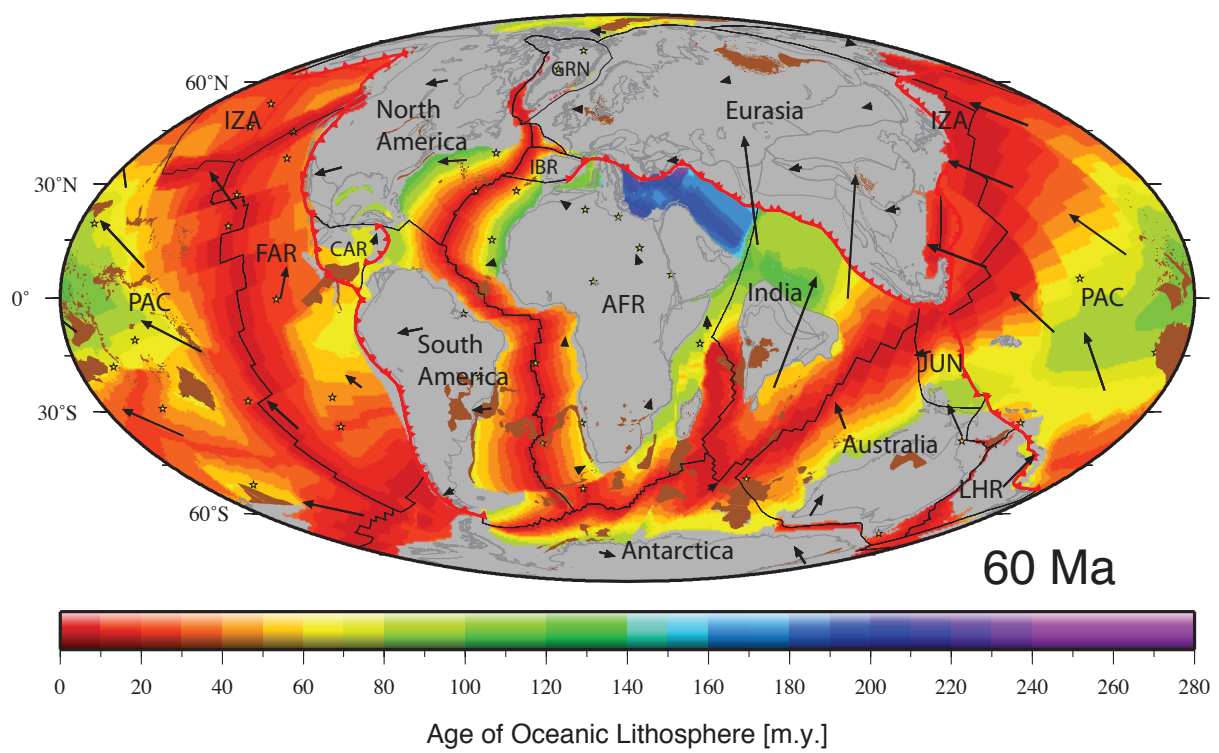


Figure 25a: Seton et. al.

Figure 25b

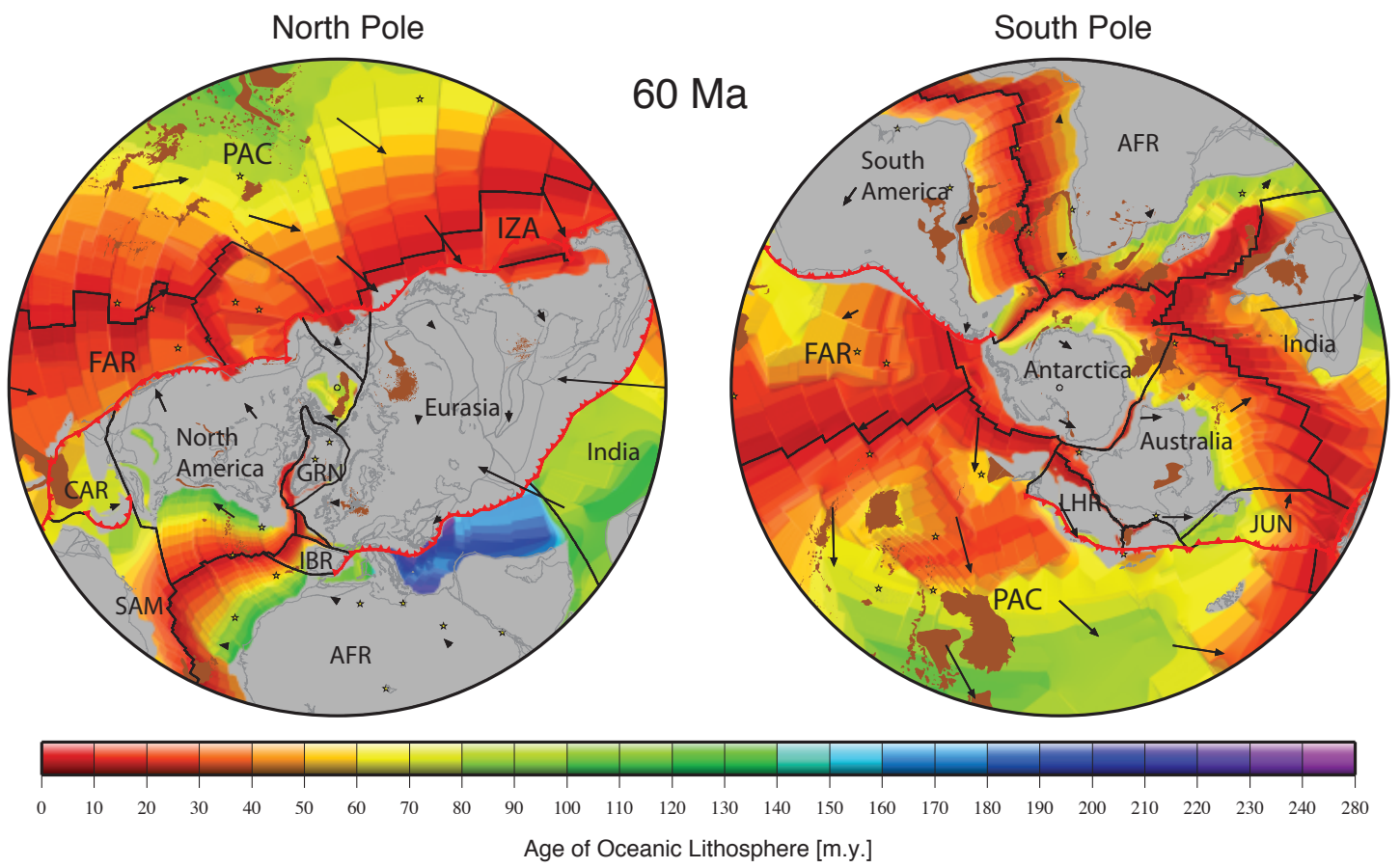


Figure 25b: Seton et. al.

Figure 26a

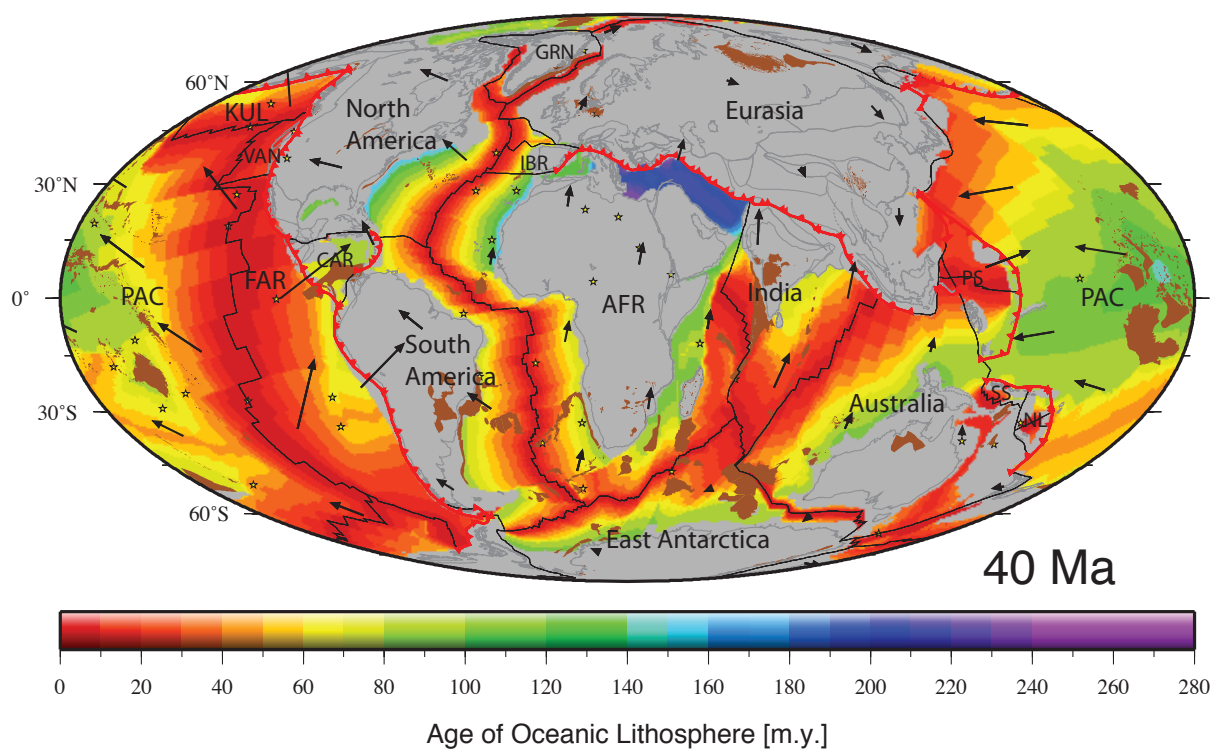


Figure 26a: Seton et. al.

Figure 26b

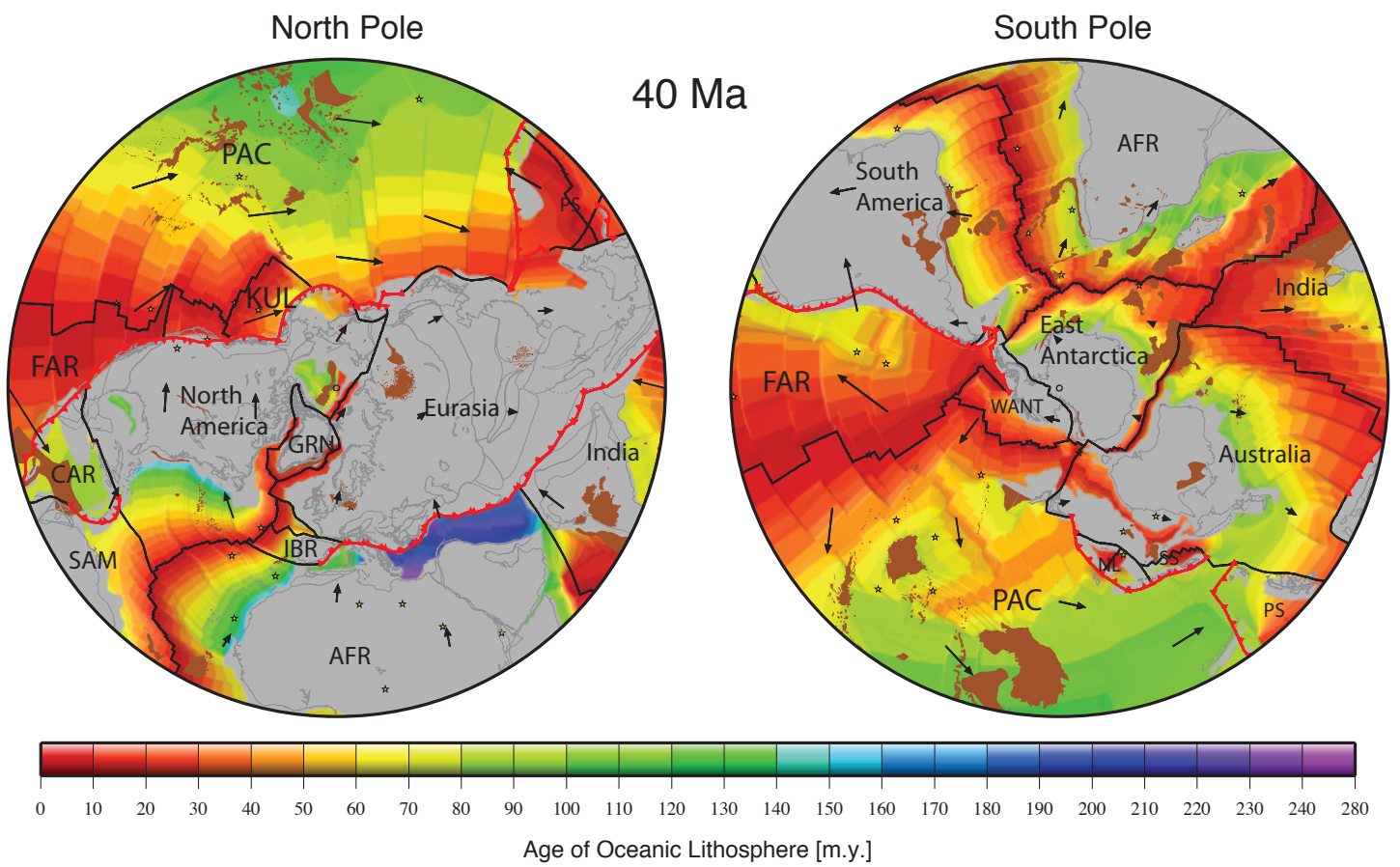


Figure 26b: Seton et. al.

Figure 27a

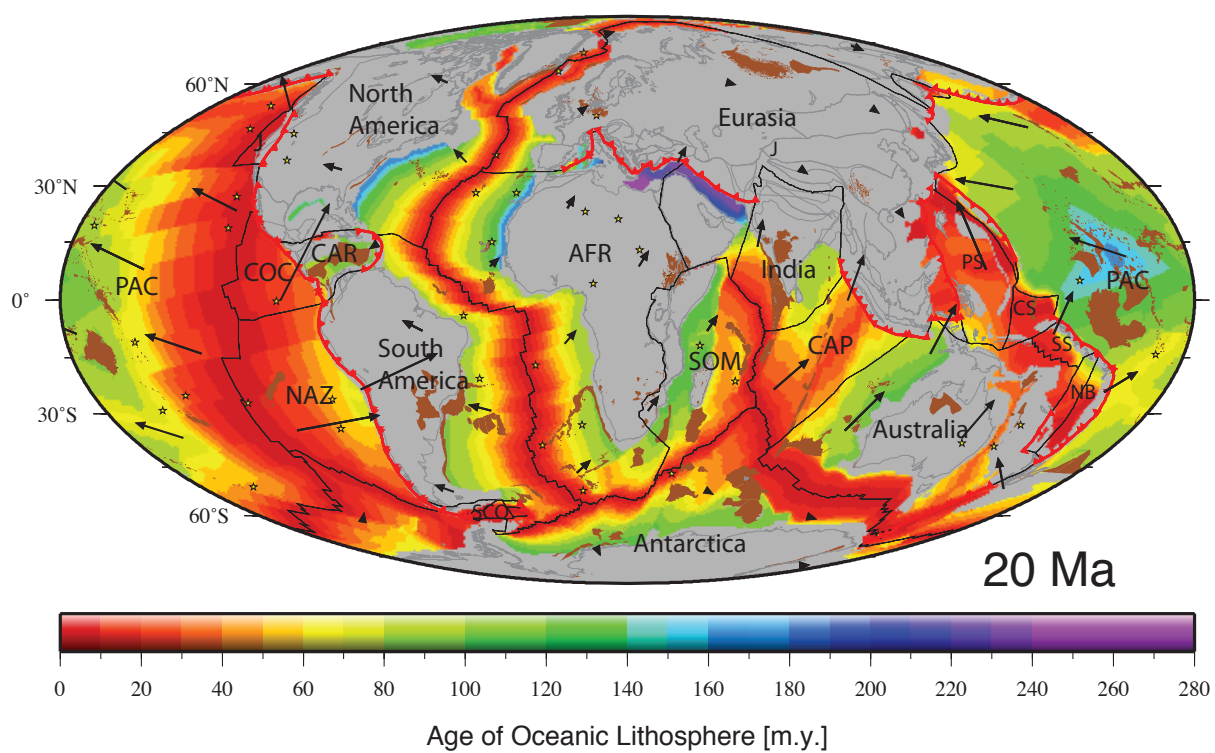


Figure 27a: Seton et. al.

Figure 27b

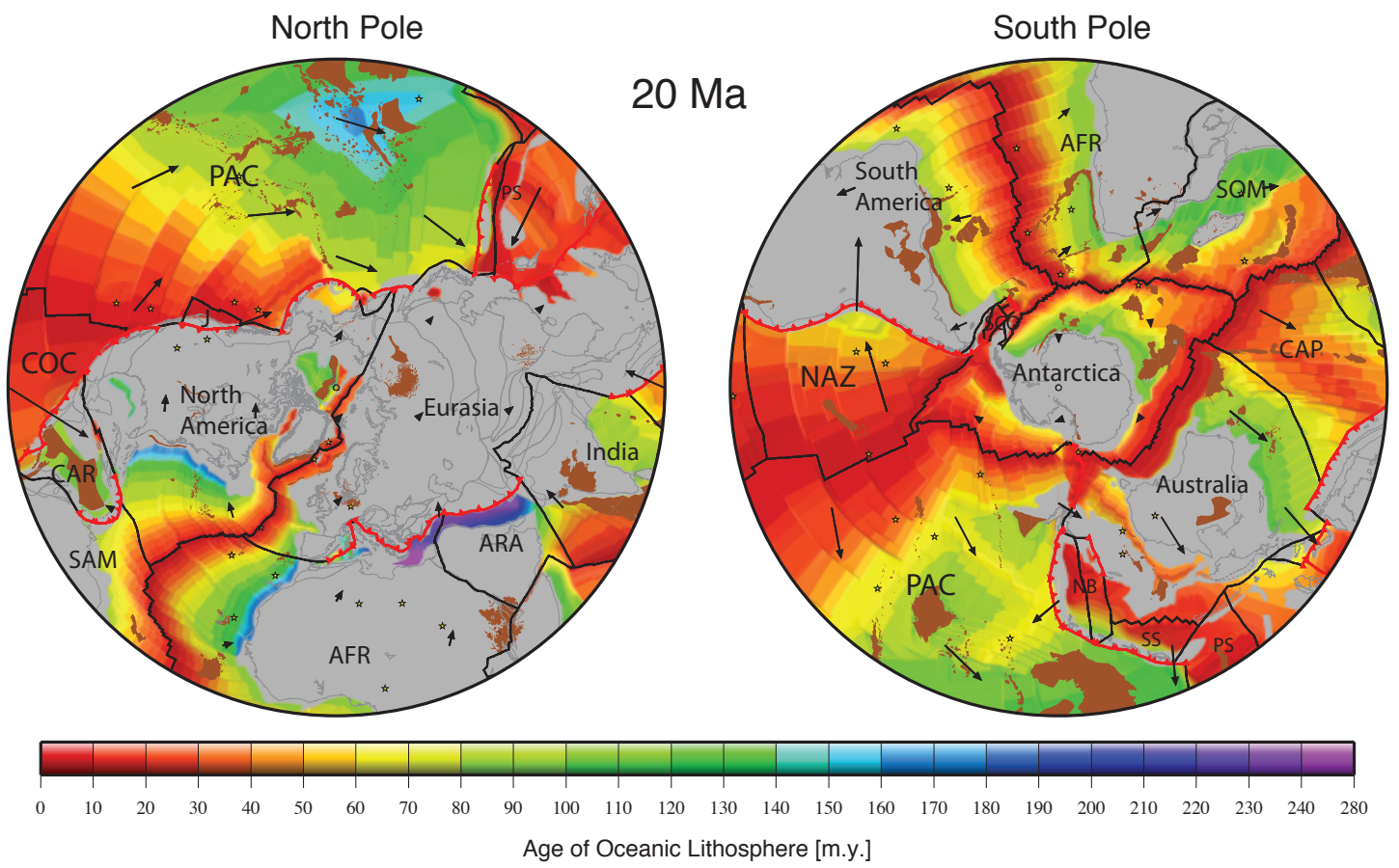


Figure 27b: Seton et. al.

Figure 28a

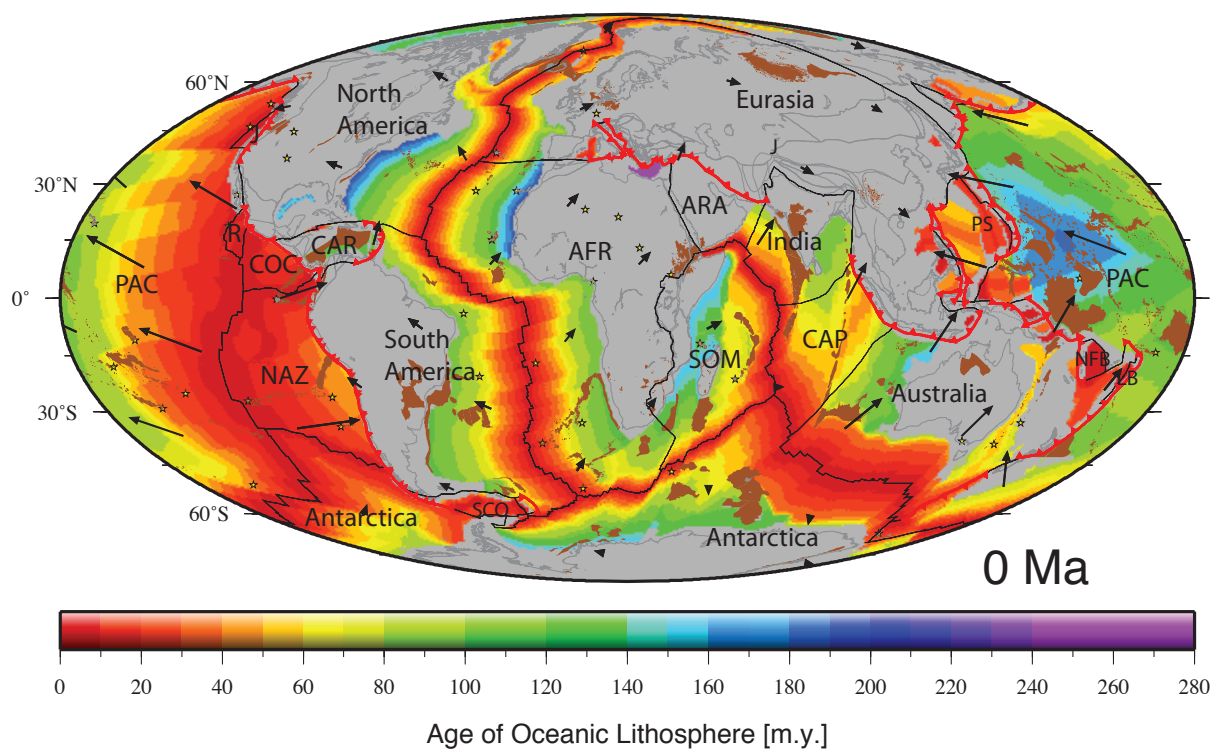


Figure 28a: Seton et. al.

Figure 28b

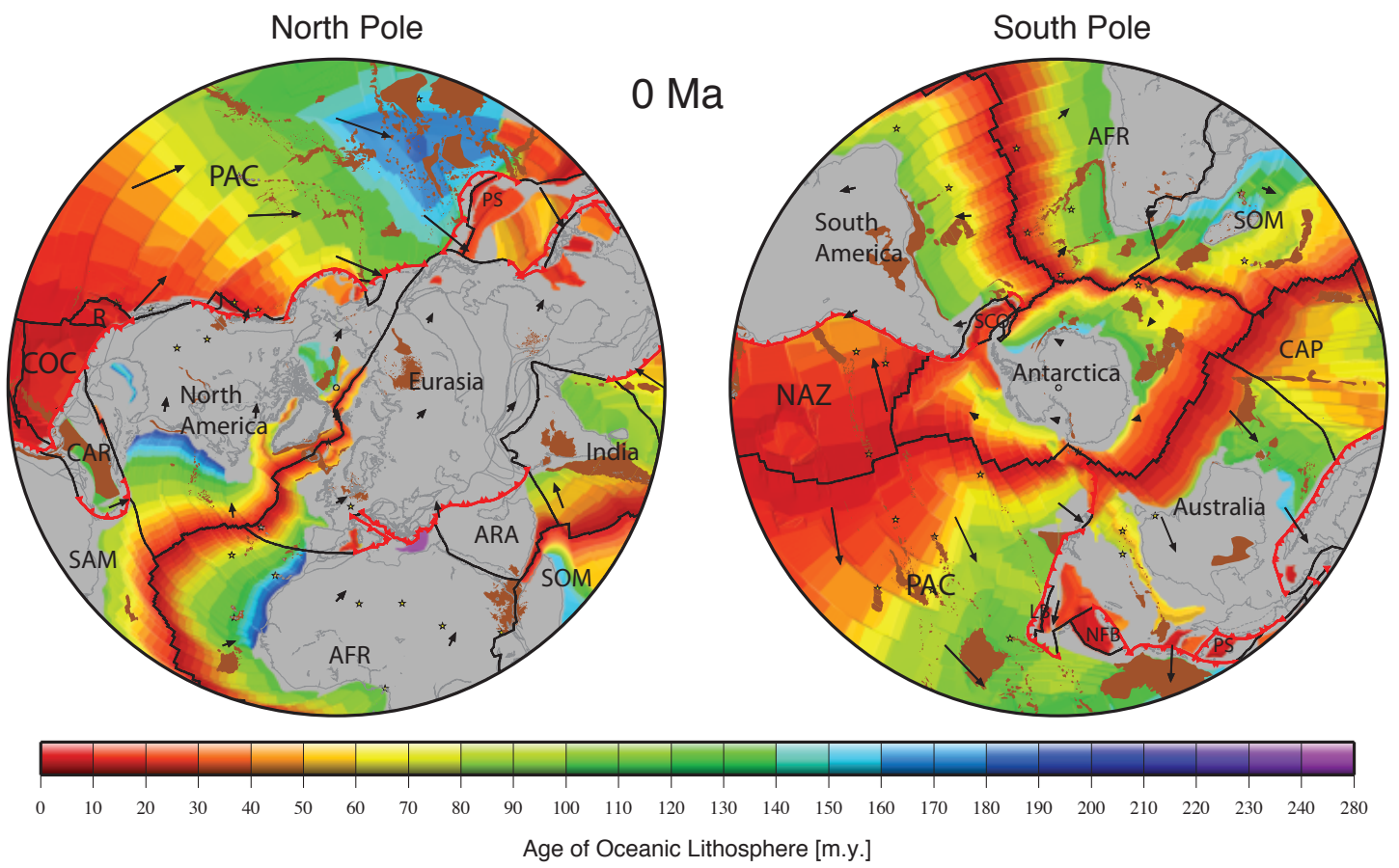


Figure 28b: Seton et. al.

Figure 29

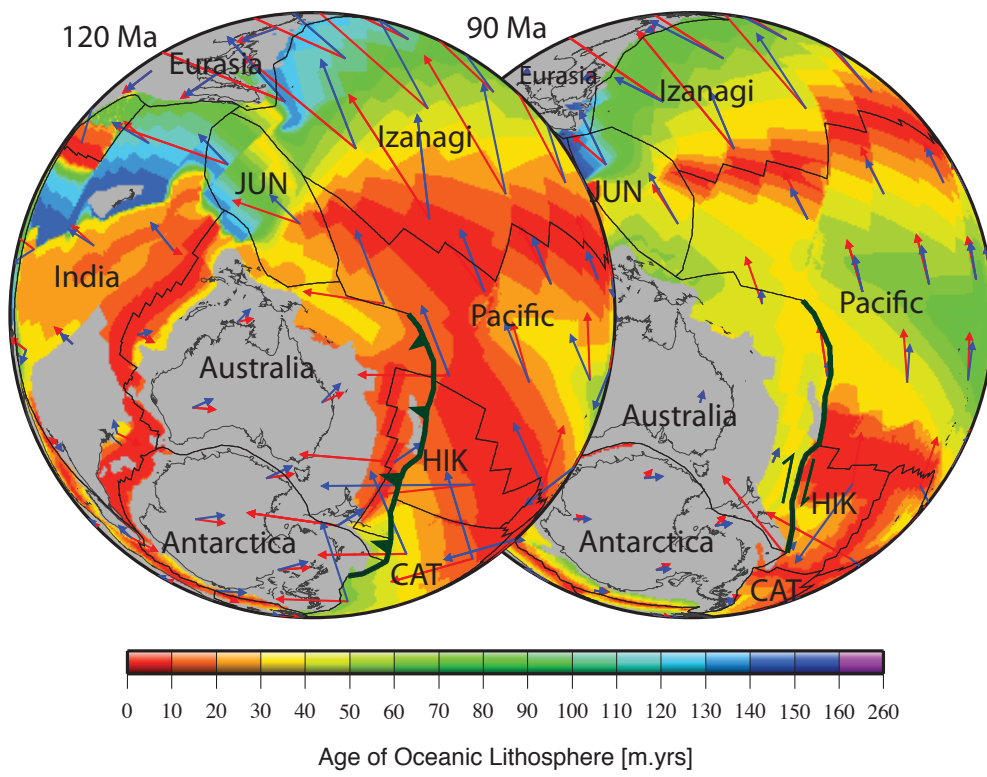


Figure 29: Seton et. al.

Chron	Abbreviation	Age - CK95, G94, T06		Age - GST 2004		Age - GK07	
		young	old	young	old	young	old
C1n	<b>1</b>	0.0	0.8	0.0	0.8	0.0	0.8
C2An.1n	<b>2</b>	2.6	3.0	2.5	3.0	2.6	3.0
C3An.1n	<b>3</b>	5.9	6.1	6.0	6.3	5.9	6.1
C4An	<b>4</b>	8.7	9.0	8.8	9.1	8.7	9.0
C5n.2n	<b>5</b>	9.9	10.9	10.0	11.0	9.9	10.9
C5Dn	<b>5D</b>	17.3	17.6	17.2	17.5	17.3	17.6
C6n	<b>6</b>	19.0	20.1	18.7	19.7	19.0	20.1
C7n.2n	<b>7</b>	24.8	25.2	24.2	24.6	24.8	25.2
C8n.2n	<b>8</b>	26.0	26.6	25.5	26.2	26.0	26.6
C9n	<b>9</b>	27.0	28.0	26.7	27.8	27.0	28.0
C10n.1n	<b>10</b>	28.3	28.5	28.2	28.5	28.3	28.5
C11n.2n	<b>11</b>	29.8	30.1	29.9	30.2	29.8	30.1
C12n	<b>12</b>	30.5	30.9	30.6	31.1	30.5	30.9
C13n	<b>13</b>	33.1	33.5	33.3	33.7	33.1	33.5
C15n	<b>15</b>	34.7	34.9	34.8	35.0	34.7	34.9
C16n.2n	<b>16</b>	35.7	36.3	35.7	36.3	35.7	36.3
C17n.1n	<b>17</b>	36.6	37.5	36.5	37.2	36.6	37.5
C18n.2n	<b>18</b>	39.6	40.1	39.0	39.5	39.6	40.1
C19n	<b>19</b>	41.3	41.5	40.4	40.7	41.3	41.5
C20n	<b>20</b>	42.5	43.8	41.6	42.8	42.5	43.8
C21n	<b>21</b>	46.3	47.9	45.3	47.2	46.3	47.9
C22n	<b>22</b>	49.0	49.7	48.6	49.4	49.0	49.7
C23n.2n	<b>23</b>	51.0	51.7	51.1	51.9	51.0	51.7
C24n.3n	<b>24</b>	52.9	53.3	53.3	53.8	52.9	53.3
C25n	<b>25</b>	55.9	56.4	56.7	57.2	55.9	56.4
C26n	<b>26</b>	57.6	57.9	58.4	58.7	57.6	57.9
C27n	<b>27</b>	60.9	61.3	61.7	62.0	60.9	61.3
C28n	<b>28</b>	62.5	63.6	63.1	64.1	62.5	63.6
C29n	<b>29</b>	64.0	64.7	64.4	65.1	64.0	64.7
C30n	<b>30</b>	65.6	67.6	65.9	67.7	65.6	67.6
C31n	<b>31</b>	67.7	68.7	67.8	68.7	67.7	68.7
C32n.1n	<b>32</b>	71.1	71.3	71.0	71.2	71.1	71.3
C33n	<b>33</b>	73.6	79.1	73.6	79.5	73.6	79.1
C34n	<b>34</b>	83.5	120.4	84.0	125.0	83.0	120.6
M0r	<b>M0</b>	120.4	121.0	124.6	125.0	120.6	121.0
M1n	<b>M1</b>	121.0	123.7	125.0	127.6	121.0	123.2
M3n	<b>M3</b>	124.1	124.7	127.6	128.1	123.6	124.1
M5n/M4	<b>M4</b>	126.7	127.7	129.8	130.8	125.7	126.6
M6n	<b>M6</b>	128.2	128.3	131.2	131.4	126.9	127.1
M7n	<b>M7</b>	128.4	128.6	131.6	131.9	127.2	127.5
M8n	<b>M8</b>	129.0	129.3	132.2	132.5	127.8	128.1
M9n	<b>M9</b>	129.5	129.8	132.8	133.1	128.3	128.6
M10n	<b>M10</b>	130.2	130.6	133.5	133.9	128.9	129.3
M10Nn.3n	<b>M10N</b>	131.6	131.9	135.0	135.3	130.2	130.5
M11n	<b>M11</b>	132.1	132.7	135.7	136.4	130.8	131.5
M12n	<b>M12</b>	134.0	134.2	137.6	137.8	132.6	132.8
M13n	<b>M13</b>	135.3	135.5	139.1	139.3	134.1	134.3
M14n	<b>M14</b>	135.8	136.0	139.5	139.8	134.5	134.8
M15n	<b>M15</b>	136.2	137.2	140.4	140.7	135.6	136.0
M16n	<b>M16</b>	137.9	139.6	141.1	142.1	136.5	137.9
M17n	<b>M17</b>	140.3	140.8	142.6	142.8	138.5	138.9
M18n	<b>M18</b>	142.4	143.0	144.0	144.6	140.5	141.2
M19n	<b>M19</b>	143.7	144.7	145.1	146.0	141.9	143.1
M20n.2n	<b>M20</b>	145.4	146.0	146.5	147.2	143.8	144.7
M21n	<b>M21</b>	146.8	147.7	147.8	148.5	145.5	146.6
M22n.1n	<b>M22</b>	148.1	149.5	148.9	150.1	147.1	148.6
M23n.1n	<b>M23</b>	150.7	151.1	151.0	151.3	150.0	150.7
M24n.1n	<b>M24</b>	152.1	152.5	152.3	152.5	151.4	151.7
M25n	<b>M25</b>	154.1	154.3	154.1	154.4	153.4	154.0
M26.1n	<b>M26</b>	155.0	155.1	155.1	155.1	154.3	155.3
M27n	<b>M27</b>	155.4	155.5	155.7	155.9	155.6	155.8
M28n	<b>M28</b>	155.7	155.8	156.0	156.3	156.1	156.2
M29.1n	<b>M29</b>	156.0	156.1	157.3	157.4	156.5	157.3
M30.1n	<b>M30</b>	156.8	157.2	N/A	N/A	N/A	N/A
M31n	<b>M31</b>	157.4	157.6	N/A	N/A	N/A	N/A
M32n	<b>M32</b>	157.7	157.9	N/A	N/A	N/A	N/A
M33n	<b>M33</b>	158.0	158.1	N/A	N/A	N/A	N/A
M34	<b>M34</b>	160.3	160.9	N/A	N/A	N/A	N/A
M35	<b>M35</b>	161.0	161.1	N/A	N/A	N/A	N/A
M36	<b>M36</b>	161.3	161.8	N/A	N/A	N/A	N/A
M37	<b>M37</b>	162.0	162.4	N/A	N/A	N/A	N/A
M38	<b>M38</b>	162.5	163.5	N/A	N/A	N/A	N/A
M39	<b>M39</b>	163.7	165.4	N/A	N/A	N/A	N/A
M40	<b>M40</b>	165.5	166.2	N/A	N/A	N/A	N/A
M41	<b>M41</b>	166.3	167.0	N/A	N/A	N/A	N/A
M42	<b>M42</b>	167.1	168.2	N/A	N/A	N/A	N/A
M43	<b>M43</b>	168.2	168.9	N/A	N/A	N/A	N/A
M44	<b>M44</b>	168.9	169.7	N/A	N/A	N/A	N/A